



Mansoura University
Faculty of Pharmacy
Department of Pharmaceutics

Development and Characterization of Certain Controlled Release Drug Delivery Systems Based on Some Polymers as Carrier Matrix

Thesis Presented by

Reham Mokhtar A. Mohamed Aman

Assistant Lecture of Pharmaceutics, Faculty of Pharmacy, Mansoura University

M. Pharm. Sci., Pharmaceutics (2014)

*Submitted in Partial Fulfillment for the Degree of Doctor of Philosophy in Pharmaceutical
Sciences (Pharmaceutics)*

Under the Supervision of

Prof. Dr.

Mahasen M. Abd El Hady Meshali

*Professor Emeritus of Pharmaceutics
Faculty of Pharmacy, Mansoura
University*

Ass. Prof. Dr.

Irhan Ibrahim Abu Hashim

*Associate Professor of Pharmaceutics
Faculty of Pharmacy, Mansoura
University*

2019

General Introduction

Controlled release drug delivery systems (DDS_S) assign to release of drug and/or biological materials in a controlled manner from dosage form to the target site. Aforementioned release behavior has benefits such as maintenance of drug concentration in systemic circulation without any more fluctuation, as well as reduction of therapeutic dose and frequency of administration. Therefore, limited side effects from high systemic or off-target exposure and improved patient compliance will be obtained (**Mansour *et al.*, 2010**).

Recently, nanomedicine can breakthrough therapeutic methods and enhance medical understanding in accordance with traditional medicine. It is the application of nanotechnology to the field of medicine by utilizing materials at the nanometer scale. The most common application of nanomedicine involves employing nanoparticles (NPs) to enhance the action of drugs in prevention and treatment of diseases (**Caster *et al.*, 2017**).

A. Nanoparticles (NP_S)

NP_S are stated precisely as solid particles or particulate dispersions with a size range of 10 to 1000 nm; where the drug is dissolved, encapsulated, entrapped, adsorbed or attached to a nanoparticle matrix.

The crucial goals in designing NP_S as a delivery system are to adjust particle size and surface properties as well as release of therapeutic agents to successfully achieve the site-specific action of the drug at the therapeutically optimum rate and dose regimen. This system also aids to increase the stability of drugs/proteins and achieve convenient controlled release properties (**Desai and Shah, 2013**).

Different methods were reported for preparation of NPs based on their types, matrices materials and characteristics of loaded drugs (**Pal *et al.*, 2011; Desai and Shah, 2013**).

After preparation, NP_s are mostly dispersed in liquid which can be administered to humans either orally, parenterally or topically after incorporation in a base matrix such as hydrogel. Otherwise, NP_s can be lyophilized to a powder which permits pulmonary delivery or further processed into tablets or capsules as well (**Desai and Shah, 2013**).

Advantages and applications of NP_s as drug carriers

NPs possess various merits over conventional DDSs as follows (**Singh et al., 2009; Goyal et al., 2016**):

- i. They are better suited for different routes of administration (oral, parenteral, topical, ocular or nasal).
- ii. They are appropriate for encapsulating both hydrophobic and hydrophilic drugs.
- iii. They protect the therapeutic agents against enzymatic degradation (i.e., nucleases and proteases).
- iv. The use of biodegradable materials for NP_s preparation permits controlled and sustained drug release inside the target site over a period of days or even weeks.
- v. Generally, these systems can be used to allow targeted (cellular or tissue) delivery of drugs, enhance bioavailability, sustain release of drugs or solubilize drugs for systemic delivery.
- vi. It has been confirmed that NP_s as drug carriers can be concentrated discriminatively to tumors, inflammatory sites, and at antigen sampling sites by merit of the enhanced permeability and retention (EPR) effect of the vasculature.

Among different nanocarriers, polymeric nanocarriers, lipid-based nanocarriers, and inorganic nanocarriers are the most extensively used as illustrated in **Figure 1** (**Arora and Jaglan, 2016**).

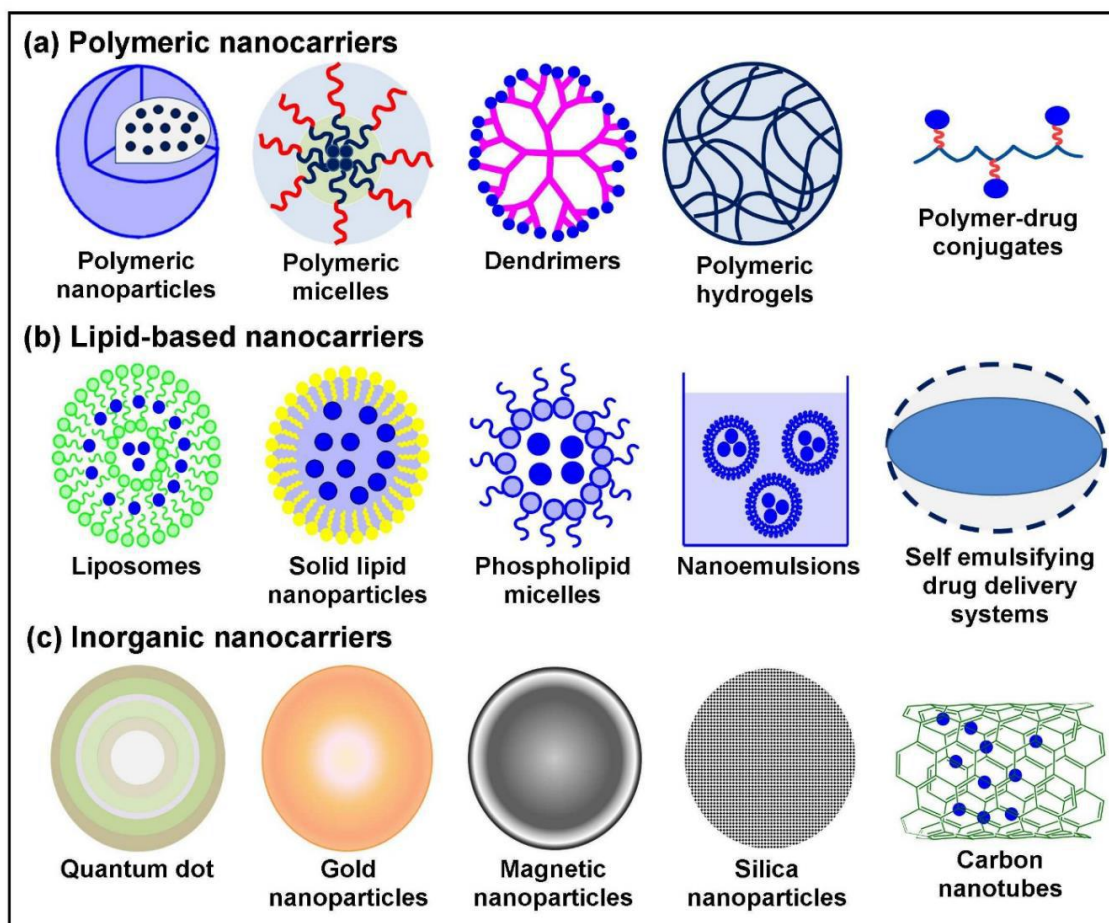


Figure 1: Different types of nanocarriers (Arora and Jaglan, 2016).

Lipid-based nanocarriers

Conspicuous research has been accomplished on lipidic systems which include mainly liposomes, solid lipid nanoparticles (SLN_s), phospholipid micelles, nanoemulsions (NE), and self-emulsifying drug delivery systems. Lipid nanoparticulate DDS_s routes of administration and applications are dependent on their architecture and particle size (Haghiralsadat *et al.*, 2018).

◆ **SLNs**

SLNs are consisted of solid lipid, emulsifier, and water. They have been widely studied as nanocarriers in the pharmaceutical fields, which are used to carry and deliver hydrophilic/hydrophobic drugs, macromolecules such as proteins and peptides, genes or gene expression-modifying compounds, antigens, and food molecules. Drugs can be carried by SLNs using either solid solution model or core-shell model. SLNs have some predominant advantages (**Haghiralsadat et al., 2018**):

- i. Biodegradable lipids are used.
- ii. The use of organic solvents can be avoided to decrease toxicity.
- iii. Large quantities can be easily prepared.
- iv. Bioavailability of drugs is enhanced.
- v. Drug mobility and biodegradability are reduced.
- vi. Controlled drug delivery can be achieved.
- vii. More stable for *in vivo* application than other lipid nanocarriers.

The broadly reported preparation techniques comprise high pressure homogenization, ultrasonication/high speed homogenization, solvent emulsification-diffusion method, solvent evaporation method, spray drying method, supercritical fluid method, microemulsion based method, and double emulsion method. Selection of preparation method depends on route of administration and type of lipid as well as solubility and stability of the drug (**Haghiralsadat et al., 2018**).

◆ **Nanoemulgel (NEG)**

Lately, there has been an increasing trend in the NEG preparation. NEG is an amalgamated formulation of two different systems in which NE containing drug is incorporated into a hydrogel matrix (**Sengupta and Chatterjee, 2017**).

Hydrogels can be prepared from natural or synthetic polymers. Natural polymers, being biocompatible and biodegradable such as collagen, gelatin, fibrin, silk, agarose, hyaluronic acid, chitosan (CS), dextran, guar gum (GG), gum acacia (GA) and alginate, contain functional groups like -OH, -COOH, and -NH₂ which are involved in forming linkages with other polymeric networks to form the hydrogels' architecture (**Rizwan *et al.*, 2017**). Hydrogels based on synthetic polymers such as polyacrylic acid (PAA), polyacrylamide, polyethylene glycol (PEG), polylactic acid (PLA), and polyvinyl alcohol (PVA) offer great flexibility in controlling polymer chemical structure and architecture, which is crucial to prepare hydrogels with tailored network and mechanical strengths (**Rizwan *et al.*, 2017**).

A plenty of advantages were reported for application of NEG enumerated as follows (**Sengupta and Chatterjee, 2017**):

- i. It has a good adhesion property and spreadability on the skin compared to other topical DDS_s as well as enhance superior delivery of lipophilic drugs, hence it is considered as potential and promising candidate for enhancing the topical delivery of lipophilic drugs with improved patient compliance.
- ii. It controls the release of drugs having shorter half-life.
- iii. It is non-toxic and non-irritant.
- iv. Stability of NE is enhanced as a result of oil droplets distribution in gel base.

B. Nanofibers (NF_s)

Since the mid-1990s, electrospinning technology has gained worldwide attention for production of NFs. A principal mechanism of electrospinning is to apply electrostatic repulsions of highly charged polymer jets to prepare nano- or microscale fibers laid down irregularly and solidified on the collector (**Shan *et al.*, 2015**). Therefore, the conventional electrospinning setup often comprises of three main parts (**Figure 2**) (**Xue *et al.*, 2017**; **Jiang *et al.*, 2018**):

- i. A high voltage power supply (usually expressed as kV),

- ii. A syringe pump and a spinneret (metallic needle, nozzle, disc or wire) for controlled flow of polymer fluid, and
- iii. A grounded collector (metal net, aluminum paper, baking paper, plate, rotating disc or drum).

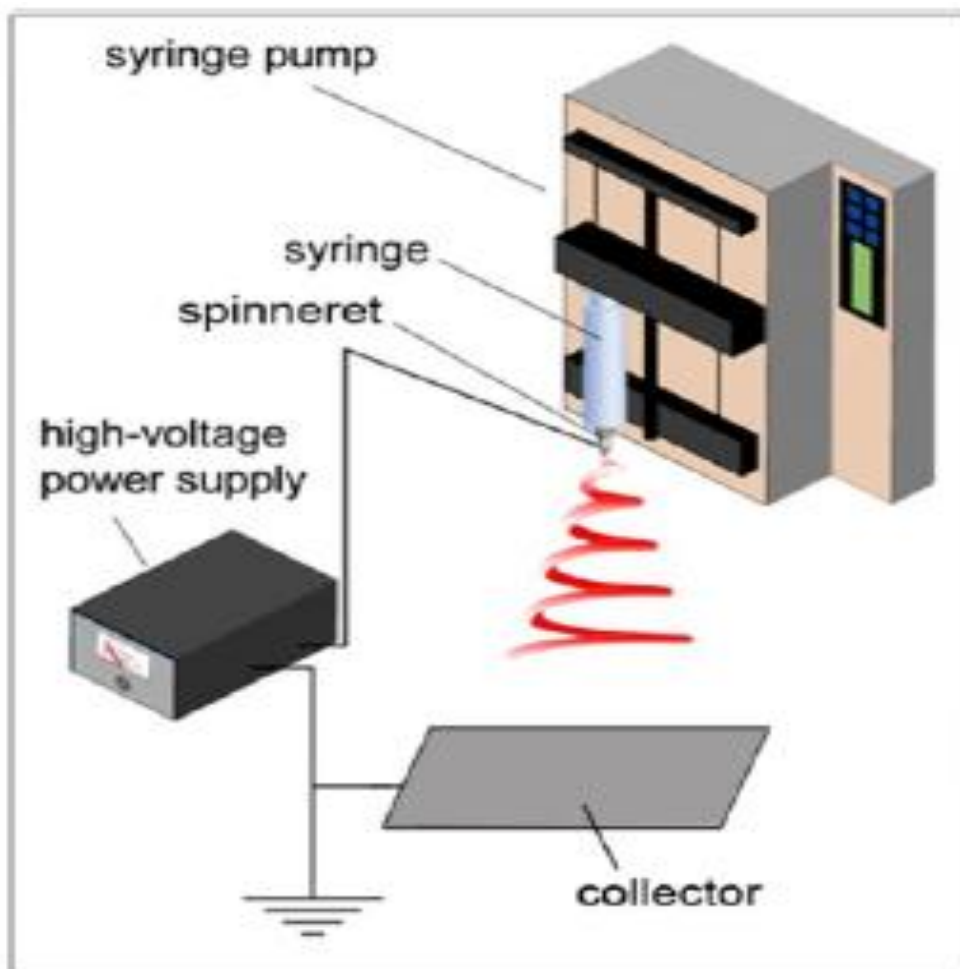


Figure 2: Schematic illustration of a typical setup for electrospinning (Xue *et al.*, 2017).

Such electrospinning setup can be used for production of NFs with different orientation and hierarchical structures. Different orientation of NFs includes random as well as aligned structures as illustrated in **Figure 3** (Shi *et al.*, 2015^a).

Recently, hierarchical nanostructured materials have attracted remarkable attention in numerous fields such as biomedicine. Hierarchical electrospun NFs structures involve core-shell, hollow, and porous structures as shown in **Figure 4** (Shi *et al.*, 2015^a).

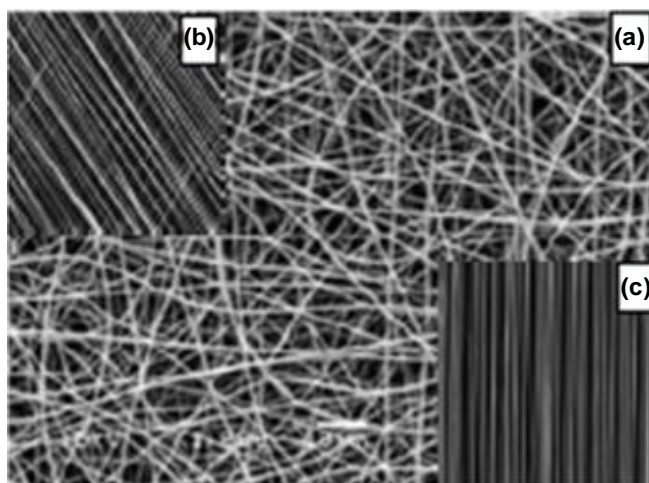


Figure 3: Scanning electron micrographs of electrospun (a) random NFs, (b) aligned fibers at an angle, and (c) aligned fibers (Shi *et al.*, 2015^a).

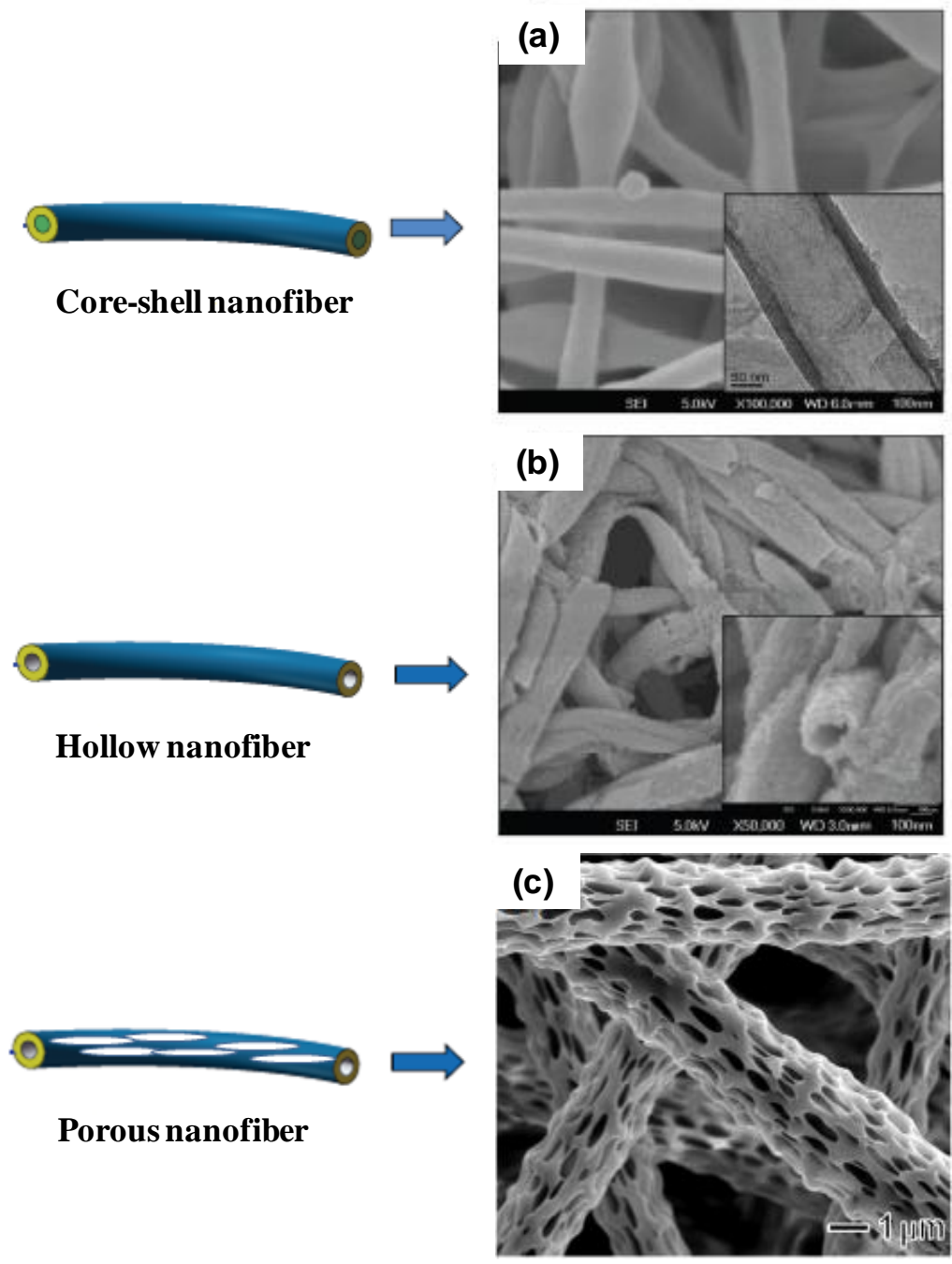


Figure 4: Schematic illustration and scanning electron micrographs of electrospun (a) core-shell NFs, (b) hollow NFs (Shi *et al.*, 2015^a), and (c) porous NFs (Xue *et al.*, 2017).

The final fiber diameter and morphology depend on three major factors (Shi *et al.*, 2015^a):

- i. Polymer solution parameters (concentration, viscosity, surface tension, and electric conductivity).
- ii. Process parameters (applied voltage, feed rate, diameter and shape of spinneret, spinneret tip to collector distance, and collector shape).
- iii. Ambient conditions (ambient temperature and relative humidity (RH)).

Electrospun NF_S mats offer several advantageous features as DDS_S including (Okuda *et al.*, 2010; Han *et al.*, 2012; Nguyen *et al.*, 2012; Shan *et al.*, 2015; Goyal *et al.*, 2016):

- i. NF_S can be fabricated from a wide variety of solutions of both natural polymers e.g., CS, gelatin, fibronectin, collagen, ethyl cellulose, silk and synthetic polymers e.g., PLA, polyglycolides (PGA), poly lactic-co-glycolic acid (PLGA), PVA, polyvinylpyrrolidone (PVP), tyrosine-derived polycarbonates, polycaprolactone, polyurethane, or combinations.
- ii. Bio-mimicking electrospun NF_S with a high surface area to volume ratio as well as satisfactory mechanical performance have received much attention owing to their structural resemblance to the extracellular matrix of biological systems as collagen fibers. Hence, these important characteristics are determinant to their use in various applications for biomedical devices, tissue engineering scaffolds, and drug delivery carriers.
- iii. In the field of drug delivery, an extensive variety of functionalization systems can be generated in terms of entrapping not only low molecular weight (low MW) drugs but also macromolecules such as proteins and nucleic acids into electrospun NF_S. As well, the drug release profile from these NF_S systems might be controlled in a fiber diameter-relative manner or other factors such as the drug to polymer ratio, morphology, and/or porosity.
- iv. NF_S meshes are flexible, making them appropriate for topical drug delivery applications.

- v. Electrospun NF_s mats can provide sustained release, which reduces the frequency of topical application and increases patient compliance.
- vi. NF_s mats can be embodied into wound dressings, as part of a drug-releasing wound treatment technology.

Nature represents an inexhaustible resource for drug development, novel pharmacophores, chemotypes, and other precious bioactive agents. Since immemorial time, bioactive natural products have been the pillar of folk remedies everywhere in the globe and have also been an indispensable part of history and culture (**Veeresham, 2012**). In spite of the wide spread use of synthetic drugs due to their time effectiveness, production cost, uncomplicated quality control, and quick effects, their safety was always remained questionable. Therefore, in recent years, there has been a renewed attentiveness on the prospective application of natural products as alternatives with dual benefits of pharmacological activity and safety profile.

Phytochemicals are naturally occurring compounds found in plants which have versatile pharmacological activities against variety of diseases. Predominant phytochemicals are phenolic compounds, alkaloids, tannins and flavonoids. Until now, it seems that the phenolic patterns of higher plants have been created by a dialog between plants and their environment for the conveniences of plants and their superior adaptation to external conditions (**Kyselova, 2011; Jabeen et al., 2014**).

Phenolic compounds, known as plant pigments, are the most broadly distributed secondary metabolites even if the type of compound present differs dependent on the phylum under consideration. Higher plants synthesize various known phenolic compounds and the number of those entirely characterized is frequently increasing (**Lattanzio, 2013**). Overall decisive data from *in vitro* and *in vivo* laboratory investigations, epidemiological studies, and human clinical trials specify that phenolic compounds are beneficial for human health. A huge number of studies have reported cellular targets of dietary plant phenolic compounds that could be involved in the health promoting actions. Epidemiological conformation showed that diets rich in fruits and

vegetables improve health and impair or delay the onset of many diseases (**Kyselova, 2011**).

The valuable effects of fruits and vegetables have been largely attributed to phenolic compounds. Ingestion of foods rich in these substances, in humans and experimental animals, has been associated with reduction in endothelial dysfunction and hypertension, platelet activation and thrombosis, dyslipidemia and atherosclerosis, as well as inflammatory processes associated with induction and perpetuation of cardiovascular diseases (**Fraga et al., 2010; Kyselova, 2011**). Additionally, the antioxidant activity of phenolic compounds can be explained instantly, in terms of their free radical scavenger activity, or incidentally as modulators of intracellular pro- and anti-oxidant enzymes (**Kyselova, 2011**).

Amongst natural phenolic compounds that need to be incorporated in promising delivery systems, are apocynin (APO) and clove essential oil (CEO).

Apocynin (APO)

Apocynin (APO) is related to vanillin in structure and originally extracted from the roots of either *Apocynum cannabinum* (Canadian hemp) or *Picrorhiza kurroa* native to the western Himalaya (**Stefanska and Pawliczak, 2008**). It is used as a folk medicine in India and Sri Lanka for treatment of liver, heart, joints, and lungs ailments (**'t Hart et al., 2014**).

APO is a specific nicotinamide adenine dinucleotide phosphate-oxidase (NADPH-oxidase) inhibitor that exhibits versatile pharmacological activities (**Hougee et al., 2006**). Likewise, the suppression effect of APO on different inflammatory mediators in experimental animals has been implicated (**Ximenes et al., 2007; Impellizzeri et al., 2011; Hwang et al., 2016**). Thus, it is considered as bioactive phenolic phytochemical with potent antioxidant and anti-inflammatory activities. The bioactivity of APO was manifested in various diseases like atherosclerosis, asthma, cancer, vascular and neurodegenerative diseases, inflammatory bowel disease and collagen-induced arthritis pharmacotherapy (**de Oliveira et al., 2017**).

Clove essential oil (CEO)

Clove essential oil (CEO) is an essential oil extracted from flower buds of *Syzygium aromaticum* L. (Family: Myrtaceae), recommended in the treatment of various diseases. Versatile pharmacological bioactivities including analgesic, antibacterial, antifungal, antiallergic, antiinflammatory, anticarcinogenic and antimutagenic activities have been documented for CEO. Several phytochemicals have been identified in CEO, with the phenolic primary constituent being eugenol (88.85%) that is mainly responsible for most of the aforementioned biological activities of CEO (Anwer *et al.*, 2014).

Recently, phytopharmaceutical preparations based on the use of nanotechnology with the phytochemicals is a rapidly developing approach since it can confer several merits involving (Ansari *et al.*, 2012; Gunasekaran *et al.*, 2014):

- Solubility and bioavailability enhancement.
- Pharmacological activity and stability improvement.
- Improving tissue macrophages distribution.
- Sustained and controlled delivery.
- Protection from physical and chemical degradation.

This context encouraged us to dedicate the current thesis on developing novel nano-sized phytopharmaceutical delivery systems of APO (orally and parenterally) and CEO (topically) to potentiate the bioavailability and pharmacological activity, respectively for prospective therapeutic application.

Scope of Work

Natural products and their application in herbal medicine field are of great importance in treating a wide spectrum of diseases owing to possessing multiple pharmacological and/or biological activities. Additionally, they have become one of the most prominent resources for discovery and developing of new effective drugs for prospective therapeutic application. Lately, the use of nanomedicine and other delivery systems with natural products is a promptly developing approach where it can offer controlled release profile as well as improved targeting and bioavailability of these products.

The thesis encompasses two phytochemicals; apocynin (APO) and clove essential oil (CEO) as solid lipid nanoparticles (SLN_S) (A), nanoemulgel (NEG) and nanofibers (NF_S) (B), respectively.

(A)- SLN_S loaded with bioactive phytochemicals have come into view as a powerful technology for the treatment of various diseases owing to considerable attractive characteristics, such as nanometric particle size, high drug loading capacity for both hydrophilic and lipophilic drugs, large-scale production, controlled delivery of pharmacologically active agents that can enhance drug bioavailability and targeting as well as long-term shelf stability. To the best of our knowledge, only few reviews with limited scopes have been published on natural product-centered nanomedicine.

Therefore, the objective of the first part of this thesis was to investigate the potential use of SLN_S as an oral and parenteral delivery systems for the bioactive phytochemical "APO" in the following manner:

- ❑ Preparation of chitosan-based APO-loaded solid lipid nanoparticles (CS,APO - loaded SLN_S) through double-emulsion solvent evaporation technique (w/o/w).
- ❑ Optimization of the prepared CS,APO - loaded SLN_S by adopting full factorial design 2⁴ with four different critical process parameters (CPPs), namely; the

amount of each of glycerol tristearate (GTS) (X_A) and sucrose monopalmitate (SMP) (X_B) as well as the concentration of both chitosan (CS) (X_C) and polyvinyl alcohol (PVA) (X_D), at two levels.

- ❑ Evaluation of all the prepared formulations in terms of drug entrapment efficiency % (DEE %), percentage yield (yield %), particle size, polydispersity index (PDI), and zeta potential (ZP), expressed as the measured critical quality attributes (CQAs).
- ❑ Characterization of the optimized CS,APO - loaded SLN_S formula using transmission electron microscopy (TEM), Fourier transform-infrared (FT-IR) spectroscopy, X-ray diffraction (XRD), and differential scanning calorimetry (DSC).
- ❑ Evaluation of the *in vitro* release pattern of APO from the optimized CS,APO - loaded SLN_S formula and kinetics analysis of the release data as well as stability study at refrigeration ($5 \pm 3^\circ\text{C}$) and ambient conditions.
- ❑ Biopharmaceutical evaluation to investigate the *in vivo* oral and parenteral bioavailability performance of the optimized formula in male Sprague–Dawley rats.

(B)- The topical route can be considered as an alternative to oral delivery of drugs as well as parenteral injection. It offers the advantages of having a large and varied surface area in addition to the ease of application via self-administration. Lately, there has been an increasing trend in the preparation of NEG and NF_S as controlled release nanoparticulate drug delivery systems for topical application with potentiated therapeutic activity and enhanced stability. Despite of the wealthy literature on the versatile pharmacological effect of CEO, little trials to formulate and evaluate CEO pharmacological activities in different delivery systems were reported.

Such a situation was encouraging to devote the second part of the thesis to investigate the potential use of NEG and NF_s as topical nano delivery systems for CEO with the following main objectives in mind:

- ❑ Preparation of nanoemulsion (NE) formulations of CEO to enhance its anti-inflammatory activity and evaluation of such formulations in terms of thermodynamic stability studies; self-nanoemulsification efficiency tests; drug content estimation; measurement of particle size, PDI, ZP, viscosity (η) as well as percentage transmittance (%T); and pH determination.
- ❑ Characterization of the chosen NE formula using FT-IR spectroscopy and TEM.
- ❑ Preparation of blank hydrogel matrices employing natural polymers, namely; guar gum (GG), gum acacia (GA) and CS, and optimization by adopting Taguchi's model with three independently controlled parameters (ICPs), namely the concentration of the three used polymers, at three levels.
- ❑ Further formulation of the optimized blank hydrogel formula and the selected NE formula into CEO-NE based NEG and evaluation of such NEG formula with regard to pH determination, viscosity (η) measurement, drug content assay, FT-IR and DSC studies.
- ❑ Preparation of CEO-NE based NF_s using the selected CEO-NE formula and PVA polymer, followed by characterization of such NF_s formula in terms of scanning electron microscopy (SEM), drug content assay, FT-IR and DSC studies.
- ❑ Further characterization of CEO-NE based NEG as well as CEO-NE based NF_s mats with respect to *ex vivo* permeation study and kinetics analysis of the permeation data, as well as stability study for a period of six months.
- ❑ Investigation of the *in vivo* anti-inflammatory activity of the developed CEO topical formulations against croton oil-induced mouse skin inflammation model via histopathological examination and immunohistochemical (IHC) detection of cyclooxygenase-2 (COX-2) expression level.

- Assessment of skin safety of the medicated formulae, CEO-NE based NEG and CEO-NE based NF_s, by histopathological examination after topical application.

PART I

Novel chitosan-based solid-lipid nanoparticles to enhance the bio-residence of the miraculous phytochemical “Apocynin”

Introduction

APO is chemically named 4-hydroxy-3-methoxyacetophenone (acetovanillone). It has the empirical formula of $C_9H_{10}O_3$, MW of 166.17, pKa value of 8.17, and hydrophobicity index of ($\log P = 0.83$). APO is an orange to red colored powder with a melting point of 115°C . It is slightly soluble in cold water but freely soluble in hot water, alcohol, benzene, chloroform and ether (Petrônio *et al.*, 2013; <http://en.wikipedia.org/wiki/Apocynin>).

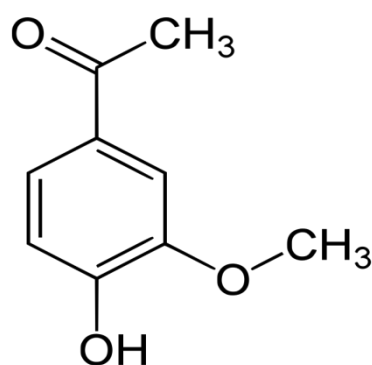


Figure 5: Chemical structure of APO.

Therapeutic uses and applications of APO

APO is a specific NADPH-oxidase inhibitor. Also, it can minimize superoxide anion (O_2^-) production from activated neutrophils and macrophages (Hougee *et al.*, 2006). The anti-inflammatory activity of APO has been revealed in a variety of cell lines and animal models of inflammation clarifying its distinguished suppressive effect on different inflammatory mediators (Ximenes *et al.*, 2007; Impellizzeri *et al.*, 2011; Hwang *et al.*, 2016). Therefore, it is considered as a promising bioactive phytochemical

with potent anti-oxidant and anti-inflammatory activities for treatment of numerous diseases such as atherosclerosis, asthma, cancer, vascular and neurodegenerative diseases, inflammatory bowel disease and collagen-induced arthritis pharmacotherapy (de Oliveira *et al.*, 2017).

Pharmacokinetics of APO

Absorption

APO was found to be rapidly absorbed within 5 min after oral administration following one compartment model kinetics. Also, the mean peak plasma concentration (C_{max}) of 2963.33 ± 747.69 ng/mL was reached within 0.083 h after oral administration (50 mg/kg) and $10,070 \pm 807.28$ ng/mL after intravenous (i.v.) administration (5 mg/kg) in male Sprague-Dawley rats (Chandasana *et al.*, 2015).

Distribution

The volume of distribution (V_d) of APO given to rats intravenously in solution form at a dose of 5 mg/kg and orally in suspension form at a dose of 50 mg/kg was 0.76 ± 0.04 and 3.75 ± 0.55 L/kg, respectively. As well, the plasma protein binding of APO was 71.39–73.34% in human plasma and 83.41–86.07% in rat plasma (Chandasana *et al.*, 2015).

Metabolism

Eighty percentage recovery of un-metabolized APO in the urine was reported when rats were fed 120 mg APO/kg (Francis *et al.*, 2016). Previously, Ximenes *et al.*, 2007 demonstrated that the activity of APO was attributed to its active metabolite (diapocynin) based on *in vitro* peroxidase assay. On the other hand, APO was rapidly metabolized to glycoconjugate not to diapocynin when injected intraperitoneally (i.p.) to adult male Sprague-Dawley rats at a dose of 5 mg/kg as documented by Wang *et al.*, 2008. Following intragastric administration, APO exhibited rapid absorption and excretion; with urinary excretion including APO's unchanged form, the glucuronide, demethylated, and ring-hydroxylated forms along with other derivatives. Additionally, fecal recoveries of the metabolites were tiny (Simonyi *et al.*, 2012).

Elimination

As reported, APO showed rapid elimination after absorption and the clearance was more than glomerular filtration rate indicating extrarenal clearance such as hepatic or biliary one. Clearance rate was almost the same for i.v. and oral route after reaching the systemic circulation (0.77 ± 0.13 and 0.75 ± 0.26 L/h/kg, respectively) but a difference in half life was observed between the aforementioned routes of administration (0.067 ± 0.07 and 3.47 ± 0.35 h, respectively) (**Chandasana *et al.*, 2015**).

Toxicity

Safety data of APO are seldom found, but those accessible show low toxicity and high stability. In mice, the median lethal dose (LD₅₀) after oral dosing has been estimated at 9 g/kg and minimal signs of toxicity after APO i.v. dose of 420 mg/kg were displayed. On the other hand, in rats, approximately 80% of APO injected i.p. at a dose of 120 mg/kg was eliminated unchanged in urine sample collected after 20 h (**'t Hart *et al.*, 2014**).

Adverse effects and precautions of APO

APO may actually increase oxidative stress under some conditions which is considered a serious potential problem. Its activation by myeloperoxidase produces an APO-free radical that is able to oxidize glutathione with subsequent decrease in glutathione expression in alveolar epithelial cells treated with APO (**Riganti *et al.*, 2006**; **Ximenes *et al.*, 2007**). Also, as claimed by **Riganti *et al.*, 2008**, APO is able to increase the hydrogen peroxide (H₂O₂) level in resting monocyte-like cells and can cause, under longer times of exposure, an oxidative damage and a cytotoxic effect.

Therefore, it is revealed that APO is an inducer of reactive oxygen species (ROS) production, regardless the cell type. It is reasonable that when NADPH-oxidase is maximally activated, the inhibition of the respiratory burst is the prevailing effect of APO. However, in absence of NADPH-oxidase stimulation, the oxidative effect of APO itself could be predominant.

Interactions

APO may enhance the anticoagulant activities of abciximab and acenocoumarol. It may decrease the antihypertensive activities of acebutolol, besides decrease in the excretion rate of aclarubicin with subsequent higher serum level. The severity of side effects can be increased when APO is combined with 16-bromoepiandrosterone, 19-norandrostenedione, 5-androstenedione, acetaminophen, aceclofenac and acetylsalicylic acid (**Apocynin**. <https://www.drugbank.ca/drugs/DB12618>).

Despite having wide spectrum of activity, APO's clinical impact is minimal due to its pharmaceutical impediment such as low aqueous solubility, poor oral bioavailability (< 10%), rapid elimination, high protein binding and narrow dose-response relationship (**Chandasana et al., 2015; de Oliveira et al., 2017**). Simultaneous increase in the bioavailability of a drug with sustaining its efficacy is a challenge. To address such challenge, encapsulation in a delivery system like NP_s has protruded as a promising avenue.

Yet, a few attempts to prepare APO NP_s were published. The first one was reported by **Brenza et al., 2017** who incorporated a synthesized mitochondria-targeted apocynin (Mito-APO) into polyanhydride NP_s by a modified anti-solvent nano-encapsulation method. The second attempt involved the preparation of bovine serum albumin (BSA) NP_s containing native APO by desolvation technique, followed by cross-linking with glutaraldehyde (**de Oliveira et al., 2018**). Nevertheless, Mito-APO synthesis process possessed certain drawbacks as expensive raw materials, tedious procedure, special conditions, and purification steps. In case of APO-loaded BSA NPs, the glutaraldehyde used in the preparation would contribute to health concern and could cause unenviable side effects. Additionally, the *in vivo* pharmacokinetic study of both aforementioned prepared NP_s was not established. A very recent attempt was published which demonstrated the *in vivo* efficacy of APO loaded PLGA in hyperoxaluric rats (**Sharma et al., 2018**).

Such survey motivated us to dedicate the present study to augment the oral and i.v. bioavailability of APO via designing a novel and facile strategy for fabricating (CS,APO/oil)/PVA (core/shell) SLN_s through double-emulsion solvent evaporation technique (w/o/w). Optimization of chitosan-based APO-loaded solid lipid nanoparticles (CS,APO - loaded SLN_s) was conducted by adopting full factorial design 2⁴ with four different critical process parameters (CPPs) at two levels. The optimized CS,APO - loaded SLN_s formula would be further characterized and extensively investigated in terms of its *in vitro* release, stability, and ultimately *in vivo* oral and i.v. bioavailability performance in rats.

To fulfill these goals, the work in this part was divided into two main chapters:

Chapter 1:

Formulation, characterization and optimization of novel chitosan-based apocynin-loaded solid lipid nanoparticles.

Chapter 2:

Oral and parenteral bioavailability of the optimized chitosan-based apocynin-loaded solid lipid nanoparticles in rats.

Chapter 1

Formulation, characterization and optimization of novel chitosan-based apocynin-loaded solid lipid nanoparticles

Introduction

Solid lipid nanoparticles (SLN_S) are recently developed as drug delivery carriers possessing the merits of both polymeric NP_S and liposomes (Shazly, 2017). Several methods have been utilized for SLN_S preparation which are convenient for their large scale production and application (Arana *et al.*, 2015). They are made up of nanosized biocompatible and biodegradable lipid base carriers that are stabilized by a surfactant. Several studies have declared that SLN_S have high drug loading capacity for both hydrophilic and lipophilic drugs, large-scale production, and long-term shelf stability. Furthermore, SLN_S are flexible nanocarriers that are used for drug delivery in almost all routes of administration, including peroral, parenteral, ocular, and dermal. Additionally, they have emerged as one of the most encouraging nanocarriers for controlled drug delivery that can enhance drug bioavailability and targeting (Shazly, 2017; Chuang *et al.*, 2018; Kumar *et al.*, 2018).

Surface modification of SLN_S with CS, a natural cationic polysaccharide derived from chitin, is an auspicious strategy to improve the penetration of encapsulated macromolecules such as insulin through mucosal surfaces (Fonte *et al.*, 2012) and to deliver phenethyl isothiocyanate, a tumor-suppressive agent, through the pulmonary route (Dharmala *et al.*, 2008). CS has been used for developing DDS_S owing to its stability, biocompatibility, biodegradability, low toxicity, antimicrobial, mucoadhesive, and absorption enhancing properties (Saikia *et al.*, 2015; Salomon *et al.*, 2017). On the other hand, PVA, a Food and Drug Administration (FDA) approved water-soluble synthetic polymer, is of great interest for various biomedical and pharmaceutical applications because of its excellent emulsifying, film-forming, and adhesive properties (Martinez *et al.*, 2017).

Replacement of liquid oil in the sub-micron sized lipid emulsions with solid lipid in SLN_s represents a turning point in attaining controlled drug release as the mobility of a drug in solid lipid is commonly lower compared to liquid oil, hence conferring conspicuous improvement in the performance of pharmaceuticals, nutraceuticals and other comparable materials. Acquired results confirmed that the SLN_s formulations prepared with triglycerides were more stable than those with mono- and diglycerides (**Pardeshi et al., 2012**). Therefore, to obtain a biocompatible formulation reasonable for human administration, glycerol tristearate (GTS) has been chosen as a biomaterial due to its high physico-chemical stability, high biocompatibility, and controlled drug release.

Sucrose fatty acid esters (sucrose esters, SE_s) are nonionic surfactants which include sucrose and one or more fatty acids as hydrophilic head and lipophilic tail groups, respectively (**Das et al., 2014**). An increased attentiveness in the employment of SE_s has been experienced within pharmaceutical and food industries based on their manufacture from natural sources (vegetable oil and sucrose), superior taste and aroma profile, high biodegradability, biocompatibility, and low toxicity compared to petrochemical-based surfactants (**Rao and McClements, 2011**). The use of sucrose monopalmitate (SMP), a hydrophilic nonionic surfactant, in the preparation of lemon oil as micro and nano sized emulsions was investigated (**Rao and McClements, 2011**). Moreover, sucrose stearate and sucrose palmitate were assessed separately or in combinations as co-emulsifying agents in aceclofenac lecithin-based nanoemulsions preparation (**Isailović et al., 2016**).

Double emulsion method is commonly used for hydrophilic drugs. The drug is dissolved in an aqueous solvent and added to the melted lipid. An emulsifier is incorporated either in the aqueous phase or in the oil phase to form the primary emulsion. Subsequently, the formed emulsion is dispersed in an aqueous phase containing hydrophilic stabilizer such as PVA to prepare the required double emulsion. The SLNs can be separated by evaporation, filtration or centrifugation (**Mishra et al., 2018**).

Consequently, the aim of the work in this chapter was to prepare CS,APO - loaded SLN_S through double-emulsion solvent evaporation technique (w/o/w). Optimization of CS,APO - loaded SLN_S was conducted by adopting full factorial design 2⁴ with four different CPPs at two levels. The CPPs were the amount of each of GTS (X_A) and SMP (X_B) as well as the concentration of both CS (X_C) and PVA (X_D). The measured critical quality attributes (CQAs) were drug entrapment efficiency % (DEE %), percentage yield (yield %), particle size, polydispersity index (PDI), and zeta potential (ZP) of CS,APO - loaded SLN_S. The optimized CS,APO - loaded SLN_S formula was further characterized by transmission electron microscopy (TEM), Fourier-transform infrared spectroscopy (FT-IR), differential scanning calorimetry (DSC), and x-ray diffractometry (XRD). Ultimately, its *in vitro* release profile, kinetic analysis, and stability at two different conditions for a period of six months were evaluated.

Experimental

Materials

- ❖ Apocynin (APO) was purchased from Sigma-Aldrich, Saint Louis, MO, USA.
- ❖ Chitosan (CS) with 90-95 % degree of deacetylation and low MW (1,526.454 g/mol) was obtained from Oxford Chemical Co., Mumbai, India.
- ❖ Glycerol tristearate (GTS) was acquired from BDH Laboratory Supplies Poole, England.
- ❖ Sucrose monopalmitate (SMP) was a gift from Gattefossé, St Priest, France.
- ❖ Polyvinyl alcohol (PVA) was purchased from Hayashi Pure Chemical industries Ltd., Japan.
- ❖ Analytical grade of glacial acetic acid (99%), absolute ethyl alcohol, potassium phosphate monobasic (KH₂PO₄), disodium hydrogen phosphate (Na₂HPO₄) and sodium chloride (NaCl) were procured from El-Nasr Pharmaceutical Chemical Co., Cairo, Egypt.
- ❖ Millipore filter, 0.45 µm, Berlin, Germany.

Equipment

- ❖ Electric balance (BEL, Model M214Ai, Ser. No. ITA1702341, Italy).
- ❖ Ultrasonic homogenizer (4710 Series, Cole-Parmer Instrument Co., Chicago, USA).
- ❖ Magnetic stirrers (Thermolyne Corporation, Dubuque Iowa, USA).
- ❖ UV–VIS spectrophotometer (double beam, Labomed Inc., USA).
- ❖ Benchtop Centrifuge (Sigma Laborzentrifugen, D-37520, Germany).
- ❖ Freeze dryer (SIM FD8-8T, SIM international, USA).
- ❖ Malvern Zetasizer Nanoseries (Malvern Instruments Limited, UK).
- ❖ Transmission electron microscopy (TEM, JEOL JEM-2100, JEOL Ltd, Tokyo, Japan).
- ❖ Fourier-transform infrared spectrophotometer (FT-IR, Madison Instruments, Middleton, Wisconsin, USA).

- ❖ Differential Scanning Calorimeter (DSC 6000, Perkin-Elmer, Waltham, MA, USA).
- ❖ X-ray diffractometer equipped with Co-K α (Diano Corp., USA).
- ❖ Ultrasonic bath (Sonix USA, SS101H230).
- ❖ Shaking incubator (GFL Gesellschaft für Labortechnik, Burgwedel, Germany).
- ❖ Spectrapor[®] membrane (MW cut off of 12,000-14,000 Da, Spectrum Medical Industries Inc., Los Angeles 90054, USA).
- ❖ Calibrated potentiometer (Consort NV P-901 pH-meter (Belgium, Europe)).

Methodology

1- Spectrophotometric scanning of λ_{\max} of APO

Spectrophotometric scanning of APO's stock solution (200 $\mu\text{g/mL}$) in deionized water was carried out to determine the λ_{\max} of APO in this medium (**Petrônio *et al.*, 2013**). A stock solution, having a concentration of 200 $\mu\text{g/mL}$, was prepared by dissolving 10 mg of APO in 50 mL deionized water. Slight stirring was performed for about 30 min to expedite and ensure complete dissolution. Then, 1.25 mL of the aqueous solution was diluted to 25 mL with deionized water to produce a clear solution with a concentration of 10 $\mu\text{g/mL}$. UV–VIS scanning at different wavelengths ranging from 250–400 nm was performed to determine λ_{\max} of APO using water as blank.

APO was dissolved similarly, to obtain a stock solution with the same concentration (200 $\mu\text{g/mL}$), at three different dissolution media with pH values simulating gastric pH (HCl, pH 1.2), intestinal pH (phosphate buffer, pH 6.8), and physiological pH of the blood (phosphate buffer, pH 7.4). The same previously described procedure was followed to determine λ_{\max} of APO at these different media.

2- Construction of calibration curve of APO

Calibration curves of APO in deionized water and three different dissolution media were constructed spectrophotometrically by measuring the absorbance at the predetermined λ_{\max} values. Different volumes of the four prepared stock solutions (0.25–2.75 mL) were transferred to 25 mL volumetric flasks and each was diluted to 25 mL, with deionized water or one of the three aforementioned dissolution media, to produce concentrations of 2–22 $\mu\text{g/mL}$. Then, the absorbance of these dilutions was measured at the predetermined λ_{\max} by using each one's corresponding blank. The mean absorbance values of triplicate measurements were plotted against the concentration of the drug, expressed as $\mu\text{g/mL}$, and the coefficients of determination (R^2) were calculated.

3- Design of experiment and statistical analysis

The design of experiment (DOE) technique, being used widely in various processes, was challenged to provide an efficient mean to optimize the w/o/w double

emulsion-solvent evaporation method. It involves a large number of runs and offers very precise and accurate analysis on the interaction between factors and its polynomial effects. An experimental design (2^4 full factorial design) was followed to systematically investigate the main effects and interactions of CPPs namely; GTS amount (X_A), SMP amount (X_B), CS concentration (X_C) and PVA concentration (X_D) on the CQAs in terms of DEE %, yield %, particle size and ZP of CS,APO - loaded SLNs. The four CPPs were tested at two levels represented by the coded values as -1 (low levels) and +1 (high levels) as mentioned in **Table 1**. These limits were selected on the basis of preliminary risk-assessment studies and the optimization procedure was carried out within these domains. Sixteen formulations, each with three runs to prepare CS,APO - loaded SLNs, are presented in **Table 2**.

The complete polynomial regression equation was generated as follows:

$$Y = \beta_0 + \beta_1 X_A + \beta_2 X_B + \beta_3 X_C + \beta_4 X_D + \beta_5 X_{AB} + \beta_6 X_{AC} + \beta_7 X_{AD} + \beta_8 X_{BC} + \beta_9 X_{BD} + \beta_{10} X_{CD} + \beta_{11} X_{ABC} + \beta_{12} X_{ABD} + \beta_{13} X_{ACD} + \beta_{14} X_{BCD} + \beta_{15} X_{ABCD}$$

Where

Y	CQAs
β_0	is the arithmetic mean response of the sixteen runs
$\beta_1, \beta_2, \beta_3,$ and β_4	linear coefficients
$\beta_5, \beta_6, \beta_7, \beta_8, \beta_9$ and β_{10}	interaction coefficients between the two CPPs
$\beta_{11}, \beta_{12}, \beta_{13},$ and β_{14}	interaction coefficients between the three CPPs
β_{15}	interaction coefficients between the four CPPs
X_A, X_B, X_C and X_D	CPPs

Table 1: CPPs and levels of a 2⁴ full factorial design.

CPPs	Minimum level	Maximum level	Minimum coded level	Maximum coded level
X_A: GTS amount (mg)	75.0	100.0	-1	+1
X_B: SMP amount (mg)	28.4	56.8	-1	+1
X_C: CS concentration (% w/v)	1.0	1.5	-1	+1
X_D: PVA concentration (% w/v)	1.0	3.0	-1	+1

4- Preparation of CS,APO - loaded SLN_s

The w/o/w double emulsion-solvent evaporation technique was applied in the preparation of CS,APO - loaded SLN_s (Rao, 2007) with little modifications. Briefly, an accurately weighed quantity of GTS (75 or 100 mg) and SMP (28.4 or 56.8 mg) were dissolved in 2 mL absolute ethyl alcohol and the organic phase was heated above GTS's melting point [oil phase]. In our laboratory, the solubility study of APO in deionized water at 37°C was carried out and it was found to be 2 mg/mL (Anter *et al.*, 2018). For preparation of the internal aqueous phase (w₁), APO was dissolved in deionized water at 40°C. After cooling, powdered CS (1 or 1.5% (w/v)) and acetic acid (1% (v/v)) were added followed by magnetic stirring for 2 h. In this solution, APO content was assayed spectrophotometrically using a blank of CS and acetic acid in deionized water. It was estimated to be 5.351 ± 0.0704 mg/mL. One milliliter of such solution was taken as an internal aqueous phase (w₁) and heated to the same temperature of the organic phase. Both phases were combined at the respective temperature and prehomogenized using an ultrasonic homogenizer for 2 min in an ice bath at the following conditions: (% Duty Cycle: 90, Output Control: 10, and Pulser: On) to form the primary emulsion (w₁/o). Then, the resultant dispersion was poured in the external aqueous phase (w₂), 25 mL (1 or 3% (w/v)) PVA aqueous solution containing 0.1 M NaCl (Mobarak *et al.*, 2014), and ultrasonic homogenization step was repeated for 10 min in an ice bath to form a double emulsion (w₁/o/w₂). The organic solvent was completely evaporated from the resulting double emulsion via magnetic stirring at room temperature for 2 h.

The CS,APO - loaded SLN_S were isolated from the non-encapsulated APO by centrifugation at 11,500 rpm (11,532 g) for 90 min, followed by washing with deionized water and freeze drying under vacuum at -80°C. Ultimately, the lyophilized CS,APO - loaded SLN_S were stored at 4°C for further evaluation. The non-encapsulated APO would be saved for DEE % determination. Plain SLN_S (P SLN_S) corresponding to each formula was prepared using 1 mL of CS solution (1 or 1.5%) in aqueous acetic acid (1% (v/v)) without APO as an internal aqueous phase (w₁).

5- Characterization of CS,APO - loaded SLN_S

All the SLN_S of the 16 formulae were subjected to estimation of CQAs such as DEE %, yield %, particle size analysis, PDI and ZP.

5.1. Determination of drug entrapment efficiency %

Efficiency of drug entrapment as percentage (DEE %) was estimated as previously reported (Vyas *et al.*, 2010). The determination of the DEE % was calculated for each formula indirectly by measuring the amount of the untrapped drug (free APO) in the clear supernatant after centrifugation spectrophotometrically using a UV-Vis double beam scanning spectrophotometer at 273 nm using the corresponding P SLN_S supernatant as blank. The DEE % was calculated according to the following equation:

$$\text{DEE \%} = \frac{(\text{Total amount of drug} - \text{Free (untrapped) drug})}{\text{Total amount of drug}} \times 100$$

5.2. Determination of percentage yield

Percentage yield (yield %) was calculated for each formula according to the following equation (Bhatt *et al.*, 2016):

$$\text{Yield (\%)} = \frac{W_m}{W_t} \times 100$$

Where, W_m represents the weight of the lyophilized SLN_S and W_t expresses the sum of the weights of the whole solid components used in the SLN_S preparation.

5.3. Particle size analysis

The hydrodynamic size and PDI of all the freshly prepared batches were determined by dynamic light scattering employing Malvern Zetasizer Nanoseries after suitable dilution with deionized water.

5.4. Zeta potential

ZP is a decisive factor to appraise the colloidal dispersion stability (**Komatsu *et al.*, 1995**). Surface charge on the CS,APO - loaded SLN_s was determined using Malvern Zetasizer Nanoseries after convenient dilution with deionized water.

6- Evaluation of the optimized formula (F-3) of CS,APO - loaded SLN_s

6.1. Transmission electron microscopy (TEM)

The morphological examination of suspended SLN_s of F-3 was performed using TEM. One milliliter of the prepared SLN_s was diluted tenfold with deionized water and sonicated for 5 min using an ultrasonic bath. One drop of the diluted sample was dropped onto carbon coated copper grid and the excess liquid was drawn-off with a Whatman filter paper. After complete drying of the sample at room temperature, the image capture and analysis were performed using Digital Micrograph and Soft Imaging Viewer software.

6.2. Fourier-transform infrared spectroscopy (FT-IR)

Spectroscopic studies of APO, GTS, SMP, their physical mixture corresponding to the optimized formula, freeze dried F-3 and its P SLN_s were done by using FT-IR spectrophotometer. Potassium bromide (KBr) discs were prepared by means of hydrostatic press. The scanning range was 500 to 4000 cm⁻¹.

6.3. Differential scanning calorimetry (DSC)

The thermal stresses of medicinal compounds, excipients, and their interactions throughout the formulation process were detected by thermodynamic techniques. DSC was implemented for F-3 using Differential Scanning Calorimeter. It was calibrated with indium (99.99% purity, melting point 156.6°C). Four milligrams samples of each of APO, GTS, SMP, physical mixture corresponding to the optimized formula as well as freeze dried F-3 and its P SLN_s were crimped in standard aluminum pans and heated

from 35 to 350°C at a heating rate of 10°C /min under constant purging of dry nitrogen at 20 mL/min.

6.4. X-ray diffractometry (XRD)

XRD analysis is a unique technique in the investigation of any changes in the crystallinity of the compounds before and after formulation. X-ray diffractograms of APO, GTS, SMP, physical mixture corresponding to the optimized formula as well as freeze dried SLN_S of optimized F-3 and its P SLN_S were obtained using X-ray diffractometer equipped with Co-K α radiation (45 kV, 9 mA, scanned from 3° to 50° at 2 θ angle).

7- *In vitro* release of APO from CS,APO - loaded SLN_S (F-3)

The modified vertical Franz diffusion cell was utilized to study the APO release from the freshly prepared medicated SLN_S (F-3) as well as its diffusion from aqueous solution (as a control) as previously reported (**Reddy *et al.*, 2006; Manjunath *et al.*, 2011**). The *in vitro* release tests were conducted in three different dissolution media with pH values simulating gastric pH (HCl, pH 1.2), intestinal pH (phosphate buffer, pH 6.8), and physiological pH of the blood (phosphate buffer, pH 7.4) for 24 h.

Franz diffusion cells having a diameter of 3 cm were placed in a shaking incubator maintained at 37 \pm 0.5°C during the entire experiment. A semipermeable cellulose membrane, that was equilibrated with the release medium for 12 h before mounting in the diffusion cell, was firmly attached between the donor and receptor compartments.

CS,APO - loaded SLN_S, containing the equivalent of 2.452 \pm 0.029 mg APO, were suspended in distilled water and introduced to the donor compartment. The receptor compartment was filled with 50 mL of the dialysis medium and shaken at 100 rpm. At predetermined intervals, 0.5, 1, 2, 3, 4, 6, 8, 10, 18, 20 and 24 h, aliquots of the release medium (3 mL) were withdrawn from receptor compartment and replenished with an equal volume of fresh medium in order to maintain the sink condition throughout the experiment. The collected aliquots were filtered, through Millipore filter (0.45 μ m), and further analyzed for drug concentration using a UV-VIS

spectrophotometer at each specified λ_{\max} value for the different release media. Each experiment was done in triplicate and the cumulative APO released (%) was calculated at each time interval. Concurrently, aqueous solution containing the same amount of APO was also tested for the process of diffusion similarly in triplicate.

8- Kinetic analysis of the drug release data

The release data were fitted to different kinetic models encompassing zero-order, first-order, Higuchi's square root of time (**Higuchi, 1963**) and Korsmeyer-Peppas equation (**Korsmeyer et al., 1983**). The (R^2) were estimated from linear regression plots of m vs. t , $\log(m_0 - m)$ vs. t and m vs. $t^{1/2}$, corresponding to zero-order, first-order, and Higuchi's model, respectively. In such plots, m represents the cumulative percent of drug released at time t , and $m_0 - m$ is the percentage of the drug remained after time t . For Korsmeyer-Peppas, the equation was:

$$M_t/M_\infty = kt^n$$

Where, M_t/M_∞ is the fraction of the drug released after time t , n is a characteristic exponent for the release mechanism and k is a release constant which is related to the formulation. On the basis of Korsmeyer-Peppas equation, the n exponent values less than or equal to 0.5 are indication of Fickian or quasi-Fickian diffusion; while those between 0.5 and 1 are characteristic of an anomalous mechanism. On the other hand, a zero-order release is considered in case of unity value for n . The selection of the best mathematical model is based on the kinetic release profile expressing the highest (R^2).

9- Physical stability of CS,APO - loaded SLN_S (F-3)

The physical stability of the optimized CS,APO - loaded SLN_S (F-3) was evaluated under different storage conditions as stated in the International Conference for Harmonization (ICH) guidelines (**Gupta et al., 2017**). CS,APO - loaded SLN_S aqueous dispersions (F-3) were freshly prepared, packed in glass bottles and maintained at refrigeration ($5 \pm 3^\circ\text{C}$) and ambient conditions without any agitation or stirring for 6 months. The stability of the selected formula was assessed in terms of physical appearance, particle size, PDI, ZP and percentage drug retention (drug retention %) at

zero time (at production day as previously described), and after 1, 2, 3, 4, 5 and 6 months of storage.

10- Statistical analysis

The *in vitro* data were presented as mean \pm standard deviation (SD) and statistically analyzed using analysis of variance (ANOVA) followed by Tukey–Kramer multiple comparisons test. GraphPad Prism 5 software (GraphPad Software Inc., San Diego, CA, version 5.03) computer program was employed for the analysis process.

The experimental design (2^4 full factorial design) was evaluated in terms of statistical significance using ANOVA by Design Expert[®] v.10. (Stat-Ease, Inc., Minneapolis, Min-nesota, USA). Statistically significant F-value ($p < 0.05$) and adjusted coefficients of determination (adjusted R^2) between 0.8-1.0 were the criteria for validation of the model chosen, according to those previously suggested (**Asasutjarit *et al.*, 2007**). The effect of CPPs on the CQAs was also presented as response surface plots and contour plots generated by fixing the X_C and X_D factors at their high and low levels and varying X_A and X_B over the range used in the study.

Results and Discussion

1- Spectrophotometric scanning of APO

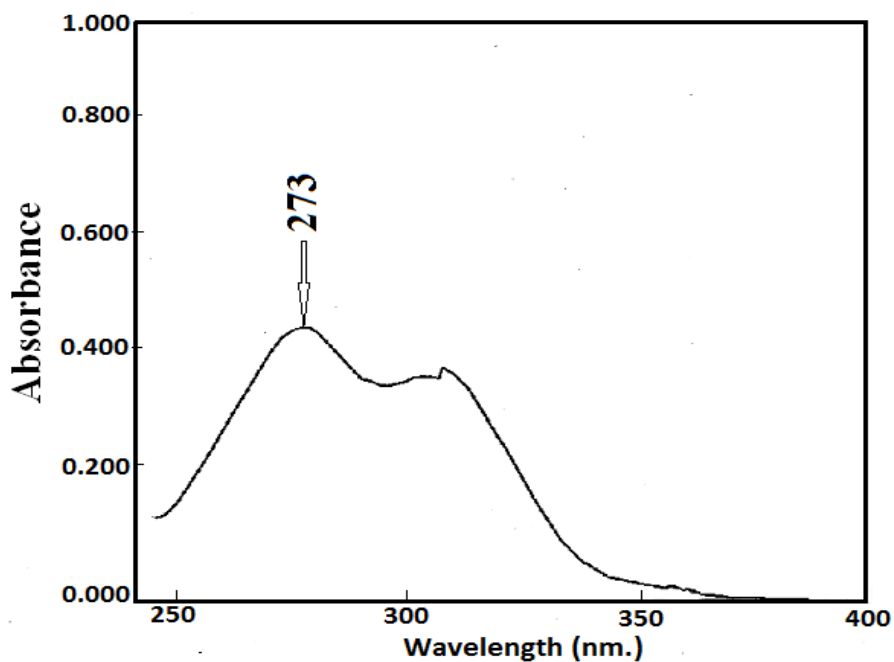
Figure 6 represents UV scanning from 250-400 nm of APO solution in deionized water and phosphate buffer at pH 7.4. It was clearly evident from this figure that the spectra of APO at these media were found to have λ_{\max} at 273 and 276 nm, respectively, as reported before (**Petrônio *et al.*, 2013**).

Figure 7 illustrates APO's UV scanning in HCl (pH 1.2) and phosphate buffer pH 6.8. The spectra of APO were found to have λ_{\max} at 274 and 277 nm at the previously mentioned media, respectively.

2- Construction of calibration curve of APO

Figures 8 and 9 illustrate the graphical plots of concentration of different APO solutions at the four used media against the absorbance at the aforementioned λ_{\max} values. It was observed that the concentration of APO obeyed Beers-Lambert law at concentration range of 2-18 and 2-22 $\mu\text{g/mL}$ with higher (R^2) (0.9996 and 0.9997) for deionized water (**Figure 8A**) and phosphate buffer, pH 7.4, respectively (**Figure 8B**). As well, a concentration range of 2-16 and 2-14 $\mu\text{g/mL}$ with high (R^2) of 0.9992 was observed for APO in HCl (pH 1.2) (**Figure 9A**) and phosphate buffer, pH 6.8 (**Figure 9B**), respectively.

(A)



(B)

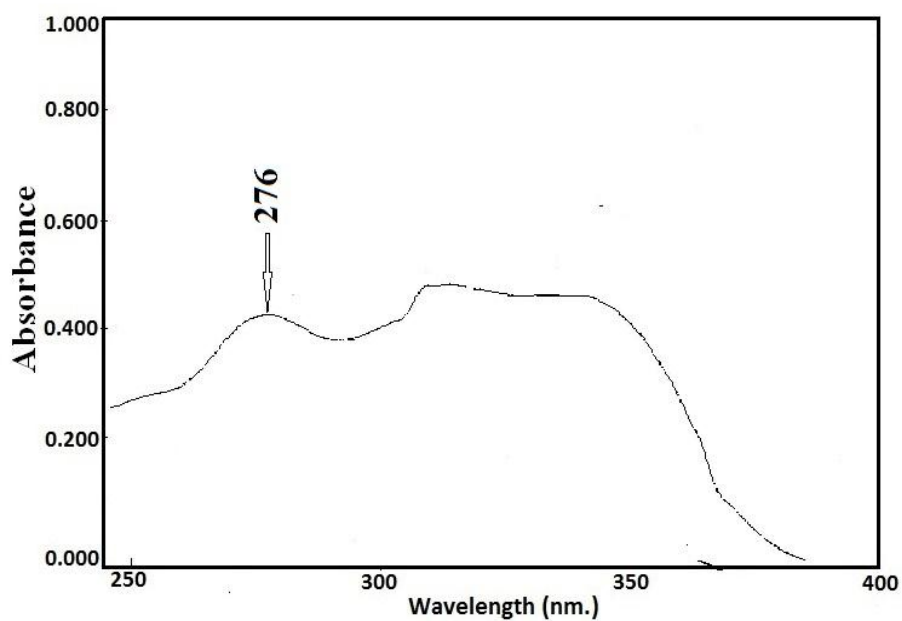
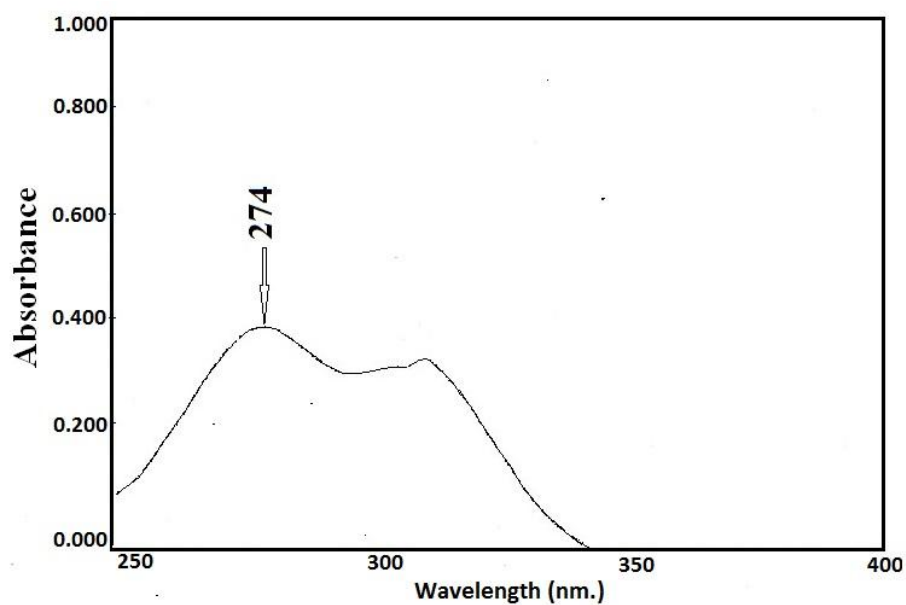


Figure 6: Spectrophotometric scanning of APO in (A) deionized water and (B) phosphate buffer, pH 7.4.

(A)



(B)

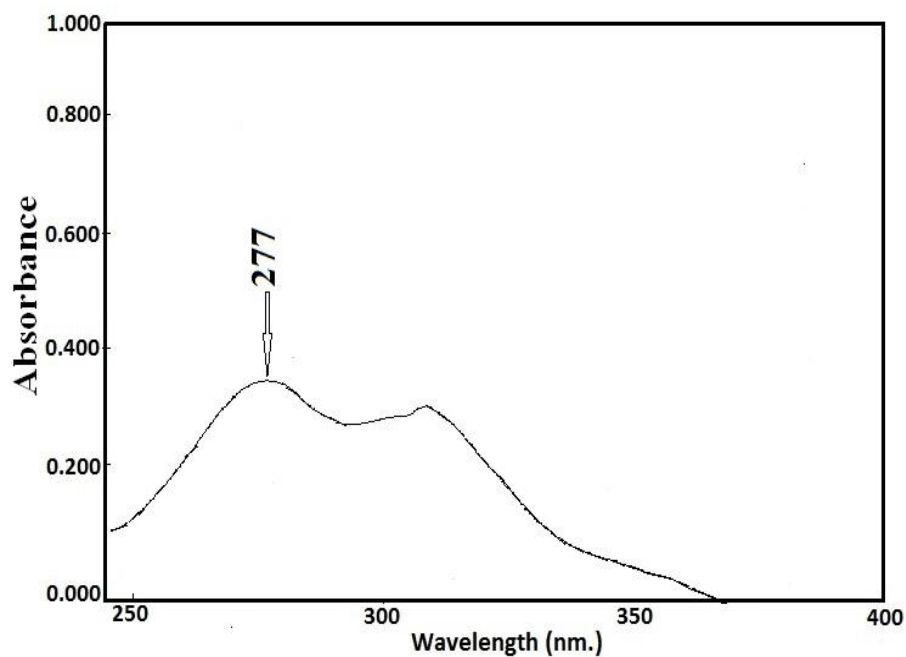


Figure 7: Spectrophotometric scanning of APO in (A) HCl (pH 1.2) and (B) phosphate buffer, pH 6.8.

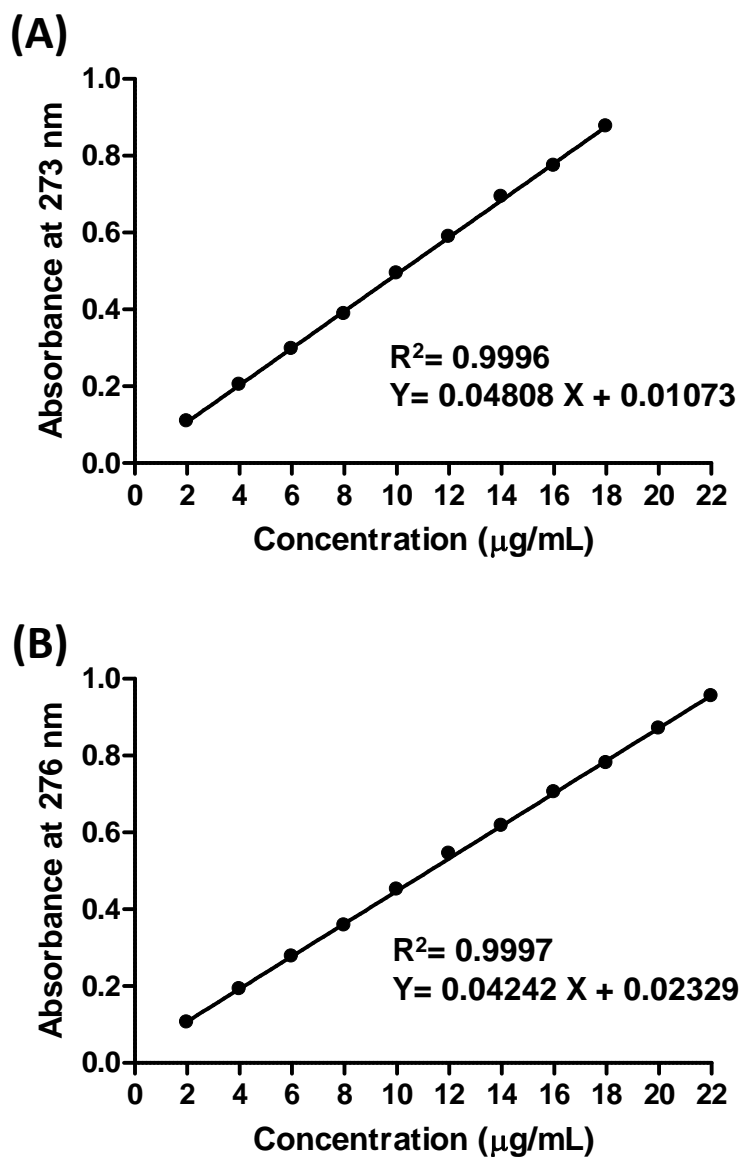


Figure 8: Calibration curves of APO in (A) deionized water and (B) phosphate buffer, pH 7.4. Each point represents the mean \pm SD (n=3).

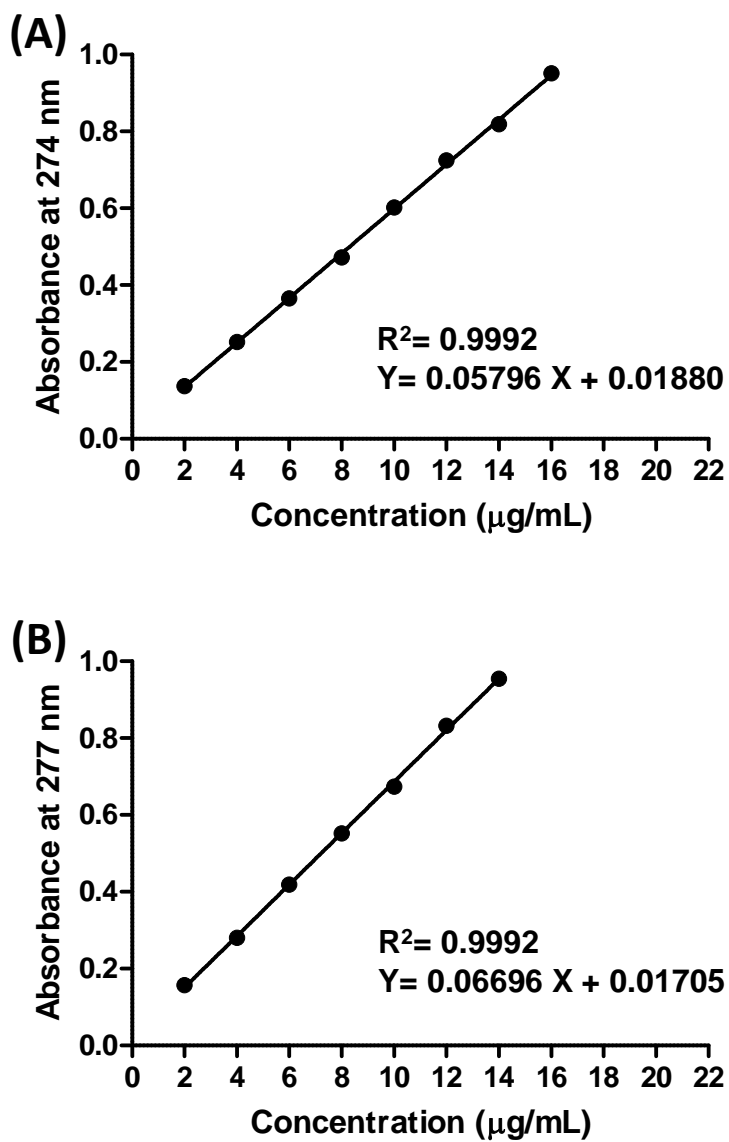


Figure 9: Calibration curves of APO in (A) HCl (pH 1.2) and (B) phosphate buffer, pH 6.8.

Each point represents the mean \pm SD (n=3).

3- Characterization of CS,APO - loaded SLN_s

Double emulsion (w/o/w) method is one of the recent distinguished techniques to prepare SLN_s loaded with hydrophilic drugs owing to its relative simplicity, efficiency, and better DEE % over single emulsion technique (**Liu *et al.*, 2011**). The applicability of SLNs for almost all routes of administration; peroral, topical, and systemic have been reported (**Gupta *et al.*, 2017**).

For enhancing the drug absorption and subsequently its bioavailability, vital CQAs encompassing minimum particle size, minimum PDI, maximum DEE %, maximum yield %, and reasonable ZP should be kept into consideration. Full factorial design is widely used in various processes. It involves moderate number of runs with very precise and accurate analysis and unveiled the CPPs interactions (**Mohtar *et al.*, 2015**).

3.1. Drug entrapment efficiency % (DEE %) and percentage yield (yield %)

These two CQAs were selected as an indication of the efficiency and reproducibility of the processing technique (**Table 2**). The DEE % and yield % of CS,APO - loaded SLN_s ranged from 13.04 ± 3.73 to 45.30 ± 2.52 % and 59.02 ± 1.27 to 86.51 ± 2.94 %, respectively. The obtained polynomial equations representing the regression models for these CQAs are as follows:

$$\text{DEE \%} = + 25.22 + 1.89\mathbf{X}_A - 0.42\mathbf{X}_B + 2.35\mathbf{X}_C + 4.31\mathbf{X}_D - 0.33\mathbf{X}_{AB} - 2.50\mathbf{X}_{AC} + 3.32\mathbf{X}_{AD} - 0.55\mathbf{X}_{BC} - 0.078\mathbf{X}_{BD} + 2.28\mathbf{X}_{CD} - 0.92\mathbf{X}_{ABC} - 0.42\mathbf{X}_{ABD} + 2.55\mathbf{X}_{ACD} - 1.11\mathbf{X}_{BCD} - 2.07\mathbf{X}_{ABCD}$$

Where $F= 40.70$, $p < 0.0001$, and adjusted $R^2=0.9268$

$$\text{Yield \%} = + 70.43 + 0.46\mathbf{X}_A - 2.78\mathbf{X}_B + 0.005625\mathbf{X}_C + 3.00\mathbf{X}_D + 1.04\mathbf{X}_{AB} - 1.15\mathbf{X}_{AC} - 0.29\mathbf{X}_{AD} - 1.47\mathbf{X}_{BC} - 2.81\mathbf{X}_{BD} + 4.72\mathbf{X}_{CD} - 2.04\mathbf{X}_{ABC} + 0.075\mathbf{X}_{ABD} + 0.76\mathbf{X}_{ACD} + 0.63\mathbf{X}_{BCD} - 1.23\mathbf{X}_{ABCD}$$

Where $F= 42.89$, $p < 0.0001$, and adjusted $R^2=0.9304$

The above equations represent the quantitative effects of CPPs which are: GTS (X_A), SMP (X_B), CS (X_C) and PVA (X_D), and their interactions on the two mentioned CQAs. Careful examination of these two equations reveals that all the CPPs have

positive effect on CQAs such as DEE % and yield % except SMP (X_B). Interestingly, the highest coefficient was that of PVA (X_D). Presumably; SMP (X_B) in the oil phase, being surface active agent, facilitates the "escape" of some of the drug from the "core" to the external aqueous medium " w_2 ". Both CS (X_C) with its viscosity inside the "core" and PVA (X_D) the "core-shell" synergistically antagonize this "escape" with a positive coefficient value of X_{CD} .

Table 2 shows that an increase in PVA (X_D) from 1 to 3 % w/v and keeping X_A , X_B and X_C constant (F-2 and 3, F-7 and 8, besides F-15 and 16) increased DEE % and yield %, while an increase in SMP (X_B) from 28.4 to 56.8 mg and keeping X_A , X_C and X_D constant (F-3 and 8, as well as F-11 and 14) decreased DEE % and yield % values.

However, in order to make the interpretation of CPPs influence on CQAs much easier than looking at all the coefficients, the model equations for DEE % and yield % were used to generate various graphical plots. **Figures 10 (A–D)** and **11 (A–D)** show the contour and response surface plots, respectively, of changes in the aforementioned CQAs against two CPPs, X_A (GTS) and X_B (SMP) at a time, keeping the other CPPs, X_C and X_D (CS and PVA), fixed at their high and low levels. The contour plots reveal that the two CQAs were highest at high level of GTS (X_A) and low level of SMP (X_B) when CS (X_C) and PVA (X_D) were at their high levels. This means that high levels of GTS (X_A), CS (X_C), PVA (X_D) and low level of SMP (X_B) in the range used are required to produce SLN_S with high DEE % and yield % (F-3). The probable explanation is that high concentration of GTS (X_A) conferred more space to accommodate the drug with an excess amount throughout SLN_S preparation. In addition, lower concentration of SMP minimizes the amount of drug escaping into the external aqueous phase (w_2), and hence resulting in an increase in DEE %. These results were in line with reported study (**Hosny, 2016**).

Table 2: Formulations and properties of CS,APO - loaded SLN_s prepared according to 2⁴ full factorial design.

Formula Code	Code of (A, B, C, D) ^a	Particle size (nm)	PDI	ZP (mV)	DEE (%)	Yield (%)
F-1	(+, -, -, -)	447.93 ± 13.88	0.333 ± 0.01	+ 30.93 ± 0.40	26.42 ± 3.58	70.90 ± 2.70
F-2	(+, -, +, -)	499.00 ± 7.01	0.364 ± 0.02	+ 32.20 ± 1.24	13.04 ± 3.73	63.47 ± 1.85
F-3	(+, -, +, +)	326.43 ± 6.79	0.201 ± 0.03	+ 22.73 ± 1.09	45.30 ± 2.52	86.51 ± 2.94
F-4	(+, -, -, +)	465.77 ± 2.71	0.299 ± 0.02	+ 27.87 ± 0.58	26.65 ± 2.69	69.63 ± 2.43
F-5	(+, +, -, -)	582.60 ± 27.28	0.363 ± 0.02	+ 30.83 ± 1.16	22.49 ± 0.43	78.69 ± 0.42
F-6	(+, +, -, +)	1744.66 ± 35.50	0.328 ± 0.04	+ 33.20 ± 0.62	33.46 ± 3.39	68.89 ± 1.91
F-7	(+, +, +, -)	535.63 ± 4.29	0.266 ± 0.07	+ 14.73 ± 2.38	15.96 ± 1.42	59.65 ± 1.48
F-8	(+, +, +, +)	1390.00 ± 56.04	0.342 ± 0.11	+ 35.90 ± 0.56	33.52 ± 2.35	69.35 ± 1.07
F-9	(-, -, +, +)	539.23 ± 27.66	0.402 ± 0.04	+ 25.90 ± 1.44	27.32 ± 0.49	82.64 ± 0.83
F-10	(-, -, +, -)	432.83 ± 5.13	0.267 ± 0.03	+ 32.13 ± 0.32	28.46 ± 3.08	66.09 ± 2.80
F-11	(-, -, -, +)	514.33 ± 16.68	0.361 ± 0.05	+ 27.40 ± 0.82	20.83 ± 0.88	77.28 ± 2.43
F-12	(-, -, -, -)	400.20 ± 46.94	0.355 ± 0.14	+ 40.57 ± 1.00	17.06 ± 1.69	69.13 ± 3.37
F-13	(-, +, -, -)	418.43 ± 13.25	0.208 ± 0.03	+ 33.43 ± 0.21	17.38 ± 0.97	69.86 ± 2.01
F-14	(-, +, -, +)	2600.00 ± 179.92	0.223 ± 0.03	+ 31.73 ± 0.81	18.67 ± 0.64	59.02 ± 1.27
F-15	(-, +, +, -)	412.33 ± 40.06	0.285 ± 0.07	+ 30.67 ± 0.50	26.44 ± 0.77	61.66 ± 1.72
F-16	(-, +, +, +)	1265.33 ± 7.64	0.257 ± 0.00	+ 25.23 ± 1.01	30.50 ± 2.25	74.12 ± 1.66

Each value represents the mean ± SD (n=3).

^a A, B, C, D are GTS amount, SMP amount, CS concentration and PVA concentration, respectively.

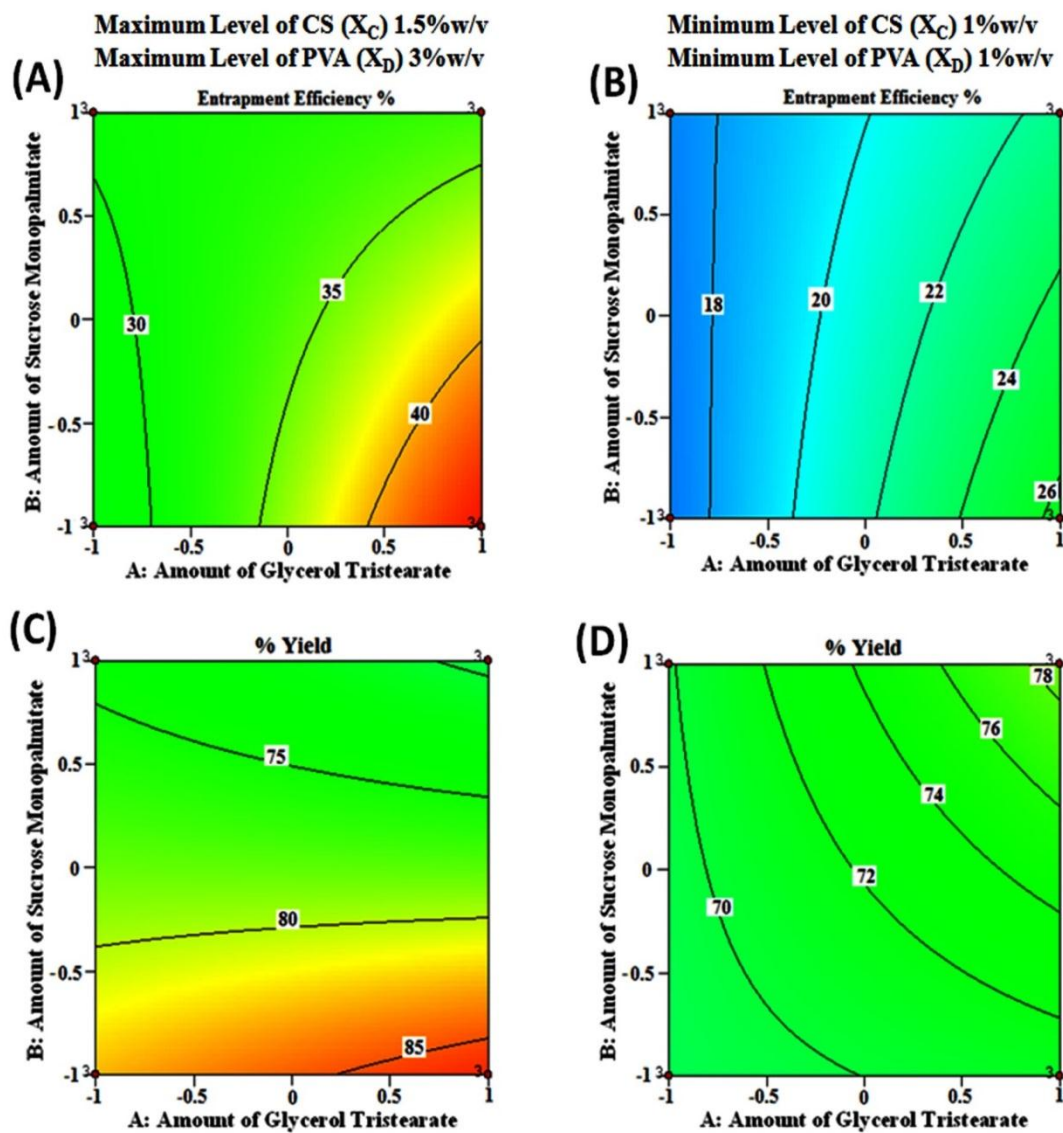


Figure 10: Contour plots representing the effect of the interaction between the amounts of both GTS (X_A) and SMP (X_B) on DEE % and yield % (A and B) and (C and D) at the maximum and minimum levels of both CS (X_C) and PVA (X_D) concentrations, respectively.

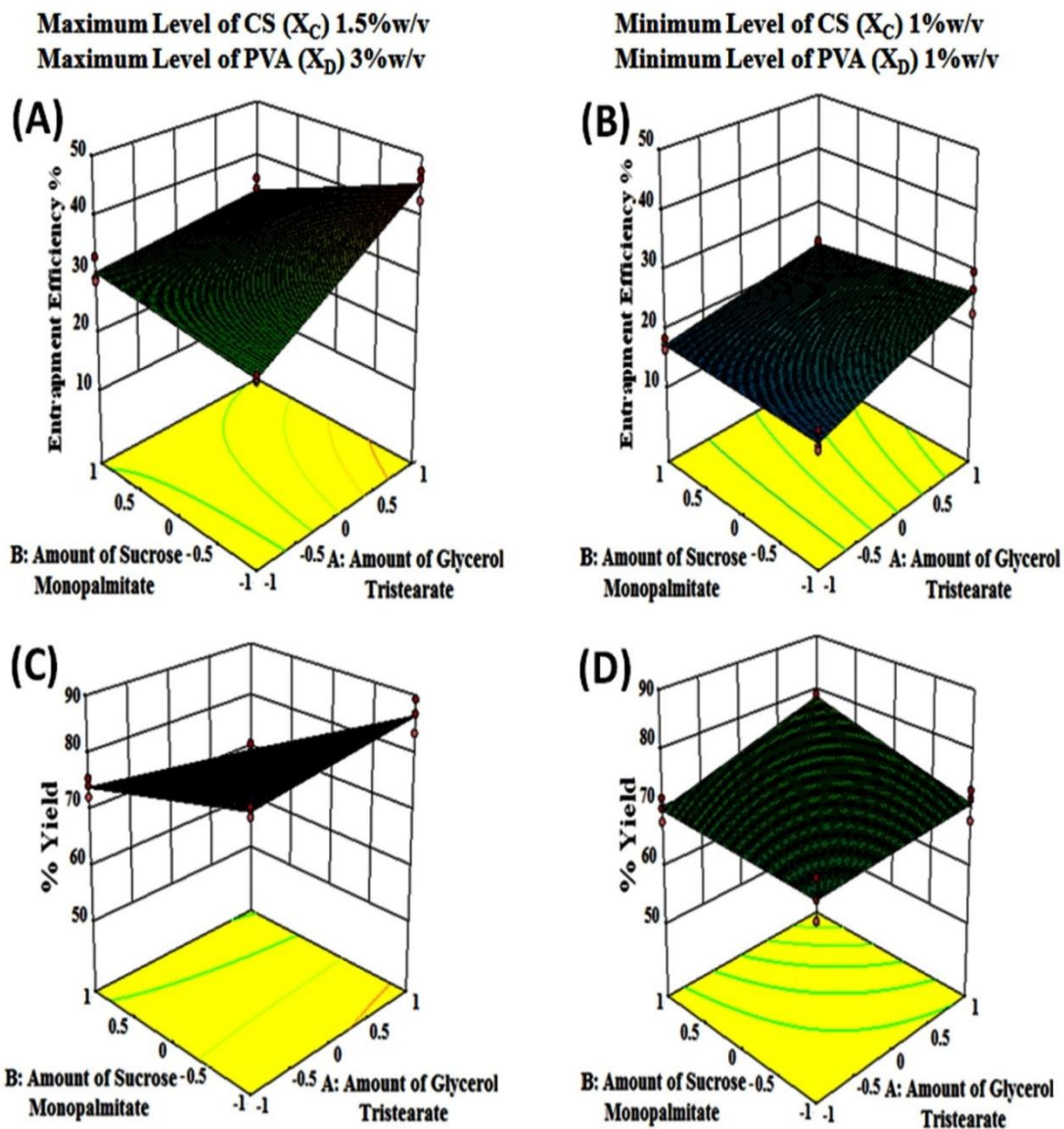


Figure 11: Three dimensional surface plots representing the effect of the interaction between the amounts of both GTS (X_A) and SMP (X_B) on DEE % and yield % (A and B) and (C and D) at the maximum and minimum levels of both CS (X_C) and PVA (X_D) concentrations, respectively.

3.2. Particle size analysis and the polydispersity index (PDI)

With respect to the size of NP_s, not only their average value (nm) is prime, but also their size variability. A metric for size variability is the PDI, a unitless quantity derived from the cumulate analysis and equivalent to the relative discrepancy of the distribution. Particle size and size distribution are two essential touchstones of NP_s as such factors influence drug release rate, bio-distribution, and mucoadhesion (Vandervoort and Ludwig, 2002; Leach *et al.*, 2005). As well, they are substantial clues for evaluating a colloidal dosage form upon storage. The issue of size stability is more crucial for NP_s than other drug delivery systems because of the large specific surface area afforded by NP_s.

Table 2 shows the particle size and PDI of the prepared CS,APO - loaded SLN_s. All formulations exhibited a PDI values ranged from 0.201 to 0.402. The small values of PDI describe narrow-average distribution and are considered to be a homogenic suspension. Also, they are desired to keep the colloidal dispersion stability without microparticles or precipitates formation (Puhl *et al.*, 2011).

The obtained polynomial equation representing the regression model for particle size is as follows:

$$\text{Particle Size} = + 785.92 - 36.92 X_A + 332.70 X_B - 110.82 X_C + 319.80 X_D - 18.48 X_{AB} + 49.58 X_{AC} - 87.09 X_{AD} - 106.98 X_{BC} + 311.58 X_{BD} - 114.65 X_{CD} + 67.81 X_{ABC} - 40.18 X_{ABD} + 52.39 X_{ACD} - 89.88 X_{BCD} + 75.22 X_{ABCD}$$

Where F= 454.69, $p < 0.0001$, and adjusted $R^2 = 0.9931$

This equation reveals that all CPPs and their interactions have highly significant influence on particle size. The amount of SMP (X_B) and PVA concentration (X_D) have the most prominent effect on particle size increment if their levels were maintained high. Meanwhile, GTS amount (X_A) and CS concentration (X_C) have a negative effect as previously reported (Hansraj *et al.*, 2015). Furthermore, careful examination of **Table 2** reveals that the interaction between SMP (X_B) and PVA (X_D), while keeping GTS (X_A) and CS (X_C) constant either at their low or high levels, is synergistic towards particle size (F-2 and 8 as well as F-12 and 14). The significant increase might be

attributed to an increase in the viscosity of the external aqueous phase (w_2) by increasing the concentration of PVA (X_D) solution resulting in a net shear stress decrease (i.e. difficulty in breaking the emulsion droplets down into smaller ones) and a corresponding particle size increase. Moreover, such increase in particle size might be due to the accumulation of excess PVA molecules at the SLN_S surface (**Keum et al., 2011; Mohanty et al., 2014**). Likewise, high level of SMP (X_B) can lead to accumulation of such surfactant and a subsequent particle size enlargement (F-3 and 8). From the aforementioned results, F-3 with ($X_A (+)$, $X_B (-)$, $X_C (+)$, $X_D (+)$) represents the lowest particle size and PDI besides the highest DEE % and yield %.

3.3. Zeta potential

ZP as well as particle size and PDI are essential parameters for evaluating the colloidal suspension. During the preparation of NP_S , the formation of an electrical double layer occurs encircling the NP_S in solution. The electrostatic potential at this “slipping plane” boundary is called the ZP and is related to the surface charge of the NP_S (**Puhl et al., 2011**). Therefore, the ZP, which can be either positive or negative in polarity, depends on the chemistry of the particles and the degree of repulsion between similarly charged ones in the dispersion medium. It is a criterion widely used to predict colloidal suspension stability. NP_S with ZP higher than +30 mV or lesser than -30 mV are to be considered very stable in the dispersion medium (**Clogston and Patri, 2011; Wu et al., 2011**). Herein, SLN_S covered by a non-ionic surfactant like PVA tend to remain stable despite having a lower value of ZP. Surface coverage of the $SLNs$ with PVA reduces the electrophoretic mobility of the particles by steric stabilization and thus lowers the ZP (**Shah et al., 2014**). In such cases, ZP of about +20 mV, as in case of F-3, is still sufficient to fully stabilize the system. Hence, ZP measurement was not considered a primary parameter in the selection of the optimal formulation F-3.

The obtained polynomial equation symbolizing the regression model for ZP is as follows:

$$\text{ZP} = + 29.98 - 0.90\mathbf{X}_A - 0.52\mathbf{X}_B - 2.01\mathbf{X}_C - 0.70\mathbf{X}_D + 0.10\mathbf{X}_{AB} + 0.39\mathbf{X}_{AC} + 2.61\mathbf{X}_{AD} - 0.82\mathbf{X}_{BC} + 2.75\mathbf{X}_{BD} + 1.24 \mathbf{X}_{CD} - 0.90\mathbf{X}_{ABC} + 1.22\mathbf{X}_{ABD} + 0.84\mathbf{X}_{ACD} + 0.64\mathbf{X}_{BCD} + 1.98\mathbf{X}_{ABCD}$$

Where $F = 90.77$, $p < 0.0001$, and adjusted $R^2 = 0.9663$

The ZP of all the prepared formulae was consistently positive and in the range of $+ 14.73 \pm 2.38$ to $+ 40.57 \pm 1.00$ mV (F-7 and 12, **Table 2**). Positive ZP is essential for increasing bioavailability through mucoadhesion. The polynomial equation reveals that all the main CPPs have negative coefficient towards ZP with comparatively low numerical values (**Mohanty et al., 2014**). **Table 3** summarizes the statistical significance of all CPPs and their interactions on ZP and other CQAs.

Since F-3 experienced optimized CPPs with the highest DEE % and yield %, lowest particle size and PDI as well as acceptable ZP values, it was subjected to further elaborate investigations.

Table 3: Statistical analysis for the effect of CPPs and their interactions on the CQAs.

			Particle size (nm)	ZP (mV)	DEE (%)	Yield (%)
CPPs	GTS amount (X_A)	F-value	< 0.0001*	< 0.0001*	< 0.0001*	0.1387
		Estimate coefficient	-36.92	-0.90	+1.89	+0.46
	SMP amount (X_B)	F-value	< 0.0001*	0.0014*	0.2073	< 0.0001*
		Estimate coefficient	+332.70	-0.52	-0.42	-2.78
CS concentration (X_C)	F-value	< 0.0001*	< 0.0001*	< 0.0001*	0.9852	
	Estimate coefficient	-110.82	-2.01	+2.35	+0.005625	
PVA concentration (X_D)	F-value	< 0.0001*	< 0.0001*	< 0.0001*	< 0.0001*	
	Estimate coefficient	+319.80	-0.70	+4.31	+3.00	
CPPs interaction	GTS amount vs. SMP amount	F-value	0.0189*	0.5035	0.3099	0.0016*
		Estimate coefficient	-18.48	+0.10	-0.33	+1.04
	GTS amount vs. CS concentration	F-value	< 0.0001*	0.0133*	< 0.0001*	0.0006*
		Estimate coefficient	+49.58	+0.39	-2.50	-1.15
	GTS amount vs. PVA concentration	F-value	< 0.0001*	< 0.0001*	< 0.0001*	0.3417
		Estimate coefficient	-87.09	+2.61	+3.32	-0.29
	SMP amount vs. CS concentration	F-value	< 0.0001*	< 0.0001*	0.1003	< 0.0001*
		Estimate coefficient	-106.98	-0.82	-0.55	-1.47
	SMP amount vs. PVA concentration	F-value	< 0.0001*	< 0.0001*	0.8110	< 0.0001*
		Estimate coefficient	+311.58	+2.75	-0.078	-2.81
	CS concentration vs. PVA concentration	F-value	< 0.0001*	< 0.0001*	< 0.0001*	< 0.0001*
		Estimate coefficient	-114.65	+1.24	+2.28	+4.72
	GTS amount vs. SMP amount vs. CS concentration	F-value	< 0.0001*	< 0.0001*	0.0076*	< 0.0001*
Estimate coefficient		+67.81	-0.90	-0.92	-2.04	
GTS amount vs. SMP amount vs. PVA concentration	F-value	< 0.0001*	< 0.0001*	0.2059	0.8044	
	Estimate coefficient	-40.18	+1.22	-0.42	+0.075	
GTS amount vs. CS concentration vs. PVA concentration	F-value	< 0.0001*	< 0.0001*	< 0.0001*	0.0170*	
	Estimate coefficient	+52.39	+0.84	+2.55	+0.76	
SMP amount vs. CS concentration vs. PVA concentration	F-value	< 0.0001*	0.0001*	0.0017*	0.0438*	
	Estimate coefficient	-89.88	+0.64	-1.11	+0.63	
GTS amount vs. SMP amount vs. CS concentration vs. PVA concentration	F-value	< 0.0001*	< 0.0001*	< 0.0001*	0.0003*	
	Estimate coefficient	+75.22	+1.98	-2.07	-1.23	

*Significant at $p < 0.05$.

4- Evaluation of the optimized formula (F-3) of CS,APO - loaded SLN_S

4.1. Transmission electron microscopy (TEM)

TEM is a method of probing the microstructure of rather delicate systems like liquid crystalline phases, emulsions, micelles, vesicles, and NP_S (Han *et al.*, 2008). The photograph of the TEM reveals that the prepared SLN_S have spherical shape with "core" encapsulating APO with CS as well as smooth surface of the "shell" (Figure 12) (Shi *et al.*, 2015^b).

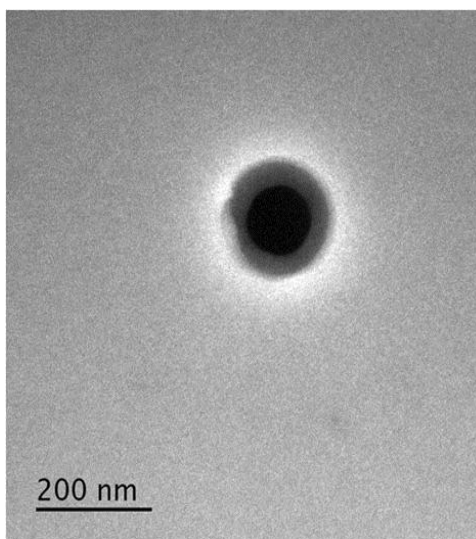


Figure 12: TEM image of CS,APO - loaded SLN_S with high level of GTS (X_A), CS (X_C) and PVA (X_D) and low level of SMP (X_B) (F-3, Table 2).

4.2. Fourier-transform infrared spectroscopy (FT-IR)

As indicated in Figure 13A, infrared shoulders at 3301, 3006, 2850-2950 and 1660 cm⁻¹ appear indicating phenolic OH, aromatic-hydrogen, alkane carbon-hydrogen and ketone C=O conjugated bonds of APO (i), respectively (Tagwireyi and Majinda, 2017).

The infrared spectrum of GTS (ii) shows distinctive peaks at 2916 and 2849 cm⁻¹ attributed to the carbon-hydrogen stretch in the -CH₂ groups present in the acyl chain of the fatty acid. The peak at 1736 cm⁻¹ is due to the stretching vibration of the C=O bond that is related to the carbonyl group present in the fatty acid ester (Yas, 2013).

Besides, the peak at 1111 cm^{-1} belongs to the C–O–C stretching in the polar head group. The obvious band at 1257 cm^{-1} is due to C–O stretch, while the bands at 1471 and 718 cm^{-1} are correlated to C–H stretching in the long aliphatic chain of the fatty acid moiety (Patel *et al.*, 2014).

In the FT-IR spectrum of SMP (iii), the distinct absorption band located in the region of $3500\text{--}3200\text{ cm}^{-1}$ typifies the O–H stretching of SMP free hydroxyl groups. The methylene and terminal methyl groups of palmitate chain of SMP are characterized by the stretching bands at 2920 and 2851 cm^{-1} , respectively. The band at 1060 cm^{-1} is related to the C–O–C stretching vibration of SMP (Ravi babu *et al.*, 2015).

The spectrum of APO (5.35 mg), GTS (100 mg) and SMP (28.4 mg) physical mixture of F-3 (iv) shows the combined bands of the two lipids, while those of the drug are with reduced intensities and some are even disappeared as a consequence of dilution effect. Similarly, the FT-IR spectra of the P SLN_S (v) and CS,APO - loaded SLN_S (F-3) (vi) coincide with that of the physical mixture. This established APO entrapment in the lipid matrix.

4.3. Differential scanning calorimetry (DSC)

As reported previously, DSC can be used to determine thermodynamic discrepancies related to morphological changes during preparation of SLN_S (Shi *et al.*, 2012).

Figure 13B shows DSC thermograms of pure APO, GTS, SMP, their physical mixture, P SLN_S as well as CS,APO - loaded SLN_S (F-3). The DSC curve of APO (i) shows a melting endotherm at 116.385°C which indicates the crystalline nature of pure APO (de Oliveira *et al.*, 2018). The corresponding endothermic peaks of GTS (ii) and SMP (iii) were at 68.222 and 46.073°C , respectively. The thermograms of their physical mixture (iv) and SLN_S experienced only one melting point of the bulk lipid (GTS). This might be due to the presence of both APO and SMP as amorphous or molecular dispersion in GTS during the run (Chaudhary *et al.*, 2016). Noticeably, the melting point of the bulk lipid (GTS) (ii) was even reduced when formulated as SLN_S. The decrease in GTS melting in both lyophilized P SLN_S (60.141) (v) and CS,APO - loaded

SLN_S (59.66) (vi) could be explained on the basis that GTS is not pure anymore. The phase transition temperature of colloidal dispersion was always much lower than that of the anhydrous lipid mixture (**Dudhipala and Veerabrahma, 2016**). No interaction between the drug and lipid was detected.

4.4. X-ray diffractometry (XRD)

The XRD patterns of APO, GTS, SMP, physical mixture, P SLN_S as well as CS,APO - loaded SLN_S (F-3) are shown in **Figure 13C**. The XRD pattern of APO (i) shows the principal peaks at angle 13.125°, 22.611°, and 26.413° (2θ) (**de Oliveira et al., 2018**). GTS (ii) has characteristic peaks at angle 19.261°, 21.358°, 22.941°, and 23.990° (2θ) (**Vivek et al., 2007**). SMP (iii) exhibits only one peak at 21.321° (2θ). The physical mixture (iv) shows the peaks of both GTS and SMP, whereas those of APO were inconspicuous owing to its comparatively small amounts.

The distinctive peaks of APO were diminished in the lyophilized CS,APO - loaded SLN_S (F-3) (vi) suggesting the entrapment of APO within the lipid core in an amorphous or molecular form. Furthermore, less ordered crystals of GTS were present in both lyophilized plain and loaded SLNs where the majority of the intense peaks were absent (**Akanda et al., 2015**). This may be referred to the incorporation of APO between parts of the crystal lattice of the lipid leading to a change in the crystallinity of the CS,APO - loaded SLN_S. Such manner matches the DSC data and distinctly indicates the possible change in crystallinity of the lipid after APO embedding and formulation as SLN_S (**Vivek et al., 2007**).

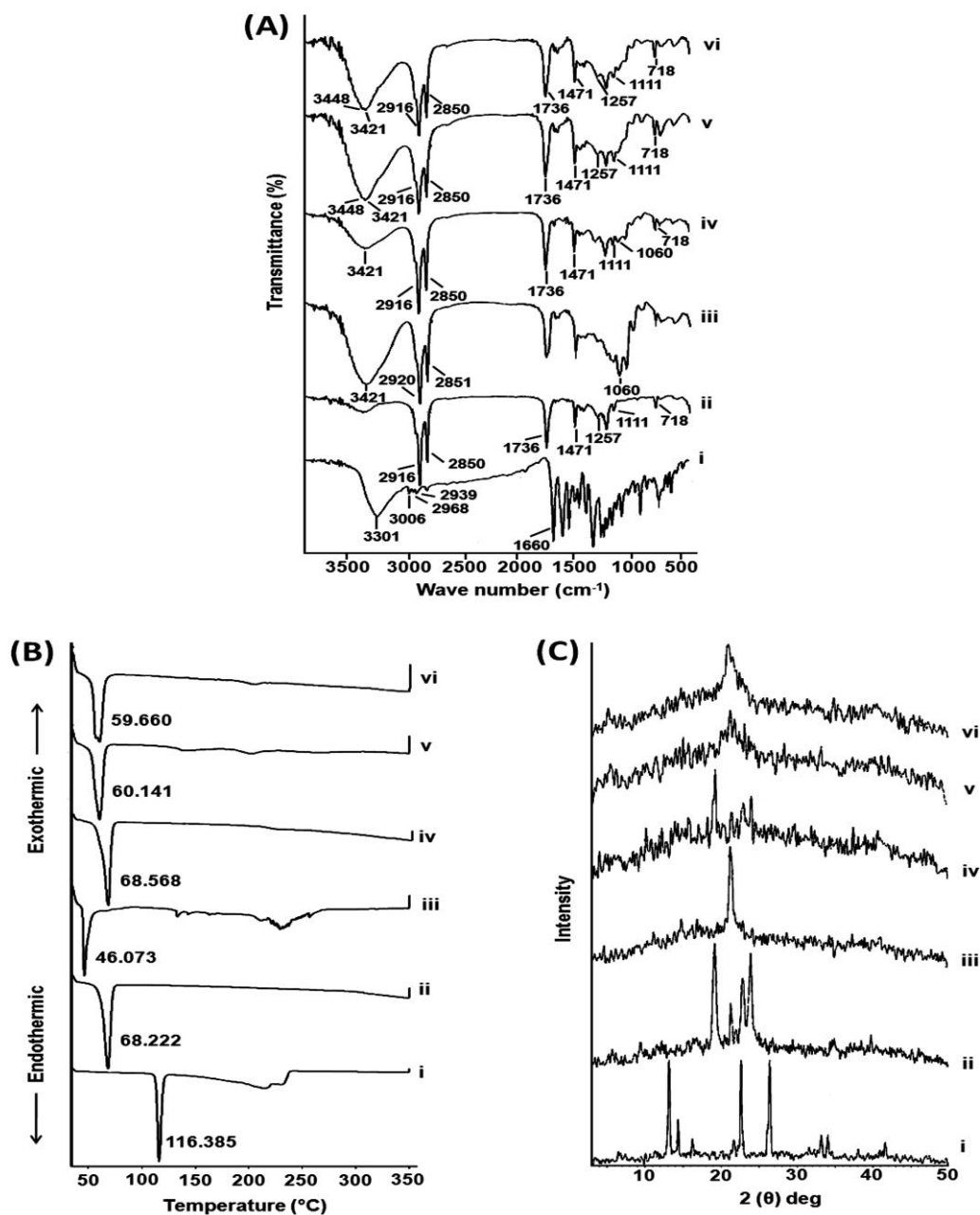


Figure 13: Solid characterization. (A) FT-IR spectra, (B) DSC thermograms, and (C) XRD patterns of pure APO (i), GTS (ii), SMP (iii), physical mixture of APO, GTS and SMP (iv), P SLNs (v) and CS,APO - loaded SLNs (F-3) (vi).

5- *In vitro* release of APO from CS,APO - loaded SLN_s

As mentioned before, SLNs are demonstrated to have a core-shell nanometer structure comprising a lipid core surrounded by surfactants (Chen *et al.*, 2015). In CS,APO - loaded SLN_s, APO was encapsulated in low MW CS as an internal phase and surrounded by lipid core. Therefore, the drug needs to be released from the core-shell nanometer structure rather than being directly exposed to the release medium. This will result in a controlled release. Low MW CS was selected owing to its significantly better oral absorption than the high MW one as well as its negligible cytotoxic effect on Caco-2 cells (Chae *et al.*, 2005).

Diffusion of free APO and *in vitro* release of the drug from the selected SLN_s formula (F-3) were investigated in different media simulating gastrointestinal tract (GIT) fluids (pH 1.2 and pH 6.8) to mimic transit of orally administered formulations. Additionally, it was studied at pH 7.4 resembling physiological pH of the blood (Figure 14).

Free APO can be considered as an amphoteric molecule where it can dissolve in acidic as well as basic media. It dissolved completely in the acidic pH of the stomach (pH 1.2) as well as in pH of the blood (pH 7.4). About 100 % of the free APO diffused in 2 h (Figure 14A and C) (Zhang *et al.*, 2013).

In acidic pH, solubility of APO might be due to hydrogen-bond formation between phenolic OH group of the drug and water (H₂O) molecules of the medium. In basic pH, free ionization of phenolic OH group of the drug, interaction with either Na⁺ or K⁺ cations of the phosphate buffer medium as well as formation of hydrogen-bond with H₂O molecules, may provoke complete diffusion of free APO.

On the other hand, free APO diffusion reached only 56 % at nearly neutral pH medium of the intestine (phosphate buffer pH 6.8) and remained constant (Figure 14B). A possible interpretation of such behavior might be assigned to the reduction in the degree of ionization of APO in neutral pH with subsequent decrease in its solubility.

The *in vitro* release data of APO from CS,APO - loaded SLN_s , however, showed no burst effect at the different release media. Such behaviour might be attributed to

limited water penetration due to the presence of 0.1 M NaCl, in the external aqueous phase (w_2), as reported before by **Mobarak *et al.*, 2014**. In pH 1.2, a negligible release prevailed for 3 h (9.719 ± 0.759 %). Meanwhile, at pH 6.8 and 7.4, the release profiles of CS,APO - loaded SLNs (F-3) were comparatively higher (28.791 ± 1.193 and 57.723 ± 2.260 %, respectively) and sustained over a period of 24 h, as shown in **Figure 14 (A–C)**. The predominant insoluble long chain GTS, used as the lipid matrix, might be responsible for such behavior (**Narala and Veerabrahma, 2013; Christophersen *et al.*, 2014**). Probably, combination of the surfactant SMP together with the lipid GTS resulted in this controlled release delivery system (**Muller *et al.*, 2000; Reddy *et al.*, 2006; Szűts *et al.*, 2010**). The excipients of these SLNs being biodegradable rarely pose any toxicity.

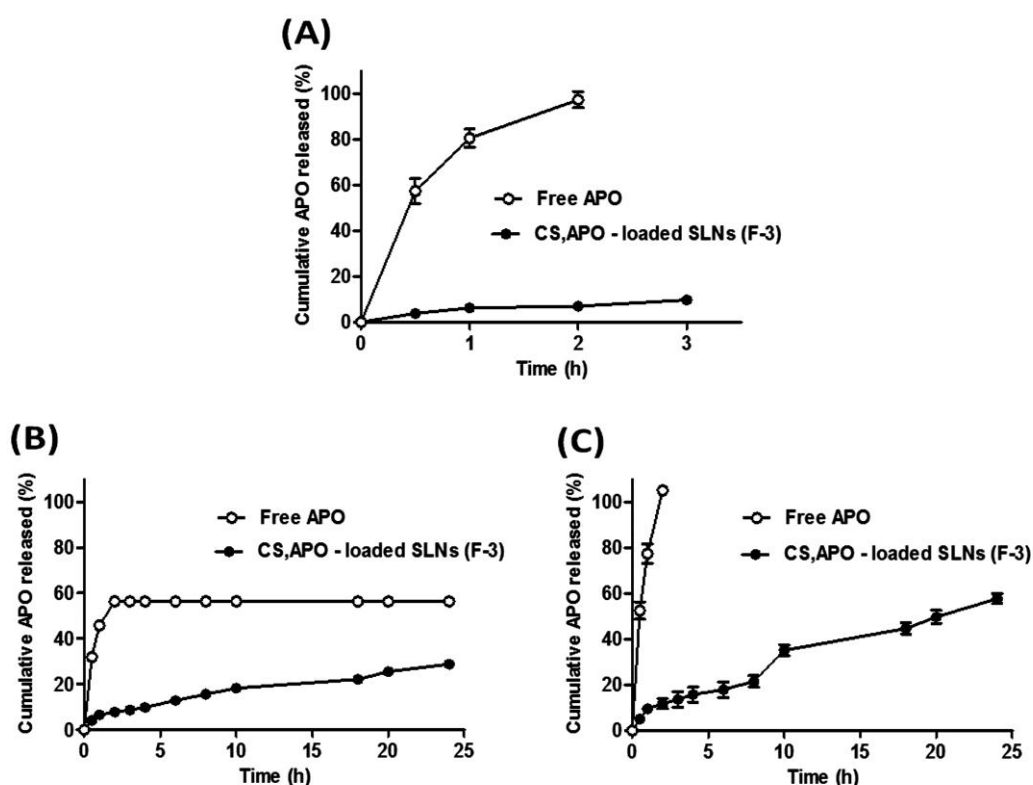


Figure 14: *In vitro* release profiles of free APO and APO from CS,APO - loaded SLNs (F-3) at three different pH values (A) pH 1.2, (B) pH 6.8 and (C) pH 7.4.

Each point represents the mean \pm SD (n=3).

6- Kinetic analysis of the drug release data

As seen in **Table 4**, the kinetic of drug release was dependent on the pH of the medium and the form of the drug; free or encapsulated in the SLN_S. Generally, it can be inferred from the (R^2) values that both Higuchi's model and Fickian diffusion mechanism prevailed for both free drug as well as entrapped one in the CS,APO - loaded SLN_S (F-3). Analogous findings were previously reported (**Sadiq and Abdul rassol, 2014**).

Table 4: Kinetic analysis of the percentage drug diffused and that released from pure APO and CS,APO - loaded SLN_S (F-3), respectively (See **Table 2** for F-3).

Formula	Coefficients of determination (R^2)			Korsmeyer-Peppas		
	Zero-order	First-order	Higuchi model	(R^2)	Diffusional exponent (n)	Main transport mechanism
Free drug (pH 1.2)	0.8060	0.9773	0.9737	0.9183	0.2814	Fickian
Free drug (pH 6.8)	0.8294	0.9065	0.9847	0.9629	0.3389	Fickian
Free drug (pH 7.4)	0.8904	0.9751	0.9950	0.9735	0.4267	Fickian
F-3 (pH 1.2)	0.8286	0.8356	0.9293	0.7822	0.2952	Fickian
F-3 (pH 6.8)	0.9331	0.9495	0.9779	0.9602	0.4467	Fickian
F-3 (pH 7.4)	0.9611	0.9705	0.9453	0.9350	0.5432	Non-Fickian

7- Physical stability of CS,APO - loaded SLN_S (F-3)

Stability is a prime concern in the development of any formulation. In the present study, CS,APO - loaded SLN_S of the optimized formulation (F-3) did not experience any physical changes or phase separation at refrigeration and ambient conditions pointing out to its good stability.

Table 5 summarizes the values of particle size, PDI, ZP, and drug retention % of the optimized CS,APO - loaded SLN_S (F-3) stored at the two different conditions. The

ANOVA results elucidated the insignificant variation in particle size and PDI throughout the storage period at refrigeration conditions. Contrary, a significant increase in particle size and PDI was recorded upon storage at ambient conditions. These data indicated the high stability of the optimized formula upon storage at $5 \pm 3^{\circ}\text{C}$ for 6 months manifested by uniform nanosize range along with homogeneous distribution. Fortunately, the values of drug retention % were found to be 99.94 ± 5.22 and 100.45 ± 2.37 % after 6 months storage at refrigeration and ambient conditions, respectively.

Hence, the obtained results exhibited a clear evidence of the stability of the prepared CS,APO - loaded SLN_s aqueous dispersion (F-3) upon storage at $5 \pm 3^{\circ}\text{C}$, hence enabling its efficacy for prolonged period of time.

Conclusions

From the previous results, it could be concluded that;

- ❖ CS,APO - loaded SLN_S were prepared successfully using double-emulsion solvent evaporation technique (w/o/w), where the core contains APO and CS with the lipid, while the shell contains PVA.
- ❖ DOE paradigm provides an efficient mean to optimize the CQAs of the w/o/w method of preparation.
- ❖ F-3, with (X_A (+), X_B (-), X_C (+), X_D (+)), was found to be the optimized CS,APO - loaded SLN_S formula with the lowest particle size and PDI besides the highest DEE % and yield %.
- ❖ TEM of the optimized F-3 revealed that the prepared SLN_S have spherical shape with "core" encapsulating APO with CS as well as smooth surface of the "shell".
- ❖ Solid characterization of F-3 employing FT-IR, DSC and XRD established the drug entrapment in the SLNs matrix.
- ❖ The *in vitro* release data of APO from CS,APO - loaded SLN_S (F-3) showed no burst effect at the different release media. In pH 1.2, a negligible release prevailed for 3 h. However, at pH 6.8 and 7.4, the release profiles of CS,APO - loaded SLN_S (F-3) were comparatively higher and sustained over a period of 24 h.
- ❖ Both Higuchi's model and Fickian diffusion mechanism prevailed for both free drug as well as entrapped one in the CS,APO - loaded SLN_S (F-3).
- ❖ The high stability of the prepared CS,APO - loaded SLN_S aqueous dispersion (F-3) was revealed upon storage at $5 \pm 3^{\circ}\text{C}$, hence enabling its efficacy for prolonged period of time.

Notwithstanding from a pharmaceutical perspective, it is evident that further elaborate biopharmaceutical evaluation is required to investigate the *in vivo* oral and parenteral bioavailability performance of F-3 in male Sprague–Dawley rats. Chapter 2 would implement this.

Table 5: Particle size, PDI, ZP and drug retention % of CS,APO - loaded SLN_s aqueous dispersions (F-3) stored at refrigeration ($5 \pm 3^\circ\text{C}$) and ambient conditions (See **Table 2** for F-3).

Storage time	Evaluation parameters							
	Refrigeration conditions ($5 \pm 3^\circ\text{C}$)				Ambient conditions			
	Particle size (nm)	PDI	ZP (mV)	Drug retention (%)	Particle size (nm)	PDI	ZP (mV)	Drug retention (%)
Zero time	389.80 \pm 19.43	0.279 \pm 0.04	+27.00 \pm 1.08	100.00 \pm 0.00	389.80 \pm 19.43	0.279 \pm 0.04	+27.00 \pm 1.08	100.00 \pm 0.00
1 month	431.30 \pm 20.69	0.249 \pm 0.04	+24.60 \pm 0.43*	102.00 \pm 2.15	598.13 \pm 13.48*	0.602 \pm 0.14	+21.27 \pm 0.42*	96.40 \pm 0.771
2 months	456.40 \pm 37.41	0.256 \pm 0.13	+20.80 \pm 1.39*	101.66 \pm 2.63	556.73 \pm 34.54	0.712 \pm 0.17*	+12.57 \pm 0.40*	101.46 \pm 2.89
3 months	444.17 \pm 28.20	0.363 \pm 0.03	+20.33 \pm 0.76*	97.31 \pm 1.66	664.23 \pm 60.05*	0.913 \pm 0.15*	+10.18 \pm 1.16*	96.54 \pm 1.31
4 months	441.90 \pm 26.39	0.245 \pm 0.09	+22.60 \pm 1.22*	99.25 \pm 2.93	634.60 \pm 41.53*	0.213 \pm 0.23	+12.27 \pm 0.60*	98.75 \pm 4.48
5 months	440.17 \pm 53.77	0.411 \pm 0.10	+22.63 \pm 0.83*	102.73 \pm 3.94	690.23 \pm 114.76*	0.873 \pm 0.11*	+10.77 \pm 0.25*	104.48 \pm 1.17
6 months	401.93 \pm 83.81#	0.224 \pm 0.03	+21.07 \pm 0.15*#	99.94 \pm 5.22	616.07 \pm 148.86*	0.135 \pm 0.09	+11.63 \pm 0.15*	100.45 \pm 2.37

Each value represents the mean \pm SD (n=3).

* Significant at $p < 0.05$ monthly vs. initial.

Significant at $p < 0.05$ refrigeration vs. ambient conditions after 6 months.

Chapter 2

Oral and parenteral bioavailability of the optimized chitosan-based apocynin-loaded solid lipid nanoparticles in rats

Introduction

The bioavailability is especially concerned with the fraction of the oral dose that absolutely reaches the blood stream, as this amount is the effective portion of the drug. However, in some acute cases such as pain, allergic response and insomnia, where a single dose of the drug is needed, a rapid and complete absorption is commonly desirable. Therefore, bioavailability is also concerned with the rate of drug absorption. The more fast the absorption, the shorter is the onset of action and the higher is the intensity of the pharmacologic response (**Lemke and Williams, 2012**). Rapid absorption could also decrease the frequency and severity of gastrointestinal distress expected after oral administration of certain drugs, including aspirin and tetracycline, by reducing the contact time in the GIT. Hence, bioavailability is believed to be the rate and the extent at which a substance or its active moiety is delivered from a pharmaceutical dosage form and becomes available in the general circulation (**Toutain and Bousquet-Mélou, 2004**).

On the other hand, absolute bioavailability is the exact percentage of the administered dose (from 0 to 100%), that reaches the general circulation. Assessment involves comparing drug exposure following extravascular (e.v.) administration of the tested dosage form with that of an i.v. administration, assumed to be 100% available (**Toutain and Bousquet-Mélou, 2004**).

Methods for assessing absolute bioavailability

There are several direct and indirect methods which may be used to assess the extent of systemic bioavailability. The bioavailability of a drug product is expressed by the rate and extent of drug absorption, as determined by comparison of measurable

parameters, e.g. concentration of the active drug moiety in the blood, cumulative urinary excretion data or pharmacological effects.

◆ **Plasma drug concentration**

The most traditional one is based on comparing plasma exposure area under the curve (AUC) after an i.v. and an e.v. administration. Classically, the bioavailability factor "*F* (%)" is obtained by the following equation:

$[F (\%) = (AUC_{(e.v.)} * Dose_{(i.v.)} / AUC_{(i.v.)} * Dose_{(e.v.)}) \times 100]$ Where, AUC is the area under the plasma or total blood drug concentration–time curve, *Dose* (i.v.) and *Dose* (e.v.) are the doses actually administered to evaluate *F* (%) (Toutain and Bousquet-Mélou, 2004).

◆ **Urinary drug excretion data**

Absolute bioavailability can be evaluated by measuring the amount of drug eliminated in urine (or any other biological fluid) using the following equation:

$[F (\%) = (X_{(u,e.v.)}^{\infty} * Dose_{(i.v.)} / (X_{(u,i.v.)}^{\infty} * Dose_{(e.v.)}) \times 100]$ Where, X_u^{∞} is the total amount of drug excreted in urine (or other biological fluid). The major limit of the urinary approach is the requirement to collect urine (or other biological fluid) until almost all the drug has been excreted (Toutain and Bousquet-Mélou, 2004).

◆ **Clinical observations**

Well-disciplined clinical trials in humans prove the safety and effectiveness of drug products and may be used to determine bioavailability. Meanwhile, the clinical trials approach is the least accurate, sensitive and reproducible of the general techniques for measuring bioavailability. The FDA resorts to this approach only when analytical methods are not adequate to determine bioavailability of drug moiety when its biological response is not directly related to blood levels (Shargel *et al.*, 2005). Blood sugar lowering promoted by an antidiabetic agent (Mohamed *et al.*, 2012^a) and changes in blood pressure provoked by an antihypertensive agent (Vasdev *et al.*, 2009) are examples of such clinical purposes.

APO's bioactivity was manifested in many diseases like atherosclerosis, asthma, cancer, vascular and neurodegenerative diseases, inflammatory bowel disease and

collagen-induced arthritis pharmacotherapy (**de Oliveira et al., 2017**). Even though, the *in vivo* pharmacokinetic study of both previously prepared synthesized Mito-APO into polyanhydride NPs and APO-loaded BSA NPs was not established (**Brenza et al. 2017; de Oliveira et al., 2018**). Only *in vivo* efficacy of APO loaded PLGA in hyperoxaluric rats was assessed recently (**Sharma et al., 2018**).

Consequently, the aim of the work in this chapter was to evaluate and compare the oral and parenteral bioavailability of the optimized CS,APO - loaded SLN_S (F-3) with that of a freshly prepared aqueous solution of APO (APO-sol) following administration to male Sprague–Dawley rats.

Experimental

Materials

- ❖ Naproxen (NAP) was purchased from Sigma-Aldrich, Saint Louis, MO, USA.
- ❖ Methanol of chromatographic grade (HPLC methanol, Fisher) was purchased from Cornell Lab, Cairo, Egypt.
- ❖ Phosphoric acid was procured from El-Nasr Pharmaceutical Chemical Co., Cairo, Egypt.
- ❖ Other materials as in part I, chapter 1.

Equipment

- ❖ Centrifuge (Hettich Micro 22R, Germany).
- ❖ Vortex tube mixer (Model VM-300, Gemmy Industrial Corp, Taiwan).
- ❖ Perkin-Elmer high performance liquid chromatography (HPLC) system (USA). This system is equipped with a Perkin-Elmer binary pump, Series 200; Perkin-Elmer variable wavelength UV-VIS detector, Series 200; Perkin-Elmer vacuum degasser, Series 200 and Perkin-Elmer chromatography interface, Series 600.
- ❖ Thermo Scientific Hypersil BDS C18 column (250 mm X 4.6 mm, 5 μ m).
- ❖ Other equipment as in part I, chapter 1.

Methodology

1- Animals

Male Sprague–Dawley rats weighing 200-250 g were used in this study. The Research Ethical Committee at Mansoura University approved the protocols regarding animal experiment in accordance with "The principles of laboratory animal care" (NIH publication No. 85-23, revised 1985). The animals were acclimatized to an environmentally controlled breeding room two weeks prior to the start of the experiment with free access to standard laboratory food and water *ad libitum*.

2- In vivo study

Male Sprague–Dawley rats were fasted for 12 h prior to dosing with free access to water *ad libitum*. All animals were randomly divided into four groups (six per group):

Group a, positive control for oral drug administration (APO-sol);

Group b, oral administration of CS,APO - loaded SLN_s (F-3);

Group c, positive control for i.v. drug administration (APO-sol); and

Group d, i.v. administration of CS,APO - loaded SLN_s (F-3).

The control groups (**a** and **c**) received 14 and 5 mg/kg of APO-sol as an oral and i.v. doses, respectively (**Hougee et al., 2006; McGee and Abdel-Rahman, 2014**). The test groups (**b** and **d**) received the same doses of APO orally and intravenously, respectively, but as SLN_s suspension prepared as previously mentioned. The oral doses were administered by oral gavage under light ether anesthesia, while the i.v. doses were injected through the tail vein.

3- High performance liquid chromatography (HPLC) analysis of APO in rat plasma

Blood samples were collected by heparinized capillary tubes in ethylenediaminetetraacetic acid (EDTA) coated tubes from the retro-orbital venous plexus of the rats at time intervals 15, 30, 45, 60, 120, 180, 240, 360, 480 and 600 min after oral and i.v. administration. Blood samples were centrifuged using a centrifuge at 5000 rpm for 10 min to separate plasma which was then transferred into Eppendorf

tubes and stored at -20°C until analysis. The plasma concentration of APO was assayed by a simple, reliable and reported HPLC-UV analysis method with slight modification (Wang *et al.*, 2013).

Briefly, standard stock solution was prepared by dissolving APO in HPLC methanol at 1 mg/mL. A series of APO standard working solutions, ranging from 2 to 40 $\mu\text{g/mL}$, were prepared by diluting the stock solution with HPLC methanol. For construction of APO calibration curve, the standard plasma samples were prepared by spiking 20 μL of different standard working APO solutions and 20 μL of NAP solution as an internal standard (I.S.) (40 $\mu\text{g/mL}$ in HPLC methanol) into separate tubes containing drug-free blank plasma (100 μL) to attain the final APO concentrations ranging from 0.4 to 8.0 $\mu\text{g/mL}$. Twenty microliters of phosphoric acid were added to adjust pH, denature and precipitate protein of plasma (Liu and Ho, 2017). Besides, 0.4 mL HPLC methanol was added. The steps of extraction were achieved by vortexing using vortex tube mixer for 5 min and centrifugation at 10,000 rpm for 15 min.

After the plasma samples from the experimental animals have been thawed, aliquots (100 μL) of each sample were well mixed using vortex tube mixer with 20 μL NAP (I.S. solution, 40 $\mu\text{g/mL}$), 20 μL phosphoric acid and 0.4 mL HPLC methanol and the steps of extraction were followed exactly as mentioned above.

Analysis was carried out on a HPLC system. Chromatographic separation was accomplished with a C18 column. The mobile phase consisted of a mixture of HPLC methanol/potassium phosphate monobasic buffer (20 mM, pH 6.0) (50:50, %v/v). The isocratic elution was run at a flow rate of 1.5 mL/min. The detection wavelength was 276 nm and the injection volume was 50 μL . Validation of this procedure was performed in order to evaluate the modified method in terms of selectivity/specificity, linearity, accuracy and precision in correspondence to the recommendations per ICH guidelines (Wang *et al.*, 2013). Also, the detection limit (DL) and the quantitation limit (QL) were estimated according to the ICH guidelines (ICH, 2005).

- **Selectivity/specificity**

The selectivity/specificity was assessed by comparing the chromatograms of blank plasma sample and blank plasma spiked with APO and NAP (I.S.).

- **Linearity**

Linearity of a method is its capability to achieve test results which are directly proportional to the sample concentration over a given range. A series of standard plasma samples were prepared with standard working solutions as described previously. The peak areas of APO and I.S. were documented to calculate peak area ratios. The calibration curves were constructed by linear regression of the peak area ratios versus the corresponding concentrations.

- **Accuracy**

The observed concentrations (C_{obs}) were compared to the nominal concentrations (C_{nom}) of APO in the plasma samples to inspect the intraday and interday % accuracy of the assay according to the formula:

$$\% \text{ Accuracy} = \frac{C_{\text{obs}}}{C_{\text{nom}}} \times 100$$

- **Precision**

The intraday and interday % precision of the assay was measured by the percentage of relative standard deviation (RSD %) over the concentration range of calibration curve of APO in rat plasma, three replicates for each concentration, during the course of validation. RSD % was calculated according to the formula:

$$\text{RSD \%} = \frac{\text{SD}}{C_{\text{obs}}} \times 100$$

Where the SD and C_{obs} are the standard deviation and the mean value of the observed concentrations, respectively.

- **Detection limit (DL) and quantitation limit (QL)**

$$\text{DL} = \frac{3.3 \sigma}{S_1}$$

$$\text{QL} = \frac{10 \sigma}{S_1}$$

Where, σ is the standard deviation (SD) of y-intercept of regression line of the calibration curve and S_1 is the slope of the calibration curve.

4- Pharmacokinetic analysis

In order to calculate the pharmacokinetic parameters, a noncompartmental model using GraphPad Prism 5 software computer program was applied to analyze the profiles of APO concentrations in rat plasma versus time. The elimination rate constant (K) was obtained from the slope of the linear regression of the log plasma concentration versus time data of the terminal phase where, $(K) = (2.303 * \text{slope})$. The area under the curve to the last measurable concentration (C_{last}) for each group ($AUC_{0-Clast}$) was calculated by the linear trapezoidal rule. The area under the plasma concentration-time curve from 0– ∞ min ($AUC_{0-\infty}$) was obtained from the summation of $AUC_{0-Clast}$ and the C_{last} divided by K ($= AUC_{0-Clast} + C_{last}/K$). The mean residence time (MRT) was calculated as the ratio of area under the first moment curve from 0– ∞ min ($AUMC_{0-\infty}$) to ($AUC_{0-\infty}$) where, $AUMC_{0-\infty} = AUMC_{0-Clast} + C_{last} * t_{last}/K + C_{last}/K^2$. From the plasma drug concentration after i.v. administration, the half-life ($t_{1/2}$) was calculated as $0.693 * MRT$ and total body clearance (CL_B) as $Dose/AUC_{0-\infty}$. The apparent volume of distribution at steady state (Vd_{ss}) was calculated as $CL_B * MRT$. In case of oral administration, the C_{max} and its occurrence time (t_{max}) were obtained directly from the concentration-time profile. The $t_{1/2}$ was calculated as $0.693/K$, and CL_B as $Dose * F/AUC_{0-\infty}$, where (F) is the fraction absorbed. From CL_B of the oral dose, Vd_{ss} was calculated as CL_B/K . Absolute bioavailability for oral APO-sol or SLN_S was calculated from the plasma data using the relationship $F (\%) = (AUC_{0-\infty(oral)} * Dose_{(i.v.)}/AUC_{0-\infty(i.v.)} * Dose_{(oral)})$, where $AUC_{0-\infty(i.v.)}$ is for APO-sol administered intravenously. Additionally, the forthcoming parameters were also calculated to describe APO absorption after oral administration. Mean absorption time (MAT) was the difference between MRT after oral route, either as APO-sol or SLN_S, and that after i.v. dose as APO-sol (control). The first order rate constant for drug absorption (K_a) was calculated as $1/MAT$. The half-life of absorption ($t_{1/2a}$) was calculated as $0.693/K_a$. Mean *in vivo* dissolution (or release) time (MDT) was obtained from the difference between MRT for oral SLN_S and oral APO-sol.

5- *In vitro-in vivo* correlation

In vitro-in vivo correlation for F-3 was implemented by plotting the *in vivo* percentage drug absorbed against the *in vitro* percentage drug released at time intervals from 1 to 3 h to estimate correlation coefficient (r). Wagner Nelson method was employed to calculate the *in vivo* percentage drug absorbed according to the subsequent equation (**Bala et al., 2014**):

$$\text{Percentage drug absorbed} = \left[\frac{(C_t + k AUC_{0-t})}{k AUC_{0-\infty}} \right] \times 100$$

Where, C_t is the plasma drug concentration at time t, k is the overall elimination rate constant, AUC_{0-t} is the area under the curve from time zero to time t, and $AUC_{0-\infty}$ is the area under the curve from time zero to infinity.

6- Statistical analysis

In vivo pharmacokinetic parameters data were expressed as mean \pm standard error of the mean (SE) and statistically analyzed by Student's *t*-test (unpaired *t*-test). GraphPad Prism 5 software computer program was employed for the analysis process.

Results and Discussion

1- Calibration curve of APO in rat plasma

Figure 15 represents the calibration curve of APO in rat plasma. The regression plot showed a linear dependence of (APO peak area/I.S. peak area) ratio values on drug concentration over the range (0.4 to 8 μg APO/mL) with high (R^2) of 0.9838.

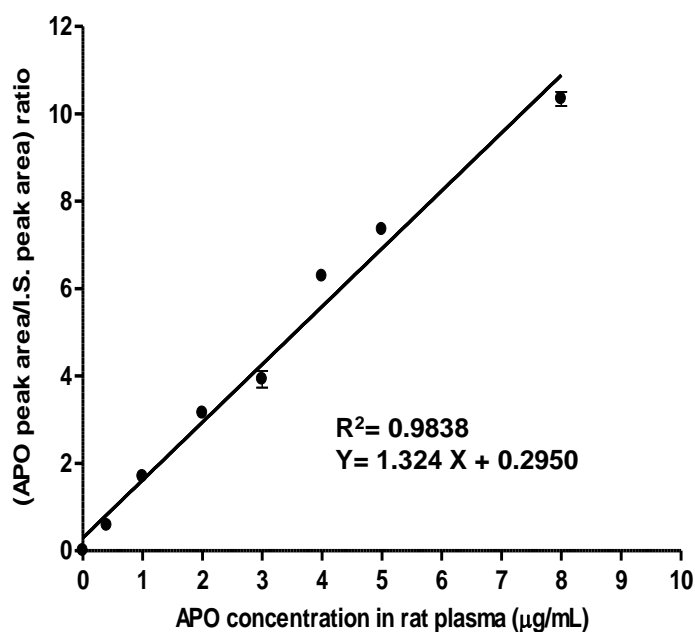


Figure 15: Calibration curve of APO in rat plasma.

Each point represents the mean \pm SE (n=3).

2- Bioavailability and pharmacokinetic study in rats

Using the optimized chromatographic conditions, the modified HPLC method was validated with respect to selectivity/specificity, linearity, accuracy and precision as per the ICH guidelines. Typical HPLC chromatogram of blank plasma spiked with APO and I.S. is shown in **Figure 16**. Neither interferences were observed at the retention times of APO and I.S. nor with the endogenous plasma components. This indicates the selectivity of this analysis for the analytes in the plasma matrix. The approximate retention time of APO and I.S. was found to be 3.32 ± 0.04 and 6.40 ± 0.01 min, respectively. The calibration curve of APO in rat plasma was linear over the concentration range of 0.4-8.0 $\mu\text{g/mL}$. The representative linear regression equation was found to be:

$y = (1.324 \pm 0.016) x + (0.295 \pm 0.020)$, with (R^2) of 0.9838, where: y is the (APO peak area/I.S. peak area) ratio, (1.324 ± 0.016) is the S_1 and its SE, x is the concentration of APO ($\mu\text{g/mL}$) in each standard plasma sample and (0.295 ± 0.020) is the intercept and its SE. The calculated DL and QL based on the SD of y-intercept (0.034) and the S_1 (1.324) were found to be 0.084 and 0.256 $\mu\text{g/mL}$, respectively.

The proposed method was accurate, reproducible and precise for the determination of APO in rat plasma. The intraday and interday % accuracy were in the range of 90.517 ± 19.773 to $110.658 \pm 1.494\%$ and 86.50743 ± 6.772 to $113.159 \pm 2.758\%$, respectively. Besides, the intraday and interday % precision were in the range of 0.371 ± 0.005 to $17.096 \pm 0.048\%$ and 0.137 ± 0.012 to $13.2001 \pm 1.064\%$, respectively. These values were within the acceptable criteria of accuracy between 85–115% and precision nearly less than 15% (**Wang et al., 2013**).

Figure 17 shows the mean plasma concentration-time profiles of APO after oral and i.v. administration of the drug solution as well as the optimized SLN_s (F-3) to Male Sprague–Dawley rats. The plasma level dropped significantly rapid and was undetectable after 60 min in case of both oral and i.v. APO-sol compared to CS, APO - loaded SLN_s. The corresponding pharmacokinetic parameters were calculated using a noncompartmental analysis and are presented in **Tables 6 and 7**.

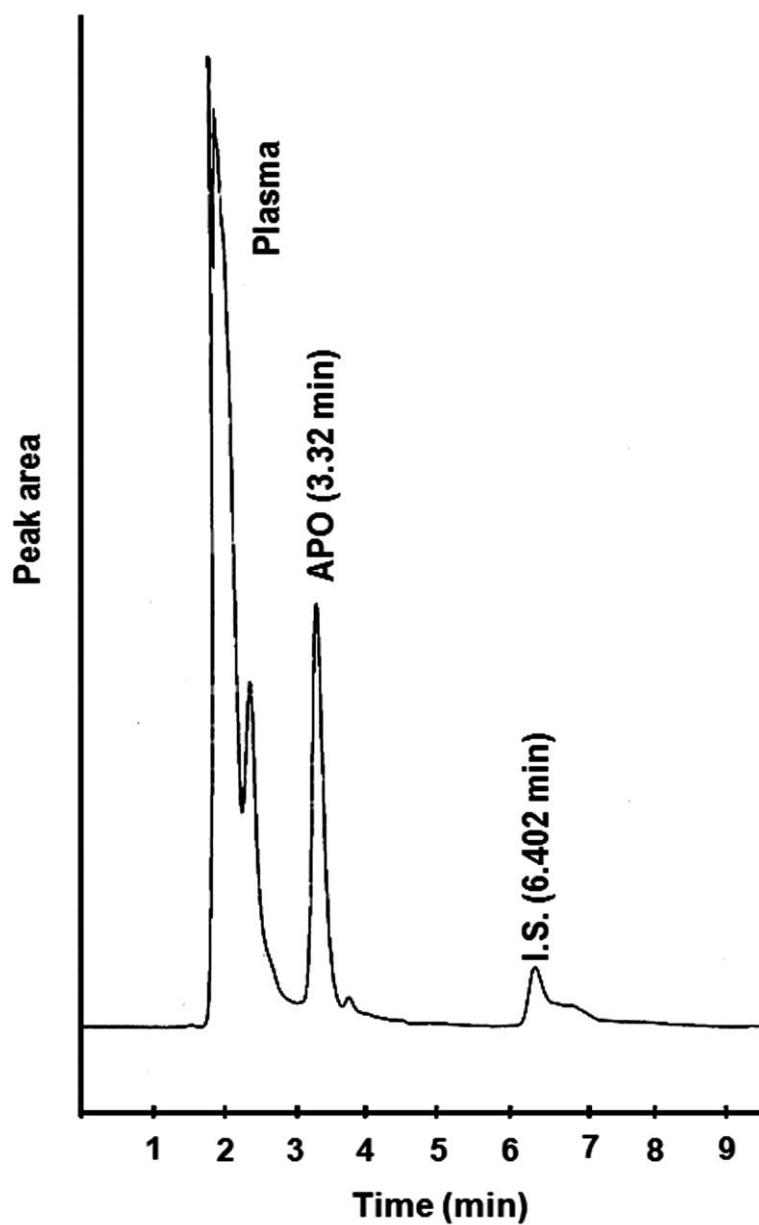


Figure 16: HPLC chromatogram of plasma spiked with APO and I.S.

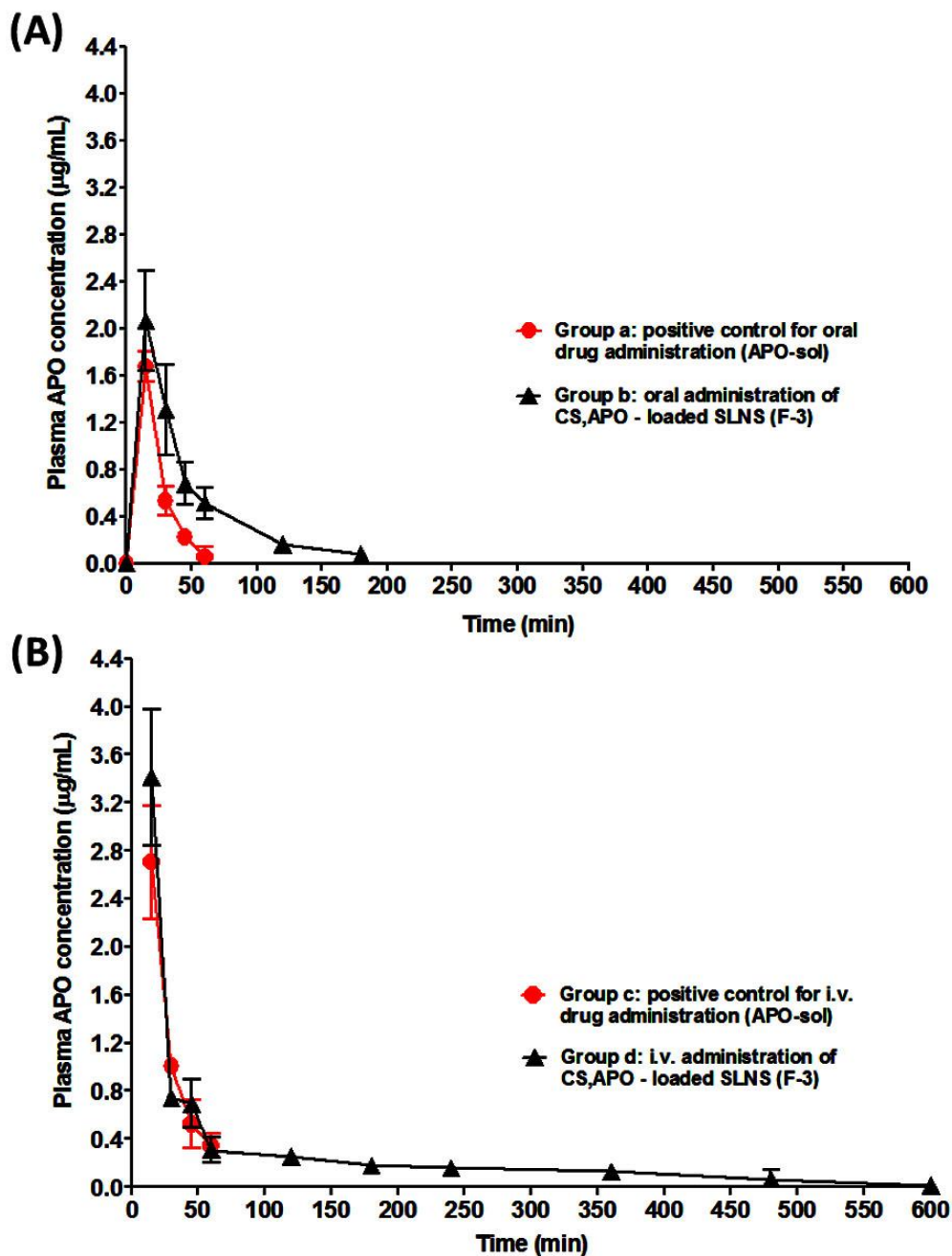


Figure 17: Mean plasma concentration-time profiles of APO after (A) oral (14 mg/kg) and (B) i.v. (5 mg/kg) administration. Drug solution (Group a and c), F-3 (Group b and d).

Each point represents the mean \pm SE (n=6).

Table 6 reveals that a significant increase ($p < 0.05$) in $AUC_{0-\infty}$, $t_{1/2}$, MRT , and Vd_{ss} (2.52, 2.77, 2.24, and 2.91 folds, respectively) exists when oral CS,APO - loaded SLN_S is compared with oral aqueous APO-sol. Additionally, C_{max} showed considerable improvement, expressed by 1.23 fold increase for oral SLN_S .

A possible explanation for such increase in the bioavailability of oral CS,APO - loaded SLN_S is that the positively charged SLN_S , experienced by the cationic CS, would increase the frequency of electrostatic interaction with the negatively charged gut mucus and adhesion of SLN_S , consequently opening up the tight junctions of epithelial cells and permit the paracellular transport pathway. These findings were in accordance with those reported (**Shi et al., 2017**). Additionally, direct uptake of SLN_S through the GIT (lymphoid) augments the above mentioned effect (**Ji et al., 2016**).

Table 6 also shows the MAT for oral SLN_S . Surprisingly, since the oral APO-sol experienced MRT (22.620 ± 1.657 min) less than that when it was given intravenously (27.431 ± 0.580 min), its MAT can't be calculated. This likely resulted from the fast elimination of drug in solution by the oral route. Intuitively, one can conclude that the SLN_S were absorbed over a longer period of time than the solution confirming its sustained release property.

From **Table 6**, one can notice that the MRT for oral CS,APO - loaded SLN_S is more than double that of the oral APO-sol. The difference between both MRT_S represents the time for release and dissolution of APO from SLN_S (MDT). This notice coincides with the above conclusion of the sustaining release of the SLN_S . Absolute oral bioavailability F (%) of oral SLN_S ($45.970 \pm 4.863\%$) is nearly about 2.5 that of oral APO-sol ($18.024 \pm 1.245\%$). Similar low bioavailability of oral APO has been reported (**Chandasana et al., 2015**).

Table 6: Pharmacokinetic parameters after oral administration of APO as an aqueous solution and CS,APO - loaded SLN_s (F-3) (See **Table 2** for F-3).

Pharmacokinetic parameters	Group a Positive oral (APO-sol)	Group b Oral CS,APO- loaded SLN _s
t_{\max} (min)	15.000 ± 0.000	15.000 ± 0.000
C_{\max} (µg/mL)	1.674 ± 0.131	2.065 ± 0.423
$AUC_{0-\infty}$ (µg min/mL)	38.181 ± 2.674	96.404 ± 27.085*
$t_{1/2}$ (min)	12.197 ± 1.289	33.798 ± 5.383*
K (min ⁻¹)	0.058 ± 0.006	0.021 ± 0.003*
MRT (min)	22.620 ± 1.657	50.770 ± 5.090*
CL_B (mL/min kg)	66.699 ± 4.369	62.509 ± 15.416
Vd_{ss} (L/kg)	1.158 ± 0.041	3.377 ± 0.248*
F	0.180 ± 0.0124	0.460 ± 0.084*
MAT (min)	-----	23.339 ± 5.090
K_a (min ⁻¹)	-----	0.0450 ± 0.010
$t_{1/2a}$ (min)	-----	16.174 ± 3.527
MDT (min)	-----	28.150 ± 5.090

Each value represents the mean ± SE (n=6).

Oral dose (14 mg/kg).

*Significant at $p < 0.05$.

In **Table 7**, the pharmacokinetic difference between APO-sol and CS,APO - loaded SLN_S in case of i.v. administration is very similar to that of the oral route. A significant increase in $AUC_{0-\infty}$, $t_{1/2}$, MRT , and Vd_{ss} (2.03, 4.86, 4.86, and 2.37 folds, respectively ($p < 0.05$)) than that of APO-sol was experienced by the CS,APO - loaded SLN_S. Importantly, CL_B value was observed to be significantly decreased ($p < 0.05$) by entrapping APO in the SLN_S.

From **Tables 6 and 7**, it is clear that the MRT is significantly higher for CS,APO - loaded SLN_S than that of the APO-sol whether the drug was given by oral or i.v. routes. The significant increment in MRT together with the reduction in K obtained with SLN_S are the two pillars on which “mostly” the sustaining efficacy of any drug depends (**Venishetty et al., 2012; Soma et al., 2017**). Interestingly, CS,APO - loaded SLN_S given intravenously showed higher $t_{1/2}$ and MRT than those administered orally. This likely resulted as the oral formulation exhibited a faster CL_B than the i.v. one through pre-systemic effect. Moreover, it might be speculated that the PVA shell-stealth SLN_S hindered opsonization and uptake of the particles by the reticuloendothelial system when given intravenously. It was reported that coating of (CS-Fe₃O₄ NP_S) with hydrophilic polymers like PVA improved their colloidal stability and also prolonged circulation kinetics through low opsonization (**Shagholani et al., 2015**).

Tables 6 and 7 also highlight the high distribution of SLN_S whether given orally or intravenously, ($Vd_{ss} = 3.377 \pm 0.248$ and 4.492 ± 0.366 L/Kg for oral and i.v. CS,APO - loaded SLN_S, respectively), through the rat tissues. This increase in Vd_{ss} exceeded the total body water (0.6 L/Kg) of a rat (**Mohamed et al., 2012^b**). Further study requires tissue analysis after SLN_S administration.

Table 7: Pharmacokinetic parameters after i.v. administration of APO as an aqueous solution and CS,APO - loaded SLN_s (F-3) (See **Table 2** for F-3).

Pharmacokinetic parameters	Group c Positive i.v. (APO-sol)	Group d i.v. CS,APO- loaded SLN_s
$AUC_{0-\infty}$ ($\mu\text{g min/mL}$)	73.508 \pm 7.573	149.710 \pm 7.401 [*]
$t_{1/2}$ (min)	19.010 \pm 0.402	92.449 \pm 2.969 [*]
K (min^{-1})	0.047 \pm 0.000	0.012 \pm 0.003 [*]
MRT (min)	27.431 \pm 0.580	133.405 \pm 4.285 [*]
CL_B (mL/min kg)	68.749 \pm 7.083	33.562 \pm 1.663 [*]
Vd_{ss} (L/kg)	1.890 \pm 0.234	4.492 \pm 0.366 [*]

Each value represents the mean \pm SE (n=6).

I.v. dose (5 mg/kg).

^{*}Significant at $p < 0.05$.

3- *In vitro-in vivo* correlation

As shown in **Figure 18**, plotting of *in vivo* percentage drug absorbed against *in vitro* percentage drug released at time intervals from 1 to 3 h revealed good *in vitro-in vivo* correlation for the optimized formula (F-3) with (r) values of 0.8853, 0.9948, and 0.9999 in case of pH 1.2, 6.8, and 7.4, respectively.

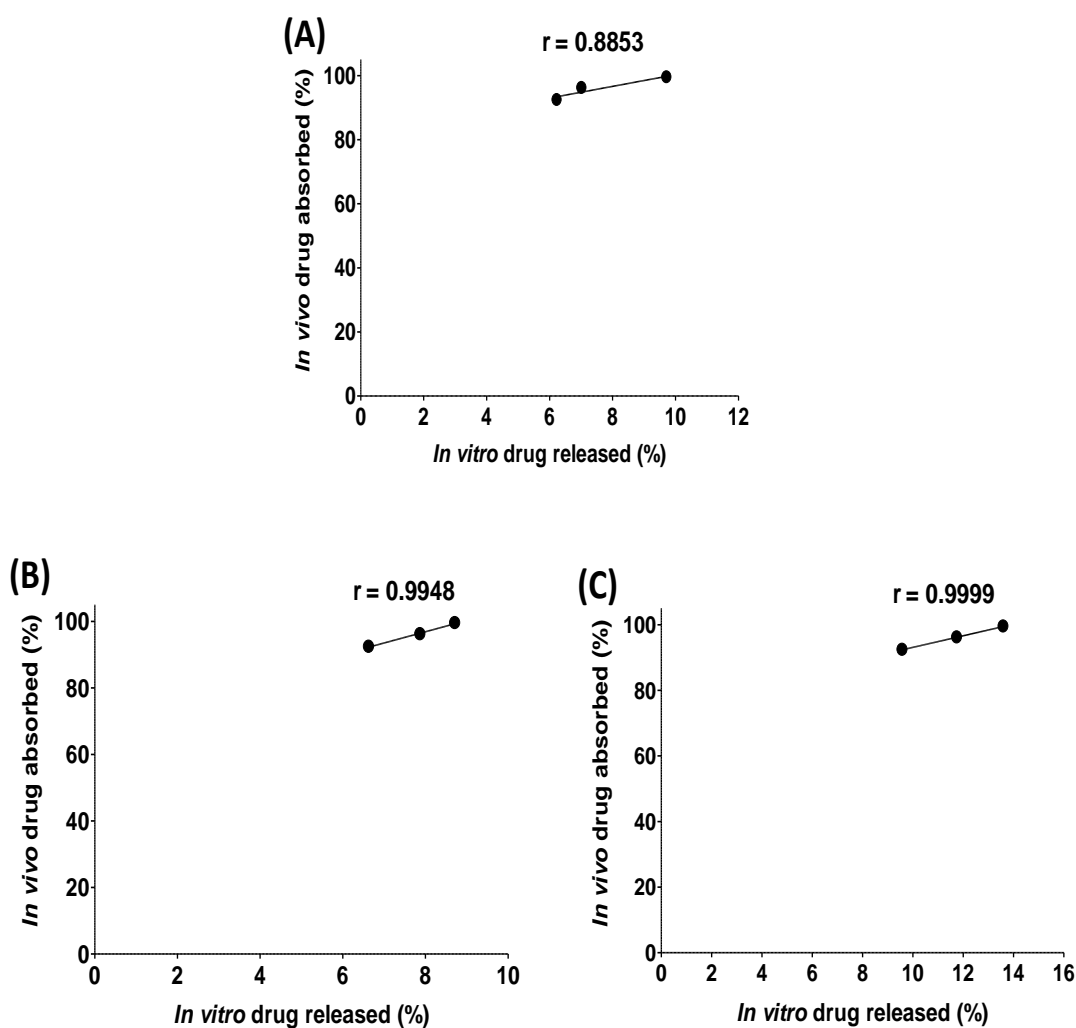


Figure 18: *In vitro-in vivo* correlation plot for the optimized formula (F-3) in different pH media (A) pH 1.2, (B) pH 6.8 and (C) pH 7.4.

Conclusions

Based on the obtained results, it could be concluded that:

- ❖ The bioavailability and *MRT* of CS,APO - loaded SLN_S in rats were higher compared to that of APO-sol regardless of the route of administration.
- ❖ SLN_S with APO, CS and PVA is a promising phytopharmaceutical delivery system for sustaining the efficacy of the “miraculous” molecule APO especially when it is necessary to administer the drug over a prolonged period of time. After which study, one may name the APO SLN_S as "nano-scaffold".
- ❖ Future study is required to trace the biodistribution of APO SLN_S in the different animal tissues.
- ❖ In conclusion, the novel CS-based SLNs system would open new vistas in potentiating the bioavailability and sustaining the effect of APO and other bioactive phytochemicals with comparable properties.

PART II

Clove essential oil nanoemulgel and scaffold-based nanofibers: phytopharmaceuticals with promising potential as cyclooxygenase-2 inhibitors in external inflammation

Introduction

CEO is a colorless to pale yellow liquid with a boiling point of 251°C and a density of 1.05 g/mL at 25°C (Clove oil. http://www.chemicalbook.com/ChemicalProductProperty_EN_CB8286611.htm). It is practically insoluble in water, whereas it is soluble in ethanol, methanol and diethyl ether (Clove oil MSDS. Material Safety Data Sheet. <http://www.sciencelab.com/msds.php?msdsId=9927498>).

CEO contains many different compounds, with the primary constituents being eugenol (49–87%), β -caryophyllene (4–21%), and eugenyl acetate (0.5–21%). Smaller quantities of α -humulene are also present, as well as trace amounts (<1%) of other constituents (Chapter 6—Clove Oil (Eugenol), <https://www.marinwater.org/DocumentCenter/View/253>). Eugenol, as the main component of CEO, is chemically named (2-Methoxy-4-(prop-2-en-1-yl) phenol) according to the International Union of Pure and Applied Chemistry system (IUPAC) (<http://en.wikipedia.org/wiki/Eugenol>, Figure 19).

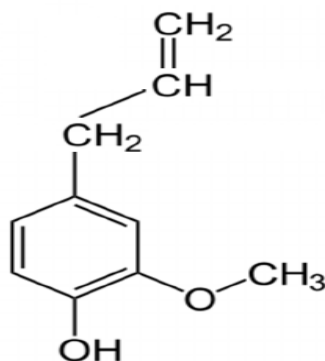


Figure 19: Chemical structure of eugenol.

Therapeutic uses and applications of CEO

The US FDA has approved and categorized CEO as generally recognized as safe (GRAS) for use in food as a flavoring agent, in odontology as an analgesic, in dental cements, in personal care products and in aromatherapy oils as an aroma, as well as in topical and transdermal drug delivery systems (TDDSs). CEO has also been found to possess antiviral, antibacterial, antifungal, anti-inflammatory, antioxidant, antitumor, and insecticidal characteristics. (**Chapter 6—Clove Oil (Eugenol)**, <https://www.marinwater.org/Document Center /View/253>; Anwer *et al.*, 2014; Tonglairoum *et al.*, 2016).

Pharmacokinetics of CEO

Absorption

CEO is rapidly absorbed through the skin and is used in TDDSs to enhance drug uptake from the skin (**Chapter 6—Clove Oil (Eugenol)**, <https://www.marinwater.org/Document Center/View/253>).

Distribution

Rapid distribution of C¹⁴ methoxy labeled eugenol to all organs, with tissue concentrations reaching 10-20 ng/mg of tissue, was perceived in male Wistar rats given i.p. a single dose of 450 mg/kg of the labeled compound (**Eugenol**, <http://www.inchem.org/documents/jecfa/jecmono/v17je10.htm>).

Metabolism

In humans, ingested eugenol is metabolized in the liver primarily to the glucuronic acid or sulfate conjugate (**Chapter 6—Clove Oil (Eugenol)**, <https://www.marinwater.org/Document Center /View/253>). On the other hand, in rats, 20-30% of eugenol is metabolized to homovanillic acid and 4-hydroxy-3-methoxymandelic acid (**Clove Oil BP**: <https://www.medicines.org.uk/emc/medicine/25134>). The fast metabolism and short half-life have provoked the viewpoint that there is a minimum risk of accumulation in body tissues (**Djilani and Dicko, 2012**).

Elimination

In humans, 95% of swallowed eugenol is excreted in the urine in conjugated form within 24 h, with the sulfate conjugates preponderating at low doses and the glucuronic acid conjugates at higher doses (>500 mg/kg-day) (**Chapter 6—Clove Oil (Eugenol)**, <https://www.marinwater.org/DocumentCenter/View/253>).

Toxicity

Acute and chronic CEO toxicity to mammals is low. Acute oral LD₅₀ values in all tested species were greater than 1.19 g/kg. In subchronic toxicity tests, no adverse effects were noticed in laboratory animals' studies up to doses of 0.9 g/kg-day. The fatal oral dose is 3.75 g/kg body weight. Overdose may cause central nervous system (CNS) depression, liver damage, urinary abnormalities, coma, seizure and low blood glucose levels. There is some ambiguous evidence for carcinogenicity, but not enough for a listing as a carcinogen. No case of overdose from oromucosal or dental use has been reported (**Clove Oil BP: <https://www.medicines.org.uk/emc/medicine/25134>**). Treatment has to be supportive and symptomatic. The literature reported that N-acetylcysteine has been auspiciously used as an antidote (**Clove Oil BP: <https://www.medicines.org.uk/emc/medicine/25134>**).

Safety during pregnancy and lactation has not been well-established. In this situation, the use during pregnancy and lactation is not endorsed. Studies on the effects on fertility have not been carried out (**Clove Oil BP: <https://www.medicines.org.uk/emc/medicine/25134>**).

Adverse effects and precautions of CEO

CEO is known to cause skin and eye irritation (**Clove oil. <https://pubchem.ncbi.nlm.nih.gov/compound/12658395>**). Irritation of the eye is characterized by redness, watering, and itching, while skin irritation is characterized by itching, scaling, erythema, or sometimes blistering (**Clove oil. <https://pubchem.ncbi.nlm.nih.gov/compound/12658395>**).

Interactions

CEO or eugenol, known to have antiplatelet activity, might increase the risk of bleeding if co-administered with anticoagulant and/or antiplatelet drugs (**Aiamsa-ard et al., 2017**).

In spite of having versatile pharmacological activities, little trials to formulate and evaluate CEO in different delivery systems were reported. Antibacterial effects of Clove essential oil nanoemulsion (CEO-NE) formulations were evaluated in comparison with pure CEO and amikacin antibiotic (as a positive control) (**Anwer et al., 2014**). Another study was implemented by Shahavi and co-authors to investigate the antibacterial activity of CEO-NE (**Shahavi et al., 2016**). Moreover, CEO was incorporated into the PVP-NF₅ mats using electrospinning process with the assistance of cyclodextrins (CDs) to prepare a fast dissolving drug delivery system. Then, antifungal activity against oral fungi and cytotoxicity were evaluated (**Tonglairoum et al., 2016**). These previously prepared NE and PVP-NF₅ mats systems exhibited fast release behavior and just *in vitro* antibacterial and antifungal activities were assessed. Consequently, different controlled release DDS_s are still required to be constructed and evaluated to exploit and potentiate the versatile CEO pharmacological activities. Although documented lines of substantiation supporting the beneficial anti-inflammatory activity of CEO, a thorough review of literature disclosed that fabricating nano topical delivery systems targeted to augment the anti-inflammatory activity of CEO has not been so far studied.

Hence, the aim of this work was to develop controlled release nanoparticulate systems of CEO for topical application with potentiated anti-inflammatory activity and enhanced stability. Firstly, clove essential oil nanoemulsions (CEO-NEs) were developed, characterized and optimized. Secondly, the employment of biopolymers like GG, GA and CS as hydrogel bases is a cost effective as well as a well-documented choice of technology, particularly in topical preparations with extended release characteristics (**Sami et al., 2018**). Based on this perspective, blank hydrogel matrices of the aforementioned polymers were prepared and optimized by adopting Taguchi model with three independently controlled parameters (ICPs) at three levels. Thereafter, the

optimized blank hydrogel formula and the optimized CEO-NE formulation were selected for further formulation into CEO-NE based NEG, which could be more suitable for better topical application. Thirdly, CEO-NE based NF_s was prepared using the optimized NE formulation and PVA. Ultimately, both CEO-NE based NEG and CEO-NE based NF_s would be further characterized and extensively investigated.

Chapter 1:

Preparation of clove essential oil nanoemulsion and its evaluation.

Chapter 2:

Preparation and evaluation of nanoemulgel tailored by Taguchi's model and nanofibers mat from clove essential oil nanoemulsion.

Chapter 3:

Ex vivo permeation, stability and *in vivo* impact of clove essential oil nanoemulgel and nanofibers mat on external inflammation.

Chapter 1

Preparation of clove essential oil nanoemulsion and its evaluation

Introduction

NE is described as a dispersion made up of oil, surfactant, cosurfactant, and aqueous phase, which is thermodynamically stable isotropic nanoparticulate system having a droplet diameter usually in range of 10–200 nm. NE is an auspicious nanovehicle for topical as well as transdermal application owing to its beneficial merits such as high physical and thermodynamic stability as well as enhancing the solubilization capacity, bioavailability and therapeutic efficacy of various drugs and pharmaceuticals (**Lovelyn and Attama 2011; Wu *et al.*, 2013; Arora *et al.*, 2014; Halnor *et al.*, 2018**).

Therefore, the aim of the work in this chapter was to develop, characterize and optimize NE formulations of CEO in order to enhance its anti-inflammatory activity.

Experimental

Materials

- ❖ Clove essential oil (CEO) was obtained from Wako JAPAN, 036-03562, Lot KP J4110.
- ❖ Glycerol monoacetate (GMA) was acquired from Koch-Light Laboratories Ltd., Colnbrook Bucks, England.
- ❖ Polyoxyethylene (20) sorbitan monooleate (tween 80[®]) was purchased from Sigma-Aldrich, Saint Louis, MO, USA.
- ❖ Caprylocaproyl macrogol-8-glyceride (Labrasol) was obtained as a gift sample from Gattefossé, St Priest, France.
- ❖ Other materials as in part I, chapter 1.

Equipment

- ❖ Hot air oven (Heraeus GS model B 5042, Germany).
- ❖ Cone and plate rotary viscometer (Haake Inc., Germany).
- ❖ Other equipment as in part I, chapter 1.

Methodology

1- Spectrophotometric scanning of λ_{\max} of CEO in ethanolic solution

A stock solution, having a concentration of 570 $\mu\text{g/mL}$, was prepared by dissolving 28.5 mg (two drops) of CEO in 50 mL absolute ethanol. Then, 0.2 mL of the ethanolic solution was diluted to 10 mL with distilled water to produce a clear solution with a concentration of 11.4 $\mu\text{g/mL}$. UV–VIS scanning at different wavelengths ranging from 250–400 nm was performed to determine λ_{\max} of CEO using the same volume of pure absolute ethanol (0.2 mL) in 10 mL distilled water as blank.

2- Construction of calibration curve of CEO in ethanolic solution

Calibration curve of CEO in distilled water was constructed spectrophotometrically by measuring the absorbance at the predetermined λ_{\max} value. Different volumes (0.1–0.9 mL) of the prepared stock solution, having a concentration of (570 $\mu\text{g/mL}$), were transferred to 10 mL volumetric flasks and each was diluted to 10 mL with distilled water to produce concentrations of 5.7–51.3 $\mu\text{g/mL}$. Then, the absorbance of these dilutions was measured at the predetermined λ_{\max} by using each one's corresponding blank. The average absorbance values of triplicate measurements were plotted against the concentration of the drug, expressed as $\mu\text{g/mL}$, and the R^2 value was estimated.

3- Preparation of CEO-NEs formulae

CEO-NEs formulae were obtained by mixing 1% w/w of CEO with required amount of GMA (oil phase, varied from 8 to 24% w/w). The fixed amount of surfactant (tween 80[®]): cosurfactant (Labrasol) mixture (S_{mix} (1:1)) (30% w/w) was added to CEO-GMA mixture and water was added in a drop-wise manner to obtain an apparent and clear solution. The composition of CEO-NEs formulae (F-1 to F-5) is listed in **Table 8**. Such NEs formulae were selected based on the pseudo-ternary phase diagram previously constructed by **Anwer et al., 2014** with slight modification by using GMA instead of triacetin as an oil phase.

Table 8: Composition (% w/w) of CEO-NEs formulae (F-1–F-5) prepared using GMA, tween-80[®], labrasol and water.

Code	Formulation composition (% w/w)				
	CEO	GMA	S _{mix} ratio (1:1)		Water
			Tween-80 [®]	Labrasol	
F-1	1	8	15	15	61
F-2	1	12	15	15	57
F-3	1	16	15	15	53
F-4	1	20	15	15	49
F-5	1	24	15	15	45

4- Characterization of CEO-NEs formulae

All the prepared CEO-NEs of the 5 formulae were subjected to thermodynamic stability studies; self-nanoemulsification efficiency tests; drug content estimation; measurement of particle size, PDI, ZP, viscosity (η) as well as percentage transmittance (%T); and pH determination.

4.1. Thermodynamic stability studies

In order to remove metastable and unstable formulations and to select stable one, different thermodynamic stability tests were performed. All prepared formulations were centrifuged at 5,000 rpm (2,180 g) for 30 min and observed for phase separation, creaming, or cracking. Those formulations that didn't show any phase separation were exposed to heating and cooling cycles (three cycles between refrigerator temperature (4°C) and hot air oven temperature (50°C) with storage at each temperature for not less than 48 h). Those formulations which were stable under these stress conditions were subjected to freeze-thaw stress cycles (three cycles between -21°C and +25°C with storage at each temperature for not less than 24 h) (Anwer *et al.*, 2014). Finally, those

formulations which passed these thermodynamic stress tests were further taken for the self-nanoemulsification efficiency tests.

4.2. Self-nanoemulsification efficiency test

The self-nanoemulsification efficiency test was carried out to assess the efficiency of NE for self-nanoemulsifying drug delivery of CEO without any precipitation or phase separation upon dilution with water. To perform this test, one milliliter of each CEO-NE formula was diluted with 500 mL of distilled water (**Anwer et al., 2014**). The *in vitro* performance of the formulations was visually assessed using the following grading system:

- Grade A: Rapidly forming clear/transparent NE (emulsify within 1 min);
- Grade B: Rapidly forming slightly less clear (bluish white) NE (emulsify within 2 min);
- Grade C: Fine milky emulsion (more than 2 min to emulsify);
- Grade D: Dull and grayish white emulsion having slightly oily appearance (more than 3 min to emulsify); and
- Grade E: Formulation with large oil globules at the surface.

4.3. Drug content estimation

The drug content for each CEO-NE formula was calculated by using UV-VIS spectrophotometer. Small volume (0.1 mL) of each formula was diluted to 10 mL using absolute ethanol as a solvent (**Ghareeb and Neamah, 2017**). Then, an appropriate dilution with distilled water was performed and the absorbance was measured at λ_{\max} 279 nm against the same dilution for the corresponding blank of each CEO-NE formula.

4.4. Particle size analysis

The particle size and PDI of all the freshly prepared CEO-NEs formulae were measured using Malvern Zetasizer Nanoseries.

4.5. Zeta potential

ZP is a measure of surface charge of droplets in CEO-NEs formulae. In order to perform this measurement, each CEO-NE formula was conveniently diluted with deionized water and its ZP was determined using Malvern Zetasizer Nanoseries.

4.6. Measurement of viscosity

The η of all CEO-NEs formulae was measured at ambient temperature without any dilution using a cone and plate rotary viscometer. Few drops of each formulation were placed on the stationary plate of viscometer having a diameter of 2.9 cm, while that of the cone was 2.8 cm. The torque value (S_T) was determined at constant speed (n_s) value of 256 rpm (**Ibrahim et al., 2013**).

Then, the η values were calculated using the following equation:

$$\eta = \frac{G \cdot S_T}{n_s}$$

Where;

η : Viscosity in millipascal.second (mPa.s) (mPa.s = 1 centipoise (cP)).

G : Instrumental factor = 14,200 (mPa.s/scale grad. min).

S_T : Torque (scale grad.).

n_s : Speed (rpm).

4.7. Measurement of the percentage transmittance (%T)

The percentage transmittance (%T) as a measurement of optical clarity for the prepared CEO-NEs formulae was assessed spectrophotometrically using UV-VIS spectrophotometer without dilution. The prepared formulae were analyzed at 650 nm using distilled water as a standard blank solution (**Ghareeb and Neamah, 2017**).

4.8. pH determination

The pH measurement was considered as an important parameter for the final product of drug loaded NEs because any amendment in pH will affect the stability of the formulated NEs. pH values of freshly prepared CEO-NEs were measured at 25°C using a calibrated potentiometer.

5- Statistical analysis

The *in vitro* data were presented as mean \pm SD (n=3) and statistically analyzed using ANOVA followed by Tukey-Kramer multiple comparisons test at $p < 0.05$. GraphPad Prism 5 software computer program was employed for the analysis process.

6- Evaluation of CEO-NE (F-1)

6.1. Fourier-transform infrared spectroscopy (FT-IR)

To look into any chemical incompatibility between incorporated CEO and other ingredients, FT-IR analysis was conducted. The FT-IR spectra of pure CEO, CEO diluted in GMA (in a ratio of 1:8 as in the composition of CEO-NE (F-1)), CEO-loaded NE (F-1), and its corresponding blank NE were obtained using an FT-IR spectrophotometer. The FT-IR analysis of pure NE components (namely; GMA, labrasol and tween 80[®]) was also carried out using the same apparatus. The FT-IR spectra of all the tested samples were recorded between 4000 and 400 cm⁻¹.

6.2. Transmission electron microscopy (TEM)

Transmission electron microscopy (TEM) was used to study the surface morphology and particle size distribution of the CEO-NE (F-1). The formula was first diluted with deionized water, then dropped onto carbon coated copper grid, and negatively stained with 2% phosphotungestic acid for 10 s. Whatman filter paper was used to draw-off the excess liquid and the prepared samples were blotted for dryness at room temperature. The samples were observed with TEM and the digital images were captured and analyzed using Digital Micrograph and Soft Imaging Viewer software.

Results and Discussion

1- Spectrophotometric scanning of CEO in ethanolic solution

Figure 20 represents UV scanning from 250-400 nm of CEO solution in distilled water. It was clearly evident from this figure that the spectrum of CEO in this medium was found to have λ_{\max} at 279 nm as reported before (**Hernández-Sánchez *et al.*, 2012**).

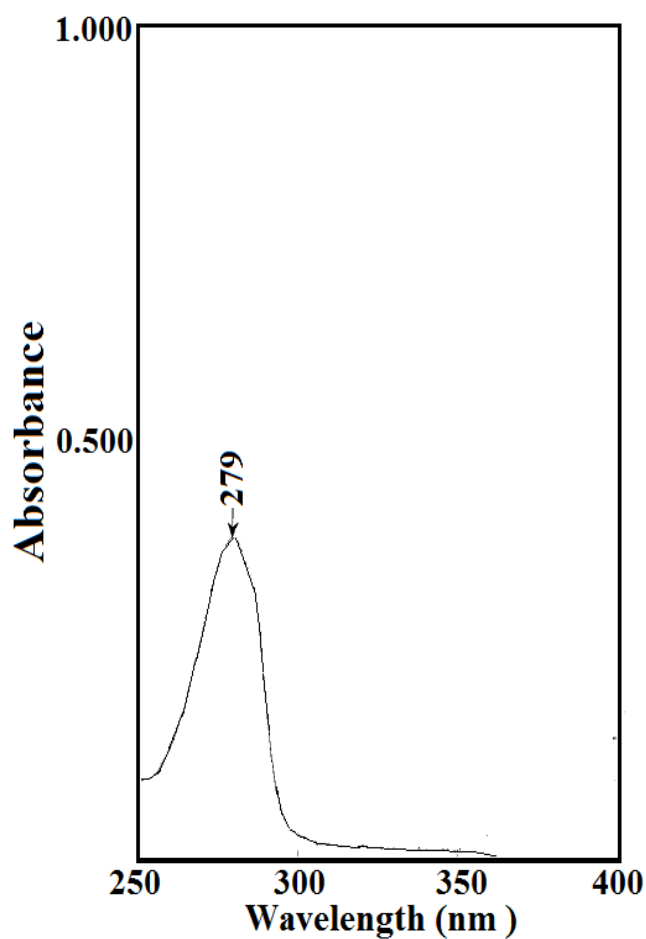


Figure 20: Spectrophotometric scanning of CEO in distilled water.

2- Construction of calibration curve of CEO in ethanolic solution

Figure 21 illustrates the graphical plot of different concentrations of CEO solutions in distilled water against the absorbance at the aforementioned λ_{\max} value. It was observed that the concentration of CEO obeyed Beers-Lambert law at a concentration range of 5.7–51.3 $\mu\text{g/mL}$ with high R^2 (0.9981).

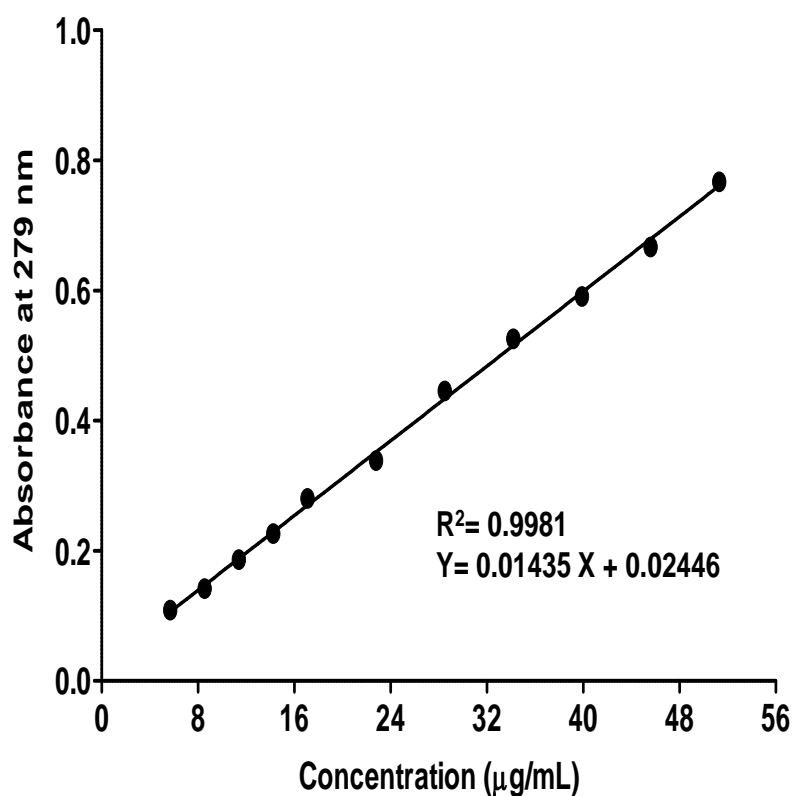


Figure 21: Calibration curves of CEO in distilled water.

Each point represents the mean \pm SD (n=3).

3- Characterization of CEO-NEs formulae

3.1. Thermodynamic stability studies

NEs are known to be thermodynamically stable systems when prepared at a specific concentration of oil, surfactant, cosurfactant and water with no phase separation, cracking or creaming. Thermostability is the key factor that discriminates nano- or microemulsions from macroemulsions that are kinetically unstable along with possibility of phase separation. Additionally, it will prevent frequent tests to be carried out during storage (**Ezealisiji et al., 2017**). Thus, the prepared CEO- NEs formulations were subjected to different thermodynamic stability stress tests in terms of centrifugation, heating/cooling cycles and freeze-thaw cycles. All the formulations were stable during each stress cycle; hence it can be described as thermodynamically stable (**Table 9**).

3.2. Self-nanoemulsification efficiency test

Thermodynamically stable CEO-NEs (F-1–F-5) were further inspected for self-nanoemulsification test using A-E grading systems (**Anwer et al., 2014**). It was observed that all CEO-NEs (F-1–F-5) formulations passed this test with grade A (**Table 9**).

3.3. Drug content estimation

Analysis of drug content for the prepared CEO-NEs (F-1–F-5) showed no evidence of drug degradation and was in the range of $(95.40 \pm 0.04$ to $103.43 \pm 3.05 \%)$ (**Table 10**).

Table 9: Thermodynamic stability and self-nanoemulsification efficiency tests of the prepared CEO-NEs (F-1–F-5).

Code	Thermodynamic stability tests			Self-nanoemulsification efficiency test	Results
	Centrifugation	Heating/cooling	Freeze-thaw		
F-1	√	√	√	A	Pass
F-2	√	√	√	A	Pass
F-3	√	√	√	A	Pass
F-4	√	√	√	A	Pass
F-5	√	√	√	A	Pass

Table 10: Physicochemical characterizations of CEO-NEs (F-1–F-5) in terms of particle size, PDI, ZP, η , % T, pH and drug content (%).

Code	Characterization parameters						
	Particle size (nm)	PDI	ZP (mV)	η (cP)	% T	pH	Drug content (%)
F-1	81.53 \pm 11.15	0.245 \pm 0.04	-14.60 \pm 2.34*	33.28 \pm 7.84*	100.38 \pm 0.75	4.01 \pm 0.07	96.62 \pm 1.78
F-2	44.48 \pm 04.19	0.354 \pm 0.09	-12.63 \pm 1.71*	48.54 \pm 9.81	101.30 \pm 0.17	4.01 \pm 0.04	98.09 \pm 6.35
F-3	57.99 \pm 15.59	0.237 \pm 0.07	-12.59 \pm 3.92*	55.47 \pm 0.00	100.73 \pm 0.75	4.00 \pm 0.05	95.40 \pm 0.04
F-4	59.28 \pm 12.46	0.375 \pm 0.10	-10.15 \pm 0.83	61.02 \pm 7.84	101.60 \pm 0.26	4.01 \pm 0.03	103.43 \pm 3.05
F-5	65.79 \pm 22.33	0.319 \pm 0.16	-04.25 \pm 1.47	73.50 \pm 5.88	100.87 \pm 0.21	4.03 \pm 0.03	101.21 \pm 0.62

Each value represents the mean \pm SD (n=3).

* Significant at $p < 0.05$ vs. F-5.

3.4. Particle size analysis

The particle size of nanocarriers such as NE is one of the most important criteria, as it controls the rate and release of the drug where smaller droplet size resulted in a large surface area providing high drug release for absorption. Also, PDI is a measure of the breadth of the size distribution of NE droplets and it varies from 0.0 to 1.0. The lower the PDI, the higher the homogeneity of the particles in the formulation (**Badran et al., 2014**).

The mean droplet size and PDI, for CEO-NEs (F-1–F-5), was found to be in the range of 44.48 ± 04.19 to 81.53 ± 11.15 nm and 0.237 ± 0.07 to 0.375 ± 0.10 , respectively (**Table 10**). The PDI values were very low designating excellent uniformity in droplet size distribution.

3.5. Zeta potential

ZP measurements carried out on CEO-NEs yielded a measure of the electrical charge carried by the droplets suspended in the aqueous phase. Their values were observed to be in the range of -14.60 ± 2.34 to -04.25 ± 1.47 mV (**Table 10**). It was reported that the spontaneous adsorption of hydroxyl ions (OH^-) from the water phase to the hydrophilic head of the nonionic surfactant (tween 80[®]) as a result of hydrogen bonding is the most distinctly possible mechanism for the small negative interfacial charging (**Teo et al., 2015**). Stabilization of NEs prepared using tween 80[®], as nonionic surfactant, occurs mainly via steric mechanisms.

3.6. Measurement of viscosity

The η of CEO-NEs (F-1–F-5) was observed to be in the range of 33.28 ± 7.84 to 73.50 ± 5.88 cP (**Table 10**). The η was found to be enhanced by increasing the concentration of GMA in the formulations (**Table 8**). A similar observation was published by **Anwer et al., 2014**. It was obvious that the developed NEs have a low η which is one of the characteristic features of the NEs exhibiting Newtonian flow behavior (**Azeem et al., 2009**).

3.7. Measurement of the percentage transmittance (%T)

The %T is an important criterion to determine the isotropic nature of the system. A value of %T closer to 100% reveals that all of the prepared formulae are clear, transparent and globules size in the nanometric range (**Table 10**). In turn, it indicates that the formulae have a large surface area for drug release, and subsequently high capacity to undergo enhanced absorption in biological matrix.

3.8. pH determination

As summarized in **Table 10**, the apparent pH of all formulations is 4 which is compatible with the skin pH of approximately 4-5, hence ensuring their appropriateness for topical and transdermal applications as well as averting any prospect of skin irritation (**Hadgraft, 2001**).

CEO-NE (F-1) was subjected to further elaborate assessments.

4- Evaluation of CEO-NE (F-1)

4.1. Fourier-transform infrared spectroscopy (FT-IR)

Figure 22 shows the FT-IR spectra of native CEO, GMA, labrasol and tween 80[®]. As a comparison, the FT-IR spectra of CEO: GMA dilution (in a ratio of 1:8), CEO-NE (F-1) and its blank are illustrated, as well.

CEO spectrum exhibited signature peaks at 3523, 3071 and 2934 cm^{-1} assigned to O-H, =C-H, and C-H stretching, respectively. As well, sharp peaks at 1609 and 1514 cm^{-1} originated from C=C stretching of the aromatic moiety, whereas peak at 1269 cm^{-1} pointed out to C-O stretching (**Figure 22a**) (**Shende et al., 2016; Tonglairoum et al., 2016**).

For GMA (**Figure 22b**), signals at 1731 and 1377 cm^{-1} from the carbonyl (C=O) stretch of the ester and alcohols (OH), respectively were observed. Additionally, characteristic (C-H alkane stretch) signals were noticed at 2953 and 2890 cm^{-1} , while a distinguished band of OH was recorded at 3406 cm^{-1} (**Lacerda et al., 2015; Arun et al., 2016**).

The infrared spectrum of labrasol (**Figure 22c**) showed broad peaks nearly at 3040-3600 (3416) cm^{-1} (O-H stretch), distinctive sharp peaks at 2925 and 2871 cm^{-1} (C-

H stretch) and at 1736 cm^{-1} (C=O stretch) as well as broad peaks at approximately $1200\text{-}1000$ (1109 cm^{-1} (C-O stretching) (**Karataş and Bekmezci, 2013**).

FT-IR spectrum of tween-80[®] (**Figure 22d**) displayed numerous sharp and intense peaks due to the presence of different functional groups. The strong band around 3449 cm^{-1} could be related to the O-H stretching vibrations. The bands centered at 2925 and 2865 cm^{-1} were associated with methyl (-CH₃) group absorption band and methylene (-CH₂) group stretching vibrations, respectively. The band at 1737 cm^{-1} could be attributed to C=O stretching of the ester group, while the band at 1111 cm^{-1} referred to stretching of C–O–C (**Kura et al., 2014**).

The FT-IR spectrum of CEO: GMA dilution, in a ratio of 1:8, (**Figure 22e**) disclosed the peaks of CEO along with that of GMA. The characteristic peaks of GMA (1731 , 1377 , 2953 , 2890 and 3406 cm^{-1}) were predominant, probably due to dilution effect.

Peaks in blank NE (3418 , 2925 , 2880 , 1731 , 1642 , 1103 cm^{-1}) were related to some peaks in GMA, labrasol, tween-80[®], with a minor shift. This might indicate the occurrence of some interactions between NE components and water, causing a shift and broadening of the peaks, as depicted in **Figure 22f** (**Rachmawati et al., 2015**). CEO-NE (F-1) peaks elicited the same peaks of its blank indicating no interaction (**Figure 22g**).

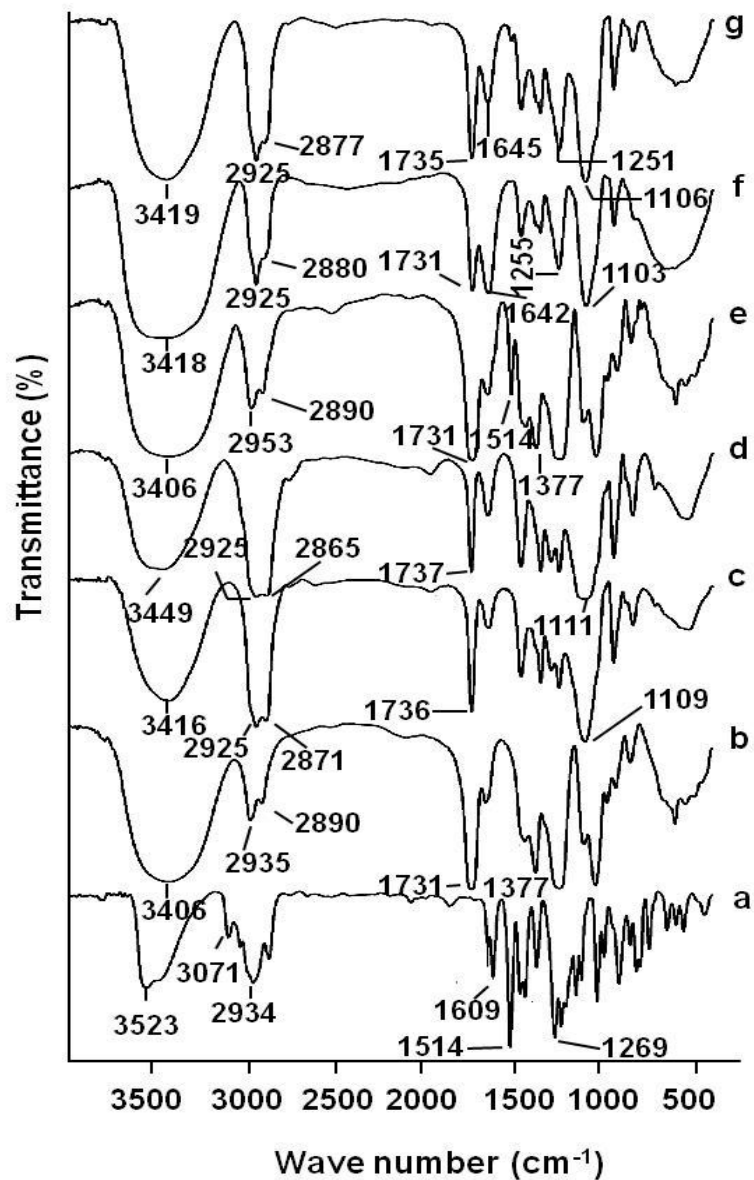


Figure 22: FT-IR spectra of pure CEO (a), GMA (b), Labrasol (c), tween-80[®] (d), CEO: GMA dilution (in a ratio of 1:8) (e) blank NE (f) and CEO-NE (F-1) (g).

4.2. Transmission Electron Microscopy (TEM)

TEM analysis has been one of the most accomplished assessment for identifying the morphology, structure and particle size frequency. **Figure 23** shows homogeneous and spherical droplets of CEO-NE (F-1). It's known that, NE with spherical morphology can disperse well without aggregation (**Izadiyan et al., 2017**).

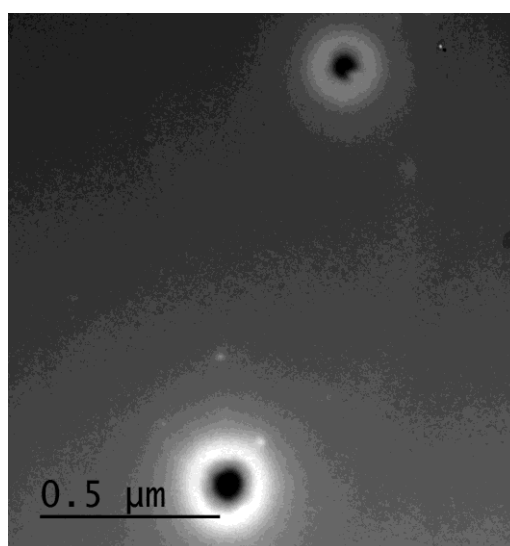


Figure 23: TEM image of CEO-NE (F-1, Table 8).

Conclusions

From the obtained results, it was found that;

- ❖ All CEO-NEs (F-1–F-5) formulae passed thermodynamic stability as well as self-nanoemulsification efficiency tests.
- ❖ All the prepared CEO-NEs formulae were found to have a negative ZP charge, a droplet diameter < 100 nm and PDI values ≤ 0.375 , indicating superior uniformity in the distribution of the droplets besides having small size.
- ❖ All the prepared CEO-NEs formulae expressed high %T values indicating optically clear solutions.
- ❖ FT-IR analysis of CEO-NE (F-1) indicated molecular dispersion of CEO in the oil phase of the NE.
- ❖ CEO-NE (F-1) has spherical shape.

The above results were encouraging to further incorporate CEO-NE (F-1) into hydrogel as well as NF_S matrices for enhanced topical application.

Chapter 2

Preparation and evaluation of nanoemulgel tailored by Taguchi's model and nanofibers mat from clove essential oil nanoemulsion

Introduction

NE formulations of CEO were successfully prepared, characterized and optimized to enhance its expected anti-inflammatory activity (Part II, Chapter 1). However, NE's low η constrains its application for topical and transdermal delivery. Therefore:-

- i. The incorporation of NE into hydrogel matrix can result in NEG with increased η which could be more suitable for better applicability compared to NE as well as better permeation potential through the skin (Arora *et al.*, 2014).
- ii. Alternatively, the incorporation of NE into NF_s matrix may also offers enhanced topical application.

i. Preparation of NEG from CEO-NE (F-1)

Various natural and synthetic polymers are employed for hydrogel preparation. A number of reports are published on hydrogels formation using biopolymers like GG and CS (Sami *et al.*, 2018).

GG, which can be extracted from the seed of the legume *Cyamopsis tetragonalobus*, is a functional polysaccharide consisted of a linear chain of d-mannose residues connected by (1→4)- β -glycosidic linkages. Owing to its biodegradability, biocompatibility, low cost, nontoxicity, high η , as well as high water solubility, GG is recently used in many industries. From the pharmaceutical point of view, its functional properties are of prime importance for controlling the release of drugs in the GIT. For instance, as a carrier for colon targeted drugs in the treatment of colorectal cancer as well as for oral rehydration solutions in the treatment of cholera in adults (Kono *et al.*, 2014).

CS is a natural cationic linear polysaccharide co-polymer consisting of D-glucosamine and N-acetyl-D-glucosamine units produced by deacetylation of chitin. It has remarkable biological properties including biodegradability, biocompatibility, mucoadhesion and nontoxicity. Furthermore, it is a pH sensitive polymer which easily dissolves at low pH while it is insoluble at high pH. Bearing in mind these properties, CS and its derivatives have been applied frequently in biomedical fields (such as wound dressing, tissue engineering and therapeutic/diagnostic agents delivery) in the form of NP_s, fibers, films and hydrogels (Shariatnia and Jalali, 2018).

GA is a dried exudation extracted from the stems and branches of *Acacia Senegal* or closely related species of acacia (family Leguminosae). Mainly, it is a water soluble gum forming solutions over a wide range of concentrations without being highly viscous. GA consists of higher MW polysaccharides as well as their calcium, magnesium and potassium salts, which yield arabinose, galactose, rhamnose and glucuronic acid on hydrolysis. Recently, its extract has been reported to be haemostatic, non-haemolytic, anti-oxidant, and antibacterial in nature (Singha *et al.*, 2017).

Natural hydrogels are more advantageous due to their biodegradability, eco-friendly nature, low-cost production, plentiful raw resources as well as their use to design controlled release DDS_s (Manjanna *et al.*, 2010). Intuitively, NE-loaded into natural hydrogel matrix, prepared by using GG, CS and GA, can result in NEG with dual benefits of facilitating the topical application and augmenting the therapeutic activity of the loaded drugs.

ii. Preparation of electrospun NF_s from CEO-NE (F-1)

NF_s have generated remarkable interest in a number of industries such as food, personal care, chemical and pharmaceutical industries due to their distinctive mechanical, optical, and thermal properties. More recently, electrospun NF_s have been evaluated for their ability to serve as novel controlled release systems, especially topical and transdermal ones. This might be attributed to the fact that NF_s size, surface area and porosity can be accurately controlled by varying different parameters. Electrospinning is the simplest and most efficient fabrication methods employed to produce NF_s with mean

diameters ranging from several tens of nanometers to a few micrometers using solutions of naturally occurring biopolymers or synthetic polymers. PVA is a biocompatible and nontoxic synthetic polymer with great electrospinnability. It has been widely applied for NF_s preparation, either alone or blended with natural polymer (such as CS), as topical and transdermal scaffolds (**Kriegel et al., 2010; Cui et al., 2017**).

A dual aim of the work in this chapter was to prepare CEO-NE based NEG as well as CEO-NE based NF_s for topical application. To achieve such goal, optimization of blank hydrogel matrix was conducted via Taguchi model. The ICPs in the blank hydrogel preparation were the concentration of each of CS (X_1), GG (X_2), and GA (X_3). The dependently measured parameters (DMPs) were pH as well as η at shear rate (γ) of 192 s^{-1} of the prepared blank hydrogels. The optimized blank hydrogel formula was then selected for further formulation into CEO-NE based NEG (using CEO-NE (F-1), Part II, Chapter 1). Moreover, the prepared NEG was inspected visually and further characterized in terms of pH determination, η measurement, and drug content assay as well as FT-IR and DSC studies.

Similarly, CEO-NE based NF_s was prepared using PVA as the polymer and then characterized utilizing scanning electron microscopy (SEM), FT-IR, and DSC along with estimating the drug content.

Experimental

Materials

- ❖ Guar gum (GG) was supplied by Premcem Gums Ltd., India.
- ❖ Polyvinyl alcohol (PVA) with a MW of 146-186 kilodaltons (KDa) and a degree of hydrolysis of 98.0-98.8 mol % was purchased from Acros Organics, New Jersey, USA.
- ❖ Dimethyl sulfoxide (DMSO) with a MW of 78.129 g/mol was obtained from SDFCL, Mumbai-400030, India.
- ❖ Gum acacia (GA) was procured from El-Nasr Pharmaceutical Chemical Co., Cairo, Egypt.
- ❖ Other chemicals were previously mentioned in part I, chapter 1 and part II, chapter 1.

Equipment

- ❖ Overhead mechanical stirrer (T-line Laboratory Stirrer, Talboys Engineering, 230 V).
- ❖ Electrospinning apparatus (MECC CO., Ltd., JAPAN).
- ❖ A sputter gold coater (Sputter Coating Evaporator, SPI Module-Sputter Carbon/Gold Coater, USA).
- ❖ Scanning electron microscopy (JSM 6150, JEOL, Tokyo, Japan).
- ❖ Other equipment as in part I, chapter 1 and part II, chapter 1.

Methodology

1- Preparation, characterization and optimization of blank hydrogels

1.1. Taguchi design of the experiment

The DOE using the Taguchi model offers a simple, efficient, and systematic procedure to determine the optimum conditions (Shahavi *et al.*, 2016; Sadrjavadi *et al.*, 2018). The Taguchi design method utilizes fractional factorial test designs called orthogonal arrays (OAs) that serve to reduce the number of experiments. The selection of a suitable orthogonal array (OA) hangs on the number of factors and their levels. For example, for three parameters at three levels, the conventional full factorial design would require 3^3 or 27 experiments. On the other hand, in the Taguchi L9 OA, the mandatory experiments are only 9 (F-1–F-9). Using OA design, multiple process variables which are concurrently affecting on the performance characteristic can be evaluated, while keeping the number of experiential tests to a minimum. Thus, performance improvement with lower costs and time saving can be achieved following such design. Based on these outstanding merits, Taguchi L9 OA design (three factors with 3-level design) was applied in the current study for statistical optimization of blank hydrogel formulations and inspecting the effects of major factors on responses.

1.1.1. Effective factors and levels

Three ICPs, namely CS concentration (X_1), GG concentration (X_2) and GA concentration (X_3) were analyzed for their paramount influence on blank hydrogels characteristics (Table 11). These levels were selected on the basis of preliminary studies and the optimization procedure was carried out within these limits.

Table 11: ICPs and their levels used in L9 Taguchi OA design.

ICPs	Units	Levels		
		1	2	3
X₁: Concentration of CS	% w/w	1	1.5	2
X₂: Concentration of GG	% w/w	0.5	1	1.5
X₃: Concentration of GA	% w/w	0	2	4

1.1.2. Selection of OA and factor assignments

In this research, L9 OA (three parameters, in three levels), where L and subscript 9 denote the Latin square and the number of the experimental runs, respectively, was used. To observe the data reliably on experiment, pH and η at γ of 192 s^{-1} (as DMPs), were repeated three times with the same conditions. For statistical analysis of the results as well as conditions optimization, Minitab 18 Statistical Software® (Minitab Inc.) was used.

1.1.3. Signal-to-noise ratio ((S/N) ratio)

With respect to the Taguchi model, “signal (S)” and “noise (N)” for output attributes and the (S/N) ratio represents the desirable (S) value and the undesirable (N) value, respectively. The desirable (S) value arises from the ICPs, while the undesirable (N) value originates from factors that cannot be controlled such as environmental factors. (S/N) ratios are computed differently by the model into three different options: “larger is better”, “nominal is the-best”, and “smaller is better”, based on the category of the performance characteristics (Shahavi *et al.*, 2016; Madan and Wasewar, 2017). The objective of this study was to prepare hydrogels with a suitable pH as well as acceptable η for topical application, hence the quality characteristic go for “larger is the better” for (S/N) ratio by the model.

After all of the (S/N) ratios have been computed for each run of an experiment, Taguchi recommends a graphical approach to analyze the data. In the graphical approach, the (S/N) ratios are plotted for each factor against each of its levels.

1.1.4. Statistical analysis

ANOVA (general linear model) was implemented to analyze the paramount influence of each ICPs on blank hydrogels characteristics (DMPs), namely pH and η at γ of 192 s^{-1} and to determine contribution (%) of each factor.

1.2. Preparation of blank hydrogels

Based on Taguchi L9 OA design, blank hydrogels were prepared by blending different concentrations of CS, GG and GA as summarized in **Table 12**. Briefly, CS was dispersed in 1% (w/w) aqueous acetic acid solution using overhead mechanical stirrer

(1,250 rpm), at room temperature for 10 min to make up CS concentrations of 1, 1.5, and 2% w/w. Then, to maintain GG concentrations of 0.5, 1, and 1.5% w/w, GG was sprinkled gently to the aqueous CS solutions while stirring for additional 10 min. For hydrogels formulae containing GA, it was added gradually to attain its concentration at 2 and 4 % w/w and stirring was continued for 5 min. Finally, the prepared hydrogels mixtures were magnetically stirred for 5 h at room temperature. The dispersions were sitted aside overnight to form a gel.

Table 12: Formulations of blank hydrogels by L9 Taguchi OA design.

Formula No.	Formula code (Levels)	Concentration (%w/w)		
		CS (X ₁)	GG (X ₂)	GA (X ₃)
F-1	C ₁ G ₁ A ₁	1	0.5	0
F-2	C ₁ G ₂ A ₂	1	1	2
F-3	C ₁ G ₃ A ₃	1	1.5	4
F-4	C ₂ G ₁ A ₂	1.5	0.5	2
F-5	C ₂ G ₂ A ₃	1.5	1	4
F-6	C ₂ G ₃ A ₁	1.5	1.5	0
F-7	C ₃ G ₁ A ₃	2	0.5	4
F-8	C ₃ G ₂ A ₁	2	1	0
F-9	C ₃ G ₃ A ₂	2	1.5	2

1.3. Physicochemical characterization of the prepared blank hydrogels

1.3.1. Visual examination

Blank hydrogels were inspected visually for their color, homogeneity (appearance and existence of any aggregates), grittiness (presence of grits or particles), and syneresis (phase separation).

1.3.2. pH determination

The pH of various hydrogels formulae was measured using a calibrated potentiometer. The electrode was immersed into each freshly prepared formula 10 min prior to recording the reading at room temperature. Each measurement was performed in triplicate and presented as mean \pm SD.

1.3.3. Rheological study

Rheology is defined as the study of material flow and deformation when external force is applied. The rheological profile of the prepared blank hydrogels formulae was studied using a cone and plate rotary viscometer. The η and the shear stress (τ) of the formulae were measured as a function of the applied γ . To enable construction of η versus γ plots, experiments were conducted by changing γ between 192 and 384 s^{-1} through arbitrary varying the speed (n_s) between 32 and 64 rpm. The η , τ and γ are calculated according to the following equations:

$$\eta = \frac{G \cdot S_T}{n_s}$$

$$\tau = A \cdot S_T$$

$$\gamma = M \cdot n_s$$

Where;

η : Viscosity in mPa.s (mPa.s = 1 cP).

G: Instrumental factor = 10^3 A/M (=14,200) (mPa.s/scale grad. min).

S_T : Torque (scale grad.).

n_s : Speed (rpm).

τ : Shear stress in pascal (Pa).

A: Shear stress factor (Pa/scale grad.).

γ : Shear rate in reciprocal second (s^{-1}).

M: Shear rate factor (minute/second = min/s).

Formulations were carefully applied to the lower stationary plate of viscometer and the upper cone was adjusted. Samples were then allowed to equilibrate for 5 min to attain the running ambient temperature before each measurement (Zakaria *et al.*, 2016)

and to facilitate relaxation of internal stresses introduced during sample loading. Experiments were done in triplicate for each sample, and results were presented as mean \pm SD.

2- Preparation and characterization of CEO-NE based NEG

2.1. Incorporation of CEO-NE (F-1) into the optimized blank hydrogel to prepare CEO-NE based NEG

Four and half milliliters of the selected CEO-NE (F-1) (composed of 1% w/w CEO, 8 % w/w GMA, 30% w/w S_{mix} (tween 80[®]: Labrasol (1:1)), and 61% w/w water (Part II, Chapter 1)) were diluted with water to a weight of 23.375 gm NE (**Lei et al., 2015**). Glacial acetic acid (0.25 gm) was added to the diluted NE to allow the subsequent dispersion of CS in the NEG. The components of the optimized F-9 hydrogel (CS 2 %w/w, GG 1.5 %w/w and GA 2 %w/w) were then added to the diluted NE as previously described under preparation of blank hydrogels to finally prepare 25 gm CEO-NE based NEG.

2.2. Characterization of the prepared CEO-NE based NEG

2.2.1. Visual examination

The prepared CEO-NE based NEG was checked for color, homogeneity, grittiness, and syneresis under normal day light.

2.2.2. pH Determination

The pH of prepared CEO-NE based NEG was measured using a calibrated potentiometer as previously described for blank hydrogels.

2.2.3. Measurement of viscosity

The CEO-NE based NEG's η was measured using a cone and plate rotary viscometer at n_s of 32 rpm (γ of 192 s^{-1}) to determine the suitability of the prepared NEG for topical application.

2.2.4. Assay of drug content

A specific quantity, (2 g) of the prepared CEO-NE based NEG and its corresponding blank, was weighed and dissolved in DMSO and 1% (v/v) aqueous acetic acid solution (10:90%) using an ultrasonic bath for 1 h. One milliliter absolute ethanol

was added to each solution and the final volume was adjusted to 10 mL in a volumetric flask using the aforementioned solvent mixture. CEO content in each formula was estimated at 279 nm spectrophotometrically against the corresponding blank solution. This test was performed in triplicate and drug content was calculated as mean \pm SD.

2.2.5. Fourier-transform infrared spectroscopy (FT-IR)

Each polymer alone (namely: CS, GG and GA) and their physical mixture corresponding to the optimized formula (F-9), as well as medicated NEG and its blank were subjected to FT-IR spectroscopy using an FT-IR spectrophotometer in the range of 4000 to 400 cm^{-1} .

2.2.6. Differential scanning calorimetry (DSC)

Differential scanning calorimetric (DSC) thermograms of pure drug (CEO), medicated CEO-NE (F-1) and its blank, as well as medicated NEG and its blank were performed using a Perkin-Elmer Differential Scanning Calorimeter. It was calibrated with indium (99.99% purity, melting point 156.6°C). The samples were crimped in standard aluminum pans and heated over a temperature range of 35 to 350°C at a constant heating rate of 10°C /min under constant purging of dry nitrogen at 20 mL/min.

3- Preparation and characterization of CEO-NE based NF_s

3.1. Preparation of CEO-NE based NF_s

3.1.1. Polymer (PVA)-CEO-NE (F-1) solution preparation

PVA solution was prepared by dissolving PVA (10% w/w) in aqueous acetic acid (1 % v/v) and heating at 80°C for 3 h to ensure complete dissolution of the polymer. After cooling to room temperature, the polymer solution was blended with CEO-NE (F-1) at a ratio of (3:1 w/w), to keep PVA concentration constant at 7.5 % w/w (Kriegel *et al.*, 2010). The obtained mixture was magnetically stirred for 2 h to ensure a homogeneous distribution and then the dispersion was immediately electrospun to prepare CEO-NE based NF_s.

3.1.2. Electrospinning apparatus

An electrospinning setup described previously by Kriegel *et al.* 2010 was used to electrospin the obtained dispersion. The electrospinning setup consisted of a syringe

pump that could be adjusted to control the solution flow rates (0.1-60 mL/h), a grounded collector plate covered with aluminum foil and a high voltage power supply (0.5-30 kV, 0-50 μ A current). An electrospinning setup was used in all experiments. The prepared dispersion of PVA: CEO-NE (F-1) was loaded into a 5-mL glass syringe with a blunt-end tip (12.3 mm diameter stainless steel capillary, 27 G) and the flow rate was 1.2 mL/h. The flow rate was determined empirically to obtain stable electrospinnable jets. The distance between the capillary tip and the grounded metal collector was 10 cm and a voltage of 20 kV was applied. These conditions were kept constant throughout all experiments. CEO-NE based NF_s were kept at -18°C for overnight, and freeze dried at -80°C under vacuum for 3 h then they were detached from the aluminum foil and stored in refrigerator (at 4°C) for further analysis (Celebioglu *et al.*, 2018). Blank NF_s, as a control, was prepared with the same composition without CEO loading.

3.2. Characterization of CEO-NE based NF_s

3.2.1. Scanning electron microscopy (SEM)

The surface morphology of electrospun CEO-NE based NF_s was observed with a scanning electron microscope (SEM) operated at an accelerating voltage of 20 kV. SEM analysis was performed on a thin piece of NF_s sheared from the center, using a sharp razor blade, and placed on double-sided adhesive tape onto the aluminum SEM stubs. It was made electrically conductive by coating with a thin layer of gold using a sputter gold coater for 60 s to reduce electron charging effects. The average diameters of the individual fibers were measured using image J analysis software (NIH, USA).

3.2.2. Drug content

The total amount of CEO loaded was evaluated by using freeze dried CEO-NE based NF_s and its blank. After freeze drying, 20 mg of the NF_s mats were dissolved in 8 mL 1% (v/v) acetic acid using an ultrasonic bath for 1 h. One milliliter absolute ethanol was added to the medicated and blank solutions and the final volume was adjusted to 10 mL in volumetric flasks using 1% (v/v) acetic acid. The amount of CEO present in the obtained clear solution was quantified at 279 nm spectrophotometrically

using the solution from blank NF_S (Tonglairoum *et al.*, 2016). The experiment was performed in triplicate and drug content was calculated as mean \pm SD.

3.2.3. Fourier-transform infrared spectroscopy (FT-IR)

Characterization of pure PVA, freeze dried CEO-NE based NF_S and its blank mats were conducted using Mattson 5000 FT-IR spectrophotometer at room temperature via KBr pellet technique. In total, the scanning range was 500 to 4000 cm⁻¹.

3.2.4. Differential Scanning Calorimetry (DSC)

Differential scanning calorimetry (DSC) was implemented for thermal characterization of CEO-NE based NF_S using a Perkin-Elmer Differential Scanning Calorimeter. It was calibrated with indium (99.99% purity, melting point 156.6°C). Samples of each of CEO, medicated CEO-NE (F-1) and its blank, pure PVA, freeze dried CEO-NE based NF_S as well as its blank were crimped in standard aluminum pans and heated from 35 to 350°C at a heating rate of 10°C /min under constant purging of dry nitrogen at 20 mL/min.

Results and Discussion

1- Physicochemical characterization and optimization of the prepared blank hydrogels

1.1. Taguchi design of the experiment

1.1.1. Signal-to-noise ratio ((S/N) ratio)

The mean value of the (S/N) ratio in decibel (dB) at different levels of ICPs for mean pH and mean η at γ of 192 s^{-1} are illustrated as (S/N) graphs in **Figure 24 a and b**, respectively. Basically, it is defined in the model that larger (S/N) ratio is the optimized quality characteristic for the prepared hydrogels and in turn will be essential for determining the optimum levels of ICPs.

The L9 OA response values for DMPs and the corresponding (S/N) ratios are shown in **Table 13**. F-9 experienced the highest mean η at γ of 192 s^{-1} as well as the highest mean (S/N) ratio. Meanwhile, the mean (S/N) ratio for every level of the three ICPs is summarized and demonstrated in **Table 14**. As shown in **Table 14**, the delta value of ((maximum–minimum) (S/N) ratios) of CS concentration (X_1) is the highest value for both tested DMPs. Hence, it can be concluded that CS concentration (X_1) is the most important one affecting both the tested DMPs (**Celep and Dincer 2017**).

1.1.2. ANOVA

The purpose of ANOVA, which is a statistically based objective decision-making tool, is to investigate which ICPs significantly affected the DMPs of the prepared hydrogels and to evaluate the contribution (%) of the error (**Table 15**).

Furthermore, **Table 15** contains the ANOVA for (a) pH and (b) η at γ of 192 s^{-1} . In the aforementioned table, the rows marked as “Error” refer to errors caused by (N) (uncontrollable or environmental factors such as temperature and humidity) that are not included in the experiment and the experimental error. Generally, the error contribution (%) value should be less than 50% (**Shahavi et al., 2016**). Fortunately, here, the calculated contribution (%) value of the error was about 0.2% for mean pH experiments and 0.09% for η at γ of 192 s^{-1} experiments. It is noticeable that these values are

significantly under the limit, which means that nearly all studied ICPs have been considered and that errors in the experiments are not significant (**Shahavi et al., 2016**).

Contribution (%) and *F*-value, for each ICPs, were traditionally used to see which design parameters have a significant effect on the quality characteristic. Additionally, the *P*-value reports the significance level (**Table 15**).

It can be observed from **Table 15** that CS concentration (X_1) has the highest contribution (%) and *F*-value as well as the lowest *P*-value compared to GG concentration (X_2) and GA concentration (X_3) for both tested DMPs. **Figure 25** shows the contribution (%) of CS concentration (X_1) which has the highest significant effect on the prepared hydrogels' performance indicators; pH as well as η at γ of 192 s^{-1} .

A profound look to ANOVA data (**Table 15**) demonstrated the discrepancy in the contribution (%) of GG and GA in both tested DMPs. For instance, GG contribution (%) was higher than that of GA in case of η measurement and vice versa in pH data. It should be kept in consideration that the η is the vital DMPs as its values were greatly influenced by the ICPs attested while pH measurements were in the acceptable range in all the prepared formulae (**Table 13**). Consequently, GG represents the secondary effective ICPs following CS compared to GA. Based on the above mentioned data, it can be deduced that CS concentration (X_1) is the most pivotal parameter affecting the tested DMPs. Such conclusion coincides with that obtained from the (S/N) ratio response tables (**Table 14**).

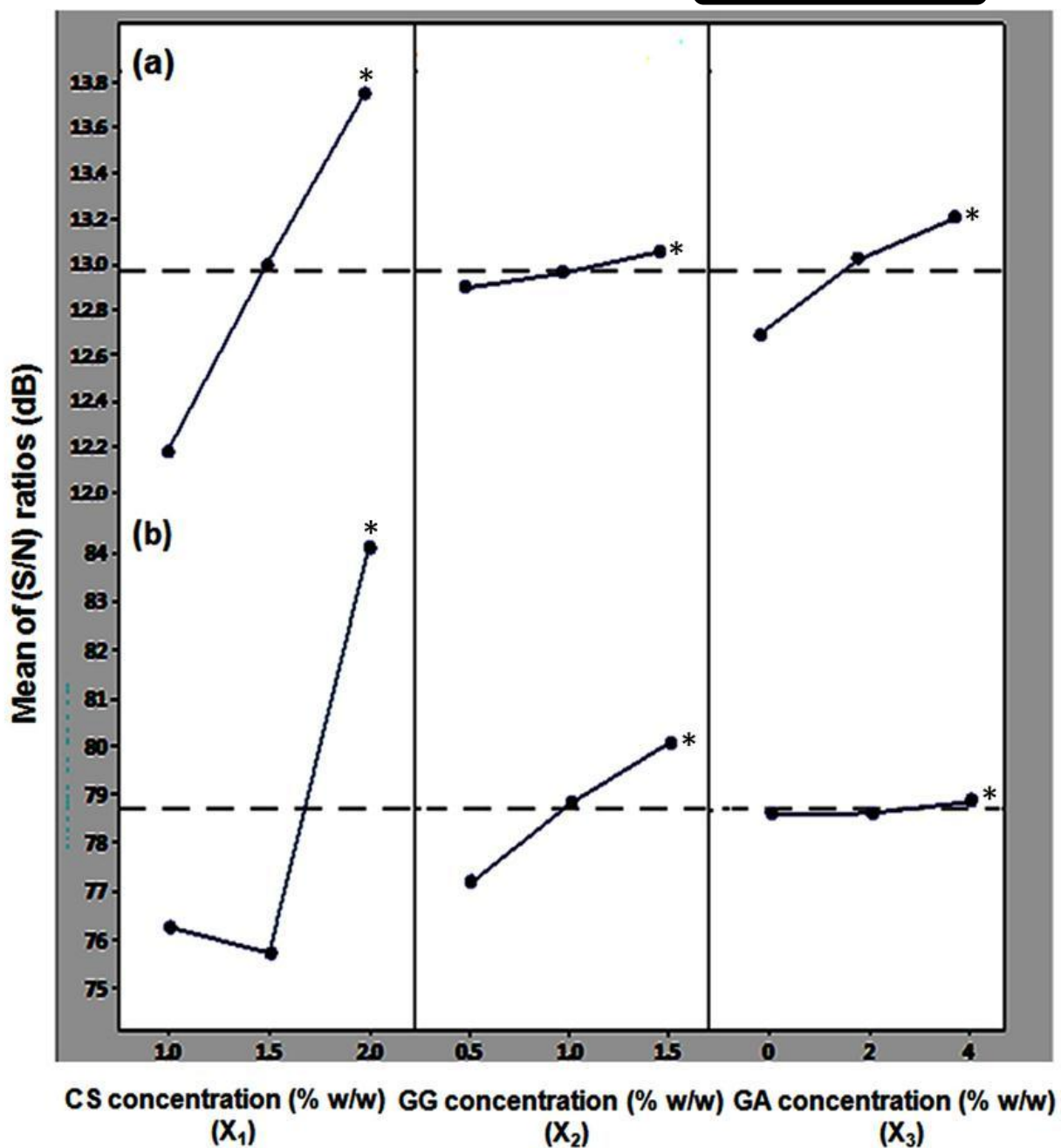


Figure 24: Graphs illustrating the mean (S/N) ratios of the DMPs against the concentration of the different ICPs.

* Are the highest values.

((a) mean pH, (b) mean η at γ of 192 s^{-1}) See **Table 14**.

Table 13: Taguchi L9 OA response values and (S/N) ratios for DMPs of the prepared blank hydrogels (See **Table 11** and **12**).

Formula No.	Mean pH*	(S/N) ratio for mean pH	Mean η (cP) at γ of 192 s^{-1}*	(S/N) ratio for mean η at γ of 192 s^{-1}
F-1	3.87 ± 0.01	11.75	5214.06 ± 156.89	74.34
F-2	4.09 ± 0.05	12.23	6767.19 ± 156.89	76.61
F-3	4.23 ± 0.03	12.53	7765.62 ± 313.78	77.80
F-4	4.47 ± 0.02	13.01	5103.12 ± 313.78	74.16
F-5	4.55 ± 0.03	13.16	6101.56 ± 470.67	75.71
F-6	4.37 ± 0.04	12.81	7321.87 ± 313.78	77.29
F-7	4.97 ± 0.04	13.93	14200.00 ± 1568.89	83.04
F-8	4.73 ± 0.05	13.50	16085.94 ± 1412.01	84.13
F-9	4.91 ± 0.02	13.82	17971.88 ± 313.78	85.09

*Average of three determinations.

Table 14: Computer calculated (S/N) ratios for the tested DMPs (a) mean pH and (b) mean η at γ of 192 s^{-1} (cP) with regard to the different ICPs (See **Table 11**).

(a)				(b)			
Level	CS concentration	GG concentration	GA concentration	Level	CS concentration	GG concentration	GA concentration
1	12.17	12.90	12.69	1	76.25	77.18	78.59
2	12.99	12.96	13.02	2	75.72	78.82	78.62
3	13.75	13.05	13.20	3	84.09	80.06	78.85
Delta	1.58	0.16	0.52	Delta	8.37	2.88	0.26
Rank	1	3	2	Rank	1	2	3

Delta = (maximum–minimum) (S/N) ratios.

Rank according to the value of delta.

Table 15: ANOVA for the tested DMPs (a) mean pH and (b) η at γ of 192 s^{-1} (cP).

ICPs	Degree of freedom (DF)	Sum of squares (SS)	F-value	P-value	Contribution (%)
(a)					
CS concentration	2	0.97609	439.24	0.002	89.60
GG concentration	2	0.00702	3.16	0.240	0.64
GA concentration	2	0.10409	46.84	0.021	9.55
Error	2	0.00222			0.20
Total	8	1.08942			100.00
(b)					
CS concentration	2	188701193	1095.18	0.001	93.61
GG concentration	2	12167661	70.62	0.014	6.04
GA concentration	2	549721	3.19	0.239	0.27
Error	2	172302			0.09
Total	8	201590877			100.00

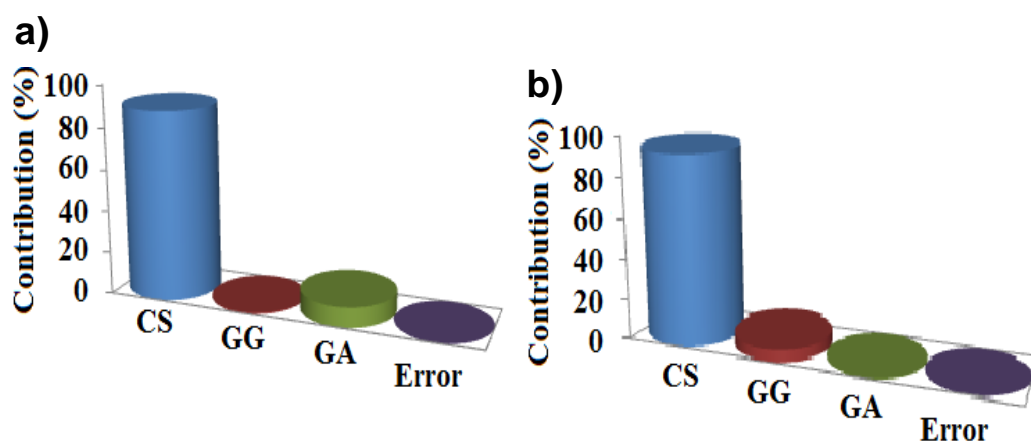


Figure 25: Results of ANOVA for contribution (%) of each factor on the performance characteristics (a) pH and (b) η at γ of 192 s^{-1} .

1.2. Physicochemical characterization of the prepared blank hydrogels

1.2.1. Visual examination

Results of the visual inspection of the blank hydrogels are presented in **Table 16**. All of the prepared blank hydrogels were either yellow transparent or off white translucent in color. All of them showed very good homogeneity, smooth homogenous texture with lack of lumps and/or syneresis. No indications of grittiness, as well.

Table 16: Results of visual inspection of the blank hydrogels prepared by Taguchi L9 OA design.

Formula No.	Color	Homogeneity	Grittiness
F-1	Yellow, transparent	+++	—
F-2	Off White, translucent	+++	—
F-3	Off White, translucent	+++	—
F-4	Off White, translucent	+++	—
F-5	Off White, translucent	+++	—
F-6	Yellow, transparent	+++	—
F-7	Off White, translucent	+++	—
F-8	Yellow, transparent	+++	—
F-9	Off White, translucent	+++	—

1.2.2. pH determination

pH values of the prepared blank hydrogels were in the range of 3.87 ± 0.01 to 4.97 ± 0.04 . The increment of CS concentration (X_1) increases the number of free amino groups which may undergo protonation, thus remarkably reducing the number of free protons and increasing pH values as shown in **Table 13**. Such manner matches the results obtained from both (S/N) ratio response as well as ANOVA tables (**Tables 14 and 15**) which approved that CS concentration (X_1) is the most important parameter

affecting pH value. The formulations containing CS (2% w/w) exhibited the highest pH values ranged from 4.73 ± 0.05 to 4.97 ± 0.04 , which are suitable for topical application (Hadgraft 2001; Abdul Rasool *et al.*, 2010).

1.2.3. Rheological study

CS and GG are known to exhibit pseudoplastic or shear-thinning behavior in aqueous solutions which refers to decrease in η with increasing γ (El-Hefian *et al.*, 2010; Mudgil *et al.*, 2014). F-9, having both CS and GG concentrations at their highest level, level 3, and GA concentration at its medium level, level 2, (Table 12), disclosed the highest η amongst all the prepared blank hydrogels at γ of 192 s^{-1} (Figure 26 and Table 13).

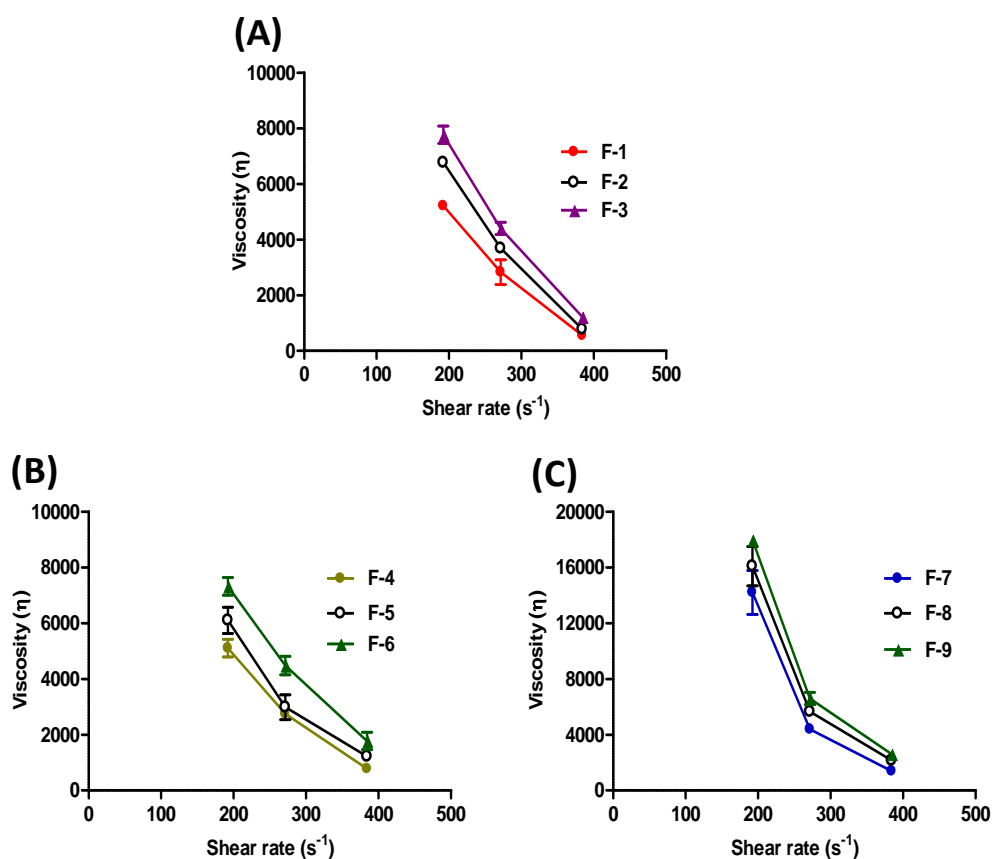


Figure 26: Shear thinning behavior of the prepared blank hydrogels with F-9 having the highest η .

Since F-9 experienced the highest η and acceptable pH of 4.91 ± 0.02 , which is suitable for skin application, it was selected for further elaborate formulation into CEO-NE based NEG.

2- Characterization of the prepared CEO-NE based NEG

2.1. Visual examination

CEO-NE based NEG was homogenous, yellow and transparent as well as free from any turbidity or grittiness.

2.2. pH Determination

CEO-NE based NEG has pH value of 4.51 ± 0.01 , which is suitable for topical application (Hadgraft 2001; Abdul Rasool *et al.*, 2010).

2.3. Measurement of viscosity

Intrestingly, the measured η of the prepared CEO-NE based NEG, 6545.31 ± 156.89 cP, is in between that of the blank hydrogel F-9 (Table 13) and that of the selected NE (CEO-NE (F-1), Table 10, Part II, Chapter 1) which will be more acceptable for topical application (Elmataeshy *et al.*, 2018).

2.4. Assay of drug content

Drug content for the prepared CEO-NE based NEG was found to be 99.350 ± 1.672 %.

2.5. Fourier-transform infrared spectroscopy (FT-IR)

Figure 27 shows the FT-IR spectra of native CS, GG, GA and their physical mixture corresponding to the optimized formula (F-9). As a comparison, the FT-IR spectra of CEO-NE based NEG and its blank are depicted, as well.

A typical characteristic polysaccharide absorption bands at 3447 and 3422 cm^{-1} ($-\text{OH}$ groups stretching) were obvious in the spectra of the three used polymers CS, GG and GA (Figure 27a, b and c, respectively). Similarly, the aforementioned spectra possess peaks at 3000 - 2800 and 1651 cm^{-1} which stand for aliphatic groups ($-\text{CH}_2$ and $-\text{CH}_3$) and carbonyl group ($-\text{C}=\text{O}$) stretching vibrations, respectively.

On the other hand, in the range of 800 - 1500 cm^{-1} , CS shows several peaks (Figure 27a). The peaks at 1425 and 1340 cm^{-1} represent oscillations characteristic for

–OH and C–H bending of CH₂ groups, respectively. The peak at 1381 cm⁻¹ is related to the C–O stretching of the primary alcoholic group (–CH₂–OH). Additionally, the broad peak at 1154-1031 cm⁻¹ represents the bridge –O– stretch of the glucosamine residues (**Modrzejewska et al., 2013; and Bianchera et al., 2014**).

In case of GG (**Figure 27b**), peak at 1007 cm⁻¹ and region around 1400 cm⁻¹ were due to O–H bending vibrations and CH₂ deformation, respectively (**Mudgil et al., 2012; Sharma et al., 2015**). Additionally, pure GA spectrum (**Figure 27c**) shows different peaks at 1426 cm⁻¹ (O–H bending of acid group), 1072 cm⁻¹ (C–O stretching) and 1030 cm⁻¹ (O–H bending) (**Borodina et al., 2011**).

FT-IR spectrum of the polymers physical mixture showed neither disappearance of existed peaks nor appearance of extra peaks, thereby establishing the absence of physical interaction between the polymers at the used ratio (**Figure 27d**).

FT-IR spectra of the blank NEG and CEO-NE based NEG (**Figure 27e and f**, respectively), elucidate the peaks of blank NE and/or that of CEO-NE (F-1) (as depicted in **Figure 22f and g**, Part II, Chapter 1) along with the used polymers' characteristic peaks reflecting the molecular dispersion of NE either blank or medicated in the prepared NE based NEG.

2.6. Differential scanning calorimetry (DSC)

Differential scanning calorimetry (DSC) was accomplished to study the thermal behavior of the CEO in the prepared CEO-NE based NEG, and the thermograms are depicted in **Figure 28**. Pure CEO, **Figure 28a**, showed well-defined endothermic events, at 155.647 and 207.968°C, attributed to the CEO boiling and evaporation processes (**Tonglairoum et al., 2016**). In the thermograms of both blank NE and CEO-NE (F-1), **Figure 28b and c**, respectively, an endothermic peak was observed around 100°C, most probably due to water evaporation. Such behavior suggests that CEO was molecularly dispersed in the oil phase of the NE (**Cekić et al., 2015**). Likewise, the same behavior was noticed in the thermograms of both blank NEG and CEO-NE based NEG, **Figure 28d and e**, respectively, revealing the molecular dispersion of CEO in the prepared NEG (**Dhibar et al., 2018**).

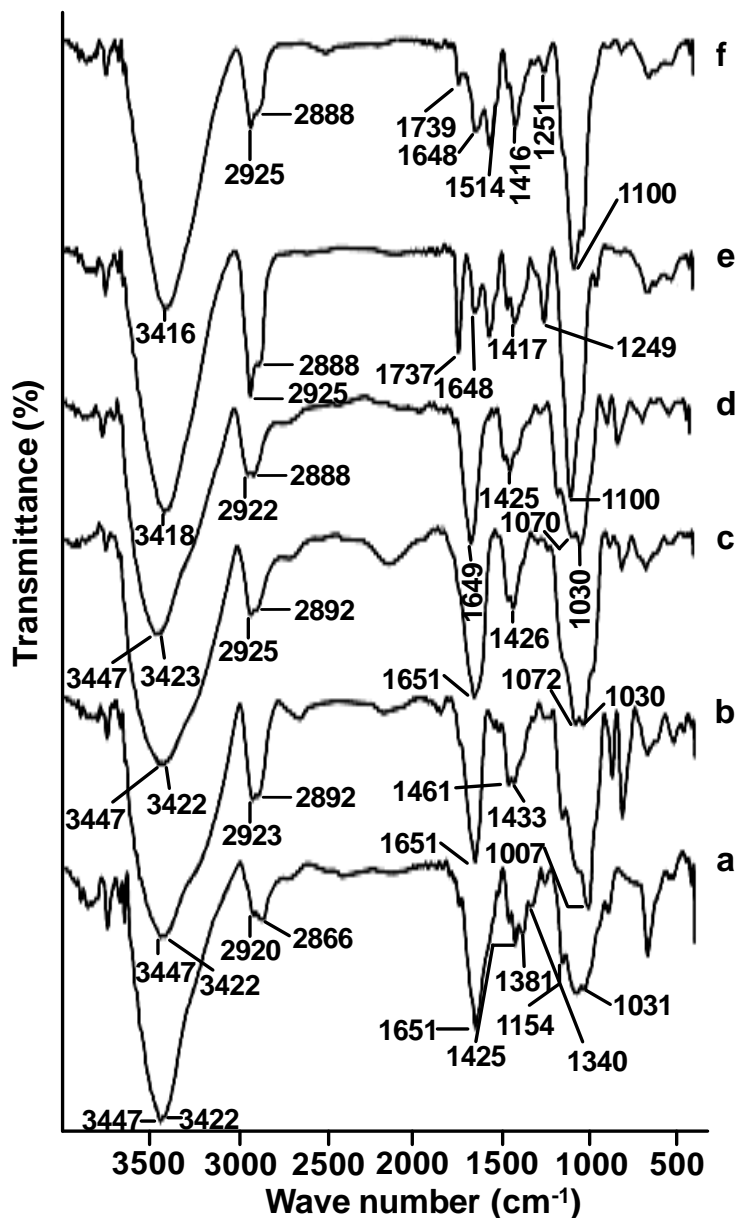


Figure 27: FT-IR spectra of pure CS (a), GG (b), GA(c), physical mixture of the optimized formula (F-9) (d), blank NEG (e) and CEO-NE based NEG (f) (See **Figure 22**, Part II, Chapter 1).

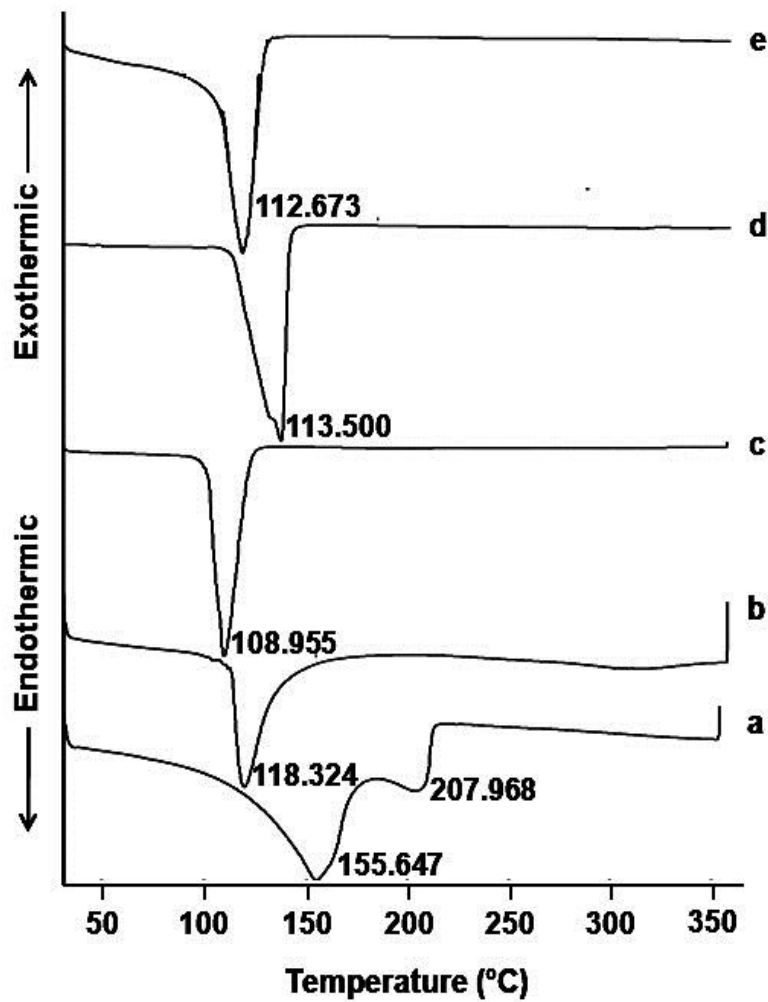


Figure 28: DSC of pure CEO (a), blank NE (b), CEO-NE (F-1) (c), blank NEG (d), and CEO-NE based NEG (e).

3- Characterization of CEO-NE based NF_S

3.1. Scanning electron microscopy (SEM)

The SEM image and the diameter distribution histogram of the CEO-NE based NF_S mats are illustrated in **Figure 29**. This image revealed bead-free and smooth NF_S without phase separation of the NE from the NF_S mats. The average diameters of the CEO-NE based NF_S were 306.4 ± 92.1 nm.

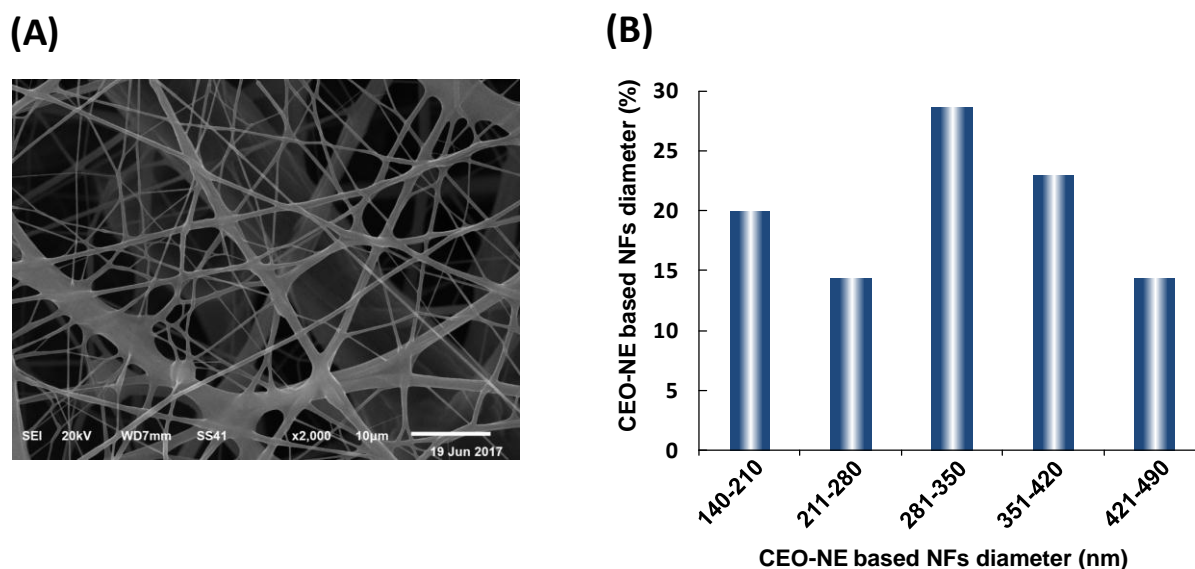


Figure 29: SEM image (A) and diameter distribution histogram (B) of CEO-NE based NF_S.

3.2. Drug content

The amount of CEO was found to be 1.00 ± 0.03 mg CEO loaded in 100 mg CEO-NE based NF_S (DEE% = 40.02 ± 1.15 %).

3.3. Fourier-transform infrared spectroscopy (FT-IR)

The FT-IR spectra of pure PVA, as well as freeze dried mats of blank and CEO-NE based NF_S are shown in **Figure 30**. In **Figure 30a**, all major peaks pertained to hydroxyl and acetate groups (residue from saponification reaction of polyvinyl acetate) were observed in the FT-IR spectrum of PVA. More particularly, the broad band

inspected between 3681 and 3129 cm^{-1} is correlated to the O-H stretch from the intermolecular and intramolecular hydrogen bonds. The vibrational peak observed between 2860 and 2987 cm^{-1} is the outcome of the C-H stretch from alkyl groups. The bands between 1773 and 1702 cm^{-1} are owing to the C=O stretching, from the existing acetate groups in PVA, while that at 1650 cm^{-1} is due to O-H bending (water absorption band). Additionally, the peaks at 1340 and 1316 cm^{-1} are due to C-H bending, while those at 1266 and 1100 cm^{-1} correspond to C=O vibration and C-O stretching in C-O-H group, respectively (**Han et al., 2009; Alhosseini et al., 2012**).

The spectra of blank NF₅ and CEO-NE based NF₅ mats (**Figure 30b and c**) showed all features of the peaks that were displayed in the spectra of both CEO-NE (F-1) and its blank (as elucidated in **Figure 22f and g**, Part II, Chapter 1) along with PVA characteristic peaks. It seems to be the evidence for the complete dispersion of the CEO-NE (F-1) into PVA polymer matrix.

3.4. Differential Scanning Calorimetry (DSC)

Differential scanning calorimetry (DSC) studies were accomplished to probe the thermal behavior of the CEO in the electrospun NF₅ mats, and the thermograms are displayed in **Figure 31**. Pure CEO, blank NE and CEO-NE (F-1) peaks, **Figure 31a, b and c**, were discussed previously (in section 2.6. DSC of CEO-NE based NEG).

Additionally, the DSC of PVA, **Figure 31d**, shows two melting endothermic peaks at 216.281 and 314.482°C (**Gökmeşe et al., 2013**). The thermograms of the blank NF₅ and CEO-NE based NF₅ mats (**Figure 31e and f**) are quite similar, where they show a broad endothermic peaks corresponding to dehydration at 77.566°C and 72.399, respectively. Besides, the two peaks of PVA melting show minor shift compared to that of the pure PVA thermogram. This DSC data clarify that CEO is molecularly dispersed into the PVA-NF₅ matrix, which matches FT-IR data.

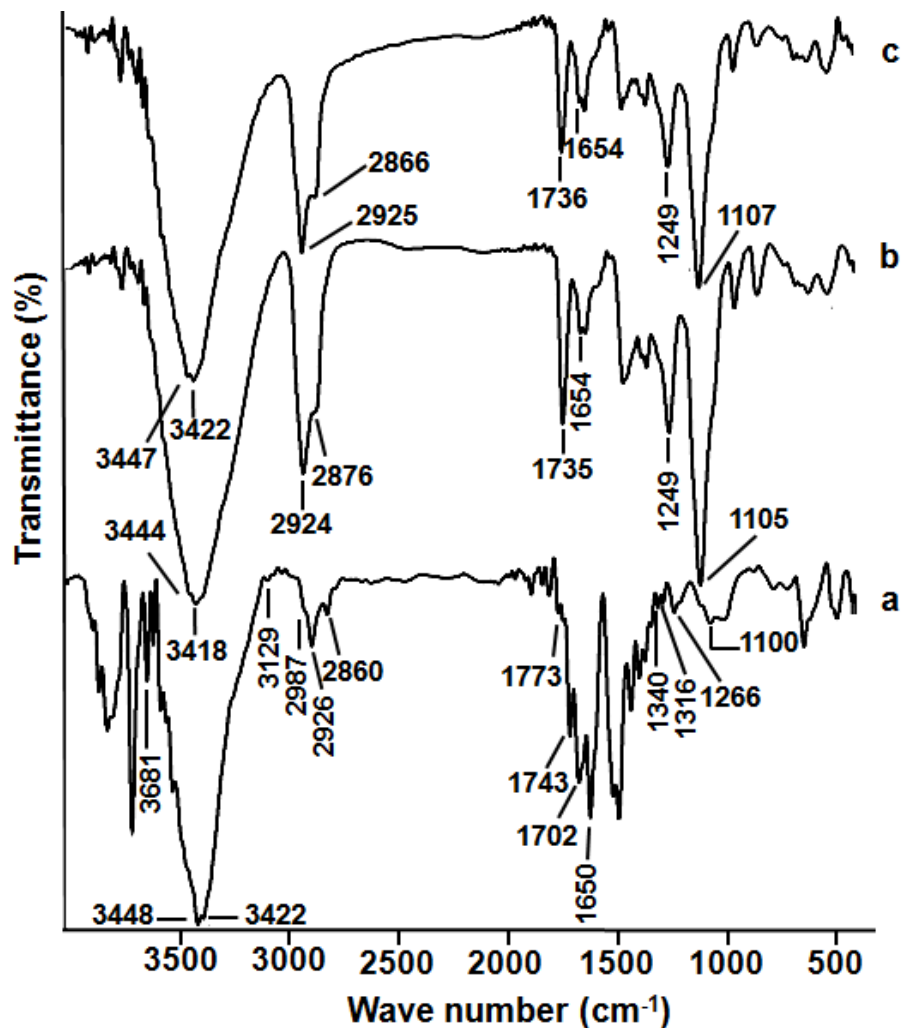


Figure 30: FT-IR spectra of pure PVA (a), blank NF_s (b), and CEO-NE based NF_s (c) (See Figure 22, Part II, Chapter 1).

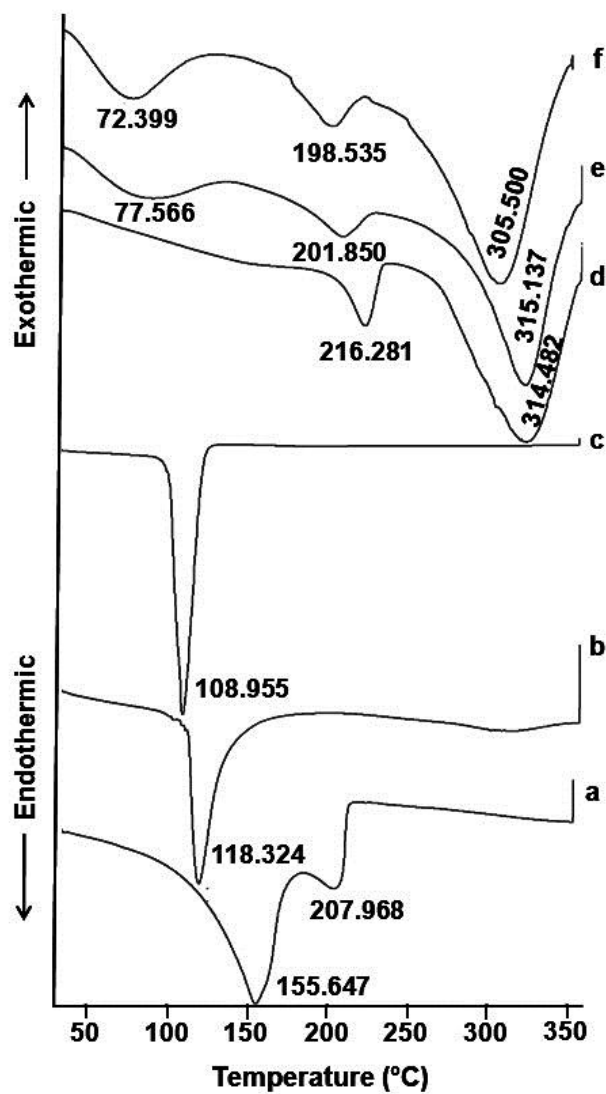


Figure 31: DSC of pure CEO (a), blank NE (b), CEO-NE (F-1) (c), PVA (d), blank NF_s (e), and CEO-NE based NF_s (f).

Conclusions

From the obtained results, it was found that;

- ❖ The DOE using the Taguchi model offers a simple, efficient, and systematic procedure to determine the optimum hydrogel formula for loading CEO-NE (F-1).
- ❖ F-9, with (X_1 (CS 2% w/w), X_2 (GG 1.5% w/w), X_3 (GA 2% w/w)), was found to be the optimized blank hydrogel formula with the highest η at γ of 192 s^{-1} and pH of 4.91 ± 0.02 , which makes it suitable for topical application.
- ❖ F-9 was subjected to further elaborate formulation into CEO-NE based NEG.
- ❖ CEO-NE based NEG is homogenous, yellow and transparent.
- ❖ CEO-NE based NEG has a suitable pH value as well as an increased η , compared to CEO-NE (F-1), being more acceptable for topical application.
- ❖ Both FT-IR and DSC data established the molecular dispersion of CEO and NE's components in the prepared NEG.
- ❖ SEM image of the CEO-NE based NF_S mats displayed a bead-free and smooth NF_S with nanometric size.
- ❖ Both FT-IR and DSC data indicated complete dispersion of the CEO-NE (F-1) into PVA polymer matrix of the NF_S.

The above results were encouraging to further evaluate CEO-NE based NEG as well as CEO-NE based NF_S mats in terms of *ex vivo* permeation, stability, and *in vivo* studies.

Chapter 3

***Ex vivo* permeation, stability and *in vivo* impact of clove essential oil nanoemulgel and nanofibers mat on external inflammation**

Introduction

In the process of biological permeation, the *ex vivo* drug permeation study through rat skin is an important step in paving the way for predicting how a drug would behave *in vivo*. Hence, an *ex vivo* skin permeation study should be performed in order to estimate the potential of the developed topical dosage form for skin targeting and permeation ability. Noteworthy, in the development of any formulation, stability evaluation is an essential prerequisite step before conducting the *in vivo* assessment study.

Consequently, the aim of the work in this chapter was to further appraise CEO-NE based NEG as well as CEO-NE based NF_s with respect to *ex vivo* permeation, kinetic analysis, and stability for a period of six months at refrigeration ($5 \pm 3^{\circ}\text{C}$) and ambient conditions. Finally, *in vivo* anti-inflammatory activity of the aforementioned medicated formulae against croton oil-induced mouse skin inflammation model in comparison with that of the corresponding plain ones and pure CEO was investigated. Assessments regarding histopathological examination and immunohistochemical (IHC) detection of cyclooxygenase-2 (COX-2) expression level were implemented. As well, the safety profile of CEO-NE based NEG and CEO-NE based NF_s was evaluated by skin irritation test.

Experimental

Materials

- ❖ Croton oil was obtained from Sigma-Aldrich, Saint Louis, MO, USA.
- ❖ Primary anti-COX-2 (Polyclonal PA137504), Thermo Fisher Scientific, Waltham, MA, USA.
- ❖ Universal kit (secondary antibody and 0.04% 3, 3'-diaminobenzidine tetrahydrochloride (DAB), DAKO, Denmark.
- ❖ Tegaderm, 3M Health Care, USA.
- ❖ Other chemicals were previously mentioned in part I, chapter 1 and part II, chapters 1 and 2.

Equipment

- ❖ Light microscope (Olympus, Tokyo, Japan).
- ❖ Other equipment as in part I, chapter 1 and part II, chapter 1.

Methodology

1- Spectrophotometric scanning of λ_{\max} of CEO in phosphate buffer, pH 7.4

Spectrophotometric scanning of CEO, in phosphate buffer, pH 7.4, was carried out to determine λ_{\max} . CEO was dissolved in absolute ethanol, as previously mentioned in part II chapter 2, to obtain a stock solution with a concentration of 570 $\mu\text{g/mL}$. An exact volume of 0.2 mL of the absolute ethanolic solution was diluted to 10 mL with phosphate buffer, pH 7.4 to produce a clear solution (11.4 $\mu\text{g/mL}$) followed by UV–VIS scanning at different wavelengths ranging from 250–400 nm to determine λ_{\max} of CEO. Pure absolute ethanol (0.2 mL) in 10 mL phosphate buffer, pH 7.4 was the blank.

2- Construction of calibration curve of CEO in phosphate buffer, pH 7.4

Calibration curve of CEO in phosphate buffer, pH 7.4 was constructed spectrophotometrically by measuring the absorbance at the predetermined λ_{\max} value. Different volumes (0.1–0.9 mL) of the prepared stock solution, having a concentration of (570 $\mu\text{g/mL}$), were transferred to 10 mL volumetric flasks and each was diluted to 10 mL with phosphate buffer, pH 7.4 to produce concentrations of 5.7–51.3 $\mu\text{g/mL}$. Then, the absorbance of these dilutions was measured at the predetermined λ_{\max} by using each one's corresponding blank. The mean absorbance values of triplicate measurements were plotted against the concentration of CEO, expressed as $\mu\text{g/mL}$, and (R^2) was estimated.

3- *Ex vivo* skin permeation study

3.1. Skin permeation experiment

All animal experiments and skin samples preparations throughout the *ex vivo* and *in vivo* studies were accomplished after approval from the Scientific Committee of the Faculty of Pharmacy, Mansoura University, Egypt, in accordance with the Principles of Laboratory Animal Care NIH publication, 1985 revision.

Before carrying out the *ex vivo* permeation experiment, the hair of the abdominal side of newborn Wistar albino rats (two weeks old) was removed using an animal hair clipper. After 24 h, the skin was carefully inspected visually for its integrity. Then, the

rats were sacrificed and the abdominal skin was excised with subsequent removal of the adhering fat and visceral debris. Ultimately, the skin was wholly rinsed with distilled water and soaked overnight in an isotonic solution (0.9% NaCl) at a refrigerator temperature, before the experiment.

Using locally fabricated Franz diffusion cells in a shaking incubator may act as a comparative tool for drug diffusion and permeation studies from topical formulations, for instance NEG and NF_S matrices. Thus, a shaking incubator maintained at $37 \pm 0.5^\circ\text{C}$ throughout the *ex vivo* skin permeation experiment as well as Franz diffusion cells consisting of donor and receptor compartments were used.

The excised rat skin was mounted on the donor half-cell, having a diameter of 1.5 cm and a surface area of 1.767 cm^2 , with the stratum corneum (SC) side faced the donor, whilst the dermal side was toward the receptor compartment. CEO in phosphate buffer, pH 7.4 ($\sim 2.33\text{ mg/mL}$), CEO-NE based NEG or CEO-NE based NF_S mat, containing the same amount of CEO, was introduced in the donor compartment and the receptor compartment was filled with 10 mL phosphate buffer, pH 7.4 and shaken at 75 rpm.

At predetermined intervals, 0.5, 1, 2, 3, 4, 5, 6, 7, 8, 24, 30 and 48 h, aliquots of the medium were withdrawn from receptor compartment and replenished with an equal volume of fresh medium in order to maintain the sink condition throughout the experiment. The collected aliquots were filtered by $0.45\ \mu\text{m}$ millipore filter and analyzed for drug amount using a UV–VIS spectrophotometer at 279 nm. Each experiment was done in triplicate. The same protocol was implemented utilizing plain formulae corresponding to each of the investigated medicated ones as blank to abolish any interference arising from rat skin and formulae components.

3.2. Skin permeation parameters

The cumulative amount of CEO permeated the Wistar albino rats skin per unit area in the receiver chamber (Q , $\mu\text{g}/\text{cm}^2$) was plotted as a function of time (t , h) for the prepared CEO-NE based NEG, CEO-NE based NF_S and pure CEO. The following skin permeation parameters were calculated as reported by **Ahmed and Rizq 2018**; **Elmataeeshy et al., 2018**:

- Q_{48h} : The cumulative amount of CEO permeating the Wistar albino rats skin after 48 h per unit area ($\mu\text{g}/\text{cm}^2$).
- J_{ss} : Steady-state flux ($\mu\text{g}/\text{cm}^2\cdot\text{h}$) which was calculated from the slope of the linear portion of the plotted permeation curve according to the succeeding equation:

$$J_{ss} = \frac{dQ}{dt} \cdot A$$

- K_p : Permeability coefficient (cm/h) was then calculated by dividing the steady-state flux (J_{ss}) by initial drug concentration (C_0 , $\mu\text{g}/\text{mL}$) in the donor compartment of the Franz diffusion cell as given below:

$$K_p = \frac{J_{ss}}{C_0}$$

- ER_{flux} : Enhancement ratio of flux was calculated by dividing the J_{ss} of the respective formulation (either CEO-NE based NEG or CEO-NE based NF_S) by the J_{ss} of pure CEO (control) as given below:

$$ER_{flux} = \frac{J_{ss} \text{ of formulation}}{J_{ss} \text{ of control}}$$

3.3. Kinetic analysis of drug permeation data

To describe the mechanism of CEO permeation through the Wistar albino rats skin from the prepared CEO-NE based NEG, CEO-NE based NF_S as well as pure CEO; the data obtained from the *ex vivo* permeation study were analyzed using different kinetic models. Three kinetic models which include zero-order (1), first-order (2), and Higuchi square root models (3) were applied to the data (**Ahmed and Rizq 2018**):

$$Q_t = K_0 t \quad (1)$$

Where Q_t is the amount of drug permeated at time t , K_0 is the zero order rate constant and t is the time.

$$\text{Log } Q_t = \text{Log } Q_0 - \frac{K_1 t}{2.303} \quad (2)$$

Where Q_0 and K_1 are the initial drug amount and the first order rate constant, respectively.

$$Q_t = K_H t^{\frac{1}{2}} \quad (3)$$

Where K_H is the Higuchi's release rate constant (**Higuchi, 1963**).

To assess the proper drug release mechanism, the data was applied in Korsmeyer-Peppas model as follows (**Korsmeyer et al., 1983**):

$$\frac{M_t}{M_\infty} = Kt^n \quad (4)$$

Where M_t/M_∞ , K and n are the fraction of drug released after time t , the release rate constant and the characteristic release exponent, respectively. The (n) value is used to characterize different release mechanisms. For example, (n) values of less than or equal to 0.5 are characteristic of Fickian or quasi-Fickian diffusion, whereas (n) values in the range of 0.5 to 1 are indication of anomalous drug release mechanism. It is worthy of note that the drug fractional release (M_t/M_∞) mechanism seems to be zero-order as n equals unity. The mathematical model that represented the best kinetic release profile was picked based on the highest (R^2).

4- Stability study

The prepared CEO-NE based NEG was subjected to stability study as per ICH guidelines. A freshly prepared NEG formula was packaged in glass bottles and subjected to stability study under different storage conditions, namely; refrigeration ($5 \pm 3^\circ\text{C}$) and ambient conditions over a period of 6 months. Physical assessment of the samples was achieved by visual inspection of any phase separation, change in color and/or odor. Furthermore, the stability of CEO-NE based NEG was assessed in terms of drug retention % and pH measurement at zero time (at production day as previously described in chapter 2), and after 1, 2, 3, 4, 5 and 6 months of storage. Its η was also determined at a rotational speed of 32 rpm (γ of 192 s^{-1}) at the designated periods of storage (**Zakaria et al., 2016; Aithal et al., 2018**). Regarding CEO-NE based NF_S formulation, its stability was evaluated with respect to drug retention % periodically throughout a 6 months period of storage in refrigerator ($5 \pm 3^\circ\text{C}$).

5- *In vivo* assessment studies

5.1. *Animals*

Male Swiss albino mice weighing 20-25 g were employed for the forthcoming *in vivo* anti-inflammatory activity and skin irritation experiments. The animals were caged and maintained for one week acclimatization period prior to conducting the experiments under standard laboratory conditions of $25 \pm 1^\circ\text{C}$ temperature, $55 \pm 5\%$ RH, and 12-h light / 12-h dark photoperiod cycles with free access to commercial laboratory chow and water *ad libitum*. Hair of the mice dorsal surface was depilated utilizing an animal hair clipper one day before executing the studies.

5.2. *In vivo anti-inflammatory activity against croton oil-induced mouse skin inflammation model*

The anti-inflammatory activity of the investigated formulae was assessed employing the documented croton oil-induced skin inflammation model (Shwaireb, 1995). The mice were divided into eight groups (6 animals per group), totaling a final number of 48 animals and served as follows:

- ◆ **Group A:** Normal control (no croton oil nor CEO).
- ◆ **Group B:** Croton oil (once topical application of single dose of 8 mg croton oil / 0.2 mL acetone and left for 24 h). These conditions (dose and time) provoked maximum inflammatory response as previously reported (Shwaireb, 1995).
- ◆ **Group C:** Pure CEO (once topical treatment/day with 1 μL of CEO after 24 h of croton oil application).
- ◆ **Group D:** CEO-NE based NEG (once topical treatment/day with 0.6 g NEG (1% w/w CEO) after 24 h of croton oil application).
- ◆ **Group E:** Plain-NE based NEG (twice topical treatment/day (every 12 hr) with 0.6 g NEG (without CEO) after 24 h of croton oil application).
- ◆ **Group F:** CEO-NE based NEG (twice topical treatment/day (every 12 hr) with 0.6 g NEG (1% w/w CEO) after 24 h of croton oil application).
- ◆ **Group G:** Plain-NE based NF_S (once topical treatment/day with 100 mg NF_S (without CEO) after 24 h of croton oil application).

- ◆ **Group H:** CEO-NE based NF_S (once topical treatment/day with 100 mg NF_S (1% w/w CEO) after 24 h of croton oil application).

Plain and medicated NEG and NF_S were prepared as previously mentioned in part II chapter 2. Such formulae were attached to the mice's dorsum by Tegaderm and additionally secured firmly by specially designed mouse Velcro jackets (**Anter et al., 2018; Ramadan et al., 2018**). In the present study, pure CEO was topically applied for comparison. It was reported that the anti-inflammatory activity of eugenol, the main component of CEO, against carrageenan-induced paw edema model was proved with no significant difference in the concentration range of 1 to 4 % (w/w) (**Esmaili et al., 2016**).

5.2.1. Preparation of skin tissue samples

The treatment regimen was continued for only one day. After that, the animals were sacrificed and dorsal skin tissue samples were excised, fixed in 10% buffered formalin solution, processed for paraffin wax embedding and sectioned into 5 μm thickness for the subsequent histopathological and IHC evaluations.

5.2.2. Histopathological evaluation

One set of skin tissue sections was deparaffinized and stained with hematoxylin and eosin (H&E) (**Bancroft and Gamble, 2007**). The intensity of the inflammatory response was assessed in 6 histological sections from each mouse per group. A minimum of 10 fields for each slide were examined (at 100× and 400× magnification) and scored. The degree of inflammation was evaluated with a score from 0 to 5. The scores were defined as follows: 0=no inflammation, 1=mild inflammation, 2=mild/moderate inflammation, 3=moderate inflammation, 4=moderate/severe inflammation and 5=severe inflammation (**Bang et al., 2009; Hussein et al., 2013**).

5.2.3. IHC evaluation of COX-2 expression

Second set of sections was subjected to IHC evaluation of COX-2 expression level employing EnVision method according to the manufacturer's instructions. After deparaffinization with xylene, rehydration with gradual descending ethanol concentrations followed by phosphate buffer saline (PBS, pH 7.4). For antigen retrieval,

tissue sections were inserted in glass jars containing 0.01M sodium citrate buffer (pH 6.0) and then placed in a microwave oven twice for 5 min to enhance immunoreactivity. Blocking the endogenous peroxidase activity was performed by 3% H₂O₂ for 5 min at room temperature. The slides were rinsed with PBS (pH7.4) and IHC staining was done utilizing ready to use anti-COX2, for cyclooxygenase isoenzymes (COX-2) antibody (1:100 in PBS w/v) overnight at 4°C. Detection was carried out using the universal kit by washing slides in PBS for 5 min and then incubating with secondary antibody that was biotinylated goat serum conjugated mouse sera for 30 min at room temperature. Sections were then washed with PBS followed by development of antigen-antibody visualization by DAB for 1 min. Sections were washed under running tap water for 10 min, then counterstained with Mayer's haematoxylin. The level of IHC staining intensity was scored 0, negative; 1, weak; 2, moderate and 3, strong staining (**Fisher *et al.*, 2005**).

To abolish a source of bias, all the stained sections were examined under light microscope and digital images were captured, and then evaluated by a qualified experienced pathologist blind to the experimental groups and treatments.

5.3. Skin irritation test

After shaving the hair of the dorsal side of the mice 24 h before starting the experiment, the animals were divided into four groups (six animals/group) as follows:

- ◆ **Group I:** Normal control without any treatment.
- ◆ **Group II:** Standard irritant (topical application of formalin aqueous solution (0.8 % v/v)).
- ◆ **Group III:** CEO-NE based NEG (twice topical application/day (every 12 hr) with 0.6 g NEG (1% w/w CEO)).
- ◆ **Group IV:** CEO-NE based NF₅ (once topical application/day with 100 mg NF₅ (1% w/w CEO)).

The same fixation method of the investigated formulae on the mice's dorsum was proceeded as previously mentioned above in the "*In vivo* anti-inflammatory activity" section. The protocol of skin irritation test was continued for only one day

followed by sacrificing the mice and dissecting the treated skin tissues for histopathological examination after (H&E) staining utilizing light microscope.

6- Statistical analysis

The *ex vivo* and stability data were presented as mean \pm SD and statistically analyzed using ANOVA followed by Tukey–Kramer multiple comparisons test except for ER_{flux} that was analyzed by Student's *t*-test (unpaired *t*-test). In case of *in vivo* study, Kruskal–Wallis test (nonparametric test) was applied followed by Dunn multiple comparison test for statistical analysis of both the inflammatory and IHC scores (**Anbar *et al.*, 2016**). GraphPad Prism 5 software computer program was employed for the analysis process. The statistical significant differences were considered at $p < 0.05$.

Results and Discussion

1- Spectrophotometric scanning of CEO in phosphate buffer, pH 7.4

Figure 32 represents UV scanning from 250-400 nm of CEO solution in phosphate buffer, pH 7.4. It was obvious from this figure that the spectrum of CEO in this medium has λ_{\max} at 279 nm.

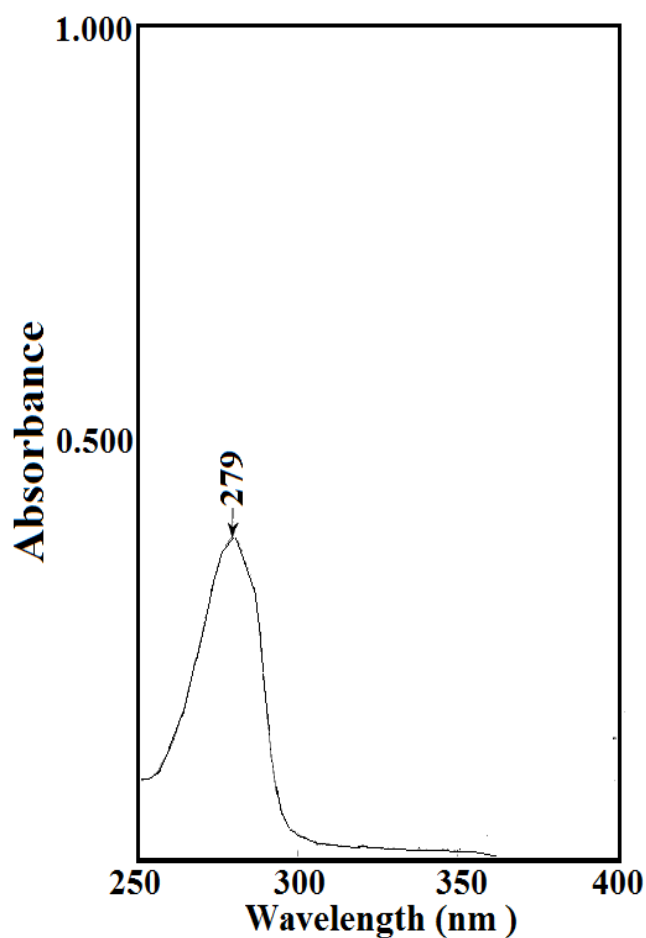


Figure 32: Spectrophotometric scanning of CEO in phosphate buffer, pH 7.4.

2- Construction of calibration curve of CEO in phosphate buffer, pH 7.4

Figure 33 demonstrates the graphical plot of different concentrations of CEO solutions in phosphate buffer, pH 7.4 against the absorbance at the aforementioned λ_{\max} value. It was observed that the concentration of CEO obeyed Beers-Lambert law at a concentration range of 5.7–51.3 $\mu\text{g/mL}$ with high (R^2) = 0.9991.

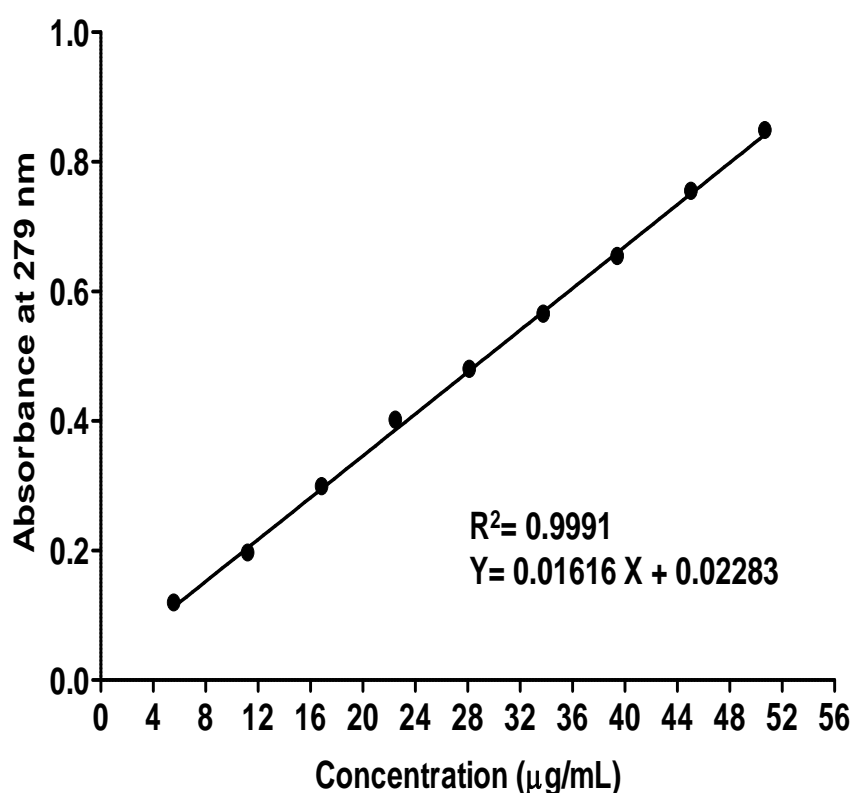


Figure 33: Calibration curves of CEO in phosphate buffer, pH 7.4.

Each point represents the mean \pm SD (n=3).

3- *Ex vivo* skin permeation study

3.1. Skin permeation experiment and parameters

As depicted in **Figure 34**, the *ex vivo* permeation profiles of CEO from the prepared CEO-NE based NEG and CEO-NE based NF_s through the excised Wistar albino rats skin were different from that of the control (pure CEO). According to the calculated Q_{48h}, the permeation rate was in the order of CEO-NE based NEG > CEO-NE based NF_s > pure CEO.

CEO-NE based NEG showed the highest permeation efficiency compared to CEO-NE based NF_s as well as pure CEO. It's known that NEG influences a better skin permeation owing to the characteristics of the gel polymeric matrix as follows: 1) good adhesion property particularly the positively charged CS that can bind to the negatively charged skin at physiological pH condition through electrostatic interaction (**Contri et al., 2016; Bussio et al., 2018**); and 2) penetration enhancement ability of CS when applied topically (**Tan et al., 2011; Bussio et al., 2018; Khademi et al., 2018**). These characteristics facilitate the controlled release of the medicated NE particles from the gel matrix, hence allowing their penetration into the SC of the skin.

On the other hand, it can be seen that CEO-NE based NF_s' permeation across the skin was gradual. Such behavior could be explained on the basis of low degradation rate of PVA NF_s, which could increase the opportunity for drug deposition and retention in the skin and subsequently sustain its permeation (**Azarbayjani et al., 2010**).

Regardless of the effect of polymeric matrix type in both investigated systems (NEG and NF_s), the influence of the NE system on the permeation of the loaded drug should be also kept into consideration. The NE's nano size and penetration enhancing capability related to its component (surfactant; tween-80[®]) greatly support and augment the drug permeation through the skin (**Elmataeshy et al., 2018**). Additionally, the high solubilization of the drug conferred by loading into NE system leads to larger concentration gradient towards the skin which further increase skin permeation of drug (**Singh et al., 2014; Elmataeshy et al., 2018; Mulia et al., 2018**).

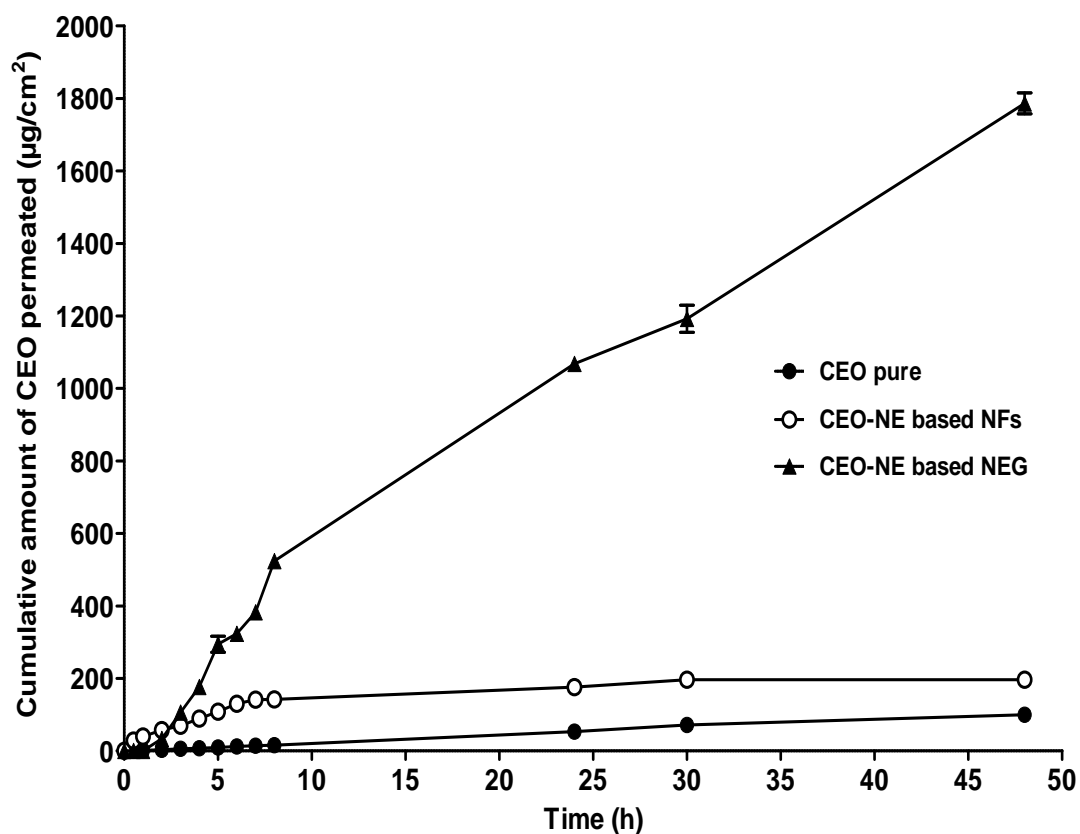


Figure 34: *Ex vivo* skin permeation profiles of CEO from pure CEO, CEO-NE based NFs and CEO-NE based NEG.

Each point represents the mean \pm SD (n=3).

As illustrated in **Table 17**, it could be concluded that CEO-NE based NF_S as well as CEO-NE based NEG formulations show significant difference ($p < 0.05$) in all the permeation parameters *vs* each other as well as *vs* the control (pure CEO). Conspicuously, CEO-NE based NEG exhibited the highest permeation parameters including Q_{48h} ($1786.61 \pm 29.14 \mu\text{g}/\text{cm}^2$), J_{ss} ($31.32 \pm 0.40 \mu\text{g}/\text{cm}^2.\text{h}$), K_p ($13.44 \pm 0.00 \times 10^{-3} \text{ cm}/\text{h}$), and ER_{flux} (16.76 ± 0.74). Hence, it can be concluded that polymeric PVA NF_S (*i.e.* CEO-NE based NF_S) can sustain the penetration of CEO through the skin, when compared to CEO-NE based NEG, and help maintaining the effective CEO concentration in the skin for prolonged period (**Azarbayjani et al., 2010**).

Table 17: *Ex vivo* skin permeation parameters of CEO from pure CEO, CEO-NE based NF_S and CEO-NE based NEG across the excised Wistar albino rats' skin after 48 h.

Formulation	Q _{48h} ($\mu\text{g}/\text{cm}^2$)	J _{ss} ($\mu\text{g}/\text{cm}^2.\text{h}$)	K _p (cm/h) $\times 10^{-3}$	ER _{flux}
pure CEO	99.97 ± 2.32	1.87 ± 0.06	0.80 ± 0.00	–
CEO-NE based NF _S	$196.81 \pm 0.36^*$	$2.41 \pm 0.12^*$	$1.04 \pm 0.00^*$	1.29 ± 0.10
CEO-NE based NEG	$1786.61 \pm 29.14^{*\#}$	$31.32 \pm 0.40^{*\#}$	$13.44 \pm 0.00^{*\#}$	$16.76 \pm 0.74^{**}$

Each value represents the mean \pm SD (n=3).

*Significant at $p < 0.05$ *vs* pure CEO using ANOVA.

#Significant at $p < 0.05$ *vs* CEO-NE based NF_S using ANOVA.

**Significant at $p < 0.05$ *vs* CEO-NE based NF_S using Student's t-test (unpaired t-test).

3.2. Kinetic analysis of drug permeation data

To inspect the drug release mechanism, the release kinetic parameters and (R^2) were calculated for the investigated pure CEO, CEO-NE based NF_S and CEO-NE based NEG (**Table 18**). It can be deduced from the (R^2) as well as (n) values that both Higuchi's kinetic model and Fickian diffusion mechanism prevailed for CEO-NE based NF_S permeation, which indicates that the release of CEO from polymeric PVA NF_S (namely CEO-NE based NF_S) seems to be a process controlled mainly by diffusion.

On the other hand, a zero-order release pattern was observed for both pure CEO and CEO-NE based NEG as estimated by (R^2) and (n) values. Similar findings were previously reported when NE based hydrogel for enhanced transdermal delivery of ketoprofen and *in situ* NEG of quercetin for periodontitis were prepared by **Arora et al., 2014** and **Aithal et al., 2018**, respectively.

The best fit of zero-order model indicated that the drug release from the prepared NEG followed controlled-release pattern. Additionally, it's known that (n) value higher than unity (1) indicates super case II transport mechanism which results from swelling and polymer chain relaxation of polymeric-blend (CS-GG-GA) matrix (**Nayaka and Pal 2013; Ghitman et al., 2018**).

Table 18: Kinetic analysis of the *ex vivo* permeation data of CEO from pure CEO, CEO-NE based NF_S and CEO-NE based NEG.

Formula	Coefficients of determination (R^2)			Korsmeyer-Peppas		
	Zero-order	First-order	Higuchi model	(R^2)	Diffusional exponent (n)	Main transport mechanism
Pure CEO	0.9946	0.9939	0.9255	0.9978	1.12	Super case II transport
CEO-NE based NF _S	0.6569	0.6745	0.8720	0.9235	0.45	Fickian
CEO-NE based NEG	0.9619	0.9401	0.8148	0.9657	1.88	Super case II transport

4- Stability study

One of the most important characteristics is the stability study of the developed formulation. In the present study, CEO-NE based NEG did not experience any physical changes, in color and/or odor, or phase separation over a storage period of 6 months at refrigeration conditions ($5 \pm 3^\circ\text{C}$) revealing its good stability. The samples have yellow colour and transparent appearance free from any turbidity or grittiness. Such good stability of the NEG formulation may be attributed to the stability of the initial NE used in its preparation. Contrary, turbidity of CEO-NE based NEG was noticed at the end of storage at ambient conditions.

Table 19 summarizes the values of drug retention %, pH and η at γ of 192 s^{-1} of the prepared CEO-NE based NEG stored at the two different conditions. The ANOVA results clarified the insignificant variation in drug retention %, pH and η at γ of 192 s^{-1} throughout the storage period at refrigeration conditions. Otherwise, a significant increase in pH as well as a decrease in drug retention % and η at γ of 192 s^{-1} was recorded upon storage at ambient conditions before the end of storage period.

Fortunately, for CEO-NE based NF_s, the value of drug retention % was found to be 97.74 ± 2.01 after 6 months storage at $5 \pm 3^\circ\text{C}$.

Consequently, the obtained results exhibited a clear evidence of the stability of the prepared CEO-NE based NEG as well as CEO-NE based NF_s upon storage at $5 \pm 3^\circ\text{C}$, therefor enabling their efficacy for prolonged period of time. Electrospun eugenol/cyclodextrin inclusion complex nanofibrous mats were reported to be kept in refrigerator (Celebioglu *et al.*, 2018).

Table 19: Drug retention %, pH, and η at γ of 192 s^{-1} of CEO-NE based NEG stored at refrigeration ($5 \pm 3^\circ\text{C}$) and ambient conditions.

Storage time	Evaluation parameters					
	Refrigeration conditions ($5 \pm 3^\circ\text{C}$)			Ambient conditions		
	Drug retention %	pH	η (cP) at γ of 192 s^{-1}	Drug retention %	pH	η (cP) at γ of 192 s^{-1}
Zero time	100.00 \pm 0.00	4.51 \pm 0.01	6545.31 \pm 156.89	100.00 \pm 0.00	4.51 \pm 0.01	6545.31 \pm 156.89
1 month	100.40 \pm 1.57	4.49 \pm 0.01	6545.31 \pm 156.89	94.88 \pm 0.63	4.46 \pm 0.03	4992.19 \pm 156.89*
2 months	99.99 \pm 2.51	4.49 \pm 0.02	6323.44 \pm 156.89	91.55 \pm 0.95*	4.48 \pm 0.02	4548.44 \pm 156.88*
3 months	98.22 \pm 0.38	4.52 \pm 0.01	6212.50 \pm 0.00	91.11 \pm 3.47*	4.50 \pm 0.03	4326.56 \pm 156.89*
4 months	98.22 \pm 3.14	4.53 \pm 0.02	6101.56 \pm 156.88	89.66 \pm 2.35*	4.85 \pm 0.04*	4104.69 \pm 156.89*
5 months	96.55 \pm 2.98	4.54 \pm 0.01	5990.62 \pm 0.00	75.85 \pm 1.79*	4.75 \pm 0.01*	3882.81 \pm 156.89*
6 months	96.29 \pm 2.48 [#]	4.55 \pm 0.03 [#]	5990.62 \pm 313.78 [#]	65.48 \pm 1.35*	4.77 \pm 0.01*	3328.12 \pm 313.78*

Each value represents the mean \pm SD (n=3).

* Significant at $p < 0.05$ monthly vs. initial.

[#] Significant at $p < 0.05$ refrigeration vs. ambient conditions after 6 months.

5- In vivo assessment studies

5.1. In vivo anti-inflammatory activity against croton oil-induced mouse skin inflammation model

Croton-oil induced skin inflammation is a well established pharmacological model for screening the anti-inflammatory activity of the investigated drugs either free or incorporated in pharmaceutical delivery systems that could be useful in the treatment of skin inflammatory diseases (Shin *et al.*, 2010; Luo *et al.*, 2014; Raposo *et al.*, 2015).

5.1.1. Histopathological evaluation

Compared with the skin from normal control mice group (**Figure 35A**), histopathological examination of mice skin tissues exposed to croton oil alone revealed epidermal damage, dermal congestion and edema in addition to marked inflammatory cells infiltration mainly polymorphonuclear (PMN) leukocytes in epidermis and dermis (**Figure 35B**). Once topical treatment with CEO alone, CEO- NE based NEG or plain-NE based NF_s did not significantly reduced the harmful effect of croton oil on the skin where separation of epidermis from basement membrane, PMN cells aggregation in epidermis and dermis with dermal congestion and edema were observed (**Figure 35C, D and G**). Epidermal damage started to disappear in plain-NE based NEG treated mice with mild reduction in dermal congestion, edema and PMN cells infiltration (**Figure 35E**). Interestingly, in case of twice application of CEO-NE based NEG, much more decreased congestion, edema and PMN cells infiltration in dermis were noticed (**Figure 35F**). Meanwhile, once application of CEO-NE based NF_s remarkably inhibited the phlogistic hallmarks of congestion, edema, and PMN cells infiltration induced in the skin by croton oil (**Figure 35H**).

5.1.2. IHC evaluation of COX-2 expression

In the current study, IHC examination was implemented to further clarify the anti-inflammatory activity of the investigated formulae by evaluating the expression level of COX-2 as a key mediator of inflammation pathways (Ricciotti and FitzGerald, 2011; Gandhi *et al.*, 2017).

As shown in **Figure 36**, COX-2 was positively stained in epidermal cells from all experimental groups (**Figure 36A-H**). However, positive signal against COX-2 was markedly increased in the skin of mice group treated with croton oil only (**Figure 36B**). Groups treated with once application of pure CEO, CEO- NE based NEG or plain-NE based NF_S experience increased number of stained PMN cells infiltrating epidermis and dermis (**Figure 36C, D and G**). Following twice application regimen, the positive signal against COX-2 decreased in skin of plain-NE based NEG treated group (**Figure 36E**) and decreased much more in CEO-NE based NEG treated one (**Figure 36F**). Since the inflammatory process was prominently suppressed by once treatment with CEO-NE based NF_S formula, the IHC staining of COX-2 appeared as in normal control mice (**Figure 36H**).

Statistical analysis of the inflammatory and IHC scores of the experimental groups is illustrated in **Figure 37**. Both groups treated with CEO-NE based NEG (twice application) and CEO-NE based NF_S (once application) disclosed a significant decrement ($p < 0.05$) in the inflammatory and IHC scores when compared with croton oil or pure CEO treated mice reflecting their superlative anti-inflammatory activity along with relatively higher efficacy of medicated NF_S than that of medicated NEG.

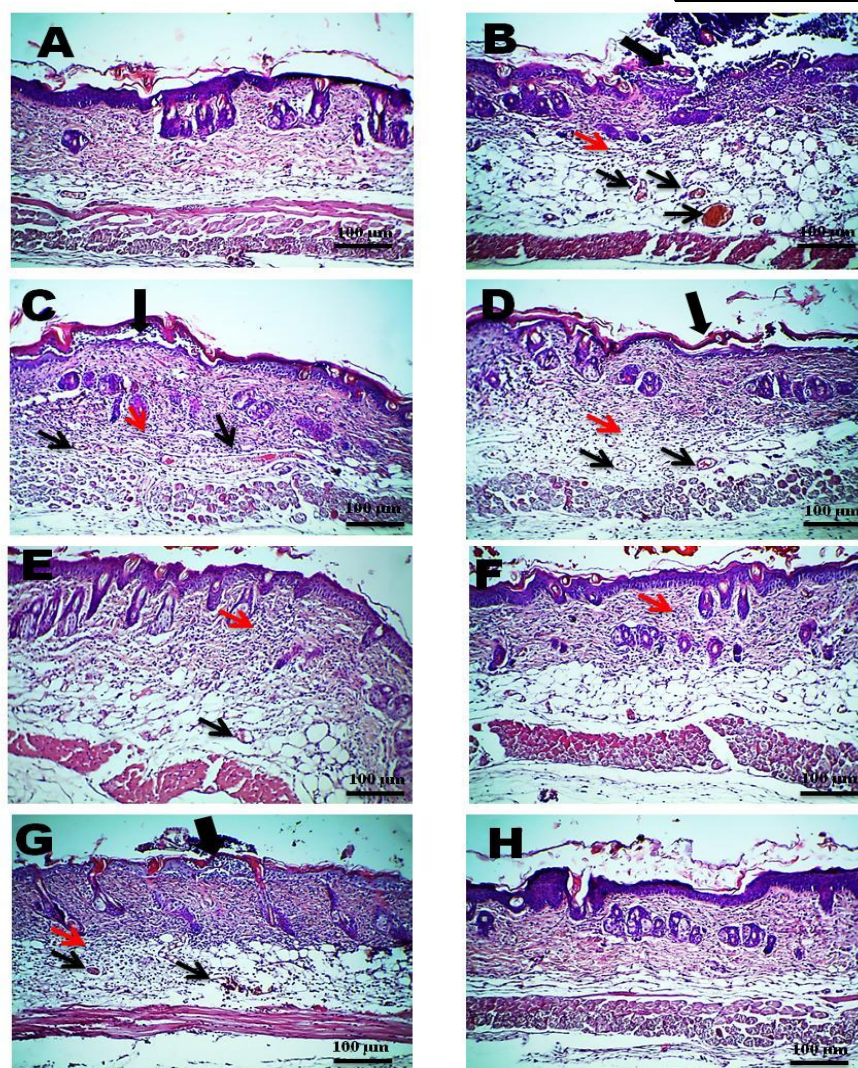


Figure 35: Photomicrographs of histopathological evaluation of the anti-inflammatory activity of the investigated formulae: (A) normal control group, (B) croton oil treated group, (C) pure CEO group (once application), (D) CEO-NE based NEG (once application), (E) plain-NE based NEG (twice application), (F) CEO-NE based NEG (twice application), (G) plain-NE based NF_s (once application) and (H) CEO-NE based NF_s (once application). Thick black arrow points to epidermal damage with marked PMN cells infiltration, thin red arrow points to PMN cells infiltration in dermis, and thin black arrow points to congested blood vessel. H&E, X: 100 bar: 100 µm.

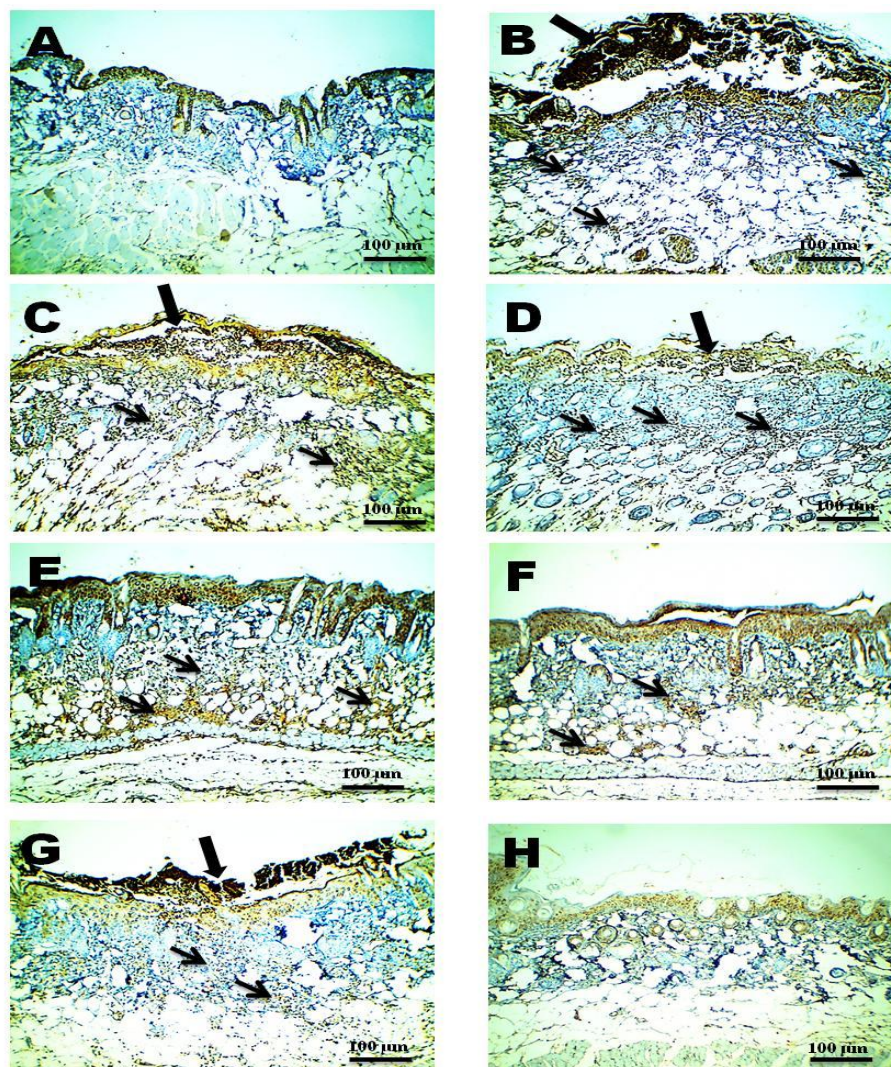


Figure 36: Photomicrographs of IHC evaluation of COX-2 expression level of the investigated formulae: (A) normal control group, (B) croton oil treated group, (C) pure CEO group (once application), (D) CEO-NE based NEG (once application), (E) plain-NE based NEG (twice application), (F) CEO-NE based NEG (twice application), (G) plain-NE based NF_s (once application) and (H) CEO-NE based NF_s (once application). Thick black arrow points to positively stained PMN cells infiltration in epidermis, and thin black arrows point to positively stained PMN cells infiltration in dermis. IHC counterstained with Mayer's hematoxylin, X: 100 bar: 100 µm.

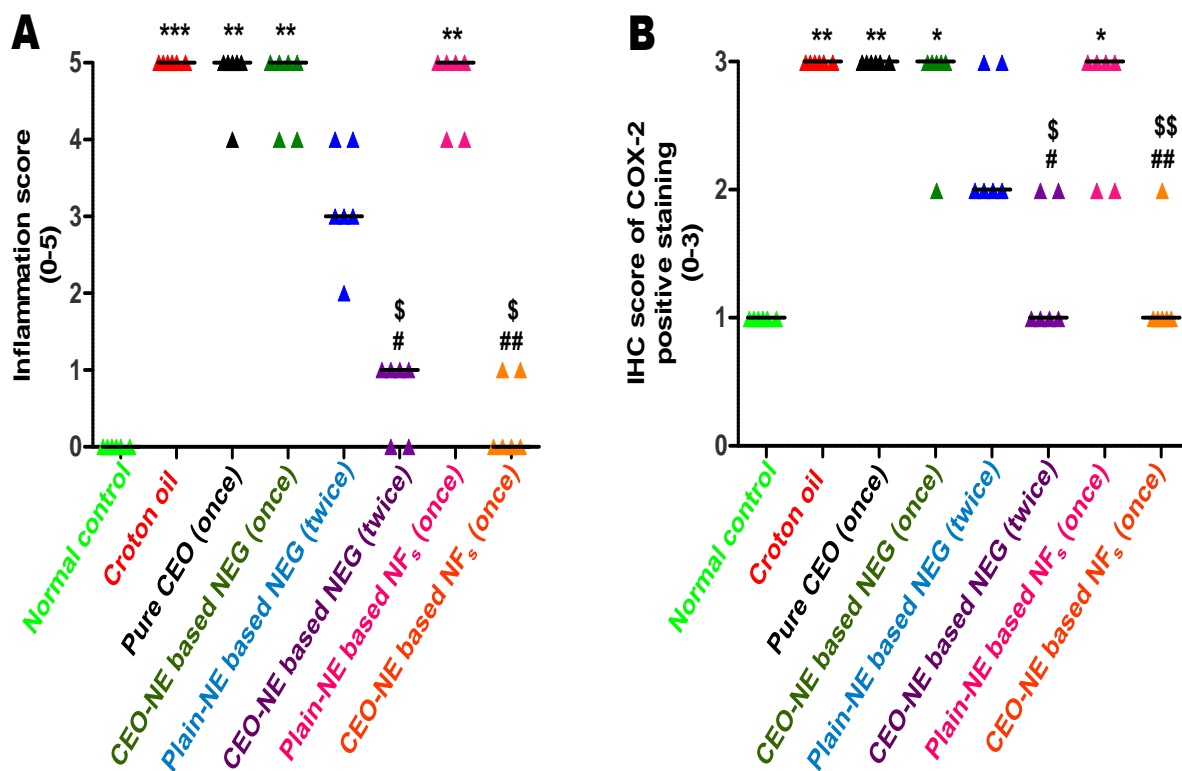


Figure 37: Statistical analysis of inflammation scores (A) and IHC scores (B) in skin from experimental groups (six animals/group). Kruskal–Wallis test (nonparametric test) was applied followed by Dunn multiple comparison test.

* $p < 0.05$, ** $p < 0.01$ and *** $p < 0.001$ vs normal control group.

$p < 0.05$ and ## $p < 0.01$ vs croton oil group.

\$ $p < 0.05$ and \$\$ $p < 0.01$ vs pure CEO group.

In this study, the anti-inflammatory activity of pure CEO and its pharmaceutical delivery systems against croton oil-induced skin inflammation was assessed. Croton oil is a phlogistic agent containing phorbol esters, mainly 12-O- tetradecanoylphorbol-13-acetate (TPA), as irritant agents. Once topical application of croton oil triggers significant inflammatory responses characterized by edema, vascular permeability increment, PMN leukocytes (mainly neutrophils) infiltration, protein kinase C (PKC) activation, prostaglandins (PGs) and leukotrienes production, and several inflammatory mediators induction involving over expression of COX-2 (**Shin *et al.*, 2010; Rahman *et al.*, 2011; Luo *et al.*, 2014**).

Although several inflammatory mediators are involved in the inflammation process, several lines of evidence suggested that over expression of COX-2, a vital key cytokine-inducible enzyme responsible for production of PGs, is robustly implicated in the pathogenesis of inflammatory diseases. Indeed, nonsteroidal anti-inflammatory drugs (NSAIDs) have been reported to alleviate the inflammation via their effect as COX-2 inhibitors (**Ricciotti and FitzGerald, 2011; Gandhi *et al.*, 2017**). However, their long-term use either orally or topically is accompanied with serious health issues (**Haroutiunian *et al.*, 2010; Sinha *et al.*, 2013**). Consequently, many endeavors have been targeted to explore COX-2 inhibitors with minimal adverse effects particularly from natural origin. Fortunately, among essential oils, CEO containing eugenol as a predominant component was very potent in suppressing COX-2 in lipopolysaccharide (LPS)-induced mouse macrophage RAW264.7 cell line (**Hong *et al.*, 2002; Kim *et al.*, 2003**) as well as in LPS-induced human macrophage U937 cell line (**Lee *et al.*, 2007**). Besides, previous study demonstrated that the anti-inflammatory activity of CEO was comparable with that of NSAIDs such as etodolac and indomethacin (**Öztürk and Özbek, 2005**).

From clinical point of view, development of topical pharmaceutical delivery systems for CEO to potentiate its anti-inflammatory activity as well as improve patient applicability is a challenge issue. The current study paved the way to achieve such goal by fabricating novel NEG and NF_s delivery systems for topical application of CEO.

According to the above mentioned *in vivo* data, the potentiated anti-inflammatory activity of such medicated formulae (CEO-NE based NEG and CEO-NE based NF_s) was clearly established.

Regarding CEO-NE based NEG, the gel polymeric matrix played an important role due to their proper rheological property, bioadhesive and penetration enhancement characteristics (mainly CS) (Contri *et al.*, 2016; Bussio *et al.*, 2018) as well as the anti-inflammatory activity (particularly CS and GA), via downregulation of several inflammatory mediators including COX-2, that may act synergistically with that of CEO (Chou *et al.*, 2003; Ali *et al.*, 2013; Kim, 2018; Xiong *et al.*, 2018; Hamid *et al.*, 2018). In case of CEO-NE based NF_s, until this moment, no articles were published concerning any anti-inflammatory activity for PVA. Therefore, the low degradation rate property of polymeric PVA NF_s could mainly contribute to CEO retention and accumulation in the skin layers (as a depot) for a prolonged period, and hence sustaining its permeation with reduced systemic effect (Azarbayjani *et al.*, 2010). Additionally, there are two common factors in both medicated formulae. The first one is the CEO-NE system with distinctive characteristics such as nano metric size that facilitates its cellular uptake by immune cells, like macrophages, in the inflamed tissues (Cortivo *et al.*, 2010) as well as penetration enhancement ability conferred by the surfactant (tween-80[®]) as one of its components, therefore augmenting the drug cutaneous permeation (Akhtar *et al.*, 2011). The second factor is the permeation pattern of both formulae either controlled (NEG) or sustained (NF_s) that has a great influence in decreasing the frequency of dosing at the application site, thence improving the patient compliance for the treatment regimen as well as being cost effective for prospective commercial production on large scale.

5.2. Skin irritation test

Skin irritation test was performed as an important prerequisite to assess the probability of any irritation episodes resulting from topical application of the developed formulae. Histopathological examination of skin from formalin treated mice, as a standard irritant group, revealed an acute inflammation characterized by extensive

congestion, edema and PMN cells infiltration in dermis particularly around capillaries (**Figure 38B**) in comparison with normal skin control group (**Figure 38A**). Contrary, normal histopathological integrity of mice skin was evident in CEO-NE based NEG (twice application) and CEO-NE based NF_s (once application) treated groups (**Figure 38C and D, respectively**) indicating their cutaneous safety profile as well as prospective patient tolerability and compliance for therapeutic use.

Considering the *ex vivo* and *in vivo* data, CEO-NE based NEG and CEO-based NF_s could be introduced to the phytomedicine field as promising topical delivery systems for effective treatment of inflammatory diseases instead of NSAIDs that possess adverse effects.

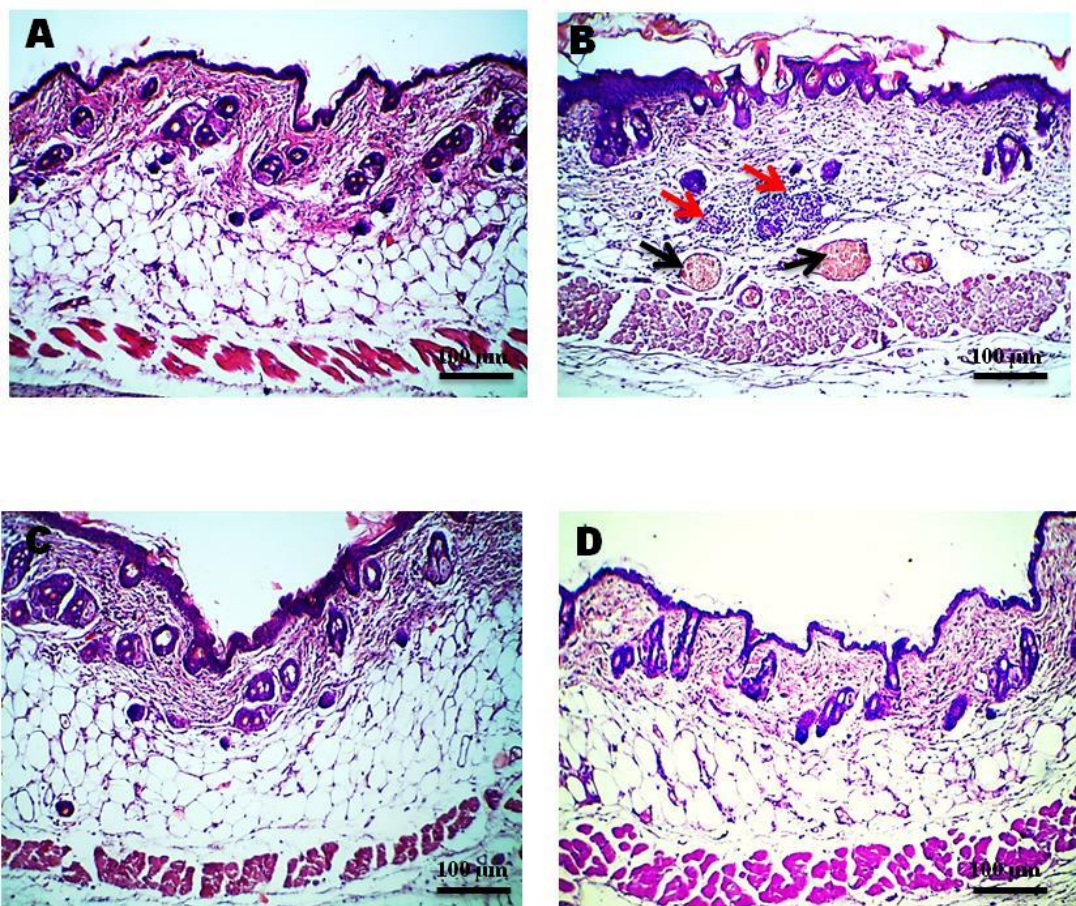


Figure 38: Photomicrographs of histopathological evaluation of skin irritation test: (A) normal control mice, (B) formalin treated mice, (C) CEO-NE based NEG (twice application), and (D) CEO-NE based NF_s (once application). Thin red arrow points to PMN cells infiltration in dermis and thin black arrow points to congested blood vessel. H&E, X: 100 bar: 100 μm.

Conclusions

Based on the obtained results, it could be concluded that:

- ❖ The *ex vivo* skin permeation data of CEO from the prepared formulations showed that CEO-NE based NF_S can sustain the penetration of CEO through the skin, when compared to CEO-NE based NEG.
- ❖ Both Higuchi's model and Fickian diffusion mechanism prevailed for CEO-NE based NF_S permeation.
- ❖ Both zero-order model and super case II transport mechanism prevailed for CEO-NE based NEG permeation.
- ❖ The high stability of the prepared CEO-NE based NEG and CEO-NE based NF_S was revealed upon storage at $5 \pm 3^{\circ}\text{C}$ for six months, hence enabling their efficacy for prolonged period of time.
- ❖ Topical treatment with CEO-NE based NEG (twice application) and CEO-NE based NF_S (once application) evoked a marvelous *in vivo* anti-inflammatory activity against croton oil-induced mouse skin inflammation model that was asserted by:
 - Histopathological evaluation which disclosed a significant decrement ($p < 0.05$) in the inflammatory scores comparably with the control pure CEO treated mice
 - Significant suppression of IHC expression level of COX-2 when compared with the control pure CEO treated mice.
- ❖ *In vivo* skin irritation test disclosed normal histopathological integrity of mice skin in case of CEO- NE based NEG (twice application) and CEO-NE based NF_S (once application) treated groups in comparison with formalin treated mice as a standard irritant group, indicating their cutaneous safety profile as well as prospective patient tolerability and compliance for therapeutic use.
- ❖ Considering the *ex vivo* and *in vivo* data; CEO-NE based NEG and CEO-based NF_S could be introduced to the phytomedicine field as promising topical delivery

systems for effective treatment of inflammatory diseases instead of NSAIDs that possess adverse effects.

References

Abdul Rasool, B. K., Abu-Gharbieh, E. F., Fahmy, S. A., Saad, H. S., and Khan, S. A., Development and evaluation of ibuprofen transdermal gel formulations, *Trop. J. Pharm. Res.*, 9(4), 355-363 (2010).

Ahmed, O. A. A., and Rizq, W. Y., Finasteride nano-transferosomal gel formula for management of androgenetic alopecia: *ex vivo* investigational approach, *Drug Des. Devel. Ther.*, 12, 2259-2265 (2018).

Aiamsa-ard, T., Lukkunaprasit, T., Lakkana, N., and Godsan, I., Anti-inflammation and antiplatelet aggregation of clove oil in rats, *BHST.*, 15(2), 32-41 (2017).

Aithal, G. C., Nayak, U. Y., Mehta, C., Narayan, R., Gopalkrishna, P., Pandiyan, S., and Garg, S., Localized in situ nanoemulgel drug delivery system of quercetin for periodontitis: development and computational simulations, *Molecules*, 23(6), E1363 (2018).

Akanda, M. H., Rai, R., Slipper, I. J., Chowdhry, B. Z., Lamprou, D., Getti, G., and Douroumis, D., Delivery of retinoic acid to LNCap human prostate cancer cells using solid lipid nanoparticles, *Int. J. Pharm.*, 493, 161-171 (2015).

Akhtar, N., Rehman, M. U., Khan, H. M. S., Rasool, F., Saeed, T. and Murtaza, G. Penetration enhancing effect of polysorbate 20 and 80 on the *in vitro* percutaneous absorption of L-ascorbic acid, *Trop. J. Pharm. Res.*, 10(3), 281-288 (2011).

Alhosseini, S. N., Moztafzadeh, F., Mozafari, M., Asgari, S., Dodel, M., Samadikuchaksaraei, A., Kargozar, S., and Jalali N. Synthesis and characterization of electrospun polyvinyl alcohol nanofibrous scaffolds modified by blending with chitosan for neural tissue engineering, *Int. J. Nanomedicine*, 7, 25-34 (2012).

Ali, B. H., Al-Husseni, I., Beegam, S., Al-Shukaili, A., Nemmar, A., Schierling, S., Queisser, N., and Schupp, N., Effect of gum arabic on oxidative stress and inflammation in adenine-induced chronic renal failure in rats, *PLoS One*, 8(2), e55242 (2013).

Anbar, H. S., Shehatou, G. S. G., Suddek, G. M., and Gameil, N. M., Comparison of the effects of levocetirizine and losartan on diabetic nephropathy and vascular dysfunction in streptozotocin-induced diabetic rats, *Eur. J. Pharmacol.*, 780, 82-92 (2016).

Ansari, S. H., Islam, F., and Sameem, M., Influence of nanotechnology on herbal drugs: a review, *J. Adv. Pharm. Tech. Res.*, 3(3), 142-146 (2012).

Anter, H. M., Abu Hashim, I. I., Awadin, W., and Meshali, M. M., Novel anti-inflammatory film as a delivery system for the external medication with bioactive phytochemical "Apocynin", *Drug Des. Devel. Ther.*, 12, 2981-3001 (2018).

Anwer, M. K., Jamil, S., Ibnouf, E. O., and Shakeel, F., Enhanced antibacterial effects of clove essential oil by nanoemulsion, *J. Oleo Sci.*, 63(4), 347-354 (2014).

Apocynin. Drug bank. <https://www.drugbank.ca/drugs/DB12618>. (Accessed January 29, 2018).

Apocynin. Int Wikipedia, the free encyclopedia. <http://en.wikipedia.org/wiki/Apocynin>. (Accessed January 29, 2018).

Arana, L., Salado, C., Vega, S., Aizpurua-Olaizola, O., de la Arada, I., Suarez, T., Usobiaga, A., Arrondo, J. L. R., Alonso, A., Goñi, F. M., and Alkort, I., Solid lipid nanoparticles for delivery of *Calendula officinalis* extract, *Colloids Surf. B: Biointerf.*, 135, 18-26 (2015).

Arora, D., and Jaglan, S., Nanocarriers based delivery of nutraceuticals for cancer prevention and treatment: a review of recent research developments, *Trends Food. Sci. Technol.*, 54, 114-126 (2016).

Arora, R., Aggarwal, G., Harikumar, S. L., and Kaur, K., Nanoemulsion based hydrogel for enhanced transdermal delivery of ketoprofen, *Adv. Pharm.*, 2014, (2014).

Arun, P., Pudi, S. M., and Biswas, P., Acetylation of glycerol over sulfated alumina: reaction parameter study and optimization using response surface methodology, *Energy Fuels*, 30(1), 584-593 (2016).

Asasutjarit, R., Lorenzen, S. I., Sirivichayakul, S., Ruxrungtham, K., Ruktanonchai, U., and Ritthidej, G. C., Effect of solid lipid nanoparticles formulation compositions on their size, zeta potential and potential for *in vitro* pHIS-HIV-Hugag transfection, *Pharm. Res.*, 24, 1098-1107 (2007).

Azarbayjani, A. F., Venugopal, J. R., Ramakrishna, S., Lim, P. F. C., Chan, Y. W., and Chan, S. Y., Smart polymeric nanofibers for topical delivery of levothyroxine, *J. Pharm. Pharmaceut. Sci.*, 13(3), 400-410 (2010).

Azeem, A., Ahmad, F. J., Khar, R. K., and Talegaonkar, S., Nanocarrier for the transdermal delivery of an antiparkinsonian drug, *AAPS PharmSciTech.*, 10(4), 1093-1103 (2009).

Badran, M. M., Taha, E. I., Tayel, M. M., and Al-Suwayeh, S. A., Ultra-fine self nanoemulsifying drug delivery system for transdermal delivery of meloxicam: dependency on the type of surfactants, *J. Mol. Liq.*, 190, 16-22 (2014).

Bala, R., Khanna, S., and Pawar, P., Design optimization and *in vitro-in vivo* evaluation of orally dissolving strips of clobazam, *J. Drug. Deliv.*, 2014, (2014).

Bancroft, J. D., and Gamble, M., Theory and practice of histological techniques (5th ed.). Churchill Livingstone, London, UK pp. 125-138 (2007).

Bang, J. S., OH, D. H., Choi, H. M., Sur, B.-J., Lim, S.J., Kim, J. Y., Yang, H. I., Yoo, M. C., Hahm, D. H., and Kim, K. S., Anti-inflammatory and antiarthritic effects of piperine in human interleukin 1 β -stimulated fibroblast-like synoviocytes and in rat arthritis models, *Arthritis Res. Ther.*, 11(2), R49 (2009).

Bhatt, P. C., Srivastava, P., Pandey, P., Khan, W., and Panda, B. P., Nose to brain delivery of astaxanthin-loaded solid lipid nanoparticles: fabrication, radio labeling, optimization and biological studies, *RSC Adv.*, 6, 10001-10010 (2016).

Bianchera, A., Salomi, E., Pezzanera, M., Ruwet, E., Bettini, R., and Elviri, L., Chitosan hydrogels for chondroitin sulphate controlled release: an analytical characterization, *J. Anal. Methods Chem.*, 2014, (2014).

Borodina, T., Grigoriev, D., Markvicheva, E., Möhwald, H., and Shchukin, D., Vitamin E microspheres embedded within a biocompatible film for planar delivery, *Adv. Eng. Mater.*, 13(3), B123-B130 (2011).

Brenza, T. M., Ghaisas, S., Ramirez, J. E. V., Harischandra, D., Anantharam, V., Kalyanaraman, B., Kanthasamy, A. G., and Narasimhan, B., Neuronal protection against oxidative insult by polyanhydride nanoparticle-based mitochondria-targeted antioxidant therapy, *Nanomedicine: NBM.*, 13, 809-820 (2017).

Bussio, J. I., Molina-Perea, C., and González-Aramundiz, J. V., Lower-sized chitosan nanocapsules for transcutaneous antigen delivery, *Nanomaterials*, 8(9), (2018).

Caster, J. M., Patel, A. N., Zhang, T., and Wang, A., Investigational nanomedicines in 2016: a review of nanotherapeutics currently undergoing clinical trials, *WIREs Nanomed. Nanobiotechnol.*, 9, 1-18 (2017).

Cekić, N. D., Đorđević, S. M., Savić, S. R., and Savić, S. D., A full factorial design in the formulation of diazepam parenteral nanoemulsions: physicochemical characterization and stability evaluation, *Adv. Technol.*, 4(1), 69-77 (2015).

Celebioglu, A., Yildiz, Z. I., and Uyar, T., Fabrication of electrospun eugenol/cyclodextrin inclusion complex nanofibrous webs for enhanced antioxidant property, water solubility, and high temperature stability, *J. Agric. Food Chem.*, 66(2), 457-466 (2018).

Celep, G. K., and Dincer, K., Application of taguchi method for the synthesis of nano-sized TiO₂ powders by acid-used sol-gel method, *Anadolu Univ. J. of Sci. and Technology A – Appl. Sci. and Eng.*, 18(3), 705-712 (2017).

Chae, S. Y., Jang, M., and Nah, J., Influence of molecular weight on oral absorption of water soluble chitosans, *J. Control. Release*, 102, 383-394 (2005).

Chandasana, H., Chhonker, Y. S., Bala, V., Prasad, Y. D., Chaitanya, T. K., Sharma, V. L., and Bhatta, R. S., Pharmacokinetic, bioavailability, metabolism and plasma protein binding evaluation of NADPH-oxidase inhibitor apocynin using LC-MS/MS, *J. Chromatogr. B*, 985, 180-188 (2015).

Chapter 6—Clove Oil (Eugenol), <https://www.marinwater.org/DocumentCenter/View/253>, (Accessed June 6, 2018).

Chaudhary, H. M., Jadhav, K. R., and Kadam, V. J., Formulation and evaluation of nanostructured lipid carriers containing glipizide, *WJPPS.*, 5, 1424-1437 (2016).

Chen, R., Wang, S., Zhang, J., Chen, M., and Wang, Y., Aloe-emodin loaded solid lipid nanoparticles: formulation design and *in vitro* anti-cancer study, *Drug Deliv.*, 22, 666-674 (2015).

Chou, T. C., Fu, E., and Shen, E. C., Chitosan inhibits prostaglandin E2 formation and cyclooxygenase-2 induction in lipopolysaccharide-treated RAW 264.7 macrophages, *Biochem. Biophys. Res. Commun.*, 308(2), 403-407 (2003).

Christophersen, P. C., Vaghela, D., Müllertz, A., Yang, M., Nielsen, H. M., and Mu, H., Solid lipid particles for oral delivery of peptide and protein drugs III — the effect of fed state conditions on the *in vitro* release and degradation of desmopressin, *AAPS J.*, 16, 875-883 (2014).

Chuang, S. Y., Lin, C. H., Huang, T. H., and Fang, J. Y., Lipid-based nanoparticles as a potential delivery approach in the treatment of rheumatoid arthritis, *Nanomaterials*, 8(1), pii: E42. (2018).

Clogston, J. D., and Patri, A. K., "Zeta potential measurement", in: "Characterization of Nanoparticles Intended for Drug Delivery", McNeil, S.E. Ed., New York: Humana Press, PP. 63-70 (2011).

Clove Oil BP: <https://www.medicines.org.uk/emc/medicine/25134>, Last Updated on eMC 16-Sep-2014 (Accessed June 5, 2018).

Clove oil MSDS. Material Safety Data Sheet. <http://www.sciencelab.com/msds.php?msdsId=9927498>. (Accessed June 6, 2018).

Clove oil. http://www.chemicalbook.com/ChemicalProductProperty_EN_CB8286611.htm. (Accessed June 6, 2018).

Clove oil. <https://pubchem.ncbi.nlm.nih.gov/compound/12658395>, (Accessed May 26, 2018).

Contri, R. V., Fiel, L. A., Alnasif, N., Pohlmann, A. R., Guterres, S. S., and Schäfer Korting, M., Skin penetration and dermal tolerability of acrylic nanocapsules: Influence of the surface charge and a chitosan gel used as vehicle, *Int. J. Pharm.*, 507(1-2), 12-20 (2016).

Cortivo, R., Vindigni, V., Iacobellis, L., Abatangelo, G., Pinton, P., and Zavan, B., Nanoscale particle therapies for wounds and ulcers, *Nanomedicine*, 5(4), 641-656 (2010).

Cui, Z., Zheng, Z., Lin, L., Si, J., Wang, Q., Peng, X., and Chen, W., Electrospinning and crosslinking of polyvinyl alcohol/chitosan composite nanofiber for transdermal drug delivery, *Adv. Polym. Technol.*, 1-12 (2017).

Das, S., Ng, W. K., and Tan, R. B., Sucrose ester stabilized solid lipid nanoparticles and nanostructured lipid carriers. I. Effect of formulation variables on the physicochemical properties, drug release and stability of clotrimazole-loaded nanoparticles, *Nanotechnology*, 25(10), 105101 (2014).

de Oliveira, J. K., Ronik, D. F. V., Ascari, J., Mainardes, R. M., and Khalil, N. M., A stability-indicating high performance liquid chromatography method to determine apocynin in nanoparticles, *JPA.*, 7, 129-133 (2017).

de Oliveira, J. K., Ronik, D. F. V., Ascari, J., Mainardes, R. M., and Khalil, N. M., Nanoencapsulation of apocynin in bovine serum albumin nanoparticles: physicochemical characterization, *Nanosci. Nanotechnol-Asia*, 8, 90-99 (2018).

Desai, D., and Shah, D., Implication of nanoparticles for controlled drug delivery system, *IJPSR*, 4(7), 2478-2488 (2013).

Dharmala, K., Yoo, J. W., and Lee, C. H., Development of chitosan–SLN microparticles for chemotherapy: *in vitro* approach through efflux-transporter modulation, *J. Control. Release*, 131(3), 190-197(2008).

Dhibar, M., Chakraborty, S., and Khandai, M., Curcumin loaded in-situ nanoemulgel: an unique dosage form for ophthalmic drug delivery, *Int. J. Pharm. Sci. Rev. Res.*, 48(1), 141-147 (2018).

Djilani, A., and Dicko, A., "The therapeutic benefits of essential oils", in: "Nutrition, Well-being and Health", Bouayed, J., and Bohn, T. eds., InTech, Croatia, PP. 155–178 (2012).

Dudhipala, N., and Veerabrahma, K., Candesartan cilexetil loaded solid lipid nanoparticles for oral delivery: characterization, pharmacokinetic and pharmacodynamic evaluation, *Drug Deliv.*, 23,395-404 (2016).

El-Hefian, E. A., Elgannoudi, E. S., Mainal, A., and Yahaya, A. H., Characterization of chitosan in acetic acid: rheological and thermal studies, *Turk. J. Chem.*, 34, 47-56 (2010).

Elmataeeshy, M. E., Sokar, M. S., Bahey-El-Din, M., and Shaker, D. S., Enhanced transdermal permeability of Terbinafine through novel nanoemulgel formulation; development, *in vitro* and *in vivo* characterization, *Future J. Pharm. Sci.*, 1-4(1), 18-28 (2018).

Esmaeili, F., Rajabnejhad, S., Partoazar, A. R., Mehr, S. E., Faridi-Majidi, R., Sahebgharani, M., Syedmoradi, L., Rajabnejhad, M. R., and Amani, A., Anti inflammatory effects of eugenol nanoemulsion as a topical delivery system, *Pharm. Dev. Technol.*, 21(7), 887-893 (2016).

Eugenol. <http://www.inchem.org/documents/jecfa/jecmono/v17je10.htm>, (Accessed June 5, 2018).

Eugenol. Int Wikipedia, the free encyclopedia. <https://en.wikipedia.org/wiki/Eugenol>. (Accessed June 5, 2018).

Ezealisiji, K. M., Mbah, C. J., Osadebe, P., and Krause, R., Pharmacokinetics studies of mirtazapine loaded nanoemulsion and its evaluation as transdermal delivery system, *J. Chem. Pharm. Res.*, 9(3), 74-84 (2017).

Fisher, E. R., Anderson, S., Dean, S., Dabbs, D., Fisher, B., Siderits, R., Pritchard, J., Pereira, T., Geyer, C., and Wolmark, N., Solving the dilemma of the immunohistochemical and other methods used for scoring estrogen receptor and progesterone receptor in patients with invasive breast carcinoma, *Cancer*, 103, 164-173 (2005).

Fonte, P., Andrade, F., Araújo, F., Andrade, C., Neves, J., and Sarmiento, B., Chitosan-coated solid lipid nanoparticles for insulin delivery, *Methods Enzymol.*, 508, 295-314 (2012).

Fraga, C. G., Galleano, M., Verstraeten, S. V., and Oteiza, P. I., Basic biochemical mechanisms behind the health benefits of polyphenols, *Mol. Aspects Med.*, 31, 435-445 (2010).

Francis, S., Laurieri, N., Nwokocha, C., and Delgoda, R., Treatment of rats with apocynin has considerable inhibitory effects on arylamine N-acetyltransferase activity in the liver, *Sci. Rep.*, 6, 26906 (2016).

Gandhi, J., Khera, L., Gaur, N., Paul, C., and Kaul, R., Role of modulator of inflammation cyclooxygenase-2 in gammaherpesvirus mediated tumorigenesis, *Front. Microbiol.*, 8, 538 (2017).

Ghareeb, M. M., and Neamah, A. J., Formulation and characterization of nimodipine nanoemulsion as ampoule for oral route, *IJPSR.*, 8(2), 591-602 (2017).

Ghitman, J., Stan, R., Ghebaour, A., Cecoltan, S., Vasile, E., and Iovu, H., Novel PEG-modified hybrid PLGA-vegetable oils nanostructured carriers for improving performances of indomethacin delivery, *Polymers*, 10(6), (2018).

Gökmeşe, F., Uslu, İ., and Aytimur, A., Preparation and characterization of PVA/PVP nanofibers as promising materials for wound dressing, *Polym. Plast. Technol. Eng.*, 52, 1259-1265 (2013).

Goyal, R., Macri, L. K., Kaplan, H. M., and Kohn, J., Nanoparticles and nanofibers for topical drug delivery, *J. Control Release*, 240, 77-92 (2016).

Gunasekaran, T., Haile, T., Nigusse, T., and Dhanaraju M. D., Nanotechnology: an effective tool for enhancing bioavailability and bioactivity of phytomedicine, *Asian Pac. J. Trop. Biomed.*, 4(Suppl 1), S1-S7 (2014).

Gupta, S., Kesarla, R., Chotai, N., Misra, A., and Omri, A., Systematic approach for the formulation and optimization of solid lipid nanoparticles of efavirenz by high pressure homogenization using design of experiments for brain targeting and enhanced bioavailability, *BioMed Res. Int.*, 2017, (2017).

Hadgraft, J., Skin, the final frontier, *Int. J. Pharm.*, 224, 1-18 (2001).

Haghirsadat, F., Amoabediny, G., Naderinezhad, S., Helder, M. N., Kharanaghi, E. A., and Zandieh-Doulabi, B., Overview of preparation methods of polymeric and lipid-based (noisome, solid lipid, liposome) nanoparticles: a comprehensive review, *Int. J. Polym. Mater. Po.*, 67(6), 383-400 (2018).

Halnor, V. V., Pande, V. V., Borawake, D. D., and Nagare, H. S., Nanoemulsion: a novel platform for drug delivery system, *JMSN.*, 6(1), (2018).

Hamid, M., Abdulrahim, Y., Liu, D., Qian, G., Khan, A., and Huang, K., The hepatoprotective effect of selenium-enriched yeast and gum arabic combination on carbon tetrachloride-induced chronic liver injury in rats, *J. Food Sci.*, 83(2), 525-534 (2018).

Han, F., Li, S., Yin, R., Shi, X., and Jia, Q., Investigation of nanostructured lipid carriers for transdermal delivery of flurbiprofen, *Drug Dev. Ind. Pharm.*, 34, 453-458 (2008).

Han, N., Johnson, J., Lannutti, J. J., and Winter, J. O., Hydrogel-electrospun fiber composite materials for hydrophilic protein release, *J. Control Release*, 158, 165-170 (2012).

Han, X., Chen, S., and Hu, X., Controlled-release fertilizer encapsulated by starch/polyvinyl alcohol coating, *Desalination*, 240, 21-26 (2009).

Hansraj, G. P., Singh, S. K., and Kumar, P., Sumatriptan succinate loaded chitosan solid lipid nanoparticles for enhanced anti-migraine potential, *Int. J. Biol. Macromol.*, 81, 467-476 (2015).

Haroutiunian, S., Drennan, D. A., and Lipman, A. G., Topical NSAID therapy for musculoskeletal pain, *Pain Med.*, 11(4), 535-549 (2010).

Hernández-Sánchez, P., López-Miranda, S., Lucas-Abellán, C., and Núñez-Delgado, E., Complexation of eugenol (EG), as main component of clove oil and as pure compound, with β - and HP- β -CDs, *Food Nutr. Sci.*, 3, 716-723 (2012).

Higuchi, T., Mechanism of sustained action medication: theoretical analysis of rate of release of solid drugs dispersed in solid matrix, *J. Pharm. Sci.*, 52, 1145-1149 (1963).

Hong, C. H., Hur, S. K., Oh, O. J., Kim, S. S., Nam, K. A., and Lee, S. K., Evaluation of natural products on inhibition of inducible cyclooxygenase (COX-2) and nitric oxide synthase (iNOS) in cultured mouse macrophage cells, *J. Ethnopharmacol.*, 83(1-2), 153-159 (2002).

Hosny, K. M., Alendronate sodium as enteric coated solid lipid nanoparticles; preparation, optimization, and *in vivo* evaluation to enhance its oral bioavailability, *PLoS One*, 11, (2016).

Hougee, S., Hartog, A., Sanders, A., Graus Y. M. F., Hoijer, M. A., Garssen, J., van den Berg, W. B., van Beuningen, H. M., and Smit, H. F., Oral administration of the NADPH-oxidase inhibitor apocynin partially restores diminished cartilage proteoglycan synthesis and reduces inflammation in mice, *Eur. J. Pharmacol.*, 531(1-3), 264-269 (2006).

Hussein, S. Z., Yusoff, K. M., Makpol, S., and Yusof, Y. A. M., Gelam honey attenuates carrageenan-induced rat paw inflammation via NF- κ B pathway, *PLoS One*, 8(8), e72365 (2013).

Hwang, Y. J., Lee, S. J., Park, J. Y., Chun, W., Nam, S. J., Park, J. M., Park, S. C., Choi, D. H., and Kang, C.D., Apocynin suppresses lipopolysaccharide-induced inflammatory responses through the inhibition of MAP kinase signaling pathway in RAW264.7 cells, *Drug Dev. Res.*, 77, 271-277 (2016).

Ibrahim, M. M., Abd-Elgawad, H. A., Soliman, O. A., and Jablonski, M. . M., Nanoparticle-based topical ophthalmic formulations for sustained celecoxib release, *J. Pharm. Sci.*, 102(3), 1036-1053 (2013).

ICH, Q2 (R1), Validation of Analytical Procedures: Text and Methodology, International Conference on Harmonization, Geneva (2005).

Impellizzeri, D., Mazzon, E., Esposito, E., Paterniti, I., Bramanti, P., and Cuzzocrea, S., Effect of apocynin, an inhibitor of NADPH oxidase, in the inflammatory process induced by an experimental model of spinal cord injury, *Free Radic. Res.*, 45, 221-236 (2011).

Isailović, T., Đorđević, S., Marković, B., Randelović, D., Cekić, N., Lukić, M., Pantelić, I., Daniels, R., and Savić, S., Biocompatible nanoemulsions for improved aceclofenac skin delivery: formulation approach using combined mixture-process experimental design, *J. Pharm. Sci.*, 105, 308-323 (2016).

Izadiyan, Z., Basri, M., Masoumi, H. R. F., Karjiban, R. A., Salim, N., and Shameli, K., Modeling and optimization of nanoemulsion containing sorafenib for cancer treatment by response surface methodology, *Chem. Cent. J.*, 11(21), (2017).

Jabeen, S., Hanif, M. A., Khan, M. M., and Qadric, R. W. K., Natural products sources and their active compounds on disease prevention: a review, *IJCBS*, 6, 76-83 (2014).

Ji, H., Tang, J., Li, M., Ren, J., Zheng, N., and Wu, L., Curcumin-loaded solid lipid nanoparticles with Brij78 and TPGS improved *in vivo* oral bioavailability and *in situ* intestinal absorption of curcumin, *Drug. Deliv.*, 23, 459-470 (2016).

Jiang, S., Chen, Y., Duan, G., Mei, C., Greiner, A., and Agarwal, S., Electrospun nanofiber reinforced composites: a review, *Polym. Chem.*, 9, 2685-2720 (2018).

Karataş, A., and Bekmezci, Ş., Evaluation and enhancement of physical stability of semi-solid dispersions containing piroxicam into hard gelatin capsules, *Acta. Pol. Pharm.*, 70(5), 883-897 (2013).

Keum, C., Noh, Y., Baek, J., Lim, J., Hwang, C., Na, Y., Shin, S., and Cho, C., Practical preparation procedures for docetaxel-loaded nanoparticles using polylactic acid-co-glycolic acid, *Int. J. Nanomedicine*, 6, 2225-2234 (2011).

Khademi, F., Taheri, R. A., Avarvand, A. Y., Vaez, H., Momtazi-Borojeni, A. A., and Soleimanpour, S., Are chitosan natural polymers suitable as adjuvant/delivery system for anti-tuberculosis vaccines?, *Microb. Pathog.*, 121, 218-223 (2018).

Kim S., Competitive biological activities of chitosan and its derivatives: antimicrobial, antioxidant, anticancer, and anti-inflammatory activities, *Int. J. Polym. Sci.*, 2018, (2018).

Kim, S. S., Oh, O. J., Min, H. Y., Park, E. J., Kim, Y., Park, H. J., Nam Han, Y., and Lee, S. K., Eugenol suppresses cyclooxygenase-2 expression in lipopolysaccharide-stimulated mouse macrophage RAW264.7 cells, *Life Sci.*, 73(3), 337-348 (2003).

Komatsu, H., Kitajima, A., and Okada, S., Pharmaceutical characterization of commercially available intravenous fat emulsions: evaluation of average particle size, size distribution and surface potential using photon correlation spectroscopy, *Chem. Pharm. Bull.*, 43, 1412-1415 (1995).

Kono, H., Otaka, F., and Ozaki, M., Preparation and characterization of guar gum hydrogels as carrier materials for controlled protein drug delivery, *Carbohydr. Polym.*, 111, 830-840 (2014).

Korsmeyer, R. W., Gurny, R., Doelker, E., Buri, P., and Peppas, N. A., Mechanism of solute release from porous hydrophilic polymers, *Int. J. Pharm.*, 15, 25-35 (1983).

Kriegel, C., Kit, K. M., McClements, D. J., and Weiss, J., Nanofibers as carrier systems for antimicrobial microemulsions. II. Release characteristics and antimicrobial activity, *J. Appl. Polym. Sci.*, 118, 2859-2868 (2010).

Kumar, R., Singh, A., Garg, N., and Siril, P. F., Solid lipid nanoparticles for the controlled delivery of poorly water soluble non-steroidal anti-inflammatory drugs, *Ultrason. Sonochem.*, 40, 686-696 (2018).

Kura, A. U., Hussein-Al-Ali, S. H., Hussein, M. Z., and Fakurazi, S., Preparation of tween 80-Zn/Al-levodopa-layered double hydroxides nanocomposite for drug delivery system, *Sci. World J.*, 2014, (2014).

Kyselova, Z., Toxicological aspects of the use of phenolic compounds in disease prevention, *Interdiscip. Toxicol.*, 4(4), 173-183 (2011).

Lacerda, C. V., Carvalho, M. J. S., Ratton, A. R., Soares, I. P., and Borges, L. E. P., Synthesis of triacetin and evaluation on motor, *J. Braz. Chem. Soc.*, 26(8), 1625-1631 (2015).

Lattanzio, V. Phenolic Compounds: Introduction. In: Ramawat, K.G., Merillon, J.M. (eds.), *Handbook of Natural Products*, Springer-Verlag Berlin Heidelberg (2013).

Leach, W. T., Simpson, D. T., Val, T. N., Yu, Z., Lim, K. T., Park, E. J., Williams, R. O., and Johnston, K. P., Encapsulation of protein nanoparticles into uniform-sized microspheres formed in a spinning oil film, *AAPS PharmSciTech.*, 6(4), E605-E617 (2005).

Lee, Y. Y., Hung, S. L., Pai, S. F., Lee, Y. H., and Yang, S. F., Eugenol suppressed the expression of lipopolysaccharide-induced proinflammatory mediators in human macrophages, *J. Endod.*, 33(6), 698-702 (2007).

Lei, L., He, Z., Chen, H., McClements, D. J., Li, B., and Li, Y., Microstructural, rheological, and antibacterial properties of cross-linked chitosan emulgels, *RSC Adv.*, 5(121), (2015).

Lemke, T. L., and Williams, D. A., “Physicochemical and biopharmaceutical properties of drug substances and pharmacokinetics”, Chapter 3, in: “Foye’s Principles of Medicinal Chemistry”, 7th Ed., Lippincott Williams & Wilkins, Philadelphia, P. 96 (2012).

Liu, D., Jiang, S., Shen, H., Qin, S., Liu, J., Zhang, Q., Li, R., and Xu, Q., Diclofenac sodium-loaded solid lipid nanoparticles prepared by emulsion/solvent evaporation method, *J. Nanopart. Res.*, 13, 2375-2386 (2011).

Liu, S., and Ho, P. C., Intranasal administration of brain-targeted HP- β -CD/chitosan nanoparticles for delivery of scutellarin, a compound with protective effect in cerebral ischaemia, *J. Pharm. Pharmacol.*, 69, 1495-1501 (2017).

Lovelyn, C., and Attama, A. A., Current state of nanoemulsions in drug delivery, *J. Biomater. Nanobiotechnol.*, 2, 626-639 (2011).

Luo, H., Lv, X. D., Wang, G. E., Li, Y. F., Kurihara, H., and He, R. R., Anti-inflammatory effects of anthocyanins-rich extract from bilberry (*Vaccinium myrtillus* L.) on croton oil-induced ear edema and *Propionibacterium acnes* plus LPS-induced liver damage in mice, *Int. J. Food Sci. Nutr.*, 65(5), 594-601 (2014).

Madan, S. S., and Wasewar, K. L., Optimization for benzenoacetic acid removal from aqueous solution using CaO₂ nanoparticles based on Taguchi method, *J. Appl. Res. Technol.*, 15(4), 332-339 (2017).

Manjanna, K. M., Pramod Kumar, T. M., and Shivakumar, B., Natural polysaccharide hydrogels as novel excipients for modified drug delivery systems: a review, *Int. J. Chemtech Res.*, 2, 509-525 (2010).

Manjunath, K., Venkateswarlu, V., and Hussain, A., Preparation and characterization of nitrendipine solid lipid nanoparticles, *Pharmazie*, 66, 178-186 (2011).

Mansour, H. M., Sohn, M., Al-Ghananeem, A. M., and Deluca, P. P., Materials for pharmaceutical dosage forms: molecular pharmaceutics and controlled release drug delivery aspects, *Int. J. Mol. Sci.*, 11(9), 3298-322 (2010).

Martinez, N. Y., Andrade, P. F., Durán, N., and Cavalitto S., Development of double emulsion nanoparticles for the encapsulation of bovine serum albumin, *Colloids Surf. B: Biointerf.*, 158, 190-196 (2017).

McGee, M. A., and Abdel-Rahman, A.A., Enhanced vascular PI3K/Akt-NOX signaling underlies the peripheral NMDAR-mediated pressor response in conscious rats, *J. Cardiovasc. Pharmacol.*, 63, 395-405 (2014).

Mishra, V., Bansal, K. K., Verma, A., Yadav, N., Thakur, S., Sudhakar, K., and Rosenholm, J. M., Solid lipid nanoparticles: emerging colloidal nano drug delivery systems, *Pharmaceutics*, 10(4), (2018).

Mobarak, D. H., Salah, S., and Elkheshen, S. A., Formulation of ciprofloxacin hydrochloride loaded biodegradable nanoparticles: optimization of technique and process variables, *Pharm. Dev. Technol.*, 19(7), 891-900 (2014).

Modrzejewska, Z., Nawrotek, K., Zarzycki, R., and Douglas, T., Structural characteristics of thermosensitive chitosan glutamate hydrogels, *PCACD.*, 17, 93-106 (2013).

Mohamed, E. A., Meshali, M. M., Foda, A. M., and Borg, T. M., Improvement of dissolution and hypoglycemic efficacy of glimepiride by different carriers, *AAPS PharmSciTech.*, 13 (3), 1013-1023 (2012)^a.

Mohamed, E. A., Zhao, Y., Meshali, M. M., Remsberg, C. M., Borg, T. M., Foda, A. M., Takemoto, J. K., Sayre, C. L., Martinez, S. E., Davies, N. M., and Forrest, M. L., Vorinostat with sustained exposure and high solubility in poly(ethylene

glycol)-b-poly(DL-lactic acid) micelle nanocarriers: characterization and effects on pharmacokinetics in rat serum and urine, *J. Pharm. Sci.*, 101, 3787-3798 (2012)^b.

Mohanty, B., Majumdar, D. K., Mishra, S. K., Panda, A. K., and Patnaik, S., Development and characterization of itraconazole-loaded solid lipid nanoparticles for ocular delivery, *Pharm. Dev. Technol.*, 20, 458-464 (2014).

Mohtar, N., Khan, N. A. K., and Darwis, Y., Solid lipid nanoparticles of atovaquone based on 2⁴ full-factorial design, *IJPR.*, 14, 989-1000 (2015).

Mudgil, D., Barak, S., and Khatkar, B. S., Guar gum: processing, properties and food applications – A Review, *J. Food Sci. Technol.*, 51(3), 409-418 (2014).

Mudgil, D., Barak, S., and Khatkar, B. S., X-ray diffraction, IR spectroscopy and thermal characterization of partially hydrolyzed guar gum, *Int. J. Biol. Macromolec.*, 50, 1035-1039 (2012).

Mulia, K., Ramadhan, R. M. A., and Krisanti, E. A., Formulation and characterization of nanoemulgel mangosteen extract in virgin coconut oil for topical formulation, *MATEC Web of Conferences*, 156, (2018).

Muller, R. H., Mader, K., and Gohla, S., Solid lipid nanoparticles (SLN) for controlled drug delivery – a review of the state of the art, *Eur. J. Pharm. Biopharm.*, 50, 161-177 (2000).

Narala, A., and Veerabrahma, K., Preparation, characterization and evaluation of quetiapine fumarate solid lipid nanoparticles to improve the oral bioavailability, *J. Pharm.*, 2013, (2013).

Nayaka, A. K., and Pal, D., Formulation optimization and evaluation of jackfruit seed starch–alginate mucoadhesive beads of metformin HCl, *Int. J. Biol. Macromol.*, 59, 264-272 (2013).

Nguyen, T. T. T., Ghosh, C., Hwang, S., Chanunpanich, N., and Park, J. S., Porous core/sheath composite nanofibers fabricated by coaxial electrospinning as a potential mat for drug release system, *Int. J. Pharm.*, 439, 296-306 (2012).

Okuda, T., Tominaga, K., and Kidoaki, S., Time-programmed dual release formulation by multilayered drug-loaded nanofiber meshes, *J. Control Release*, 143, 258-264 (2010).

Öztürk, A., and Özbek, H., The anti-inflammatory activity of eugenia caryophyllata essential oil: an animal model of anti-inflammatory activity, *Eur. J. Gen. Med.*, 2, 159-163 (2005).

Pal, S. L., Jana, U., Manna, P. K., Mohanta, G. P., and Manavalan, R., Nanoparticle: an overview of preparation and characterization, *JAPS.*, 1(6), 228-234 (2011).

Pardeshi, C., Rajput, P., Belgamwar, V., Tekade, A., Patil, G., Chaudhary, K., and Sonje, A., Solid lipid based nanocarriers: an overview, *Acta Pharma.*, 62, 433-472 (2012).

Patel, M. N., Lakkadwala, S., Majrad, M. S., Injeti, E. R., Gollmer, S. M., Shah, Z. A., Boddu, S. H. S., and Nesamony, J., Characterization and evaluation of 5-fluorouracil-loaded solid lipid nanoparticles prepared via a temperature-modulated solidification technique, *AAPS PharmSciTech.*, 15, 1498-1508 (2014).

Petrônio, M. S., Zeraik, M. L., Marcos da Fonseca, L., and Ximenes, V. F., Apocynin: chemical and biophysical properties of a NADPH oxidase inhibitor, *Molecules*, 18, 2821-2839 (2013).

Puhl, A. C., Fagundes, M., Cristina dos Santos, K., Polikarpov, I., Fernandes da Silva, M. F., Fernandes, J. B., Vieira, P. C., and Forim, M. R., Preparation and characterization of polymeric nanoparticles loaded with the flavonoid luteolin, by using factorial design, *Int. J. Drug Deliv.*, 3, 683-698 (2011).

Rachmawati, H., Budiputra, D. K., and Mauludin, R., Curcumin nanoemulsion for transdermal application: formulation and evaluation, *Drug Dev. Ind. Pharm.*, 41(4), 560-566 (2015).

Rahman, S., Ansari R. A., Rehman, H., Parvez, S., and Raisuddin, S., Nordihydroguaiaretic acid from creosote bush (*Larrea tridentata*) mitigates 12-O-tetradecanoylphorbol-13-acetate-induced inflammatory and oxidative stress responses of tumor promotion cascade in mouse skin, *Evid. Based Complement. Alternat. Med.*, 2011, (2011).

Ramadan, E., Borg, Th., Abdelghani, G. M., and Saleh, N. M., Design and *in vivo* pharmacokinetic study of a newly developed lamivudine transdermal patch, *Future J. Pharm. Sci.*, 4, 166-174 (2018).

Rao, J., and McClements, D. J., Food-grade microemulsions, nanoemulsions and emulsions: fabrication from sucrose monopalmitate & lemon oil, *Food Hydrocoll.* 25, 1413-1423 (2011).

Rao, K. K., Polymerized solid lipid nanoparticles for oral or mucosal delivery of therapeutic proteins and peptides, US Patent 0,237,826 A1 (2007).

Raposo, S., Tavares, R., Gonçalves, L., Simões, S., Urbano, M., and Ribeiro, H. M., Mometasone furoate-loaded cold processed oil-in-water emulsions: *in vitro* and *in vivo* studies, *Drug Deliv.*, 22(4), 562-572 (2015).

Ravi babu, V., Pugazhenth, G., and Katiyar, V., Fabrication and characterization of sucrose palmitate reinforced poly (lactic acid) bionanocomposite films, *J. Appl. Polym. Sci.*, 132(3), (2015).

Reddy, L. H., Vivek, K., Bakshi, N., and Murthy, R. S. R., Tamoxifen citrate loaded solid lipid nanoparticles (SLN): preparation, characterization, *in vitro* drug release, and pharmacokinetic evaluation, *Pharm. Dev. Technol.*, 11, 167-177 (2006).

Ricciotti, E., and FitzGerald, G. A., Prostaglandins and inflammation, *Arterioscler. Thromb. Vasc. Biol.*, 31(5), 986-1000 (2011).

Riganti, C., Costamagna, C., Bosia, A., and Ghigo, D., The NADPH oxidase inhibitor apocynin (acetovanillone) induces oxidative stress, *Toxicol. Appl. Pharmacol.*, 212(3), 179-187 (2006).

Riganti, C., Costamagna, C., Doublier, S., Miraglia, E., Polimeni, M., Bosia, A., and Ghigo, D., The NADPH oxidase inhibitor apocynin induces nitric oxide synthesis via oxidative stress, *Toxicol. Appl. Pharmacol.*, 228(3), 277-285 (2008).

Rizwan, M., Yahya, R., Hassan, A., Yar, M., Azzahari, A. D., Selvanathan, V., Sonsudin, F., and Abouloula, C. N., pH sensitive hydrogels in drug delivery: brief history, properties, swelling, and release mechanism, material selection and applications, *Polymers*, 9(137), (2017).

Sadiq, A. A., and Abdul rassol, A. A., Formulation and evaluation of silibinin loaded solid lipid nanoparticles for peroral use targeting lower part of gastrointestinal tract, *Int. J. Pharm. Pharm. Sci.*, 6, 55-67 (2014).

Sadrjavadi, K., Shahbazi, B., and Fattahi, A., De-esterified tragacanth-chitosan nano-hydrogel for methotrexate delivery; optimization of the formulation by Taguchi design, *Artif. Cells Nanomed. Biotechnol.*, (2018).

Saikia, C., Gogoi, P., and Maji, T. K., Chitosan: a promising biopolymer in drug delivery applications, *J. Mol. Genet. Med.*, S4:006 (2015).

Salomon, C., Goycoolea, F. M., and Moerschbacher, B., Recent trends in the development of chitosan-based drug delivery systems, *AAPS PharmSciTech.*, 18(4), 933-935 (2017).

Sami, A. J., Khalid, M., Jamil, T., Aftab, S., Mangat, S. A., Shakoori, A. R., and Iqbal, S., Formulation of novel chitosan guar gum based hydrogels for sustained drug release of paracetamol, *Int. J. Biol. Macromol.*, 108, 324-332 (2018).

Sengupta, P., and Chatterjee, B., Potential and future scope of nanoemulgel formulation for topical delivery of lipophilic drugs, *Int. J. Pharm.*, 526(1-2), 353-365 (2017).

Shagholani, H., Ghoreishi, S. M., and Mousazadeh, M., Improvement of interaction between PVA and chitosan via magnetite nanoparticles for drug delivery application, *Int. J. Biol. Macromol.*, 78, 130-136 (2015).

Shah, R., Eldridge, D., Palombo, E., and Harding, I., Optimisation and stability assessment of solid lipid nanoparticles using particle size and zeta potential, *J. Phys. Sci.*, 25, 59-75 (2014).

Shahavi, M. H., Hosseini, M., Jahanshahi, M., Meyer, R. L., and Darzi, G. N., Clove oil nanoemulsion as an effective antibacterial agent: Taguchi optimization method, *Desalin. Water Treat.*, 57(39), 18379-18390 (2016).

Shan, X., Liu, C., Li, F., Ouyang, C., Gao, Q., and Zheng, K., Nanoparticles vs. nanofibers: a comparison of two drug delivery systems on assessing drug release performance *in vitro*, *Des. Monomers Polym.*, 18(7), 678-689 (2015).

Shargel, I., Wu-Pong, S., and Yu, A. B. C., "Bioavailability and bioequivalence", in: "Applied Biopharmaceutics and Pharmacokinetics", 5th Ed., McGraw-Hill, Asia, P. 460 (2005).

Shariatnia, Z., and Jalali, A. M., Chitosan-based hydrogels: preparation, properties and applications, *Int. J. Biol. Macromol.*, 115, 194-220 (2018).

Sharma, R., Kaith, B. S., Kalia, S., Pathania, D., Kumar, A., Sharma, N., Street, R. M., and Schauer, C., Biodegradable and conducting hydrogels based on guar gum polysaccharide for antibacterial and dye removal applications, *J. Environ. Manage.*, 162, 37-45 (2015).

Sharma, S., Parmar, A., Bhardwaj, R., and Kaur, T., Design and characterization of apocynin loaded PLGA nanoparticles and their *in vivo* efficacy in hyperoxaluric rats, *Curr. Drug Deliv.*, (2018).

Shazly, G. A., Ciprofloxacin controlled-solid lipid nanoparticles: characterization, *in vitro* release, and antibacterial activity assessment, *BioMed Res. Int.*, 2017, (2017).

Shende, P. K., Gaud, R. S., Bakal, R., and Yeole, Y., Clove oil emulsified buccal patch of serratiopeptidase for controlled release in toothache, *J. Bioequiv. Availab.*, 8(3), 134-139 (2016).

Shi, F., Zhao, J. H., Liu, Y., Wang, Z., Zhang, Y. T., and Feng, N. P., Preparation and characterization of solid lipid nanoparticles loaded with frankincense and myrrh oil, *Int. J. Nanomedicine*, 7, 2033-2043 (2012).

Shi, L., Cao, Y., Zhu, X., Cui, J., and Cao, Q., Optimization of process variables of zanamivir-loaded solid lipid nanoparticles and the prediction of their cellular transport in Caco-2 cell model, *Int. J. Pharm.*, 478, 60-69 (2015)^b.

Shi, L., Lu, J., Cao, Y., Liu, J., Zhang, X., Zhang, H., Cui, J., and Cao, Q., Gastrointestinal stability, physicochemical characterization and oral bioavailability of chitosan or its derivatives-modified solid lipid nanoparticles loading docetaxel, *Drug Dev. Ind. Pharm.*, 43, 839-846 (2017).

Shi, X., Zhou, W., Ma, D., Ma, Q., Bridges, D., Ma, Y., and Hu, A., Electrospinning of nanofibers and their applications for energy devices, *J. Nanomater.*, 2015, (2015)^a.

Shin, S., Joo, S. S., Park, D., Jeon, J. H., Kim, T. K., Kim, J. S., Park, S. K., Hwang, B. Y., and Kim, Y. B., Ethanol extract of *Angelica gigas* inhibits croton oil-induced inflammation by suppressing the cyclooxygenase - prostaglandin pathway, *J. Vet. Sci.*, 11(1), 43-50 (2010).

Shwaireb, M. H., Inflammatory effects of the tumor promoter croton oil in BALB/c mice skin, *Oncol. Rep.*, 2(1), 133-135 (1995).

Simonyi, A., Serfozo, P., Lehmidi, T. M., Cui, J., Gu, Z., Lubahn, D. B., Sun, A. Y., and Sun, G. Y., The neuroprotective effects of apocynin, *Front. Biosci.*, 4, 2183-2193 (2012).

Singh, R. P., Parpani, S., Narke, R., and Chavan, R., Emulgel: a recent approach for topical drug delivery system, *AJPRD*, 2(2), 13-15 (2014).

Singh, R., and Lillard, J. W. Jr., Nanoparticle-based targeted drug delivery, *Exp. Mol. Pathol.*, 86(3), 215-223 (2009).

Singha, B., Sharmab, S., and Dhiman, A., Acacia gum polysaccharide based hydrogel wound dressings: synthesis, characterization, drug delivery and biomedical properties, *Carbohydr. Polym.*, 165, 294-303 (2017).

Sinha, M., Gautam, L., Shukla, P. K., Kaur, P., Sharma, S., and Singh, T. P., Current perspectives in NSAID-induced gastropathy, *Mediators Inflamm.*, 2013, (2013).

Soma, D., Attari, Z., Reddy, M. S., Damodaram, A., and Koteswara, K. B. G., Solid lipid nanoparticles of irbesartan: preparation, characterization, optimization and pharmacokinetic studies, *Braz. J. Pharm., Sci.* 53, (2017).

Stefanska, J., and Pawliczak, R., Apocynin: molecular aptitudes, *Mediators Inflamm.*, 2008, 691-698 (2008).

Szűts, A., Budai-Szűcs, M., Erős, I., Otomo, N., and Szabó-Révésza, P., Study of gel-forming properties of sucrose esters for thermosensitive drug delivery systems, *Int. J. Pharm.*, 383, 132-137 (2010).

't Hart, B. A., Copray, S., and Philippens, I., Apocynin, a low molecular oral treatment for neurodegenerative disease, *BioMed Res. Int.*, 2014, 298020 (2014).

Tagwireyi, D., and Majinda, R. R., Isolation and identification of acetovanillone from an extract of *Boophone disticha* (L.f.) herb (Amaryllidaceae), *S. Afr. J. Bot.*, 108, 100-101 (2017).

Tan, Q., Liu, W., Guo, C., and Zhai, G., Preparation and evaluation of quercetin-loaded lecithin-chitosan nanoparticles for topical delivery, *Int. J. Nanomedicine*, 6, 1621-1630 (2011).

Teo, S. Y., Lee, S. Y., Ong, H. L., Ong, C. L., Gan, S. N., Rathbone, M. J., and Coombes, A. G. A., Evaluation of biosourced alkyd nanoemulsions as drug carriers, *J. Nanomater.*, 2015, (2015).

Tonglairoum, P., Ngawhirunpat, T., Rojanarata, T., Kaomongkolgit, R., and Opanasopit, P., Fabrication and evaluation of nanostructured herbal oil/

hydroxypropyl- β -cyclodextrin/polyvinylpyrrolidone mats for denture stomatitis prevention and treatment, *AAPS PharmSciTech.*, 17(6), 1441-1449 (2016).

Toutain, P. L., and Bousquet-Mélou, A., Bioavailability and its assessment, *J. Vet. Pharmacol. Therap.*, 27, 455-466, (2004).

Vandervoort, J., and Ludwig, A., Biocompatible stabilizers in the preparation of PLGA nanoparticles: a factorial design study, *Int. J. Pharm.*, 238, 77-92 (2002).

Vasdev, S., Singal, P., and Gill, V., The antihypertensive effect of cysteine, *Int. J. Angiol.*, 18 (1), 7-21 (2009).

Veeresham, C., Natural products derived from plants as a source of drugs, *J. Adv. Pharm. Tech. Res.*, 3(4), 200-201 (2012).

Venishetty, V. K., Chede, R., Komuravelli, R., Adepu, L., Sistla, R., and Diwan, P. V., Design and evaluation of polymer coated carvedilol loaded solid lipid nanoparticles to improve the oral bioavailability: a novel strategy to avoid intraduodenal administration, *Colloids Surf. B: Biointerf.*, 95, 1-9 (2012).

Vivek, K., Reddy, H., and Murthy, R .S. R., Investigations of the effect of the lipid matrix on drug entrapment, *in vitro* release, and physical stability of olanzapine-loaded solid lipid nanoparticles, *AAPS PharmSciTech.*, 8(4), 16-24 (2007).

Vyas, A., Saraf, S., and Saraf, S., Encapsulation of cyclodextrin complexed simvastatin in chitosan nanocarriers: a novel technique for oral delivery, *J. Incl. Phenom. Macrocycl. Chem.*, 66(3), 251-259 (2010).

Wang, K., Li, L., Song, Y., Ye, X., Fu, S., Jiang, J., and Li, S., Improvement of pharmacokinetics behavior of apocynin by nitron derivative: comparative pharmacokinetics of nitron-apocynin and its parent apocynin in rats, *PLoS One*, 8, (2013).

Wang, Q., Smith, R. E., Luchtefeld, R., Sun, A. Y., Simonyi, A., Luo, R., and Sun, G. Y., Bioavailability of apocynin through its conversion to glycoconjugate but not to diapocynin, *Phytomedicine*, 15(6-7), 496-503 (2008).

Wu, L., Zhang, J., and Watanabe, W., Physical and chemical stability of drug nanoparticles, *Adv. Drug Deliv. Rev.*, 63, 456-469 (2011).

Wu, Y., Li, Y., Gao, X., and Chen, H., The application of nanoemulsion in dermatology: an overview, *J. Drug Target.*, 21(4), 321-327 (2013).

Ximenes, V. F., Kanegae, M. P., Rissato, S. R., and Galhiane, M. S., The oxidation of apocynin catalyzed by myeloperoxidase: proposal for NADPH oxidase inhibition, *Arch. Biochem. Biophys.*, 457(2), 134-141 (2007).

Xiong, H., Wu, M., Zou, H., Jiang, S., Yi, H., Yi, T., Wang, Q., Liu, D., Zhou, Y., Wei, C., and Zhou, X., Chitosan inhibits inflammation and adipogenesis of orbital fibroblasts in Graves ophthalmopathy, *Mol. Vis.*, 24, 509-517 (2018).

Xue, J., Xie, J., Liu, W., and Xia, Y., Electrospun nanofibers: new concepts, materials, and applications, *Acc. Chem. Res.*, 50, 1976-1987 (2017).

Yas, A. A., "Solid Lipid Microparticles for Controlling Theophylline Pulmonary Delivery and Local Retention", "PhD Thesis", College of Pharmacy, Pharmaceutics Department, Baghdad University, Iraq (2013).

Zakaria, A. S., Afifi, S. A., and Elkhodairy, K. A., Newly developed topical cefotaxime sodium hydrogels: antibacterial activity and *in vivo* evaluation, *BioMed Res. Int.*, 2016, (2016).

Zhang, C., Gu, C., Peng, F., Liu, W., Wan, J., Xu, H., Lam, C. W., and Yang, X., Preparation and optimization of triptolide-loaded solid lipid nanoparticles for oral delivery with reduced gastric irritation, *Molecules*, 18, 13340-13356 (2013).

Supervisors

Thesis Title: Development and Characterization of Certain Controlled Release Drug Delivery Systems Based on Some Polymers as Carrier Matrix.

Student Name: Reham Mokhtar Ahmed Mohamed Aman

Supervisors:

	Name	Occupation	Signature
1	<i>Prof. Dr. Mahasen M. Abd El Hady Meshali</i>	Professor Emeritus of Pharmaceutics, Faculty of Pharmacy, Mansoura University	
2	<i>Ass. Prof. Dr. Irhan Ibrahim Abu Hashim</i>	Associate Professor of Pharmaceutics, Faculty of Pharmacy, Mansoura University	

***Head of the Department
of Pharmaceutics***

***Vice Dean for Research
and Graduate Studies***

***Dean of
Faculty of Pharmacy***

***Prof. Dr.
Osama Abd El-Azeem
Soliman***

***Prof. Dr.
Manal M. Eid***

***Prof. Dr.
Nahed M. El-Enany***

Approval Sheet

Thesis Title: Development and Characterization of Certain Controlled Release Drug Delivery Systems Based on Some Polymers as Carrier Matrix.

Student Name: Reham Mokhtar Ahmed Mohamed Aman

Supervisors:

	Name	Occupation	Signature
1	<i>Prof. Dr. Mahasen M. Abd El Hady Meshali</i>	Professor Emeritus of Pharmaceutics, Faculty of Pharmacy, Mansoura University	
2	<i>Ass. Prof. Dr. Irhan Ibrahim Abu Hashim</i>	Associate Professor of Pharmaceutics, Faculty of Pharmacy, Mansoura University	

Thesis has been approved by:

	Name	Occupation	Signature
1	<i>Prof. Dr. Mahasen M. Abd El Hady Meshali</i>	Professor Emeritus of Pharmaceutics, Faculty of Pharmacy, Mansoura University	
2	<i>Prof. Dr. Omaima Ahmed Amin Samour</i>	Professor of Pharmaceutics & Industrial Pharmacy, Faculty of Pharmacy, Ain Shams University	
3	<i>Prof. Dr. Nahed Dawood Saleh Mortada</i>	Professor of Pharmaceutics & Industrial Pharmacy, Faculty of Pharmacy, Ain Shams University	
4	<i>Ass. Prof. Dr. Irhan Ibrahim Abu Hashim</i>	Associate Professor of Pharmaceutics, Faculty of Pharmacy, Mansoura University	

*Head of the Department
of Pharmaceutics*

*Vice Dean for Research
and Graduate Studies*

*Dean of
Faculty of Pharmacy*

*Prof. Dr.
Osama Abd El-Azeem
Soliman*

*Prof. Dr.
Manal M. Eid*

*Prof. Dr.
Nahed M. El-Enany*

المخلص العربي

أنظمة توصيل الأدوية محكمة الإنطلاق تشير إلى إطلاق العقار أو المواد البيولوجية بصورة محكمة من المستحضر الصيدلي إلى الهدف المحدد. وبالتالي تجنب الآثار الجانبية للعقار وكذلك تحسين استجابة المرضى ورضاهم.

حاليا، طب النانو، والمعروف بأنه تطبيق تقنية النانو في المجال الطبي باستخدام مواد نانومترية الأبعاد، بإمكانها أن تعزز المجال الطبي تماشيا مع الطب التقليدي. كما أن تطبيق طب النانو كإستراتيجية مفيدة لتوصيل الأدوية تتيح الفرص لإحكام إنطلاق الأدوية وتوصيلها إلى الهدف المحدد وكذلك حمايتها من التدهور الإنزيمي أو البيئي.

حظت الحاملات النانوية باهتماما عالميا في مجال توصيل الأدوية ومن ضمنها الجسيمات الصلبة الدهنية نانوية الحجم، و الإيمجل ذو الحجم النانو و ألياف النانو.

تعتبر الطبيعة مورد لا ينضب في مجال تطوير الأدوية واكتشاف الجديدة منها ذو نشاط حيوي. ومنذ زمن بعيد، أصبحت المنتجات الطبيعية النشطة حيويا دعامة العلاجات الشعبية في كافة أنحاء العالم وتمثل جزء لا يتجزأ من التاريخ والحضارة. ومن ثم، يوجد حاليا اهتمام متجدد بالتطبيق المستقبلي للمنتجات الطبيعية كبدايل للأدوية المصنعة، وذلك لما تتميز به من فوائد مزدوجة متعلقة بالنشاط الفارماكولوجي والسلامة.

العقارات من أصل نباتي هي المركبات التي تتكون بشكل طبيعي في النبات ولها أنشطة دوائية متعددة ضد مجموعة متنوعة من الأمراض. وتعد المركبات الفينولية، أشباه القلويات، التانينات ومركبات الفلافونويد من العقارات ذات الأصل النباتي. والجدير بالذكر أن الأوسينين و زيت القرنفل العطري من ضمن المركبات الفينولية الطبيعية والتي تحتاج إلى صياغتها في أنظمة توصيل واعدة.

الأوسينين هو مثبط محدد لفسفات ثنائي نيوكليوتيد النيكوتين و الأدينين المختزل أكسيداز (NADPH-oxidase inhibitor) له أنشطة فارماكولوجية متنوعة ومع ذلك فهو غير متوفر في السوق في أشكال صيدلية.

زيت القرنفل هو زيت عطري يمتلك العديد من الأنشطة الفارماكولوجية وقد تم الموافقة عليه من قبل إدارة الغذاء والدواء علي أنه آمن لإستخدامات متعددة. و مع ذلك فقد تم نشر محاولات قليلة لصياغة وتقييم الأنشطة الفارماكولوجية لزيت القرنفل العطري في بعض أنظمة التوصيل الدوائي. وبناءا عليه فإن هناك نهج سريع التطور لتحضير المستحضرات الصيدلانية النباتية التي تقوم أساسا علي إستخدام تكنولوجيا النانو مع العقارات ذات الأصل النباتي.

تحديث وتوصيف أنظمة توصيل عقار معينة محكمة الإنطلاق بإستخدام بعض البوليمرات كوسادة حاملة.

المخلص العربي

وبالتالي، فإن الهدف الرئيسي لهذه الرسالة هو تطوير مستحضرات صيدلانية نباتية جديدة نانومترية الأبعاد و محكمة الإنطلاق لتعزيز توصيل الألبوسينين (بالفم أو بالحقن) وكذلك التوصيل الموضعي لزيت القرنفل العطري لتحسين التوافر الحيوي و النشاط الفارماكولوجي على التوالي، من أجل تطبيقات علاجية مستقبلية. لتحقيق هذه الأهداف إشتملت الرسالة على جزئين:

الجزء الأول: الجسيمات الصلبة الدهنية نانوية الحجم الجديدة القائمة على الشيتوزان لتحسين الإتاحة الحيوية للعقار المذهل من أصل نباتي "الألبوسينين"

الجزء الثاني: الإيمجل ذو الحجم النانو وألياف النانو المحملين بزيت القرنفل العطري: مستحضرات صيدلانية نباتية بإمكانات واعدة كمثبطات لإنزيم السيكلو اوكسيجيناز-2 في الالتهاب الخارجي

الجزء الأول

الجسيمات الصلبة الدهنية نانوية الحجم الجديدة القائمة على الشيتوزان لتحسين الإتاحة الحيوية للعقار المذهل من أصل نباتي "الألبوسينين"

الألبوسينين هو عقار من أصل نباتي نشط بيولوجياً وله أنشطة بارزة مضادة للإلتهاب ومضادة للأكسدة تم إثباتها على مجموعة متنوعة من الخلايا والنماذج الحيوانية. أيضاً، في الأونة الأخيرة تم تطوير الجسيمات الصلبة الدهنية نانوية الحجم كحاملات نانوية واعدة تتميز بالقدرة العالية علي تحميل الأدوية المحبة للماء والمحبة للدهون على حد سواء وكذلك تطبيقها في توصيل الأدوية عن طريق جميع مسارات التناول. بالإضافة إلى ذلك، فقد ثبت أن الشيتوزان والكحول عديد الفايثيل من المرشحين الواعدين لتحضير العديد من أنظمة توصيل النانو التي تهدف إلى تحفيز الفعالية العلاجية للأدوية المحملة ويرجع ذلك إلي خصائصهم الممتازة.

بناءً على ذلك، تم توجيه هذا الجزء من أجل تصنيع، توصيف، تعظيم الإستفادة وتقييم مستحضر صيدلي نباتي معد في شكل نظام الجسيمات الصلبة الدهنية نانوية الحجم الجديدة سهلة التحضير (الشيتوزان والألبوسينين/الكحول عديد الفايثيل) (النواة/الغلاف). تم تحضير ذلك المستحضر باستخدام تقنية المستحلب المزدوج وتبخير المذيب والمكون من (الشيتوزان و الألبوسينين) كطبقة مائية داخلية، ثلاثي ستيرات الجليسرول كطبقة زيتية، والكحول عديد الفايثيل كطبقة مائية خارجية. كذلك، تم تطبيق التصميم المعاملي الكامل (٢٤) للمفاضلة في إختيار أمثل تحضير للمستحضر بناءً على نتائج التقييم.

في هذا الجزء تم إجراء دراسات تفصيلية لتقييم الجسيمات الصلبة الدهنية نانوية الحجم القائمة علي الشيتوزان والمحملة بالألبوسينين من خلال التجارب المعملية والحيوية (بالفم أو بالحقن).

تحديث وتوصيف أنظمة توصيل عقار معينة محكمة الإنطلاق باستخدام بعض البوليمرات كوسادة حاملة.

المُلخَص العربي

الفصل الأول: تحضير، توصيف وتعظيم الإستفادة للجسيمات الصلبة الدهنية نانوية الحجم القائمة علي الشيتوزان والمُحملة بالأبوسينين.

الفصل الثاني: التوافر الحيوي للجسيمات الصلبة الدهنية نانوية الحجم الأمثل القائمة علي الشيتوزان والمُحملة بالأبوسينين عن طريق الفم والحقن في الجرذان.

الفصل الأول

تحضير، توصيف وتعظيم الإستفادة للجسيمات الصلبة الدهنية نانوية الحجم القائمة علي الشيتوزان والمُحملة بالأبوسينين.

يتناول العمل في هذا الفصل تصنيع مستحضر صيدلي نباتي جديد في شكل جسيمات صلبة دهنية نانوية الحجم من أجل توصيل الأبوسينين (بالفم أو بالحقن) وذلك باستخدام تقنية المستحلب المزدوج وتبخير المذيب. تم توصيف وتعظيم الإستفادة باتباع التصميم المعاملي الكامل (2^4) والذي إعتد علي إستخدام أربع متغيرات حاسمة ومستويان للتصميم. المتغيرات الحاسمة الأربعة هي كمية كل من ثلاثي ستيرات الجليسرول (X_A) و أحادي بالميتان السكروز (X_B) و تركيز كل من الشيتوزان (X_C) والكحول عديد الفايثيل (X_D). وقد تم دراسة خصائص الجودة الحاسمة للجسيمات الصلبة الدهنية نانوية الحجم المحضرة من حيث كفاءة الإحتواء الدوائي، نسبة الإنتاج، حجم الجزيئات، معامل تعدد الإنتشار وجهد الزيتا. بالإضافة الى تقييم الصيغة الأمثل المحضرة من خلال المجهر الإلكتروني النافذ، التحليل الطيفي للأشعة تحت الحمراء، المسح الحراري التفاضلي وحيود الأشعة السينية. وأخيرا تم دراسة خواص الانطلاق المعمللي للعقار، التحليل الرياضي لنتائج معدل الإنطلاق المعمللي ودراسه الثبات عند درجة حرارة التلاجة (5 ± 3 درجة سيليزية) ودرجة حرارة الغرفة للصيغة الأمثل المحضرة.

وبناءً على النتائج التي تم التوصل اليها تبين الآتي:

- (1) تم تحضير الجسيمات الصلبة الدهنية نانوية الحجم القائمة علي الشيتوزان والمُحملة بالأبوسينين بنجاح بواسطة تقنية المستحلب المزدوج وتبخير المذيب، بحيث تحتوي النواة علي الشيتوزان والأبوسينين مع الدهن بينما يحتوي الغلاف علي الكحول عديد الفايثيل.
- (2) يوفر نموذج التصميم البحثي المستخدم وسيلة فعالة تنسم بالكفاءة لتقييم التقنية المستخدمة في التحضير من خلال دراسة خصائص الجودة الحاسمة.
- (3) الصيغة الأمثل المحضرة (ف-3) والتي تتكون من (X_A ثلاثي ستيرات الجليسرول 100 ملجرام)، (X_B أحادي بالميتان السكروز 28,4 ملجرام)، (X_C الشيتوزان 1,5%) و (X_D الكحول عديد

تحديث وتوصيف أنظمة توصيل عقار معينة محكمة الإنطلاق بإستخدام بعض البوليمرات كوسادة حاملة.

المخلص العربي

- الفانيل ٣,٠%) تتميز بأصغر حجم للجزيئات وأصغر قيمة لمعامل تعدد الإنتشار وكذلك أعلى كفاءة إحتواء دوائي وإنتاجي.
- (٤) أوضحت صور المجهر الإلكتروني النافذ للصبغة الأمثل أنها كروية الشكل تتكون من نواة تشتمل علي الأوبوسينين مع الشيتوزان وكذلك سطح أملس للغلاف.
- (٥) أكدت نتائج التحليل الطيفي للأشعة تحت الحمراء، المسح الحرارى التفاضلى وحيود الأشعة السينيه للصبغة الأمثل المحضرة (ف-٣) إحتباس العقار داخل الجسيمات الصلبة الدهنية نانوية الحجم.
- (٦) أوضح نمط إنطلاق الأوبوسينين من الجسيمات الصلبة الدهنية نانوية الحجم للصبغه الأمثل المحضرة (ف-٣) أنه لا يتميز بسرعة الإنطلاق في مختلف المحاليل المستخدمة لدراسة الإنطلاق المعملية. فى وسط ذو حامضية الأس الهيدروجيني ١,٢ كان الانطلاق المعملية ضئيل وكان سائدا لمدة ٣ ساعات. ومع ذلك، فإن نمط إنطلاق الأوبوسينين من الجسيمات الصلبة الدهنية نانوية الحجم للصبغه الأمثل المحضرة (ف-٣)، فى أوساط ذات حامضية الأس الهيدروجيني ٦,٨ و ٧,٤، كان أعلى نسبيا ومستمر لمدة ٢٤ ساعة.
- (٧) أظهرت النتائج أن معدل الانطلاق المعملية للأوبوسينين يتبع نموذج "هيجوشى" والإنتشار "فيكيان" ميكانيكية محتملة لإنتشار العقار سواء الحر أو المحتبس داخل الجسيمات الصلبة الدهنية نانوية الحجم للصبغه الأمثل المحضرة (ف-٣).
- (٨) أثبتت دراسة ثبات الجسيمات الصلبة الدهنية نانوية الحجم للصبغه الأمثل المحضرة (ف-٣) فى شكلها المعلق الثبات الفائق لها عند درجة حرارة الثلجة (٥ ± ٣ درجة سيليزية) مما يتيح فعاليتها لفترة طويلة من الوقت.

الفصل الثانى

التوافر الحيوي للجسيمات الصلبة الدهنية نانوية الحجم الأمثل القائمة علي الشيتوزان والمحملة بالأوبوسينين عن طريق الفم والحقن في الجرذان.

الهدف من هذا الفصل هو تقييم التوافر الحيوي (بالفم أو بالحقن) للجسيمات الصلبة الدهنية نانوية الحجم للصبغه الأمثل (ف-٣) ومقارنة ذلك بالمحلول المائي من الأوبوسينين في الجرذان.

كشفت النتائج التي تم الحصول عليها عن الآتي:

- (١) أن الإتاحة الحيوية ومتوسط فترة البقاء للجسيمات الصلبة الدهنية نانوية الحجم للصبغه الأمثل (ف-٣) أعلى من مثيلاتها لمحلول الأوبوسينين المائي بغض النظر عن طريقة التناول.
- (٢) تعتبر الجسيمات الصلبة الدهنية نانوية الحجم المحضرة بإستخدام الأوبوسينين، الشيتوزان والكحول عديد الفانيل نظام توصيل واعد للمستحضرات الصيدلانية النباتية مما يحقق فعالية ممتدة للعقار المذهل

تحديث وتوصيف أنظمة توصيل عقار معينة محكمة الإنطلاق بإستخدام بعض البوليمرات كوسادة حاملة.

المخلص العربي

"الأبوسينين" خاصة عندما يتطلب الأمر تناول العقار لفترة طويلة من الزمن. بعد تلك الدراسة، من الممكن أن نطلق علي الجسيمات الصلبة الدهنية نانوية الحجم والمُحملة بالأبوسينين "دعامة نانوية".
(٣) وفي الختام، فإن الجسيمات الصلبة الدهنية نانوية الحجم القائمة علي الشيتوزان ستفتح آفاقا جديدة لتحسين الإتاحة الحيوية وتحقيق المفعول الممتد للأبوسينين وغيره من العقارات ذات الأصل النباتي النشطة حيويا والتي تتميز بخصائص مشابهة.

﴿الجزء الثاني﴾

الإيمجل ذو الحجم النانو وألياف النانو المُحمّلين بزيت القرنفل العطري: مستحضرات صيدلية نباتية بإمكانات واعدة كمثبطات لإنزيم السيكلو اوكسيجيناز-٢ في الالتهاب الخارجي

بالرغم من كثرة البيانات عن التأثير الدوائي العلاجي المتنوع لزيت القرنفل العطري، فقد نشرت محاولات قليلة لصياغة وتقييم الأنشطة الفارماكولوجية لزيت القرنفل العطري في مختلف أنظمة التوصيل الدوائي. ومن ثم، تم إجراء هذا البحث لتطوير وتقييم أنظمة توصيل نانوية مضادة للإلتهابات للإستخدام الموضعي وتمتع بدرجة ثبات عالية مُحملة بزيت القرنفل العطري، على وجه التّحديد الإيمجل ذو الحجم النانو وألياف النانو. في هذا الجزء تم إجراء دراسات تفصيلية لتقييم أنظمة التوصيل الدوائية الموضعية سالفة الذكر من خلال التجارب المعملية والحيوية.

الفصل الأول: تحضير وتقييم مستحلبات نانوية متناهية الصغر مُحملة بزيت القرنفل العطري.

الفصل الثاني: تحضير وتقييم الإيمجل ذو الحجم النانو وفقا لنموذج تاجوشي وكذلك ألياف النانو باستخدام مستحلب النانو متناهي الصغر المُحمّل بزيت القرنفل العطري.

الفصل الثالث: دراسة نفاذية العقار عبر الجلد، الثبات وكذلك التأثير الحيوي للإيمجل ذو الحجم النانو وألياف النانو المُحمّلين بزيت القرنفل العطري في الالتهاب الخارجي.

الفصل الأول

تحضير وتقييم مستحلبات نانوية متناهية الصغر مُحملة بزيت القرنفل.

الهدف من هذا الفصل هو تصنيع مستحلبات نانوية متناهية الصغر مُحملة بزيت القرنفل وتقييمها واختيار الأفضل. وكذلك إدراج الصيغة المختارة في قاعدة الهيدروجيل، لتحضير الإيمجل ذو الحجم النانو، وأيضا إدراجها في تحضير ألياف النانو وذلك لتحسين التوصيل الموضعي.

وبناءً على النتائج التي تم التوصل إليها تبين الآتي:

(١) لقد اجتازت كل المستحلبات النانوية متناهية الصغر المُحملة بزيت القرنفل العطري اختبارات الاستقرار الديناميكي الحراري وكذلك اختبارات كفاءة الاستحلاب النانو-الذاتي.

تحديث وتوصيف أنظمة توصيل عقار معينة محكمة الإنطلاق بإستخدام بعض البوليمرات كوسادة حاملة.

المخلص العربي

- ٢) جميع المستحلبات النانوية متناهية الصغر المُحضرة والمُحملة بزيت القرنفل العطري لها جهد زيتا سالب، وحجمها يقل عن ١٠٠ نانومتر، ومعامل تعدد الإنتشار يقل عن أو يساوي ٠.٣٧٥. مما يدل على صغر حجم القطيرات بالإضافة إلي التجانس و التقارب في حجمها.
- ٣) أظهرت قيم معامل الانكسار العالية أن المستحلبات النانوية متناهية الصغر تميزت بالشفافية .
- ٤) أكدت نتائج التحليل الطيفي للأشعة تحت الحمراء لمستحلب النانو متناهي الصغر (ف-١) التشتت الجزيئي لزيت القرنفل العطري في الطبقة الزيتية من المستحلب النانو متناهي الصغر.
- ٥) المستحلب النانو متناهي الصغر (ف-١) له شكل كروي.

الفصل الثاني

تحضير وتقييم الإيمجل ذو الحجم النانو وفقا لنموذج تاجوشي وكذلك ألياف النانو باستخدام مستحلب النانو متناهي الصغر المُحمّل بزيت القرنفل العطري.

الهدف من هذا الفصل هو تحضير الإيمجل ذو الحجم النانو وكذلك ألياف النانو القانمان علي مستحلب النانو متناهي الصغر لتحسين التوصيل الموضعي بصورة محكمة الإنطلاق. ولتحقيق هذا الهدف:

أولاً: تم تحضير وسائد هيدروجيل فارغة (لا تحتوي علي عقار) باستخدام البوليمرات وهي على وجه التحديد كل من صمغ الجوار، الصمغ العربي والشيتوزان وكذلك تم توصيف وتعظيم الإستفادة باستخدام نموذج تاجوشي والذي إعتد علي إستخدام ثلاث متغيرات مستقلة وثلاث مستويات للتصميم. المتغيرات المستقلة الثلاث هم تركيز كل من الشيتوزان (X_1)، صمغ الجوار (X_2) والصمغ العربي (X_3). و المتغيرات التابعة المقاسة هي قيم الأس الهيدروجيني واللزوجة عند معدل تدفق (١٩٢ ثانية^{-١}) لوسائد الهيدروجيل الفارغة المحضرة. وبعد ذلك، فقد تم اختيار وسادة الهيدروجيل الفارغ الأمثل ومستحلب النانو متناهي الصغر المُحمّل بزيت القرنفل العطري (ف-١) لتحضير الإيمجل ذو الحجم النانو القائم علي مستحلب النانو متناهي الصغر. تم فحص ذلك الإيمجل بصريا وكذلك تمت دراسة خصائصه من حيث تعيين الأس الهيدروجيني، قياس اللزوجة، تعيين كمية الدواء و كذلك دراسة التحليل الطيفي للأشعة تحت الحمراء والمسح الحرارى التفاضلى.

ثانياً: تم تحضير ألياف النانو القائمة علي مستحلب النانو متناهي الصغر باستخدام مستحلب النانو متناهي الصغر المُحمّل بزيت القرنفل العطري (ف-١) وبوليمر الكحول عديد الفايثيل، وبعد ذلك تم تقييمها باستخدام الميكروسكوب الإلكتروني الماسح، التحليل الطيفي للأشعة تحت الحمراء، المسح الحرارى التفاضلى وكذلك تعيين المحتوي الدوائي.

تحديث وتوصيف أنظمة توصيل عقار معينة محكمة الإنطلاق باستخدام بعض البوليمرات كوسادة حاملة.

المخلص العربي

وقد تم التوصل للنتائج التالية:

- (١) يوفر التصميم البحثي باستخدام نموذج تاجوشي طريقة سهلة وفعالة ومنهجية لتحديد وسادة الهيدروجيل الفارغ الأمثل لتحميل مستحلب النانو متناهي الصغر المحمل بزيت القرنفل العطري (ف-١) عليه وتحضير الإيمجل ذو الحجم النانو القائم علي مستحلب النانو متناهي الصغر المحمل بالعقار.
- (٢) الصيغة الأمثل المحضرة (ف-٩) والتي تتكون من ((X_1 الشيتوزان ٢%) (X_2 صمغ الجوار ١,٥%) (X_3 الصمغ العربي ٢%)) تتميز بأعلي لزوجة عند معدل التدفق (١٩٢ ثانية^{-١}) وأس هيدروجيني قيمته $٤,٩١ \pm ٠,٠٢$ والذي يعتبر مناسباً للإستخدام الموضعي.
- (٣) تعرضت الصيغة الأمثل المحضرة (ف-٩) لصياغة أكثر تفصيلاً في شكل الإيمجل ذو الحجم النانو القائم علي مستحلب النانو متناهي الصغر المحمل بزيت القرنفل العطري.
- (٤) الإيمجل ذو الحجم النانو القائم علي مستحلب النانو متناهي الصغر المحمل بزيت القرنفل العطري كان متجانساً، شفافاً وأصفر اللون.
- (٥) الإيمجل ذو الحجم النانو القائم علي مستحلب النانو متناهي الصغر المحمل بزيت القرنفل العطري يمتاز بقيمة مناسبة من الأس الهيدروجيني وكذلك لزوجة أعلي من مستحلب النانو متناهي الصغر المحمل بزيت القرنفل العطري (ف-١)، مما يجعله أكثر قبولاً للإستخدام الموضعي.
- (٦) أكدت نتائج التحليل الطيفي للأشعة تحت الحمراء والمسح الحراري التفاضلي التشتت الجزيئي لزيت القرنفل العطري ومكونات مستحلب النانو متناهي الصغر في الإيمجل صاحب الحجم النانو المحضر.
- (٧) أوضح المسح المجهر الإلكتروني أن ألياف النانو القائمة علي مستحلب النانو متناهي الصغر المحمل بزيت القرنفل العطري تظهر ألياف ملساء خالية من العقد وأن حجمها في نطاق النانو.
- (٨) أظهرت نتائج التحليل الطيفي للأشعة تحت الحمراء والمسح الحراري التفاضلي التشتت الجزيئي لمستحلب النانو متناهي الصغر المحمل بزيت القرنفل العطري في قاعدة بوليمر الكحول عديد الفايثيل المكون لألياف النانو.

الفصل الثالث

دراسة نفاذية العقار عبر الجلد، الثبات وكذلك التأثير الحيوي للإيمجل ذو الحجم النانو وألياف النانو المحملين بزيت القرنفل العطري في الالتهاب الخارجي.

الهدف من هذا الفصل تقييم الإيمجل ذو الحجم النانو وكذلك ألياف النانو القائم علي مستحلب النانو متناهي الصغر المحمل بزيت القرنفل العطري من حيث نفاذية العقار عبر الجلد والتحليل الرياضي لنتائج معدل النفاذية ودراسه الثبات عند درجة حرارة التلاجة (٥ ± ٣ درجة سيليزية) ودرجة حرارة الغرفة لمدة ستة أشهر. وكذلك تم التحقيق من فاعليتهما ضد الإلتهابات التي تُحدثها مادة زيت الكروتون عند وضعها علي جلد الفئران من خلال الفحص الهيستولوجي والتقييم الكيميائي الهيستولوجي

تحديث وتوصيف أنظمة توصيل عقار معينة محكمة الإنطلاق بإستخدام بعض البوليمرات كوسادة حاملة.

المخلص العربي

المناعي لإنزيم السيكلو اوكسيجيناز-٢. ايضاً تم تقييم الإستخدام الآمن علي الجلد للإيمجلج ذو الحجم النانو وكذلك ألياف النانو القائم علي مستحلب النانو متناهي الصغر المحمّل بزيت القرنفل العطري من خلال إجراء إختبار تهيج الجلد.

كشفت النتائج التي تم الحصول عليها عن الآتي:

- (١) كشفت دراسة النفاذية عبر الجلد نمط نفاذيه العقار الممتد من ألياف النانو القائمة علي مستحلب النانو متناهي الصغر مقارنة بالإيمجلج ذو الحجم النانو القائم علي مستحلب النانو متناهي الصغر.
- (٢) أظهر التحليل الرياضي لنتائج نفاذية زيت القرنفل العطري عبر الجلد من ألياف النانو القائمة علي مستحلب النانو متناهي الصغر أنه يتبع نموذج "هيجوشي" و"الانتشار" فيكيان"
- (٣) أوضح التحليل الرياضي لنتائج نفاذية زيت القرنفل العطري عبر الجلد من الإيمجلج ذو الحجم النانو القائم علي مستحلب النانو متناهي الصغر أنه يتبع نموذج صفر الترتيب و"حالة خاصة-٢".
- (٤) أثبتت دراسة ثبات الإيمجلج ذو الحجم النانو وكذلك ألياف النانو القائم علي مستحلب النانو متناهي الصغر المحمّل بزيت القرنفل العطري الثبات العالي لهما عند درجة حرارة الثلجة (5 ± 3 درجة سيليزية) لمدة ستة أشهر مما يتيح فعاليتها لفترة طويلة من الوقت.
- (٥) أثار العلاج الموضعي باستخدام الإيمجلج ذو الحجم النانو القائم علي مستحلب النانو متناهي الصغر المحمّل بزيت القرنفل العطري (مرتين يومياً) وكذلك ألياف النانو القائمة علي مستحلب النانو متناهي الصغر المحمّل بزيت القرنفل العطري (مرة يومياً) نشاطاً بارزاً مضاداً للإلتهابات جلد الفئران التي تم حثها بمادة زيت الكروتون وتم تأكيد ذلك من خلال:
 - الفحص الهيستولوجي الذي أثبت إنخفاض ملحوظا ($p < 0.05$) في درجات الإلتهاب مقارنة مع أنسجة جلد الفئران المعرضة لزيت القرنفل العطري الخام.
 - إنخفاض ملحوظ في مستوى التقييم الكيميائي الهيستولوجي المناعي لإنزيم السيكلو اوكسيجيناز-٢ مقارنة مع أنسجة جلد الفئران المعرضة لزيت القرنفل العطري الخام.
- (٦) أثبت الفحص الهيستولوجي، بعد إختبار تهيج الجلد، سلامة أنسجة جلد الفئران في حالة الإستخدام الموضعي للإيمجلج ذو الحجم النانو القائم علي مستحلب النانو متناهي الصغر المحمّل بزيت القرنفل العطري (مرتين يومياً) وكذلك ألياف النانو القائمة علي مستحلب النانو متناهي الصغر المحمّل بزيت القرنفل العطري (مرة يومياً) مقارنة مع أنسجة جلد الفئران المعرضة للفورمالين (باعتباره مادة معيارية مهيجة)، مما يشير إلي سلامة الإستخدام الموضعي الآمن وكذلك ترقب مستقبلي لتقبل المريض للعلاج.
- (٧) وإذا وضعنا في الاعتبار تلك التجارب العملية عبر الجلد والحيوية، يمكن تقديم الإيمجلج ذو الحجم النانو وكذلك ألياف النانو القائم علي مستحلب النانو متناهي الصغر المحمّل بزيت القرنفل العطري كصياغات

تحديث وتوصيف أنظمة توصيل عقار معينة محكمة الإنطلاق باستخدام بعض البوليمرات كوسادة حاملة.

المخلص العربي

موضعية واعدة وكبدائل فعالة لعلاج الأمراض الالتهابية بدلا من الأدوية الغير ستيرويدية المضادة للإلتهابات (NSAIDs) والتي تتمتع باثار جانبية.

إقرار بحدائثة الموضوع

أقر أنا الباحثة / ريهام مختار أحمد محمد أمان أن موضوع هذه الرسالة مبتكر وأصيل ولا ينتهك حقوق الملكية الفكرية أو حقوق النشر لأحد. وقد استشهدت بأمانة وبصورة صحيحة واقترت في جزء المراجع من هذه الرسالة بكل مصادر المعلومات وبتقنيات وإقتباسات الآخرين.

لجنة الإشراف

عنوان الرسالة : تحديث وتوصيف أنظمة توصيل عقار معينة محكمة الإنطلاق
بإستخدام بعض البوليمرات كوسادة حاملة.

إسم الباحث : ريهام مختار أحمد محمد أمان

لجنة الإشراف :

م	الاسم	الوظيفة	التوقيع
(١)	أ.د. محاسن محمد عبدالهادي مشالي	أستاذ الصيدلانيات المتفرغ كلية الصيدلة - جامعة المنصورة	
(٢)	أ.م.د/ إرهان إبراهيم أبو هاشم	أستاذ مساعد الصيدلانيات كلية الصيدلة - جامعة المنصورة	

عميد الكلية

وكيل الكلية للدراسات
العلياوالبحوث

رئيس القسم

أ.د. ناهد محمود العناني

أ.د/ منال محمد عيد

أ.د/ أسامه عبد العظيم سليمان

لجنة المناقشة والحكم

عنوان الرسالة : تحديث وتوصيف أنظمة توصيل عقار معينة محكمة الإنطلاق
بإستخدام بعض البوليمرات كوسادة حاملة.

إسم الباحث : ريهام مختار أحمد محمد أمان

لجنة الإشراف :

م	الاسم	الوظيفة	التوقيع
(١)	أ.د. محاسن محمد عبدالهادي مشالي	أستاذ الصيدلانيات المتفرغ كلية الصيدلة - جامعة المنصورة	
(٢)	أ.م.د/ إرهان إبراهيم أبو هاشم	أستاذ مساعد الصيدلانيات كلية الصيدلة - جامعة المنصورة	

لجنة المناقشة والحكم:

م	الاسم	الوظيفة	التوقيع
(١)	أ.د. محاسن محمد عبدالهادي مشالي	أستاذ الصيدلانيات المتفرغ كلية الصيدلة - جامعة المنصورة	
(٢)	أ.د. أميمة أحمد أمين سمور	أستاذ الصيدلانيات والصيدلة الصناعية - كلية الصيدلة - جامعة عين شمس	
(٣)	أ.د. ناهد داود صالح مرتضي	أستاذ الصيدلانيات والصيدلة الصناعية - كلية الصيدلة - جامعة عين شمس	
(٤)	أ.م.د/ إرهان إبراهيم أبو هاشم	أستاذ مساعد الصيدلانيات كلية الصيدلة - جامعة المنصورة	

عميد الكلية

وكيل الكلية للدراسات
العلياوالبحوث

رئيس القسم

أ.د. ناهد محمود العناني

أ.د/ منال محمد عيد

أ.د/ أسامه عبد العظيم سليمان



جامعة المنصورة
كلية الصيدلة
قسم الصيدلانيات

تحديث وتوصيف أنظمة توصيل عقار معينة محكمة الإنطلاق بإستخدام بعض البوليمرات كوسادة حاملة

رسالة مقدمة من

ريهام مختار أحمد محمد أمان

مدرس مساعد الصيدلانيات، كلية الصيدلة، جامعة المنصورة

ماجستير العلوم الصيدلانية – جامعة المنصورة (2014)
للحصول على درجة دكتوراة الفلسفة في العلوم الصيدلانية
(صيدلانيات)

تحت إشراف

الأستاذ المساعد الدكتور

إرهان إبراهيم أبوهاشم

أستاذ مساعد الصيدلانيات
كلية الصيدلة
جامعة المنصورة

الأستاذ الدكتور

محاسن محمد عبد الهادي مشالي

أستاذ الصيدلانيات المتفرغ
كلية الصيدلة
جامعة المنصورة

بِسْمِ اللَّهِ الرَّحْمَنِ الرَّحِيمِ

وَقُلْ أَعْلَمُ

فَسِيرِي اللَّهُ عَزَّ وَجَلَّ وَرَسُولِي وَالْمُؤْمِنُونَ

صدق الله العظيم

سورة التوبة (١٠٤-١٠٥)

List of publication

Aman RM, Abu Hashim II, Meshali MM. Novel chitosan-based solid-lipid nanoparticles to enhance the bio-residence of the miraculous phytochemical “Apocynin”. *European Journal of Pharmaceutical Sciences*. 124: 304–318 (2018). DOI. 10.1016/j.ejps.2018.09.001.

Publisher: ELSEVIER

Impact factor (2017/2018): 3.46

Rank: Q2

Declaration

We hereby certify that this thesis is our original work that encompassed topics not published before and does not violate anyone's intellectual proprietary rights or copyrights.

We have faithfully and properly cited all sources of information; and fully acknowledged, in the references part of this thesis, others' techniques and quotations.

Dedication

I want to thank *my respected mother, my brother, my sister and my husband's family*, who endured this long process with me. Words could not express my deep appreciation to them. God always bless them.

I would like to warmly thank my *lovely husband "Mohamed Emad El-Zeki"* for his encouragement and continuous support not only throughout this work but also throughout my whole life.

Really this work would never have been accomplished if they were not around.

Reham Mokhtar Aman

2019

Acknowledgement

First and foremost, thanks to ALLAH, the most merciful and the most gracious, for helping us all to complete this work.

*I am so fortunate to come under the guidance of **Prof. Dr. Mahasen M. Abd El Hady Meshali**, Professor Emeritus of Pharmaceutics, Faculty of Pharmacy, Mansoura University. I wish to express my deepest appreciation and sincere gratitude to her, for suggesting the topic of the thesis, the plan of work, her kind supervision, valuable advice, constructive criticism, infinite support and continuous guidance to provide all the facilities throughout this work.*

*I would like to express my deepest gratitude, thankfulness and appreciation to **Ass. Prof. Dr. Irhan Ibrahim Abu Hashim**, Associate Professor of Pharmaceutics, Faculty of Pharmacy, Mansoura University, for her continuous help and guidance from the beginning and throughout the whole work, faithful participation, sincere cooperation and everlasting effort to overcome the difficulties which I met during my work. Really, without her guidance and persistent help, this thesis would not have been possible.*

*I am particularly grateful for the assistance given by **Ass. Prof. Dr. Walaa Awadin**, Associate Professor of Pathology, Faculty of Veterinary Medicine, Mansoura University, Egypt in the Pathological part of the thesis.*

*Special thanks to all my **professors, colleagues, the technical staff** of the Department of Pharmaceutics and those people who stand behind me all the time.*

*Really words won't be sufficient any more to express how much I owe to **all my family members** for their kind care, continuous support and encouragement since the first moment till the last.*

**Reham Mokhtar Aman
2019**

*To
The Soul
of My
Father*



Contents

<input type="checkbox"/> Acknowledgement	
<input type="checkbox"/> List of Abbreviations	I
<input type="checkbox"/> List of Figures	VIII
<input type="checkbox"/> List of Tables	XII
<input type="checkbox"/> Abstract	1
<input type="checkbox"/> General Introduction	11
<input type="checkbox"/> Scope of work	23

Part I

Novel chitosan-based solid-lipid nanoparticles to enhance the bio-residence of the miraculous phytochemical “Apocynin”

♦ Introduction	27
----------------	----

Chapter 1

Formulation, characterization and optimization of novel chitosan-based apocynin-loaded solid lipid nanoparticles.

♦ Introduction	32
♦ Experimental	35
♦ Results & discussion	45
♦ Conclusions	68

Chapter 2

Oral and parenteral bioavailability of the optimized chitosan-based apocynin-loaded solid lipid nanoparticles in rats.

♦ Introduction	69
♦ Experimental	72
♦ Results & discussion	78
♦ Conclusions	87

Part II

Clove essential oil nanoemulgel and scaffold-based nanofibers: phytopharmaceuticals with promising potential as cyclooxygenase-2 inhibitors in external inflammation

♦ Introduction	88
-----------------------	-----------

Chapter 1

Preparation of clove essential oil nanoemulsion and its evaluation.

♦ Introduction	93
♦ Experimental	94
♦ Results & discussion	100
♦ Conclusions	110

Chapter 2

Preparation and evaluation of nanoemulgel tailored by Taguchi's model and nanofibers mat from clove essential oil nanoemulsion.

♦ Introduction	111
♦ Experimental	114

♦ Results & discussion	123
♦ Conclusions	139

Chapter 3

Ex vivo permeation, stability and *in vivo* impact of clove essential oil nanoemulgel and nanofibers mat on external inflammation.

♦ Introduction	140
♦ Experimental	141
♦ Results & discussion	150
♦ Conclusions	167
□ References	169
□ Arabic Summary	i

List of Abbreviations

Abbreviations	Full name
Adjusted R²	Adjusted coefficients of determination
ANOVA	Analysis of variance
APO	Apocynin
APO-sol	Aqueous solution of APO
AUC	Area under the curve
AUC_{0-∞}	Area under the plasma concentration-time curve from 0-∞ min
AUC_{0-Clast}	The area under the curve to the last measurable concentration (<i>C_{last}</i>)
AUC_{0-t}	Area under the curve from time zero to time t
AUMC_{0-∞}	Area under the first moment curve from 0-∞ min
BSA	Bovine serum albumin
-C=O	Carbonyl group
C₀	Initial drug concentration
CEO	Clove essential oil
CEO-NE	Clove essential oil nanoemulsion
CEO-NEs	Clove essential oil nanoemulsions
<i>C_{last}</i>	Last measurable concentration
<i>CL_B</i>	Total body clearance
<i>C_{max}</i>	Peak plasma concentration
C_{nom}	Nominal concentrations
CNS	Central nervous system

C_{obs}	Observed concentrations
COX-2	Cyclooxygenase-2
cP	Centipoise
CPPs	Critical process parameters
CQAs	Critical quality attributes
CS	Chitosan
CS,APO - loaded SLN_s	Chitosan-based APO-loaded solid lipid nanoparticles
C_t	Plasma drug concentration at time t
DAB	3, 3'-diaminobenzidine tetrahydrochloride
dB	Decibel
DDS_s	Drug delivery systems
DEE %	Drug entrapment efficiency %
DL	Detection limit
DMPs	Dependently measured parameters
DMSO	Dimethyl sulfoxide
DOE	Design of experiment
Drug retention %	Percentage drug retention
DSC	Differential scanning calorimetry
e.v.	Extravascular
EDTA	Ethylenediaminetetraacetic acid
EPR	Enhanced permeability and retention
ER_{flux}	Enhancement ratio of flux
F	Fraction absorbed

F (%)	Bioavailability factor
FDA	Food and Drug Administration
FT-IR	Fourier-transform infrared spectroscopy
G	Instrumental factor
GA	Gum acacia
GG	Guar gum
GIT	Gastrointestinal tract
GMA	Glycerol monoacetate
GRAS	Generally recognized as safe
GTS	Glycerol tristearate
H&E	Hematoxylin and eosin
H₂O	Water
H₂O₂	Hydrogen peroxide
HPLC	High performance liquid chromatography
HPLC methanol	Methanol of chromatographic grade
i.p.	Intraperitoneally
I.S.	Internal standard
i.v.	Intravenous
ICH	International Conference for Harmonization
ICPs	Independently controlled parameters
IHC	Immunohistochemical
IUPAC	International Union of Pure and Applied Chemistry
J_{ss}	Steady-state flux

K_a	First order rate constant for drug absorption
KBr	Potassium bromide
KDa	Kilodaltons
K	Elimination rate constant
KH_2PO_4	Potassium phosphate monobasic
K_p	Permeability coefficient
LD_{50}	Median lethal dose
Low MW	Low molecular weight
LPS	Lipopolysaccharide
MAT	Mean absorption time
MDT	Mean <i>in vivo</i> dissolution (or release) time
min/s	Minute/second
Mito-APO	Mitochondria-targeted apocynin
mPa.s	Millipascal.second
MRT	Mean residence time
N	Noise
Na_2HPO_4	Disodium hydrogen phosphate
NaCl	Sodium chloride
NADPH-oxidase	Nicotinamide adenine dinucleotide phosphate-oxidase
NAP	Naproxen
NE	Nanoemulsions
NEG	Nanoemulgel
NF_s	Nanofibers

NPs	Nanoparticles
n_s	Speed
NSAIDs	Nonsteroidal anti-inflammatory drugs
O₂⁻	Superoxide anion
OA	Orthogonal array
OAs	Orthogonal arrays
P SLN_s	Plain SLN_s
Pa	Pascal
PAA	Polyacrylic acid
PBS	Phosphate buffer saline
PDI	Polydispersity index
PEG	Polyethylene glycol
PGA	Polyglycolides
PGs	Prostaglandins
PKC	Protein kinase C
PLA	Poly lactic acid
PLGA	Poly lactic-co-glycolic acid
PMN	Polymorphonuclear
PVA	Polyvinyl alcohol
PVP	Polyvinylpyrrolidone
Q	The cumulative amount of CEO permeated the Wistar albino rats skin per unit area
Q_{48h}	The cumulative amount of CEO permeating the Wistar albino rats skin after 48 h per unit area

QL	Quantitation limit
(r)	Correlation coefficient
(R²)	Coefficients of determination
RH	Relative humidity
ROS	Reactive oxygen species
RSD %	Relative standard deviation
(S/N) ratio	Signal-to-noise ratio
S	Signal
s⁻¹	Reciprocal second
SC	Stratum corneum
SD	Standard deviation
SE	Standard error of the mean
SEM	Scanning electron microscopy
SE_s	Sucrose esters
S_i	Slope of the calibration curve
SLN_s	Solid lipid nanoparticles
S_{mix}	Surfactant (tween 80[®]): cosurfactant (Labrasol) mixture
SMP	Sucrose monopalmitate
S_T	Torque value
t	Time
t_{1/2a}	Half-life of absorption
t_{1/2}	Half-life
TDDS_s	Transdermal drug delivery systems

TEM	Transmission electron microscopy
t_{max}	C_{max} occurrence time
Vd_{ss}	Apparent volume of distribution at steady state
w_1	Internal aqueous phase
w_1/o	The primary emulsion
$w_1/o/w_2$	Double emulsion
w_2	External aqueous phase
X_1	CS concentration (Taguchi model)
X_2	GG concentration
X_3	GA concentration
X_A	GTS amount
X_B	SMP amount
X_C	CS concentration (2^4 full factorial design)
X_D	PVA concentration
XRD	X-ray diffractometry
Yield %	Percentage yield
ZP	Zeta potential
%T	Percentage transmittance
η	Viscosity
γ	Shear rate
τ	Shear stress

List of Figures

Figure No.	Title	Page No.
Figure 1:	Different types of nanocarriers (Arora and Jaglan, 2016).	13
Figure 2:	Schematic illustration of a typical setup for electrospinning (Xue <i>et al.</i> , 2017).	16
Figure 3:	Scanning electron micrographs of electrospun (a) random NFs, (b) aligned fibers at an angle, and (c) aligned fibers (Shi <i>et al.</i> , 2015 ^a).	17
Figure 4:	Schematic illustration and scanning electron micrographs of electrospun (a) core-shell NFs, (b) hollow NFs (Shi <i>et al.</i> , 2015 ^a), and (c) porous NFs (Xue <i>et al.</i> , 2017).	18
Figure 5:	Chemical structure of APO.	27
Figure 6:	Spectrophotometric scanning of APO in (A) deionized water and (B) phosphate buffer, pH 7.4.	46
Figure 7:	Spectrophotometric scanning of APO in (A) HCl (pH 1.2) and (B) phosphate buffer, pH 6.8.	47
Figure 8:	Calibration curves of APO in (A) deionized water and (B) phosphate buffer, pH 7.4.	48
Figure 9:	Calibration curves of APO in (A) HCl (pH 1.2) and (B) phosphate buffer, pH 6.8.	49
Figure 10:	Contour plots representing the effect of the interaction between the amounts of both GTS (X_A) and SMP (X_B) on DEE % and yield % (A and B) and (C and D) at the maximum and minimum levels of both CS (X_C) and PVA (X_D) concentrations, respectively.	53

Figure 11:	Three dimensional surface plots representing the effect of the interaction between the amounts of both GTS (X_A) and SMP (X_B) on DEE % and yield % (A and B) and (C and D) at the maximum and minimum levels of both CS (X_C) and PVA (X_D) concentrations, respectively.	54
Figure 12:	TEM image of CS,APO - loaded SLN _S with high level of GTS (X_A), CS (X_C) and PVA (X_D) and low level of SMP (X_B) (F-3, Table 2).	59
Figure 13:	Solid characterization. (A) FT-IR spectra, (B) DSC thermograms, and (C) XRD patterns of pure APO (i), GTS (ii), SMP (iii), physical mixture of APO, GTS and SMP (iv), P SLN _S (v) and CS,APO - loaded SLN _S (F-3) (vi).	62
Figure 14:	<i>In vitro</i> release profiles of free APO and APO from CS,APO - loaded SLN _S (F-3) at three different pH values (A) pH 1.2, (B) pH 6.8 and (C) pH 7.4.	64
Figure 15:	Calibration curve of APO in rat plasma.	78
Figure 16:	HPLC chromatogram of plasma spiked with APO and I.S.	80
Figure 17:	Mean plasma concentration-time profiles of APO after (A) oral (14 mg/kg) and (B) i.v. (5 mg/kg) administration. Drug solution (Group a and c), F-3 (Group b and d).	81
Figure 18:	<i>In vitro-in vivo</i> correlation plot for the optimized formula (F-3) in different pH media (A) pH 1.2, (B) pH 6.8 and (C) pH 7.4.	86
Figure 19:	Chemical structure of eugenol.	88
Figure 20:	Spectrophotometric scanning of CEO in distilled water.	100
Figure 21:	Calibration curves of CEO in distilled water.	101

Figure 22:	FT-IR spectra of pure CEO (a), GMA (b), Labrasol (c), tween-80 [®] (d), CEO: GMA dilution (in a ratio of 1:8) (e) blank NE (f) and CEO-NE (F-1) (g).	108
Figure 23:	TEM image of CEO-NE (F-1, Table 8).	109
Figure 24:	Graphs illustrating the mean (S/N) ratios of the DMPs against the concentration of the different ICPs. * Are the highest values. (a) mean pH, (b) mean η at γ of 192 s ⁻¹) See Table 14.	125
Figure 25:	Results of ANOVA for contribution (%) of each factor on the performance characteristics (a) pH and (b) η at γ of 192 s ⁻¹ .	128
Figure 26:	Shear thinning behavior of the prepared blank hydrogels with F-9 having the highest η .	130
Figure 27:	FT-IR spectra of pure CS (a), GG (b), GA(c), physical mixture of the optimized formula (F-9) (d), blank NEG (e) and CEO-NE based NEG (f) (See Figure 22, Part II, Chapter 1).	133
Figure 28:	DSC of pure CEO (a), blank NE (b), CEO-NE (F-1) (c), blank NEG (d), and CEO-NE based NEG (e).	134
Figure 29:	SEM image (A) and diameter distribution histogram (B) of CEO-NE based NF _s .	135
Figure 30:	FT-IR spectra of pure PVA (a), blank NF _s (b), and CEO-NE based NF _s (c) (See Figure 22, Part II, Chapter 1).	137
Figure 31:	DSC of pure CEO (a), blank NE (b), CEO-NE (F-1) (c), PVA (d), blank NF _s (e), and CEO-NE based NF _s (f).	138
Figure 32:	Spectrophotometric scanning of CEO in phosphate buffer, pH 7.4.	150

Figure 33:	Calibration curves of CEO in phosphate buffer, pH 7.4.	151
Figure 34:	<i>Ex vivo</i> skin permeation profiles of CEO from pure CEO, CEO-NE based NF _S and CEO-NE based NEG.	153
Figure 35:	Photomicrographs of histopathological evaluation of the anti-inflammatory activity of the investigated formulae: (A) normal control group, (B) croton oil treated group, (C) pure CEO group (once application), (D) CEO-NE based NEG (once application), (E) plain-NE based NEG (twice application), (F) CEO-NE based NEG (twice application), (G) plain-NE based NF _S (once application) and (H) CEO-NE based NF _S (once application).	160
Figure 36:	Photomicrographs of IHC evaluation of COX-2 expression level of the investigated formulae: (A) normal control group, (B) croton oil treated group, (C) pure CEO group (once application), (D) CEO-NE based NEG (once application), (E) plain-NE based NEG (twice application), (F) CEO-NE based NEG (twice application), (G) plain-NE based NF _S (once application) and (H) CEO-NE based NF _S (once application).	161
Figure 37:	Statistical analysis of inflammation scores (A) and IHC scores (B) in skin from experimental groups (six animals/group). Kruskal–Wallis test (nonparametric test) was applied followed by Dunn multiple comparison test.	162
Figure 38:	Photomicrographs of histopathological evaluation of skin irritation test: (A) normal control mice, (B) formalin treated mice, (C) CEO-NE based NEG (twice application), and (D) CEO-NE based NF _S (once application).	166

List of Tables

Table No.	Title	Page No.
Table 1:	CPPs and levels of a 2 ⁴ full factorial design.	39
Table 2:	Formulations and properties of CS,APO - loaded SLN _s prepared according to 2 ⁴ full factorial design.	52
Table 3:	Statistical analysis for the effect of CPPs and their interactions on the CQAs.	58
Table 4:	Kinetic analysis of the percentage drug diffused and that released from pure APO and CS,APO - loaded SLN _s (F-3), respectively (See Table 2 for F-3).	65
Table 5:	Particle size, PDI, ZP and drug retention % of CS,APO - loaded SLN _s aqueous dispersions (F-3) stored at refrigeration (5 ± 3°C) and ambient conditions (See Table 2 for F-3).	67
Table 6:	Pharmacokinetic parameters after oral administration of APO as an aqueous solution and CS,APO - loaded SLN _s (F-3) (See Table 2 for F-3).	83
Table 7:	Pharmacokinetic parameters after i.v. administration of APO as an aqueous solution and CS,APO - loaded SLN _s (F-3) (See Table 2 for F-3).	85
Table 8:	Composition (% w/w) of CEO-NEs formulae (F-1–F-5) prepared using GMA, tween-80 [®] , labrasol and water.	96
Table 9:	Thermodynamic stability and self-nanoemulsification efficiency tests of the prepared CEO-NEs (F-1–F-5).	103
Table 10:	Physicochemical characterizations of CEO-NEs (F-1–F-5) in	104

	terms of particle size, PDI, ZP, η , % T, pH and drug content (%).	
Table 11:	ICPs and their levels used in L9 Taguchi OA design.	115
Table 12:	Formulations of blank hydrogels by L9 Taguchi OA design.	117
Table 13:	Taguchi L9 OA response values and (S/N) ratios for DMPs of the prepared blank hydrogels (See Table 11 and 12).	126
Table 14:	Computer calculated (S/N) ratios for the tested DMPs (a) mean pH and (b) mean η at γ of 192 s^{-1} (cP) with regard to the different ICPs (See Table 11).	127
Table 15:	ANOVA for the tested DMPs (a) mean pH and (b) η at γ of 192 s^{-1} (cP).	128
Table 16:	Results of visual inspection of the blank hydrogels prepared by Taguchi L9 OA design.	129
Table 17:	<i>Ex vivo</i> skin permeation parameters of CEO from pure CEO, CEO-NE based NF _S and CEO-NE based NEG across the excised Wistar albino rats' skin after 48 h.	154
Table 18:	Kinetic analysis of the <i>ex vivo</i> permeation data of CEO from pure CEO, CEO-NE based NF _S and CEO-NE based NEG.	155
Table 19:	Drug retention %, pH, and η at γ of 192 s^{-1} of CEO-NE based NEG stored at refrigeration ($5 \pm 3^\circ\text{C}$) and ambient conditions.	157

Abstract

Controlled release drug delivery systems (DDS_s) refer to release of drug and/or biological materials in a controlled manner from dosage form to the site of action. Hence, restricted side effects from high systemic or off-target exposure as well as improved patient compliance will be achieved.

Currently, nanomedicine, which is defined as the application of nanotechnology to the field of medicine by using materials at the nanometer scale, can improve medical understanding in accordance with traditional medicine. The application of nanomedicine, as an advantageous drug delivery strategy, can confer opportunities for controlled release, provide specific or targeted drug delivery, and protect active ingredients from enzymatic or environmental degradation.

Among different nanocarriers, solid lipid nanoparticles (SLN_s), nanoemulgel (NEG), and nanofibers (NFs) have gained worldwide attention in the field of drug delivery.

Nature represents an inexhaustible resource for drug development, novel pharmacophores, chemotypes, and other precious bioactive agents. Since immemorial time, bioactive natural products have been the pillar of folk remedies everywhere in the globe and have also been an indispensable part of history and culture. Hence, recently, there has been a renewed attentiveness on the prospective application of natural products, as alternatives to synthetic drugs, with dual benefits of pharmacological activity and safety profile.

Phytochemicals are naturally occurring compounds found in plants which have numerous pharmacological activities against variety of diseases. Prevalent phytochemicals are phenolic compounds, alkaloids, tannins and flavonoids.

Among natural phenolic compounds that need to be incorporated in auspicious delivery systems, are apocynin (APO) and clove essential oil (CEO).

APO is a specific nicotinamide adenine dinucleotide phosphate-oxidase (NADPH) inhibitor that exhibits versatile pharmacological activities. However, it isn't available in the market as a dosage form.

CEO is an essential oil possessing numerous pharmacological activities and it has been approved and categorized by Food and Drug Administration (US FDA) as generally recognized as safe (GRAS) for multiple use. Yet, little trials to formulate and evaluate CEO pharmacological activities in different delivery systems were reported.

Hence, phytopharmaceutical preparations based particularly on the use of nanotechnology with the phytochemicals is a rapidly evolving approach. Consequently, the main objective of this thesis was to develop novel nano-sized phytopharmaceutical controlled delivery systems of APO (orally and parenterally) and CEO (topically) to potentiate the bioavailability and pharmacological activity, for prospective therapeutic application. To fulfill these goals, this thesis comprises the following two parts:

Part I: Novel chitosan-based solid-lipid nanoparticles to enhance the bio-residence of the miraculous phytochemical "Apocynin"

Part II: Clove essential oil nanoemulgel and scaffold-based nanofibers: phytopharmaceuticals with promising potential as cyclooxygenase-2 inhibitors in external inflammation

Part I

Novel chitosan-based solid-lipid nanoparticles to enhance the bio-residence of the miraculous phytochemical "Apocynin"

APO is a bioactive phytochemical having remarkable anti-inflammatory and anti-oxidant activities that were confirmed on a variety of cell lines and animal models. Also, SLN_s are recently developed as promising nanocarriers acquiring the merits of having high drug loading capacity for both hydrophilic and lipophilic drugs as well as application for drug delivery in almost all routes of administration.

Additionally, chitosan (CS) and polyvinyl alcohol (PVA) have been proved as promising candidates, owing to their excellent properties, for preparation of several nano-sized delivery systems aimed to enhance the therapeutic efficacy of the loaded drugs.

In such a way, this part was directed to fabricate, optimize, by adopting full factorial design 2^4 , and evaluate a novel and facile phytopharmaceutical SLN_S system ((CS,APO/oil)/PVA (core/shell)), through double-emulsion solvent evaporation technique (w/o/w), composed of (CS,APO) as an internal aqueous phase (w_1), glycerol tristearate (GTS) as an oil phase and PVA as an external aqueous phase (w_2). In this part, the detailed studies on *in vitro* and *in vivo* oral and parenteral bioavailability performance of chitosan-based APO-loaded solid lipid nanoparticles (CS,APO - loaded SLN_S) were investigated. This part involves two chapters:-

Chapter 1:

Formulation, characterization and optimization of novel chitosan-based apocynin-loaded solid lipid nanoparticles.

Chapter 2:

Oral and parenteral bioavailability of the optimized chitosan-based apocynin-loaded solid lipid nanoparticles in rats.

Chapter 1

"Formulation, characterization and optimization of novel chitosan-based apocynin-loaded solid lipid nanoparticles."

The work in this chapter deals with the preparation of a novel phytopharmaceutical SLN_S system for oral and parenteral delivery of APO. CS,APO - loaded SLN_S were prepared by double-emulsion solvent evaporation method (w/o/w).

The prepared CS,APO - loaded SLN_S were optimized by adopting full factorial design 2⁴ with four different critical process parameters (CPPs) at two levels. The CPPs were the amount of each of GTS (X_A) and SMP (X_B) as well as the concentration of both CS (X_C) and PVA (X_D). The prepared SLN_S were evaluated in terms of drug entrapment efficiency % (DEE %), percentage yield (yield %), particle size, polydispersity index (PDI), and zeta potential (ZP), as critical quality attributes (CQAs). As well, the optimized formula was further characterized by transmission electron microscopy (TEM), Fourier transform-infrared (FT-IR) spectroscopy, differential scanning calorimetry (DSC) and X-ray diffractometry (XRD). Finally, its *in vitro* release profile, kinetic analysis and stability at two different conditions for a period of six months, namely refrigeration (5 ± 3°C) and ambient conditions were evaluated. Based on the obtained results, it could be deduced that:

1. CS,APO - loaded SLN_S were prepared successfully using double-emulsion solvent evaporation technique (w/o/w), where the core contains APO and CS with the lipid, while the shell contains PVA.
2. The design of experiment (DOE) paradigm provides an efficient mean to optimize the CQAs of the w/o/w method of preparation.
3. F-3, with (X_A (+) 100.0 mg, X_B (-) 28.4 mg, X_C (+) 1.5% w/v, X_D (+) 3.0% w/v), was found to be the optimized CS,APO - loaded SLN_S formula with the lowest particle size and PDI besides the highest DEE % and yield %.
4. TEM of the optimized F-3 revealed that the prepared SLN_S have spherical shape with "core" encapsulating APO with CS as well as smooth surface of the "shell".
5. Solid characterization of F-3 employing FT-IR, DSC and XRD established the drug entrapment in the SLNs matrix.
6. The *in vitro* release data of APO from CS,APO - loaded SLN_S (F-3) showed no burst effect at the different release media. In pH 1.2, a negligible release prevailed

for 3 h. However, at pH 6.8 and 7.4, the release profiles of CS,APO - loaded SLN_S (F-3) were comparatively higher and sustained over a period of 24 h.

7. Both Higuchi's model and Fickian diffusion mechanism prevailed for both free drug as well as entrapped one in the CS,APO - loaded SLN_S (F-3).
8. The high stability of the prepared CS,APO - loaded SLN_S aqueous dispersion (F-3) was revealed upon storage at $5 \pm 3^{\circ}\text{C}$, hence enabling its efficacy for prolonged period of time.

Chapter 2

"Oral and parenteral bioavailability of the optimized chitosan-based apocynin-loaded solid lipid nanoparticles in rats."

The aim of this chapter was to evaluate and compare the oral and parenteral bioavailability of the optimized CS,APO - loaded SLN_S (F-3) with that of a freshly prepared aqueous solution of APO (APO-sol) following administration to male Sprague–Dawley rats. The obtained results revealed that:

1. The bioavailability and the mean residence time (*MRT*) of CS,APO - loaded SLN_S in rats were higher compared to that of APO-sol regardless of the route of administration.
2. SLN_S with APO, CS and PVA is a promising phytopharmaceutical delivery system for sustaining the efficacy of the "miraculous" molecule APO especially when it is necessary to administer the drug over a prolonged period of time. After which study, one may name the APO SLN_S as "nano-scaffold".
3. In conclusion, the novel CS-based SLNs system would open new vistas in potentiating the bioavailability and sustaining the effect of APO and other bioactive phytochemicals with comparable properties.

Part II

Clove essential oil nanoemulgel and scaffold-based nanofibers: phytopharmaceuticals with promising potential as cyclooxygenase-2 inhibitors in external inflammation

Inspite of the wealth literature data on the versatile pharmacological effect of CEO, little trials to formulate and evaluate CEO pharmacological activities in different delivery systems were reported. Thereby, this research was conducted to develop and evaluate controlled release nanoparticulate DDS_s loaded with CEO, namely; NEG and NFs, for the topical application with potentiated anti-inflammatory activity and enhanced stability. In this part, the detailed studies on *in vitro* and *in vivo* evaluations of such medicated topical delivery systems were investigated. This part involves three chapters:-

Chapter 1:

Preparation of clove essential oil nanoemulsion and its evaluation.

Chapter 2:

Preparation and evaluation of nanoemulgel tailored by Taguchi's model and nanofibers mat from clove essential oil nanoemulsion.

Chapter 3:

Ex vivo permeation, stability and *in vivo* impact of clove essential oil nanoemulgel and nanofibers mat on external inflammation.

Chapter 1

Preparation of clove essential oil nanoemulsion and its evaluation.

The aim of this chapter was to develop, characterize and optimize nanoemulsion (NE) formulations of CEO. The chosen CEO-NE formula was to be further incorporated into hydrogel matrix, to prepare NEG, as well as NF_s matrix for enhanced topical application. From the obtained results, it was evident that:

1. All clove essential oil nanoemulsions (CEO-NEs) formulae passed thermodynamic stability as well as self-nanoemulsification efficiency tests.
2. All the prepared CEO-NEs formulae were found to have a negative ZP charge, a droplet diameter < 100 nm and PDI values ≤ 0.375 , indicating superior uniformity in the distribution of the droplets besides having small size.
3. All the prepared CEO-NEs formulae expressed high percentage transmittance (%T) values indicating optically clear solutions.
4. FT-IR analysis of CEO-NE (F-1) indicated molecular dispersion of CEO in the oil phase of the NE.
5. CEO-NE (F-1) has spherical shape.

Chapter 2

Preparation and evaluation of nanoemulgel tailored by Taguchi's model and nanofibers mat from clove essential oil nanoemulsion.

The aim of this chapter was to prepare CEO-NE based NEG as well as CEO-NE based NF_s for enhanced topical application with controlled release characteristics. To achieve such goal, firstly, blank hydrogel matrices of the polymers, namely; guar gum (GG), gum acacia (GA) and CS, were prepared and optimized by adopting Taguchi model with three independently controlled parameters (ICPs) at three levels. The ICPs were the concentration of each of CS (X_1), GG (X_2), and GA (X_3). The dependently

measured parameters (DMPs) were pH as well as viscosity (η) at shear rate (γ) of 192 s^{-1} of the prepared blank hydrogels. Then, the optimized blank hydrogel formula and the selected CEO-NE formulation (F-1) were chosen for further formulation into CEO-NE based NEG. Such prepared NEG was inspected visually and further characterized in terms of pH determination, η measurement, and drug content assay as well as FT-IR and DSC studies. Secondly, CEO-NE based NF_S was prepared using the selected CEO-NE formulation (F-1) and PVA, then characterized utilizing scanning electron microscopy (SEM), FT-IR, and DSC along with estimating the drug content. The obtained results revealed that:

1. The DOE using the Taguchi model offers a simple, efficient, and systematic procedure to determine the optimum hydrogel formula for loading CEO-NE (F-1).
2. F-9, with (X_1 (CS 2% w/w), X_2 (GG 1.5% w/w), X_3 (GA 2% w/w)), was found to be the optimized blank hydrogel formula with the highest η at γ of 192 s^{-1} and pH of 4.91 ± 0.02 , which makes it suitable for topical application.
3. F-9 was subjected to further elaborate formulation into CEO-NE based NEG.
4. CEO-NE based NEG is homogenous, yellow and transparent.
5. CEO-NE based NEG has a suitable pH value as well as an increased η , compared to CEO-NE (F-1), being more acceptable for topical application.
6. Both FT-IR and DSC data established the molecular dispersion of CEO and NE's components in the prepared NEG.
7. SEM image of the CEO-NE based NF_S mats displayed a bead-free and smooth NF_S with nanometric size.
8. Both FT-IR and DSC data indicated complete dispersion of the CEO-NE (F-1) into PVA polymer matrix of the NF_S.

Chapter 3

***Ex vivo* permeation, stability and *in vivo* impact of clove essential oil nanoemulgel and nanofibers mat on external inflammation.**

The goal of this chapter was to further evaluate CEO-NE based NEG as well as CEO-NE based NF_S mats in terms of *ex vivo* permeation, kinetic analysis, and stability for a period of six months at refrigeration ($5 \pm 3^{\circ}\text{C}$) and ambient conditions. *In vivo* anti-inflammatory activity against croton oil-induced mouse skin inflammation model was assessed by histopathological examination and immunohistochemical (IHC) detection of cyclooxygenase-2 (COX-2) expression level. Additionally, the safety profile of CEO-NE based NEG and CEO-NE based NF_S was evaluated by skin irritation test. From the obtained results, it could be concluded that:

1. The *ex vivo* skin permeation data of CEO from the prepared formulations showed that CEO-NE based NF_S can sustain the penetration of CEO through the skin, when compared to CEO-NE based NEG.
2. Both Higuchi's model and Fickian diffusion mechanism prevailed for CEO-NE based NF_S permeation.
3. Both zero-order model and super case II transport mechanism prevailed for CEO-NE based NEG permeation.
4. The high stability of the prepared CEO-NE based NEG and CEO-NE based NF_S was revealed upon storage at $5 \pm 3^{\circ}\text{C}$ for six months, hence enabling their efficacy for prolonged period of time.
5. Topical treatment with CEO-NE based NEG (twice application) and CEO-NE based NF_S (once application) evoked a marvelous *in vivo* anti-inflammatory activity against croton oil-induced mouse skin inflammation model that was asserted by:
 - Histopathological evaluation which disclosed a significant decrement ($p < 0.05$) in the inflammatory scores comparably with the control pure CEO treated mice.

- Significant suppression of IHC expression level of COX-2 when compared with the control pure CEO treated mice.
- 6. *In vivo* skin irritation test disclosed normal histopathological integrity of mice skin in case of CEO-NE based NEG (twice application) and CEO-NE based NF_s (once application) treated groups in comparison with formalin treated mice as a standard irritant group, indicating their cutaneous safety profile as well as prospective patient tolerability and compliance for therapeutic use.
- 7. Considering the *ex vivo* and *in vivo* data; CEO-NE based NEG and CEO-based NF_s could be introduced to the phytomedicine field as promising topical delivery systems for effective treatment of inflammatory diseases instead of nonsteroidal anti-inflammatory drugs (NSAIDs) that possess adverse effects.



Abstract





General Introduction





Scope of Work





PART I
**Novel chitosan-based solid-lipid nanoparticles to enhance the
bio-residence of the miraculous phytochemical "Apocynin"**





Chapter 1
Formulation, characterization and optimization
of novel chitosan-based apocynin-loaded solid lipid nanoparticles





Chapter 2
**Oral and parenteral bioavailability of the optimized
chitosan-based apocynin-loaded solid lipid nanoparticles in rats**





PART II
Clove essential oil nanoemulgel and scaffold-based nanofibers:
phytopharmaceuticals with promising potential as cyclooxygenase-2
inhibitors in external inflammation





Chapter 1

Preparation of clove essential oil nanoemulsion and its evaluation





Chapter 2
**Preparation and evaluation of nanoemulgel tailored by Taguchi's model
and nanofibers mat from clove essential oil nanoemulsion**





Chapter 3
**Ex vivo permeation, stability and in vivo impact of clove essential oil
nanoemulgel and nanofibers mat on external inflammation**





References





Arabic Summary





الملخص العربي

